

Characterising Quantitative Spontaneous Retinal Venous Pulsations in Glaucoma

by Sahar Shariflou

Thesis submitted in fulfilment of the requirements for
the degree of

Doctor of Philosophy: Orthoptics

Under the supervision of Dr Mojtaba Golzan, Professor Kathryn
Rose and Dr Ashish Agar.

University of Technology Sydney
Graduate School of Health

April 2022

Certificate of Original Authorship

I, Sahar Shariflou declare that this thesis, is submitted in fulfilment of the requirements for the award of Doctor of Philosophy, in the Graduate School of Health at the University of Technology Sydney. This thesis is wholly my own work unless otherwise referenced or acknowledged. In addition, I certify that all information sources and literature used are indicated in the thesis. This document has not been submitted for qualifications at any other academic institution.

This research is supported by the Australian Government Research Training Program.

Signature: Production Note:
Signature removed prior to publication.

Date: 4th April 2022

Acknowledgments

First and foremost, I would like to express sincere gratitude to my supervisors, Dr Mojtaba Golzan, Prof Kathryn Rose and Dr Ashish Agar for their support throughout the duration of my research. It has been a privilege to grow under the supervision of such intelligent and kind people. I am thankful to Dr Golzan for his clear guidance, generosity in time and for providing the opportunities to develop my skills in research. I am grateful to Prof Rose for the opportunities she has provided me in research and academia, for being so understanding and for making time to listen and console me in some of the most challenging times of my life. My sincere thanks to Dr Agar for facilitating this research from the very beginning by making his clinics available to me, and for his clinical expertise and guidance along the way. I'd also like to acknowledge both clinical and administrative staff across the Marsden Eye Specialists clinics who were incredibly accommodating to me. My sincere thanks also to Dr Jack Phu and Prof Michael Kalloniatis who assisted in facilitating this research by making their clinic available to me. The assistance of the administrative staff at the Centre for Eye Health is also greatly appreciated.

I have also been blessed with a strong network of PhD students and academic staff at UTS Orthoptics who I thank. I will forever cherish the many memories that I share with my fellow Orthoptic PhD students from this rollercoaster of a journey together. I would like to specifically thank Mythili Ilango - we began this journey together as master's students. She has been a consistent source of support, laughter and friendship throughout not only this research journey, but also in the ups and downs of life that have accompanied us in this journey.

The completion of my PhD thesis would not have been possible without the unparalleled support and love from my wonderful family. I am extremely grateful to my sister, Sana, who has proven to be wise beyond her years. She has been an immense source of joy and shared laughter throughout this journey. Your radiating energy inspires me every day. I am forever grateful to my parents who have showered me in immeasurable support, encouragement, patience and love. Thank you for always believing in my abilities and for giving me the opportunities and experiences that have made me who I am. If not for my parents, this thesis would not have been possible, and so, I dedicate this milestone to them.

Table of contents

Certificate of Original Authorship	ii
Acknowledgments.....	iii
Table of contents	iv
Thesis abstract	x
Publications, Presentations and Awards.....	xii
List of figures.....	xiv
List of tables.....	xvii
Glossary of Abbreviations.....	xviii
Chapter 1	1
1. Anatomy and blood supply of the eye	2
1.1 Overview of basic ocular anatomy	2
1.2 RGCs in the retina.....	5
1.3 RGCs at the optic nerve and beyond the eye	7
1.4 Overview of basic ocular vasculature	9
1.4.1 Arterial supply to the retina	9
1.4.2 Venous drainage of the retina.....	10
2. Overview of Glaucoma	12
2.1 Definition of glaucoma.....	12
2.2 Epidemiology of glaucoma	14
2.2.1 Prevalence of glaucoma across the globe.....	14
2.2.2 Risk factors for the development and progression of glaucoma.....	14
2.3 Quality of life with glaucoma	18

3.	Pathophysiology of glaucoma	20
3.1	Glaucoma as a disease continuum	20
3.1.1	Alternative concepts in the structure-function relationship.....	21
3.2	Clinical diagnosis of glaucoma.....	22
3.2.1	RGCs in glaucoma	23
3.2.2	RNFL assessment.....	25
3.2.3	VF assessment.....	35
3.2.4	RGC assessment	40
3.3	Vascular markers in Glaucoma.....	41
3.3.1	Static vascular markers.....	42
3.3.2	Dynamic vascular markers	44
3.3.3	Retinal vein characteristics	47
4.	Spontaneous retinal venous pulsations (SVPs).....	49
4.1	Aetiology and mechanism of SVPs.....	49
4.2	SVPs in healthy eyes	52
4.3	SVP alterations in glaucoma.....	52
4.4	Current SVP detection techniques.....	53
4.4.1	Subjective techniques.....	53
4.4.2	Objective techniques	53
5.	Gaps in current literature and thesis outline.....	56
	Chapter 2	60
1.	Human ethics	61
2.	Participant recruitment	61
2.1	Clinical diagnosis and classification	62
3.	Power Calculation.....	63
4.	Data breakdown per chapter	64

5.	Data collection	65
5.1	Standard ophthalmic workup.....	65
5.2	Retinal videoscropy (SVP recording).....	65
5.3	Data management.....	66
5.4	SVP quantification	66
5.5	Retinal ganglion cell estimation.....	66
5.6	Staging glaucoma.....	67
6.	Statistical analysis.....	68

Chapter 3 69

1.	Introduction	70
2.	Methodology.....	71
2.1	Data collection.....	71
2.2	Retinal Videoscropy	72
2.3	Data analysis.....	73
2.4	Ethics.....	76
3.	Results.....	76
3.1	SVPs were identified in 100% of patients when assessed objectively	76
3.2	SVPs are correlated with RNFL thickness	77
3.3	SVP measures are reproducible using the tablet-based ophthalmoscope.....	77
4.	Discussion	78

Chapter 4 83

1.	Introduction	84
2.	Methods.....	85

2.1	Data collection.....	85
2.2	SVP Quantification.....	85
2.3	Ethics.....	86
3.	Results.....	86
3.1	SVP and age.....	87
3.2	SVP and gender	89
4.	Discussion and conclusions.....	89
Chapter 5		92
1.	Introduction	93
2.	Methodology.....	95
2.1	Data collection.....	95
2.2	Ethics.....	96
2.3	Retinal videoscapy.....	96
2.4	Estimating retinal ganglion cell count.....	97
2.5	Statistical analysis.....	98
3.	Results.....	98
3.1	SVP amplitudes and their association with structural-functional parameters in NTG.....	99
3.2	SVP amplitudes and their association with structural-functional parameters in POAG and glaucoma suspects.....	101
4.	Discussion	104
4.1	RGC estimation and its limitations.....	105
4.2	Study limitations.....	107
5.	Conclusions	108
Chapter 6		109

1. Introduction	110
2. Methods.....	111
2.1 Ethics.....	112
2.2 Retinal venous circulation videoscropy and SVP analysis.....	112
2.3 Retinal ganglion cell estimates.....	112
2.4 Data analysis.....	112
3. Results.....	113
4. Discussion	116
4.1 POAG vs glaucoma suspects.....	116
4.2 POAG vs NTG	118
4.3 Limitations.....	118
5. Conclusions	119
Chapter 7	120
1. Introduction	121
2. Methods.....	122
2.1 Retinal videoscropy and SVP quantification	122
2.2 Retinal ganglion cell estimates	123
2.3 Statistical analysis.....	123
2.4 Ethics.....	123
3. Results.....	124
4. Discussion and conclusion	128
Chapter 8	131
1. Conclusions	132

2. Future directions	136
References	141
Appendix 1: Participant information sheet	170
Appendix 2: Participant consent form	174
Appendix 3: Participant questionnaire	176
Appendix 4a: Image of SVP assessment using a tablet-based ophthalmoscope mounted on a slit lamp	180
Appendix 4b: Image of SVP-setup on slit lamp.....	181
Appendix 5: A combined convolutional and recurrent neural network for enhanced glaucoma detection	182
Appendix 6: Objective Quantification of Spontaneous Retinal Venous Pulsations Using a Novel Tablet-Based Ophthalmoscope	194

Thesis abstract

Spontaneous retinal venous pulsations (SVPs) are a dynamic vascular marker for glaucoma, which is a leading cause of irreversible blindness across the globe. Since the discovery of SVPs, their presence has been variably reported in patients with glaucoma, some even reporting absent SVPs. Recent objective quantification of SVPs has led to an increase in their detection. There is a need to explore the possibility of SVPs being used as a potential marker for glaucoma screening in clinical practice. Current devices that are used to assess SVPs pose limitations that deem current SVP detection unfeasible for screening outside metropolitan and in remote areas and for use in mobile clinics that service underprivileged and remote communities where there is likely to be many cases of undetected glaucoma.

This thesis aims to assess the effectiveness of a novel tablet-based ophthalmoscope to detect and quantify SVPs in glaucoma with the aid of computer analysis. This device was used to perform fundus videography in 170 participants recruited from three ophthalmic clinics in Sydney. All participants had a confirmed diagnosis of glaucoma or glaucoma suspect. SVP amplitudes were extracted from raw videos using a custom-written algorithm. Standard structural (RNFL thickness) and functional (VF loss) clinical markers for glaucoma, as well as intraocular pressure (IOP) and retinal ganglion cell (RGC) estimates were also recorded and documented. SVP distribution, and its association with the established clinical structural and functional measures were assessed.

Using tablet-based ophthalmoscopy, SVPs were detected and quantified in all participants, regardless of glaucoma status. The largest SVP amplitudes were detected in normal tension glaucoma (NTG; 32.5%), followed by primary open-angle glaucoma (POAG; 28.7%) and glaucoma suspects (26.3%). A significant association was found between SVP amplitudes and clinical markers in NTG and POAG with the highest correlations being between SVP amplitude - RNFL thickness ($p=0.1$) and SVP amplitude - RGC count ($p<0.001$) in NTG and POAG respectively. When evaluating which clinical marker can distinguish between confirmed glaucoma and glaucoma suspects, SVP analysis was found to be comparable to standard clinical markers. More specifically, SVPs can separate POAG from glaucoma

suspects as effectively as RNFL thickness. SVPs can also separate POAG from NTG as effectively as IOP measurements.

The novel device used in this thesis overcomes many of the disadvantages of current commercial techniques, particularly portability and ease of use. The novel device and technique can be used to detect and quantify SVPs in all participants with glaucoma, regardless of glaucoma severity. The findings of this thesis indicate that SVPs are associated with clinical markers that are known to occur during the early glaucomatous changes. The potential benefits that this may offer in the early detection of glaucoma, consequent management and evaluation of progression are substantial. When combined with RGC count, SVP amplitude analysis may provide benefits to traditional glaucoma assessments where often structural and functional glaucomatous loss are only clinically detected once substantial RGC loss has already occurred. Further studies are required to determine if longitudinal SVP changes are associated with progressive glaucoma and whether SVPs can be used as a marker for monitoring disease progression.

Publications, Presentations and Awards

Journal publications:

Gheisari, S., Shariflou, S., Phu, J., Kennedy, P.J., Agar, A., Kalloniatis, M. and Golzan, S.M., 2021. A combined convolutional and recurrent neural network for enhanced glaucoma detection. *Scientific reports*, 11(1), pp.1-11. (Appendix 5)

Shariflou, S., Agar, A., Rose, K., Bowd, C. and Golzan, S.M., 2020. Objective quantification of spontaneous retinal venous pulsations using a novel tablet-based ophthalmoscope. *Translational Vision Science & Technology*, 9(4), pp.19-19. (Appendix 6)

National and international presentations:

Shariflou, S., Agar, A., Rose, K. and Golzan, S.M., 2019. Assessment of spontaneous retinal venous pulsations in glaucoma patients on medical treatment over two years. 8th World Glaucoma Congress, Melbourne, Australia.

Shariflou, S., Agar, A., Rose, K. and Golzan, S.M., 2019. The accuracy of spontaneous venous pulsation assessment in discriminating glaucoma from glaucoma suspects. ARVO, The Association for Research in Vision and Ophthalmology Conference, Vancouver, Canada.

Shariflou, S., Agar, A., Rose, K. and Golzan, S.M., 2018. Spontaneous venous pulsations assessed using a novel tablet-based ophthalmoscope are associated with retinal ganglion cell counts in glaucoma and glaucoma suspects. The Royal Australian and New Zealand College of Ophthalmologists (RANZCO); 50th Annual Scientific Congress, Adelaide, Australia.

Shariflou, S., Agar, A., Rose, K. and Golzan, S.M., 2018. Dynamic retinal vascular assessment: An innovative approach for early glaucoma screening. Orthoptic Association of Australia; 75th Annual Scientific Conference, Adelaide, Australia

Shariflou, S., Agar, A., Rose, K. and Golzan, S.M., 2018. Amplitudes of spontaneous venous pulsations are associated with retinal ganglion cell count estimates in glaucoma. ARVO, The Association for Research in Vision and Ophthalmology Conference, Honolulu, Hawaii.

Shariflou, S., Agar, A., Rose, K. and Golzan, S.M., 2017. Quantifying spontaneous retinal venous pulsations using a novel tablet-based ophthalmoscope. RANZCO Cossom Scientific Meeting, Sydney, Australia.

Shariflou, S., Agar, A., Rose, K. and Golzan, S.M., 2017. Quantifying spontaneous retinal venous pulsations using a novel tablet-based ophthalmoscope. Orthoptic Association of Australia; 74rd Annual Scientific Conference, Perth, Australia.

Awards:

This thesis was supported by the National Health & Medical Research Council Postgraduate Scholarship.

Ophthalmic Research Institute of Australia (ORIA) Star awarded at the RANZCO 50th Annual Scientific Congress, Adelaide, Australia (2018).

ARVO hot topics highlight at The Association for Research in Vision and Ophthalmology Conference, Honolulu, Hawaii (2018).

Best research presentation awarded at the RANZCO Cossom Scientific Meeting, Sydney, Australia (2017).

List of figures

Figure 1. Schematic cross-section of eye. Digitally drawn by author; image adapted from Snell, R.S. and Lemp, M.A. (2013). ¹	3
Figure 2. Retinal cells within the 10 retinal layers. Digitally drawn by author; image adapted from Remington and Goodwin (2011). ³	4
Figure 3. Characteristic RNFL pattern. Digitally drawn by author; image adapted from Remington (2011) ³ [Original image from Harrington (1965)]. ⁶	6
Figure 4. Schematic of the course of the optic nerve. Digitally drawn by author; image adapted from Yanoff and Duker (2004). ¹⁰	7
Figure 5. Schematic of the venous drainage of the eye. Digitally drawn by author; image adapted from Browning (2012). ²⁴	11
Figure 6. Anatomy of the anterior chamber angle and aqueous humour pathway. Digitally drawn by author; image adapted from Vaajanen and Vapaatalo (2011). ³⁶	13
Figure 7. Age specific prevalence of OAG across six ethnic groups. Figure taken with .permission from Quigley and Broman (2006). ³⁹	15
Figure 8. Simplified schematic of glaucoma continuum. Adapted from Weinreb et al 2004. ¹⁰⁰	20
Figure 9. (a) Sample fundus photograph of the optic nerve and surrounding retina. (b) Glaucomatous indicators highlighted: RNFL detect outline demarcated by yellow arrows; peripapillary atrophy highlighted in green; limits of optic cup and disc outlined in white. Image taken with permission from Joshi et al (2012). ¹²⁸	24
Figure 10. Cirrus HD-OCT ONH and RNFL OU Analysis (Optic Disc Cube 200x200) sample results.	29
Figure 11. Standard RNFL Single Exam Report OU sample results.....	33

Figure 12. GMPE algorithm RNFL Single Exam Report OU sample results. 34

Figure 13. Sample HFA Single Field Analysis results for a right eye. 39

Figure 14. A rat retina showing individual RGC apoptosis at each white spot (fluorescing spots) using DARC Technology. Image taken with permission from Crodeiro et al (2011).¹⁵³ 41

Figure 15. Optic nerve head vessel density map showing declining vessel density with increasing glaucoma severity and visual field loss. Image taken with permission from Yarmohammadi and colleagues (2016).²⁰⁵ 46

Figure 16. Schematic of SVPs in relation to IOP and ICP. Arrows on the left side correspond to relative increase or decrease of IOP to that of ICP (arrows in the grey area). 51

Figure 17. Mathematical model illustrating flattening of the retinal vein from round (**a**) to flat or ribbon shaped (**d**) along the z-axis at higher external chamber pressures. Image taken with permission from Heil (1997).²⁷¹ 55

Figure 18. Flow diagram of data collected and used in each chapter of this thesis. 64

Figure 19. Schematic of image enhancement process using Image J. Image taken from Chapter 3. 66

Figure 20. Magnified frames from an SVP video (left eye) from a 68 year-old female captured using a 20D tablet-based ophthalmoscope. Left image is a magnified original frame. The right image is the green channel of the same frame with CLAHE application. 73

Figure 21. Schematic of image enhancement process using Image J..... 74

Figure 22. *Left images:* Two magnified, cropped and enhanced frames from the same eye at 7 frames apart (approximately 0.25 seconds). The yellow arrow points to the vessel location at maximum venous collapse and the red arrow points to the vessel

location at maximum venous dilation. *Right image*: Corresponding SVP trace with yellow and red arrows indicating resultant troughs and peaks. 75

Figure 23. Correlation between SVP amplitude and RNFL thickness ($p=0.006$, $r=0.49$). 77

Figure 24. Distribution of SVPs in NTG (n=37), POAG (n=64) and glaucoma suspects (n=63).
..... 88

Figure 25. The association between SVP amplitudes and age in each of the three groups.
..... 88

Figure 26. SVP amplitude in females and males across the three groups (* $p<0.05$). 89

Figure 27. ROC curve of various markers in differentiating between POAG and glaucoma suspects. 114

Figure 28. ROC curve of various markers in differentiating between NTG and POAG. 114

Figure 29. Changes in SVP amplitude across three visits in the subset of patients who had three visits (glaucoma n=10; glaucoma suspects n=5). 125

Figure 30. SVP changes relative to the baseline visit in glaucoma suspects (A, B n=5), and POAG (C, D, n=10). A significant difference in slopes between A and B was observed ($p=0.01$). 127

List of tables

Table 1. Summary of static vascular changes in glaucoma	43
Table 2. Patient Demographics and mean values.....	76
Table 3. Comparison of SVP detection devices.....	79
Table 4. Summary of total average findings across clinic sites.	87
Table 5. Patient demographics and means.....	99
Table 6. Associations between SVP amplitudes and individual parameters in NTG.....	100
Table 7. Associations between SVP amplitudes and individual parameters in POAG.	101
Table 8. Association between SVP amplitudes and individual parameters in glaucoma suspects.	103
Table 9. Patient demographics and mean outputs.....	113
Table 10. AUROC for both ROC curves (POAG vs glaucoma suspects and NTG vs POAG).	115
Table 11. Pairwise comparison of AUROC.	116
Table 12. Number of glaucoma (and glaucoma suspect) patients assessed at each visit. ..	124
Table 13. Mean values for all measured parameter over two visits in patients with glaucoma and glaucoma suspects.....	126

Glossary of Abbreviations

Abbreviation	Full term
%	Percentage
%Δ	Percentage change
μm	Micrometre
ACA	Anterior ciliary artery
ACG	Angle-closure glaucoma
AI	Artificial intelligence
ANCOVA	Analysis of covariance
ANOVA	Analysis of variance
ART	Automatic real-time
AUD	Australian dollar
AUROC	Area under the receiver operating characteristic curve
CA	California
CD	Cup to disc
CFEH	Centre for Eye Health
CLAHE	Contrast Equalization plugin
CNS	Central nervous system
CRA	Central retinal artery
CRAE	Central retinal artery equivalent
CRV	Central retinal vein
CRVE	Central retinal vein equivalent
CSFp	Cerebrospinal fluid pressure
D	Dioptres

DARC	Detection of Apoptosing Retinal Cells
dB	Decibels
DCPx	Deep capillary plexus
DVA	Dynamic Vessel Analyzer
FAZ	Foveal avascular zone
FNR	False negative rate
FPR	False positive rates
fps	Frames per second
GHT	Glaucoma hemifield test
GMPE	Glaucoma Module Premium Edition
HFA	Humphery Visual Field Analyser
HR	High resolution
HS	High speed
HTG	High-tension glaucoma
ICA	Internal carotid artery
ICP	Intracranial pressure
ICPx	Intermediate capillary plexus
IOP	Intraocular pressure
iOS	iPhone operating system
IR	Infrared reflectance
LDF	Laser Doppler Flowmetry
LGN	Lateral geniculate nucleus
LPCA	Long posterior ciliary artery
LSF	Laser Speckle Flowgraphy
MD	Mean deviation

MES	Marsden Eye Specialists
MGC	M ganglion cell
mmHg	Millimetre of mercury
mPPG	Modified photoplethysmography
NIH	National Institutes of Health
NTG	Normal tension glaucoma
OAG	Open-angle glaucoma
OCT	Optical coherence tomography
OCT-A	Optical coherence tomography-angiogram
OD	Optic disc
P1G cell	P1 midget ganglion cell
PACG	Primary angle-closure glaucoma
PCA	Posterior ciliary artery
PDP	Pattern deviation plot
POAG	Primary open-angle glaucoma
PPG	Photoplethysmography
PSD	Pattern standard deviation
r	Correlation coefficient
RGC	Retinal ganglion cell
RNFL	Retinal nerve fibre layer
RPCP	Radial peripapillary capillary plexus
RVBA	Retinal vascular bifurcation angle
RVP	Retinal venous pressure
SAP	Standard automated perimetry
SPCA	Short posterior ciliary artery

SVP	Spontaneous retinal venous pulsation
TD	Total deviation
UNSW	University of New South Wales
USA	United States of America
UTS	University of Technology Sydney
V-CDR	Vertical cup to disc ratio
VF	Visual field
VFA	Visual field analysis
VFI	Visual field index

Chapter 1

Review of the literature: Glaucoma and Spontaneous Retinal Venous Pulsations

Chapter Summary

Background information about glaucoma and its pathophysiology are covered in this chapter, as well as an in-depth insight into the vascular features of glaucoma with a focus on dynamic vascular changes.

1. Anatomy and blood supply of the eye

1.1 Overview of basic ocular anatomy

The human eye is a complex sense organ that uses information from the environment in the form of light rays and transforms them to neural signals in order to process and decipher our surroundings in the form of visual perception and sight. The eye is made of three layers:

1. Outer fibrous layer: this layer is composed of connective tissue that comprises the sclera and cornea.
2. Middle vascular layer: this layer is also referred to as the uvea, which include the iris, ciliary body and choroid.
3. Inner neural layer: the retina.

These three layers create the globe-shaped appearance of the eye, as seen in Figure 1, and can be described in two segments: the anterior chamber and posterior chamber. The anterior chamber of the eye is bound anteriorly by the cornea and posteriorly by the anterior surface of the iris and crystalline lens. This chamber is filled with aqueous humour. The posterior chamber is a vitreous-filled cavity lined anteriorly by the posterior surface of the iris. The vitreous humour surrounds the equator of the crystalline lens and fills the space between the crystalline lens and the inner retinal layer. At the posterior pole of the eye lies the optic nerve, which emerges from a meshwork-like structure called the lamina cribrosa. The most anterior portion of the optic nerve is visible in the retina and is called the optic nerve head, or optic disc.

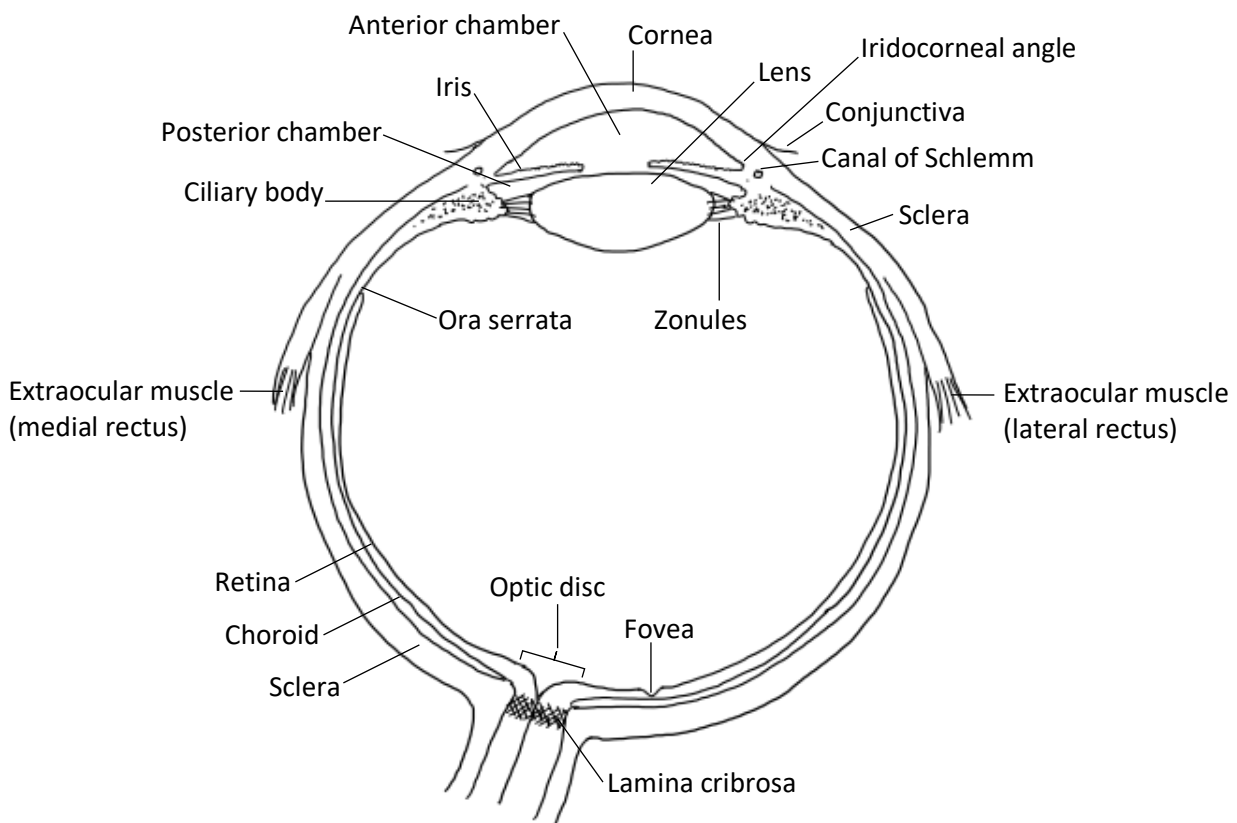


Figure 1. Schematic cross-section of eye. Digitally drawn by author; image adapted from Snell, R.S. and Lemp, M.A. (2013).¹

Each of these structures play a specific role in the transformation of light into chemical signals for transmission to the brain for visual perception. The cornea, crystalline lens and tear film are responsible for the refraction of light so that it focuses on the retina. The ciliary muscle contracts and relaxes to change the curvature of the crystalline lens to adjust the refractive power and therefore the distance that light will focus within the eye. The ciliary body produces aqueous humour that is excreted into the posterior chamber. The iris is a circular structure consisting of two muscles with a central aperture called the pupil. The iris muscles contract and dilate according to different levels of light intensity and in response to various stimuli to control the amount of light entering the eye.

The retina consists of 10 layers (Figure 2) – the outermost layer being the retinal pigment epithelium followed by the photoreceptor layer, external limiting membrane, outer nuclear layer, outer plexiform layer, inner nuclear layer, inner plexiform layer, retinal ganglion cell (RGC) layer, retinal nerve fibre layer (RNFL) and the internal limiting membrane being the

innermost layer that is in direct contact with the vitreous humour. The photoreceptors convert light into neuronal signals. These are passed to the retinal bipolar cells and then to the RGCs, whose axons are then sent to the brain along the optic nerve and visual pathway. The fovea is a small depression on the macular portion of the retina and is the site of densely arranged photoreceptors of high spatial frequency that enable sharp resolution of images and colour vision. The retina is thinnest posteriorly at the fovea, and at the anterior edge of the retina, called the ora serrata (Figure 1).²

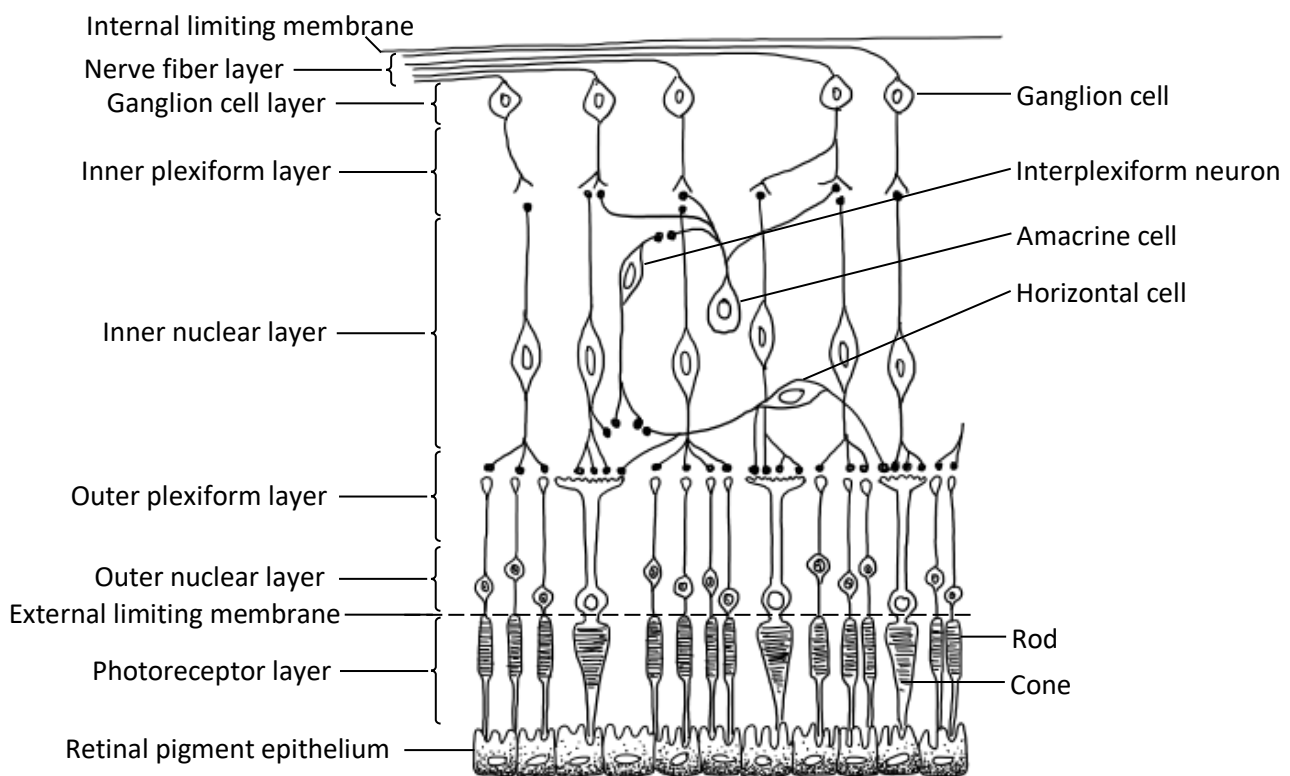


Figure 2. Retinal cells within the 10 retinal layers. Digitally drawn by author; image adapted from Remington and Goodwin (2011).³

Each RGC has a single axon that travels parallel to the inner surface of the retina, along the nerve fibre layer, towards the optic nerve. The axons all come together to form the optic disc. Each axon then passes through the lamina cribrosa and exit the eye cumulatively as the optic nerve. The retina and optic nerve are also considered as an extension of the central nervous system (CNS).

1.2 RGCs in the retina

The RGC cell bodies are housed in the ganglion cell layer of the retina (Figure 2), which is generally a single cell thick except around the macula and temporal optic disc. At the macula the RGC layer can be up to 8-10 cells thick and 2 cells thick at the temporal disc. Where the RGCs approach the ora serrata, their numbers diminish. Each ganglion cell is separated by its neighbouring RGC by the glial processes of Müller cells.³ The RGC axons run towards the optic nerve in various axonal bundles, parallel to the retinal surface and form the RNFL.

The characteristic patterns in the RNFL, as seen in Figure 4 are due to orientation that the RGC axons follow to the optic nerve. The group of fibers (RGC axons) that travel from the macular area to the optic nerve is called the papillomacular bundle. Axons that arch around the macular area to travel to the optic nerve form characteristic arcuate patterns named the superior and inferior temporal fibers that are separated along the horizontal retinal raphe. The superior and inferior nasal axons that travel directly to the optic nerve are referred to as radiating axons.⁴ All of the axons come together at the optic disc to create a specific orientation. The nasal axons create the nasal portion of the optic disc and the papillomacular bundle creates the temporal portion of the optic disc. Fibers from the superior temporal arch travel over the papillomacular bundle to create the superior pole of the optic disc and inferior temporal fibers travel below the papillomacular bundle to create the inferior pole of the optic disc.³⁻⁵ While the macular fibers encompass only about 5% of the retinal area, they create approximately 33% of the optic disc.³

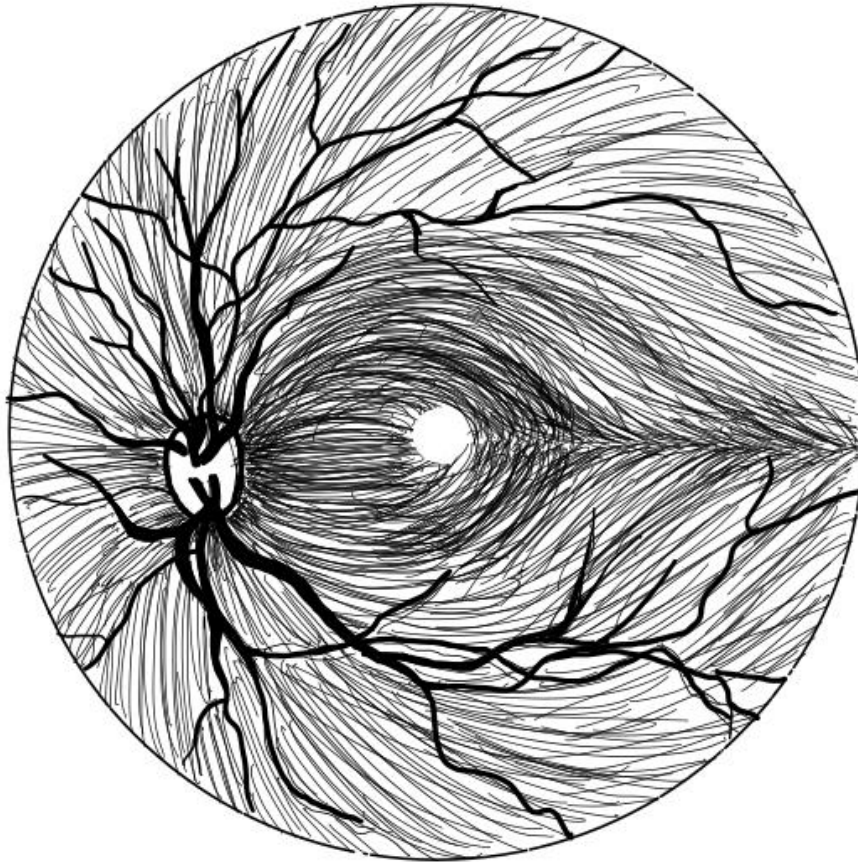


Figure 3. Characteristic RNFL pattern. Digitally drawn by author; image adapted from Remington (2011)³ [Original image from Harrington (1965)].⁶

At the optic disc, the RGC axons turn at a right angle and exit the eye through the lamina cribrosa as the optic nerve. The RNFL is thickest at the optic disc margins where all of the RGC axons accumulate.³

Clinically, a measure of local retinal ganglion cell layer thickness is possible using optical coherence tomography (OCT) over the macular area where RGC somas are multiple layers and create the thickest region of the ganglion cell layer.^{7,8} Moreover, the regular RGC axon orientation in the RNFL is reflective of specific patterns of visual field loss assessed using standard automated perimetry (SAP) in conditions affecting the RGCs and their axons (RNFL), as seen in glaucoma.³

1.3 RGCs at the optic nerve and beyond the eye

The optic nerve totals 5-6cm in length and is made of four segments (

Figure 4).³

1. Intraocular portion (0.7-1mm)

This is the point where the RGC axons join at the optic disc (also referred to as the optic nerve head) where they collectively pass through approximately 300 fenestrations at the lamina cribrosa and are redirected posteriorly.⁹

2. Intraorbital portion (25-30mm)

3. Intracanalicular (6-10mm)

4. Intracranial (10-16mm)

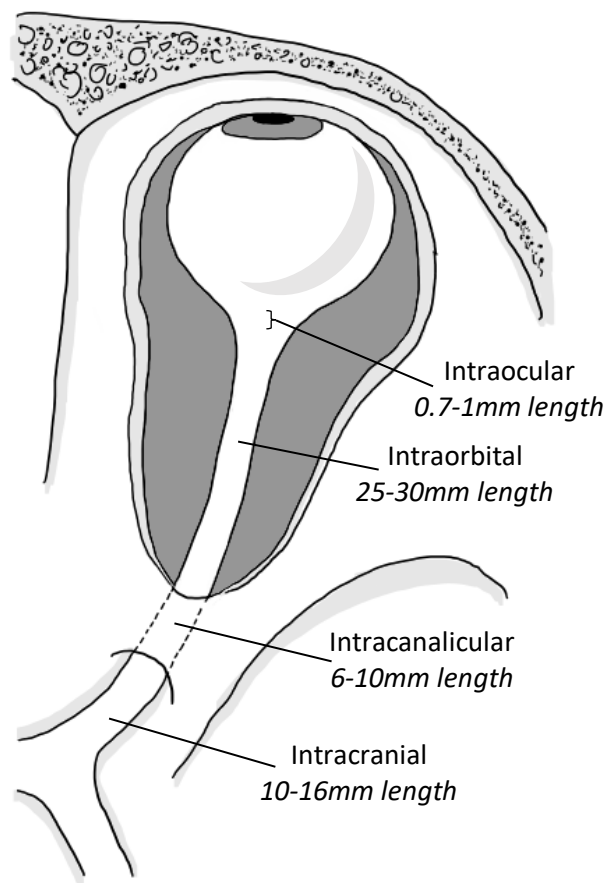


Figure 4. Schematic of the course of the optic nerve. Digitally drawn by author; image adapted from Yanoff and Duker (2004).¹⁰

Approximately 90% of RGCs will terminate at the Lateral geniculate nucleus (LGN), while the remaining 10% of axons project to areas controlling pupillary responses and circadian rhythms.³

The functionality of RGCs have been extensively studied in animal models, primarily cat, where they have been classified according to their responses to light.¹¹ Additionally, some RGCs have been found to respond to motion, orientation, contrast and colour, as well as having variations in their centre and surround configuration (ON and OFF RGC). Comparison of anatomical features of RGC and their function has shown substantial correlation, with small-field beta RGC correlating to brisk-sustained or X-RGCs, and large-field alpha RGCs with brisk-transient or Y-RGCs. In humans, RGCs at the fovea are almost exclusive of the sub-types known as ON – midget, OFF – midget and ON – parasol, OFF – parasol cells,¹² though a variety of other, less common, subtypes have been more recently described.¹³

Once at the LGN, the RGCs are further classified by the LGN layer that they terminate at. There are two classifications at this level: P cells that terminate at the parvocellular layer and M cells that terminate at the magnocellular layer. Each type of cell increases in size as its proximity from the fovea increases. The most common type of P cell is the P1 midget ganglion cell (P1G cell). The P1G cells have two subcategories depending on the arrangement of its dendritic branching.¹⁴ Some P1G cells are connected to only one midget bipolar cell that may be linked to a single cone receptor in order to process high-contrast detail and colour resolution, most commonly seen at the fovea.¹⁵ Alternatively, other P1G cells receive input from two midget bipolar cells, facilitating a convergent pathway.³ The P2 ganglion cells differ from the P1G cells in that they have densely branched and compact dendritic trees that spread horizontally.¹⁴

The M ganglion cells (MGCs; also referred to as parasol ganglion cells) are larger in size compared to the P cells and project to the magnocellular layers of the LGN. MGCs have thicker dendrites with spiny features that enlarge from the central to peripheral retina.¹⁴ These cells are responsible for detecting the orientation of objects in space.³

1.4 Overview of basic ocular vasculature

The ocular blood circulation system has intricacies allowing for varied amounts of blood supply to different structures within the eye. However, some structures, including the lens and cornea must remain avascular to maintain optical transparency. In contrast, the choroid is extremely rich in its blood supply. These variations in blood supply allow optimal visual function.

1.4.1 Arterial supply to the retina

Blood to the eye is supplied primarily through the first branch of the internal carotid artery (ICA) known as the ophthalmic artery. This blood vessel enters the optic canal and runs along the optic nerve where it branches off into various vessels that supply different portions of the eye. One of these branches, the central retinal artery (CRA), at about 10-20mm posterior to the globe, pierces the optic nerve. Once within the central portion of the optic nerve, the CRA extends anteriorly towards the sclera.^{16,17} Here, the CRA pierces through the fenestrated lamina cribrosa, into the eye, where it bifurcates and then forms further branches that supply the retina.¹⁷ There are four major arterioles that each supply one quadrant of the retina. Retinal arterioles and venules lie within the superficial RNFL, while retinal capillaries lie parallel to the surface of the retina and are more concentrated towards and around the optic nerve than the peripheral retina.⁷

There are up to four retinal vascular networks throughout the retinal thickness. In some eyes, there is a superficial network of fine capillaries in the peripapillary region known as the radial peripapillary capillary plexus (RPCP). The RPCP are uniquely organised as they run parallel to the RNFL axons, compared to the three other vascular plexuses that display a lobular configuration.^{2,18} The superficial vascular plexus is the most superficial of the remaining three vascular plexuses. It is composed of larger arteries, arterioles, capillaries, venules, and veins in the RGC layer. Above and below the inner nuclear layer, are the two deeper networks referred to as the intermediate capillary plexus (ICPx) and deep capillary plexus (DCPx). These two plexuses are supplied by vertical anastomoses from the superficial vascular plexus. These networks are spread throughout the retina and are segmented differently depending on the portion of the retina that is being supplied. Peripherally, the

superficial and deep vascular plexuses are the only two distinguishable layers. At the macula, both of these layers are distinguishable, however the deep vascular plexus can be further separated into the ICPx and DCPx. At the peripapillary region, the superficial vascular plexus can be distinguished from the RPCP. At the fovea there is an avascular zone termed the foveal avascular zone (FAZ) that has its border defined by a single capillary loop. Similar to the FAZ, 1.5mm around the posterior retinal edge and areas of the retina that are adjacent to major retinal arteries (and/or veins) are avascular.¹⁸

Other structures of the eye are supplied by other branches from the ophthalmic artery, such as the anterior ciliary arteries (ACA), medial and lateral posterior ciliary artery (PCA) that each divide into one long (LPCA) and seven to ten short posterior ciliary arteries (SPCAs) prior to their insertion through the sclera.¹⁷ The choroid supplies the outer retina. The SPCAs supply the posterior and peripapillary portion of the choroid while, the LPCAs supply the anterior portion of the choroid. The ACAs also branch from the ophthalmic artery that travel to the anterior of the eye along the tendons of the recti muscles. The ACAs supply the recti muscles, conjunctiva, sclera, iris and ciliary body.^{17,19}

1.4.2 Venous drainage of the retina

Venous drainage of the eye occurs primarily through the retinal veins and vortex veins, as seen in Figure 5. Similar to the CRA branches, the retinal venules form hemiveins that eventually join to form the central retinal vein (CRV). The CRV exits the eye through the lamina cribrosa and travels alongside the CRA in the optic nerve and pierces the optic nerve alongside the CRA where it exits into the optic nerve subarachnoid space.¹⁷ This space is one of two pressure compartments that the CRV is exposed to. Posterior to the lamina cribrosa, the CRV is subjected to the pressure within the optic nerve subarachnoid space in the form of cerebrospinal fluid pressure (CSFp). Anterior to the lamina cribrosa, at the optic disc (and retina), the CRV is subjected to the pressure directly from the vitreous humour in the form of intraocular pressure (IOP).^{20,21} The CRV usually drains into the superior ophthalmic vein, however can sometimes directly drain into the cavernous sinus. All venous blood from the eye drains into either the superior or inferior ophthalmic veins that both drain directly into the cavernous sinus.^{17,22,23}

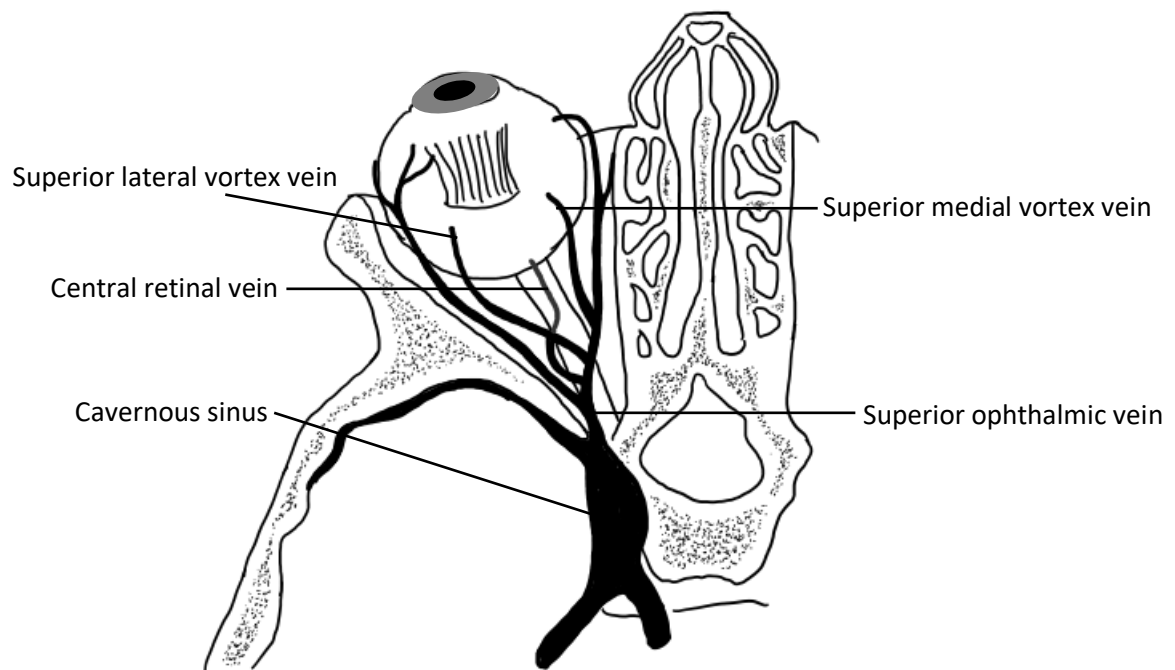


Figure 5. Schematic of the venous drainage of the eye. Digitally drawn by author; image adapted from Browning (2012).²⁴

2. Overview of Glaucoma

2.1 Definition of glaucoma

Glaucoma is a leading cause of irreversible blindness worldwide.²⁵⁻²⁷ The current definition used in epidemiological studies dates from 1998.²⁸ Glaucoma describes a class of optic neuropathies characterised by specific structural changes at the optic disc and/or RNFL, as well as functional changes detected by visual field testing.²⁹ While raised IOP was previously a defining characteristic of glaucoma, it is now only recognised as an important risk factor²⁹ and as the primary modifiable risk factor for glaucoma progression, as progression is said to stop if IOP is lowered by up to 30-50% from the baseline IOP.³⁰ The differences between the types of glaucoma lie in their cause and risk factors, demographics, symptoms, treatment and prognosis. However, a shared characteristic is that progressive structural and functional changes can lead to a gradual permanent loss of vision if undiagnosed and unmanaged. These changes are all related to progressive pathological degeneration of RGC somas and axons leading to thinning of the RNFL and cupping of the optic disc.³⁰⁻³³

The optic nerve, although named as a “nerve”, is in fact a CNS white matter tract. As seen in other parts of the CNS, the optic nerve is surrounded by meninges and is contained within the blood-brain barrier.³⁴ As with all neurons of the CNS, once RGC death occurs, they cannot regenerate. Therefore, glaucoma can be classified as a neurodegenerative disease which ultimately causes deficits in neuronal function, similar to other neurodegenerative conditions such as Alzheimer’s disease.³⁵

The morphology of the anterior chamber of the eye can determine the classification of glaucoma being open-angle glaucoma (OAG) or angle-closure glaucoma (ACG). The anterior chamber is home to Schlemm’s canal that runs the circumference of the anterior chamber angle, which is at the junction of the peripheral cornea and peripheral iris. The trabecular meshwork and Schlemm’s canal (canal of Schlemm) are the first structures in the pathway of aqueous humour drainage and each play an important role in the regulation of IOP, as seen in Figure 6. In OAG, there is unobstructed access from the anterior chamber to the trabecular meshwork and Schlemm’s canal. In contrast, in ACG the trabecular meshwork is

obstructed by the peripheral iris that is in contact with the trabecular meshwork and peripheral cornea, therefore blocking aqueous humour from the drainage system.³⁰

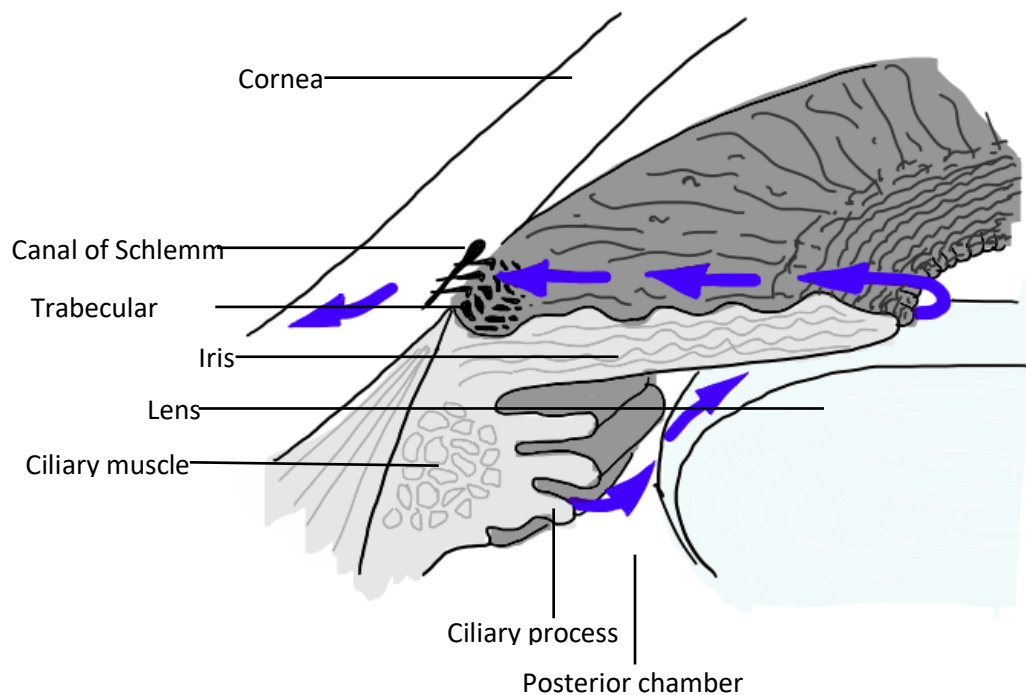


Figure 6. Anatomy of the anterior chamber angle and aqueous humour pathway. Digitally drawn by author; image adapted from Vaajanen and Vapaatalo (2011).³⁶

As one of the most important risk factors for glaucoma, IOP can be in many instances increased, but can also be within the normal range. The normal range of IOP in healthy adults is 10-21mmHg and if found alongside glaucomatous signs, the condition is termed “normal tension” glaucoma (NTG).^{30,37} Rise in IOP, if present, is often asymptomatic, therefore chronic glaucoma can progress unnoticed by the patient until significant changes to vision such as severe reduction in peripheral vision or loss of central vision and significant reduction of visual function occurs.³⁰ Hence, early detection is essential in glaucoma patients. Individuals who have glaucomatous risk factors are termed as “glaucoma suspects” and are monitored regularly in order to detect the disease before subjective symptoms develop. Ocular hypertension is elevated IOP in the absence of glaucomatous damage and is a leading risk factor for the development of OAG.³⁸

2.2 Epidemiology of glaucoma

2.2.1 Prevalence of glaucoma across the globe

An estimated 79.6 million people are currently affected by glaucoma across the globe, over 8.4 million of those being blinded by the disease. It is estimated that by 2040 the incidence of worldwide glaucoma will increase to over 111 million.^{25,39} In Tham et al (2014)'s meta-analysis, 50 population-based articles were included alongside data from the World Population Prospects of the United Nations to estimate the prevalence of glaucoma through to 2040.²⁵ The authors concluded an overall global prevalence of 3.54%, with OAG accounting for 3.05% and ACG accounting the remaining 0.5% in the year 2013.²⁵

2.2.2 Risk factors for the development and progression of glaucoma

Age

One of the main risk factors for the development and progression of glaucoma is older age,^{25,40-42} with the odds ratio of OAG prevalence increasing 1.73 with each decade beyond the age of 40.²⁵ Quigley and Broman's (2006) review compiled data from population based studies and constructed age specific prevalence models as seen in Figure 7. Their results also demonstrate increased prevalence of glaucoma with increasing age, mostly dramatically seen beyond the age of 50 (Figure 7).³⁹

Elevated IOP

Results of a randomised control trial demonstrated that IOP reduction has preservative effects on the visual field of patients with OAG.⁴³ Multiple studies have also demonstrated elevated IOP as a risk factor for development and progression of glaucoma.⁴⁴⁻⁴⁷ Elevated IOP throughout the globe and is said to cause stretching of the retina, RGCs and their axons and the optic nerve head (disc). This stretching can damage these cells, leading to glaucomatous changes. Moderate elevations in IOP produce strain that is concentrated at the optic nerve head and its surrounds, with gradual damage and remodelling of the lamina cribrosa, peripapillary connective tissue and vascular processes within the region.⁴⁸

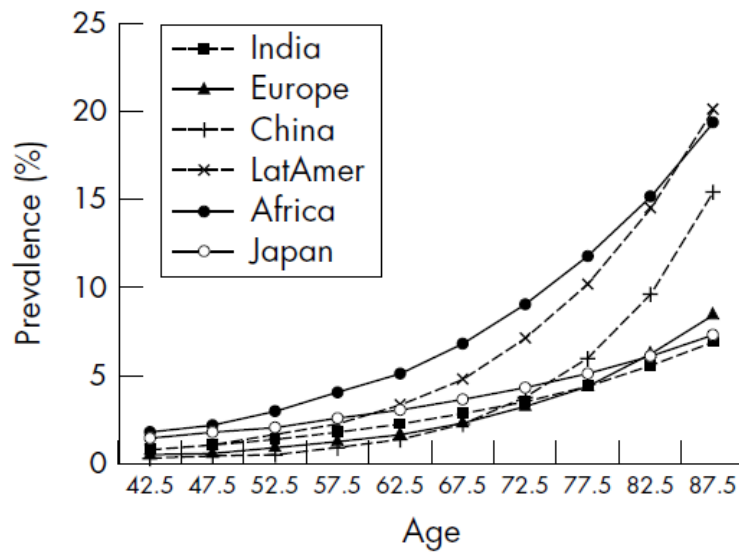


Figure 7. Age specific prevalence of OAG across six ethnic groups. Figure taken with permission from Quigley and Broman (2006).³⁹

Gender

Although there is inconsistency in the reported prevalence and gender predilection of OAG in various studies, there are two large meta-analyses of population-based glaucoma studies that have revealed a greater prevalence of glaucoma in women. Over half (59.1%) of glaucoma cases have been reported as women, as well as 55.4% of all OAG and 69.5% of all ACG cases. This is greater than the estimated 51.5% of the global population of women over the age of 40 at that time period (2010).³⁹ Another two meta-analyses also reported higher prevalence of OAG in women than men.^{25,49} However, this is contrasted by work by Rudnicka et al (2006) who combined two meta-analyses and found that men were at a higher risk for OAG than women.⁴¹ Although there are inconsistencies in studies reporting gender predilections of OAG, the higher overall prevalence in women has been attributed to their longer lives which increases their risk for glaucoma.⁴¹ Anatomical predisposition has also been reported as a factor that puts females at a higher risk of ACG.^{39,50,51} Further, it has been postulated that the overall higher risk of glaucoma in females is attributed to fluctuations in sex hormones that may have influences in the circulation at the optic nerve head as well as influences on IOP.⁵²

Ethnic background

There are clear links between ethnic background and glaucoma with a number of prevalence studies conducted in various racial groups. There is a general consensus among these studies that the highest prevalence of OAG is in people of African descent,^{25,29,39} however the prevalence of ACG is a matter of debate.

A summary of 27 glaucoma prevalence study reports have been compiled and presented in Cook and Foster's (2012) work.²⁹ They report greater OAG in people of African descent than those with European or Asian ethnicity. The prevalence of OAG in African Americans in the United States of America is five times higher than European Americans, with the greatest prevalence of OAG in African populations in the Caribbean (8.8%).²⁹ Similarly, Tham and colleagues (2014) reported OAG to have the highest prevalence in Africa.²⁵ People of African descent were reported as having the highest prevalence of glaucoma (6.11%) and OAG (5.40%). After adjusting for age and gender, the authors found that the odds ratio of OAG in people living in Africa was 2.39 compared to those in Asia.²⁵ The authors also adjusted for habitation type, response rate and year of study conducted and found that in fact the odds ratio of OAG in African descendants is lower (2.05) when compared to Asian descendants (2.80) when compared to European descendants.²⁵ Quigley and colleagues (2006) reported people of African descent having the highest prevalence of OAG. However, they noted that in older age groups people from Chinese regions and Latin America had a prevalence that approached that of the people of African descent. They reported lower (and similar) prevalence of OAG in people of Indian, European and Japanese descent.³⁹

ACG has been reported to be more prevalent in people of Asian ethnicity compared to those of African or European descent.^{25,29,39,53,54} In Tham and colleagues (2014) work, people of Asian descent were found to have the highest prevalence of ACG (1.20%).²⁵ Moreover, Quigley and colleagues (2006) reported the highest prevalence of ACG in people of Chinese descent, followed by those of Japanese descent.³⁹ In contrast, other studies have stated that the prevalence of OAG in East Asian populations is higher than that of ACG,^{55,56} except for people of Mongolian and Burmese descent who are more affected by ACG.^{57,58} Quigley and Broman's (2006) study found that people of Indian and European descent had the lowest

(and similar) prevalence of ACG, although they have not reported ACG prevalence in African populations.³⁹

Myopia

High myopia greater than 8.00 dioptres is a strong risk factor for the development and progression of glaucoma.⁵⁹⁻⁶² Myopia greater than 4.00 dioptres has also been shown to have higher prevalence of OAG.⁶³ It is thought that the increased axial length in myopic eyes may contribute to a stretching of the optic disc making it more susceptible to glaucomatous changes.^{64,65} Secondary stretching and thinning of the lamina cribrosa, in association with increased axial length, causing stretching of the peripapillary tissue, may also increase glaucoma susceptibility. Yet another theory is that the pull of the peripapillary sclera by the optic nerve dura mater during eye movements increases the stress and strain on the lamina cribrosa.⁶⁶ However, the detection of glaucomatous optic neuropathy can be difficult in highly myopic eyes due to the myopia related changes in appearance of the optic nerve head. While this is a topic of debate, high myopic changes in the eye including optic disc (OD) tilting, large ovalness index, OD deformation, OD palor, large cup to disc ratio, peripapillary crescent in myopia have been reported to hinder accurate glaucoma diagnosis.^{67,68} Moreover, the ability to distinguish high myopia related RNFL thinning from glaucomatous thinning is reduced,⁶⁹ and RGC count has been suggested a better parameter for clinical diagnosis of glaucoma in highly myopic patients.⁷⁰

Family history

Positive family history of glaucoma is a well-known risk factor for the development of glaucoma and there have been several genes associated with OAG.^{30,71-76} Thus far, there have been eight genetic loci that show strong associations with OAG.^{77,78} Moreover, there have also been genes linked specifically to childhood glaucoma, glaucoma in young adults as well as pseudoexfoliative glaucoma.^{71,72,79} A first-degree relative with glaucoma increases a patient's risk of developing POAG. Siblings of affected individuals have about an eight times increase in risk of developing POAG and a five times increased risk of developing ACG compared to individuals with unaffected siblings.³⁰

Central corneal thickness

Thin central corneal thickness has been reported as a risk factor for glaucoma, due to the falsely low IOP measurements associated with thin corneas.^{40,80} Although there is no confirmed association between corneal thickness and lamina cribrosa thickness,⁸¹ there has been some speculation that thin corneas may have an association with a thin lamina cribrosa.⁸¹⁻⁸³

2.3 Quality of life with glaucoma

In 2010 it was estimated that overall a total of 8.4 million people were blind from glaucoma, with 4.5 million people blind due to OAG and the remaining 3.9 million due to ACG. Since 2010, it has been estimated that there has been an increase of 1.4 million in each category, equating to a rise of 2.8 million people blinded, bringing the total number of people with blindness due to glaucoma in 2020 to 11.2 million people.³⁹

However, blindness is not the only factor that affects quality of life. An individual's perception of their health (physical, psychological and social), comfort and happiness in context of their life goals, standards and values are what define quality of life. The diagnosis of chronic, irreversible and potentially blinding disease can induce significant anxiety in an individual thereby adversely affecting an individual's sense of well-being and significantly reducing their quality of life.⁸⁴ Loss of peripheral vision in glaucoma can affect walking, driving, reading and scotopic vision.^{85,86} Individuals with glaucoma have reported mobility through driving and walking outside as two of the most important tasks of daily living.^{87,88} Near and central vision tasks such as reading have been reported as the most valued visual function in individuals with glaucoma.⁸⁹ All of these have been reported to be reduced in individuals with glaucoma, particularly those with more advanced glaucoma.⁸⁴ Decline in these functions may lead to an individual's loss of independence and increased dependence on assistive aids and/or carers, reducing mental health and quality of life.⁸⁴

Many studies have investigated the relationship between glaucoma and psychological disorders such as anxiety and depression. Loss or an individual's perception of loss of visual function, particularly limitations in driving^{90,91} and fear of falling^{92,93} have been associated with depression in glaucoma. Anxiety and depression were significantly higher in

participants with glaucoma ($p=0.030$ and $p=0.026$ respectively) in a case-control study conducted by Mabuchi and colleagues (2008). The authors reported a 13% and 10.9%, prevalence of anxiety and depression respectively in their cohort of over 230 individuals with glaucoma. These values were both almost double the prevalence in the age-matched control group without glaucoma.⁹⁴

As well as psychological disorders, glaucoma has also been linked to neurocognitive decline. Glaucomatous degeneration affects the whole visual pathway, including degeneration of the LGN and decreased metabolic activity and thinning of the visual cortex.⁹⁵ Magnetic Resonance Imaging has shown a correlation between the amount of damage at the LGN and the progression of glaucoma.⁹⁶ The optic tract and optic radiations have also been found to be damaged proportionate to the amount of structural and functional damage that has occurred in the eye.⁹⁷ It has also been reported that there is a greater risk of individuals with glaucoma developing dementia, particularly Alzheimer's disease.^{98,99}

Socioeconomic status has been found to influence the prognosis of glaucoma in the sense that studies have revealed that socioeconomic status affects the possibility of early detection of glaucoma as well as compliance to treatment.^{100,101}

3. Pathophysiology of glaucoma

3.1 Glaucoma as a disease continuum

Glaucoma has been described as a group of optic neuropathies that can be classified using a 3-stage disease continuum, gradually leading to permanent vision loss when undiagnosed and unmanaged (Figure 8).^{33,102} The cascade of glaucomatous vision loss is initiated by progressive loss of RGCs through apoptosis, and/or necrosis,¹⁰³ forming the basis of glaucomatous structural damage.

In stage one, RGC loss is not detectable using current technology,^{45,102,104-110} and there is no agreement on diagnosis criteria of early glaucomatous damage at this stage.¹⁰² Hence the disease continuum progresses until irreversible damage is sufficient for diagnosis.¹⁰² In stage two, RNFL loss and neuroretinal rim thinning is evident on fundus imaging. These RNFL changes are said to be the earliest observable defects in glaucoma.^{111,112} However, these changes are unable to be detected through functional testing such as visual field (VF) assessment and individuals with this level of glaucoma remain asymptomatic.^{45,106-110}

Therefore, irreversible damage and disease progression will have already ensued by the time glaucoma becomes symptomatic and can be definitively diagnosed. It is estimated that half of all glaucoma cases currently remain undiagnosed, even in well-resourced countries such as Australia.¹¹³ By stage three, visual dysfunction and blindness may develop due to increasing damage to the RGCs and their axons and therefore the optic nerve.¹⁰²

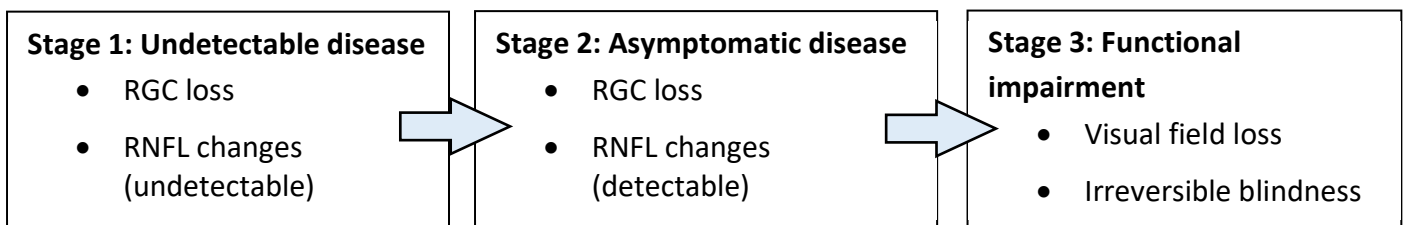


Figure 8. Simplified schematic of glaucoma continuum. Adapted from Weinreb et al 2004.¹⁰⁰

3.1.1 Alternative concepts in the structure-function relationship

While it is traditionally accepted that structural changes precede functional changes in glaucoma, there is evidence to suggest that in some patients these changes can present concurrently, and either structural or functional changes can present first in others.^{114,115}

This phenomenon may be explained by the concept of RGC dysfunction rather than RGC death. In the early stages of RGC damage, RGC dysfunction may precede cell death, leading to a reduction in VF sensitivity while structural measurements do not represent the functioning RGCs and axons. In such cases, functional deficits can exceed the reduction predicted from structural measures alone.¹¹⁶

Studies exploring the relative onset of structural and functional change in glaucoma have displayed conflicting results. Data from a large clinical trial has revealed that functional changes precede structural changes in as low as 35% percent of patients,⁴⁵ while other studies have reported functional changes to precede structural changes in up to 60-86% of patients.^{117,118} However, these results have been questioned as the identification of relative frequency and onset of these changes (structural vs functional) depend on the accuracy of the criteria to define that structural or functional change has taken place (specificity and sensitivity).¹¹⁵ The effect of this is demonstrated in a study of 198 patients with ocular hypertension who were followed over 7 years.¹¹⁹ When test specificity was set at 90%, functional deterioration alone was observed in approximately 20% of participants and 13% of participants demonstrated concurrent structural and functional deterioration. In the same study, when test specificity was increased to 97%, the frequency of functional changes occurring before structural changes dropped to 15% and the frequency of concurrent changes dropped to 4%.¹¹⁹

3.2 Clinical diagnosis of glaucoma

Glaucoma can be diagnosed on the basis of three categories of evidence found in cross-sectional studies:²⁸

Category 1 (structural and functional evidence): Vertical cup to disc ratio (V-CDR) or V-CDR asymmetry ≥ 97.5 th percentile of the normal population with the presence of definite glaucomatous visual field (VF) defect.

Category 2 (advanced structural damage with unproven VF loss): Significantly damaged optic disc (V-CDR ≥ 99.5 th percentile of the normal population) with a lack of reliable VF results.

Category 3 (optic disc not visible; VF test not possible): No view of the optic disc with the presence of:

- a) IOP readings > 99.5 th percentile of the normal population and visual acuity $< 3/60$.
- b) Visual acuity $< 3/60$ and evidence of glaucoma filtering surgery or previous medical history of glaucoma.

Note: Category 1 and 2 diagnoses can only be made in the absence of alternative CDR and VF explanations.

Further to these categories, as detailed in section 2.1, the morphology of the anterior chamber of the eye is what determines the classification of glaucoma as either OAG or ACG. In primary OAG (POAG), the anterior chamber is unremarkable and IOP can vary.³⁰ If IOP in POAG is within normal range, glaucoma is classified as NTG.^{30,37} Secondary OAG is when the cause of increased resistance to aqueous outflow through the trabecular meshwork and Schlemm's canal is due to a cause that is detectable on anterior segment examination, such as pigmentary glaucoma and pseudoexfoliative glaucoma.^{30,120,121}

Glaucoma is classified as primary ACG (PACG) if the forward bulging of the iris is due to a pressure difference between the anterior and posterior chambers, where there is higher pressure in the posterior chamber than the anterior chamber. This "push mechanism" causes iridocorneal contact that obstructs the aqueous drainage system. This pressure

difference can be caused by anatomical variations such as anterior lens vault (greater forward bulging of the anterior crystalline lens pole) and/or a larger contact area between the posterior iris and crystalline lens surface and/or abnormal insertion of the iris root on the ciliary body, all which lead to increased resistance of aqueous humour flow between the posterior iris and anterior crystalline lens.^{30,122,123} In secondary ACG, there is a physical “pull mechanism” where the iris is pulled forward to cause iridocorneal contact due to pathology such as iris neovascularisation and/or uveitis.³⁰

Congenital glaucoma is classified when the trabecular meshwork and/or Schlemm’s canal are underdeveloped, causing resistance to aqueous humour drainage.³⁰

3.2.1 RGCs in glaucoma

In its healthy state, the RNFL has uniform striations arising from the separation of highly reflective RGC axon bundles by non-reflective Müller cell glial septa, which appear as darker bands.¹²⁴ These striations are most visible at the vertical poles of the optic disc, where the RNFL is thickest.¹²⁵ Müller cells provide structural support throughout the retina by filling the spaces not occupied by neuronal elements in the retina. Among other structural roles, Müller cells regulate ions and metabolic wastes in the retina.³ Loss of localised RGC axons, such as in early-mid glaucoma, produces a reduction in RNFL reflectivity, hence creating a darkened appearance in the affected area of the retina, often seen as wedge-shaped defects narrowing towards the disc margin with sharply demarcated borders, as seen in Figure 9.^{126,127}

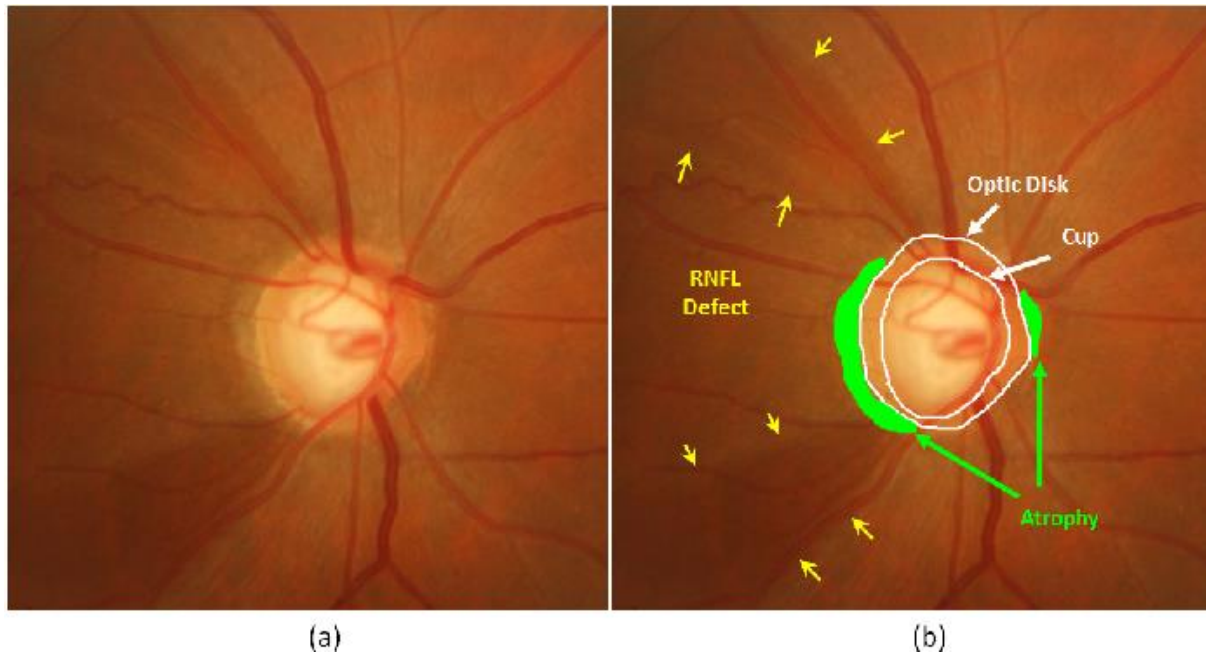


Figure 9. (a) Sample fundus photograph of the optic nerve and surrounding retina. (b) Glaucomatous indicators highlighted: RNFL defect outline demarcated by yellow arrows; peripapillary atrophy highlighted in green; limits of optic cup and disc outlined in white. Image taken with permission from Joshi et al (2012).¹²⁸

A global loss of RGC axons, as seen in advanced glaucoma cases, results in an overall dull appearance of the retina and clearer visibility of retinal blood vessels.^{124,129,130} While some have reported RNFL defects as the earliest observable defect in glaucoma,^{111,112} an older histology study has determined that up to 50% of RNFL loss is required for detectable RNFL loss on fundus imaging in animals and up to 45% loss of RNFL thickness in humans.¹²⁹ This suggests that significant RGC loss must occur before the detection of visible RNFL defects. Hence, quantification of RGCs may provide a better indication of glaucoma onset and progression. RGCs have been calculated in glaucomatous eyes using clinical data, as well as in histology studies, described in detail in section 3.2.4.^{105,131} The age related loss of RGCs has been reported to be approximately 7200 to 7900 RGCs per year in adult eyes both in histology and calculation studies that are based on clinical results.^{105,131} Medeiros and colleagues (2012) report faster rates of RGC loss in eyes with glaucoma over an average of 4.5 years, compared to age-matched controls. They also report that a larger proportion of

patients with glaucoma showed disease progression based on RGC counts than isolated clinical results from HFA and OCT (22.1%, 8.5% and 14.6% respectively; $p < 0.01$).¹³¹

Structural glaucomatous changes to the RNFL and neuroretinal rim can be quantified objectively and subjectively using techniques such as OCT and ophthalmoscopy respectively.^{132,133} This is covered in detail in section 3.2.2.

Functional glaucomatous changes including visual field sensitivity can be quantified objectively through visual field analysis (VFA).¹²⁶ Quantification of structural and functional RNFL changes through OCT and VFA are part of standard clinical monitoring of glaucomatous change and progression. However, structural RNFL or optic nerve changes have been reported before detection through functional tests.^{45,106-110} On the contrary, some have reported functional deterioration before detection through structural tests.^{45,117,134} Therefore, combining results from structural and functional tests to estimate RGC counts, as demonstrated by Harwerth and colleagues,³³ can be used as a more accurate method to improve detection and monitoring of glaucoma compared to isolated measures of structure and function.^{33,131}

3.2.2 RNFL assessment

Assessment of the RNFL is essential in both the detection and monitoring of glaucoma.¹³⁵ Since the introduction of OCT, non-invasive objective measurements of the RNFL thickness have become possible. The development of spectral domain OCTs have greatly enhanced scan resolution while reducing acquisition time, therefore increasing reproducibility when compared to older OCTs such as time domain OCTs.^{132,136,137} The most commonly used spectral domain OCTs are the Spectralis (Heidelberg Engineering, Dossenheim, Germany) and the Cirrus (Carl Zeiss Meditec, Dublin, CA).¹³⁸ These devices work by collecting three dimensional images of the parapapillary region to gather information about the RNFL thickness using a diode laser scan.¹³⁸

Cirrus OCT

The Cirrus HD-OCT algorithm for peripapillary and optic nerve head scanning takes 200 horizontal linear scans (B-scans) over a 6mm x 6mm area. The algorithm is called Optic Disc Cube 200x200 and provides the most common report used to evaluate the RNFL thickness in patients with glaucoma and glaucoma suspects. Each report has information about various aspects as shown in Figure 10 and detailed below.¹³⁹ Data presented on the left side of the printout depict results from the right eye, while results printed on the right side depict results from the left eye, as per clinical ophthalmic convention.

1. Patient data and signal strength: Figure 10(a). This information is presented along the top strip of the printout. Patient data including name, identification number, date of birth, gender and clinician/technician have been removed from Figure 10 in the interest of patient confidentiality.
2. Key parameters table: Figure 10 (b). A tabulated summary of key parameters is presented for each eye. Results presented in this table are colour coded based on comparison to Cirrus HD-OCT normative data. The colours are based on the colour block scale (Figure 10 (c)), where grey represents measurements that are beyond the range of normative data. White represents measurements that fall within the thickest 5% of normative data. Measurements that are normal (between the 5-95% prediction limits of normative data) are green, borderline results (measurements that fall between the 1-5% prediction limits of normative data) are yellow, and measurements that are outside normative data (thinner than the thinnest 1% of normative data) are red.
3. RNFL thickness map: Figure 10 (d). There is one RNFL thickness map for each eye on either side of the printout. Each map displays raw RNFL thickness data that is unique to the Cirrus HD-OCT. This is the only data in the printout that is not compared to normative data. The colours shown in the maps follow the colour scale on the left side of the map (Figure 10 (e)) which ranges from 0 μ m to 350 μ m (deep blue to white respectively). Cold colours (blue and green) represent thinner measurements while warm colours (yellow, orange and red) represent thicker measurements. If an area

cannot be scanned or cannot be calculated it will be coloured black and this will significantly affect the remaining results of the data.

4. Neuroretinal rim thickness plot: Figure 10 (f). These measurements are taken from Bruch's membrane opening (black circle in Figure 10 (g)) and the border of the optic cup (red circle in Figure 10 (g)). The results are compared to normative data and fall within different coloured areas that correspond to the colour block scale (Figure 10 (c)) and the plot is in "TSNIT" (Temporal- Superior-Nasal-Inferior-Temporal) configuration.
5. RNFL deviation map: (Figure 10 (g)). There is one map for each eye on either side of the printout. The RNFL thickness is compared to normative data. Areas that fall within normal thickness measures have no colour overlay. Areas with yellow and red coloured overlay correspond to the colour block scale mentioned earlier.
6. RNFL thickness plot Figure 10 (h)): This plot shows measurements from a 3.46mm diameter calculation circle (purple circle on the RNFL deviation map) centred at the Bruch's membrane opening and creates a TSNIT configuration plot against a colour coded background that corresponds to age matched normative data (colours follow the colour block scale described above). This plot is also summarised in the quadrant and clock hour graphs (Figure 10 (i)).
7. RNFL quadrant and clock hour thickness measurements: Figure 10 (i). There is one of each pie graph for each eye. These pie graphs summarise RNFL thickness from the RNFL thickness plot. The colours used in these graphs follow the colour block scale based on normative data.¹³⁹ Healthy eyes will follow the "ISNT rule", where the inferior RNFL thickness is the thickest measurement, followed by the superior RNFL thickness, followed by nasal and temporal RNFL thickness which would be the thinnest RNFL measurement.
8. Extracted horizontal and vertical tomograms: Figure 10 (j). There is one horizontal and vertical tomogram (B-scans) displayed for each eyes optic disc. The colours used in these images represent tissue reflectance where warm colours (red, orange and

yellow) represent high reflectivity and cold colours (blue, black) represent low reflectivity.

9. RNFL circular tomogram: Figure 10 (k). There is one displayed for each eye. These are the raw OCT images of the calculation circle (purple circle on the RNFL deviation map) used to develop the RNFL thickness plot and pie graphs (RNFL quadrants and clock hour thickness).¹³⁹

OD OS

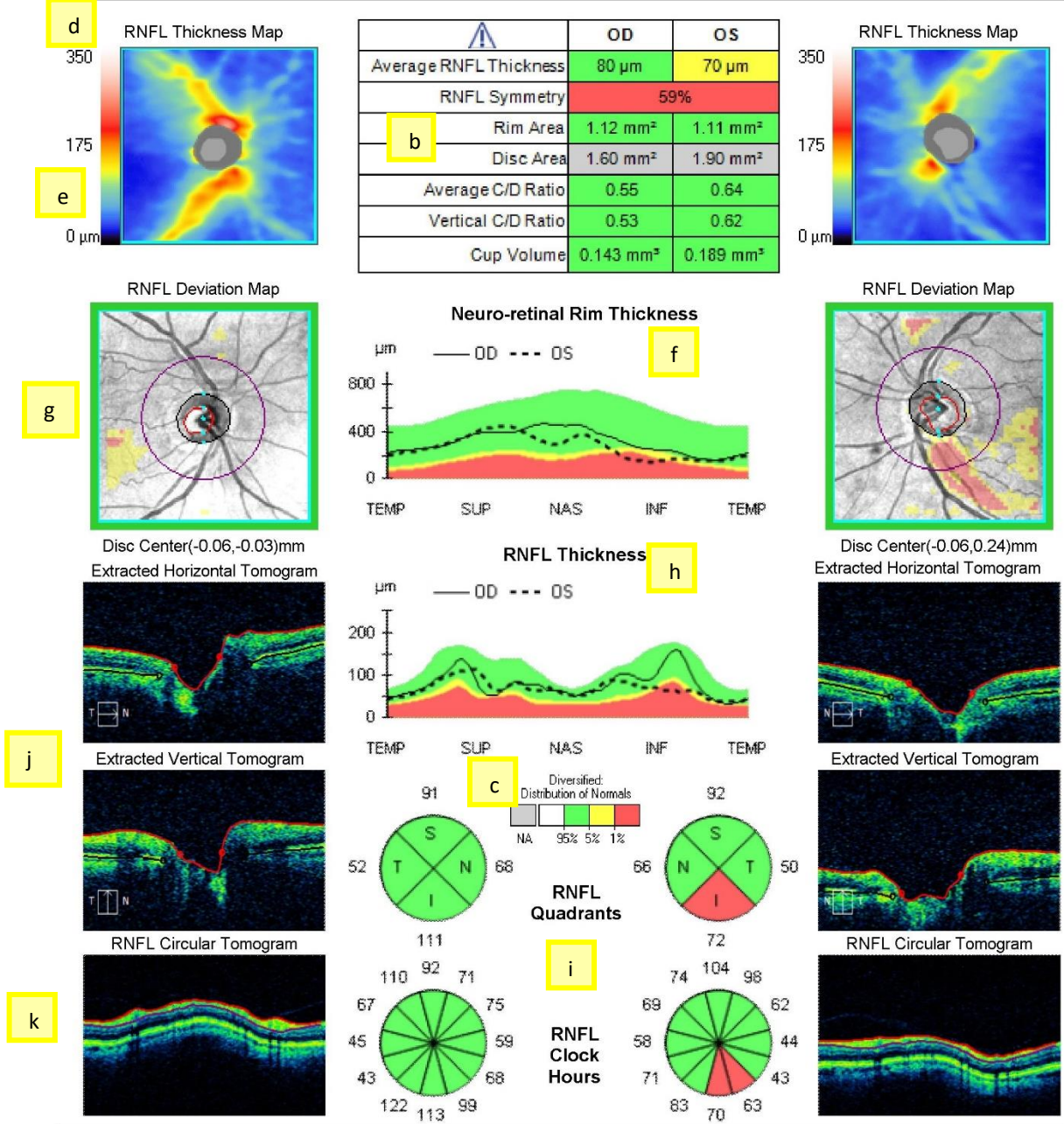
a Exam Date: 25/01/2019 25/01/2019 CZMI

Exam Time: 4:42 PM 4:44 PM

Serial Number: 4000-4912 4000-4912

Signal Strength: 7/10 7/10

ONH and RNFL OU Analysis: Optic Disc Cube 200x200 OD ● ● OS



Comments: _____

Doctor's Signature: _____

CFEH-0002
SW Ver: 9.5.0.8712
Copyright 2016
Carl Zeiss Meditec, Inc
All Rights Reserved
Page 1 of 1

Figure 10. Cirrus HD-OCT ONH and RNFL OU Analysis (Optic Disc Cube 200x200) sample results.

Spectralis OCT

The Spectralis OCT has an advanced automated anatomic positioning system where a fovea to disc alignment function corrects unwanted eye turns or torsion. This ensures that all scans start and stop at the same anatomical positions and therefore increases the accuracy and decreases test variability in follow-up scans, as well as increases the accuracy of comparison to normative data.¹⁴⁰ The angular difference between the foveal centre and ONH (or Bruch's membrane opening) centre relative to the horizontal meridian has been reported to be on average 7° lower (fovea lower than ONH).¹⁴¹ The Spectralis OCT also has a Glaucoma Module Premium Edition (GMPE) software that automatically aligns follow-up scans with their baseline image according to the alignment of the fovea and ONH.

The original RNFL imaging algorithm takes 768 data point measurements of 1.9mm depth along a 3.46mm diameter (12°) circle around the centre of the optic disc (Figure 11). The new GMPE software algorithm takes 768 data point measurements along three different diameter circles (3.5mm, 4.1mm and 4.7mm) centred at the optic disc (Figure 12). The two additional larger diameter circles are beneficial when the inner circle cannot be interpreted due to pathology such as peripapillary atrophy. Each of these algorithms provide useful information, and are the most common reports used to evaluate the RNFL thickness in patients with glaucoma and glaucoma suspects when using the Spectralis OCT device.¹⁴⁰ Each report has information about various aspects of the retina as shown in Figures 10 and 11 and detailed below. Data presented on the left side of the printouts depicts results from the right eye, while results printed on the right side depict results from the left eye. Analysis of the RNFL Single Exam Report OU in both the standard and GMPE algorithms are very similar:

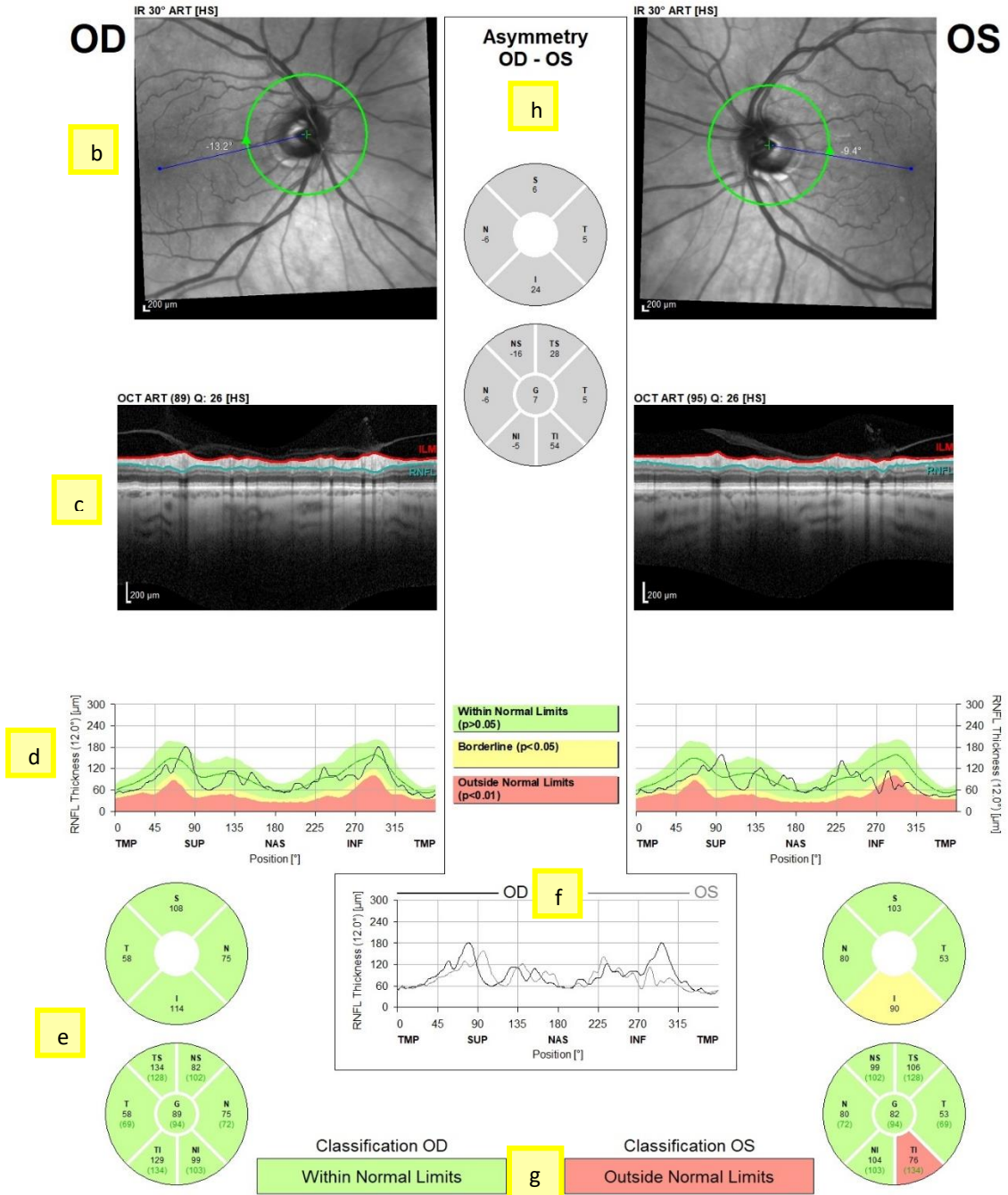
1. Patient and test information: Figure 11 (a) and Figure 12 (a). This information is presented along the top strip of the printout. Patient data including name, identification number, date of birth, examination date, gender and clinician/technician have been removed from Figure 10 and 11 in the interest of patient confidentiality.

2. Fundus image information: Figure 11 (b), Figure 12 (b). There is one image of each eye on either side of the printout. These images are infrared reflectance (IR) images with a 30° field of view of the fundus. If the top of the image states “ART”, this indicates that the automatic real-time function was active during image acquisition. The resolution setting is also printed at the top left of each scan, where “[HR]” is high resolution and “[HS]” is high speed. The image also has information on fovea to disc alignment and the green circle delineates the area of the peripapillary scan (3.46mm diameter circle centred at the optic disc, which is marked with a green “+”). The GMPE algorithm printout will have three concentric circles depicting the 3.5mm, 4.1mm and 4.7mm diameter circular scans Figure 12 (b). The setting of the scan shown in the printout is a brighter and bolder green compared to the other two settings. The scan diameter and Bruch’s membrane opening area are noted in the lower right corner of the fundus image.
3. RNFL profile image: Figure 11 (c), Figure 12 (c). There is one of each eye on each side of the printout. These are raw images that show the boundaries of the internal limiting membrane (ILM, delineated in red) and the RNFL (delineated in blue). On the top left border of each image notes are printed about the image settings used. There is a number in parentheses that indicates the number of averaged frames (i.e. how many times the circular scan was repeated) as well as a quality score on a scale of 1-40 recorded as “Q:26” in Figure 11 (c), Figure 12 (c). ART and [HS] or [HR] are also displayed, as described above.
4. RNFL thickness profile: Figure 11 (d), Figure 12 (d). There is one for each eye on either side of the printout. These graphs have a black line that indicates the RNFL thickness around the optic disc plotted in TSNIT configuration against a colour coded background that corresponds to age matched normative data. RNFL thickness within normal limits (i.e. results within the 95% prediction limits) are shown in green. Borderline results that are outside the 95% prediction limit but within 99% prediction of normal data are shown in yellow. Results that are outside normal limits, i.e. being thinner than 99% of the normative data, are shown in red. This plot

is also summarised in the classification charts (similar to quadrant and clock hour graphs in the Cirrus OCT) (Figure 11 (e), Figure 12 (e)).

5. Combined RNFL thickness profile: Figure 11 (f), Figure 12 (f). This graph combines the RNFL thickness graphs from each eye for comparative purposes.
6. Classification charts: Figure 11 (e), Figure 12 (e)). Classification charts for the right and left eye are on the left and right side of the printout respectively. These charts show the average RNFL in each quadrant and six sectors, as well as an average global RNFL thickness in μm . These results are colour coded according to the colour code described above. Normative age-matched values are recorded in green in parentheses under each sector result. The classification bar (Figure 11 (g), Figure 12 (g)) displays the sector result that is most deviated from normative data. The GMPE algorithm printout has does not present normative data. Instead, the number in parentheses under the average RNFL thickness of each sector, the ranking of the average RNFL thickness of that sector in the percentile within the normative database is presented.
7. Asymmetry charts: Figure 11 (h), Figure 12 (h). The top chart displays the difference in RNFL thickness in corresponding quadrants between each eye. The bottom chart displays the difference in RNFL thickness in corresponding sectors between the two eyes. ¹⁴⁰

Patient:
Patient ID: **a**



Reference database: European Descent (2009)

Software Version: 6.9.5

www.HeidelbergEngineering.com

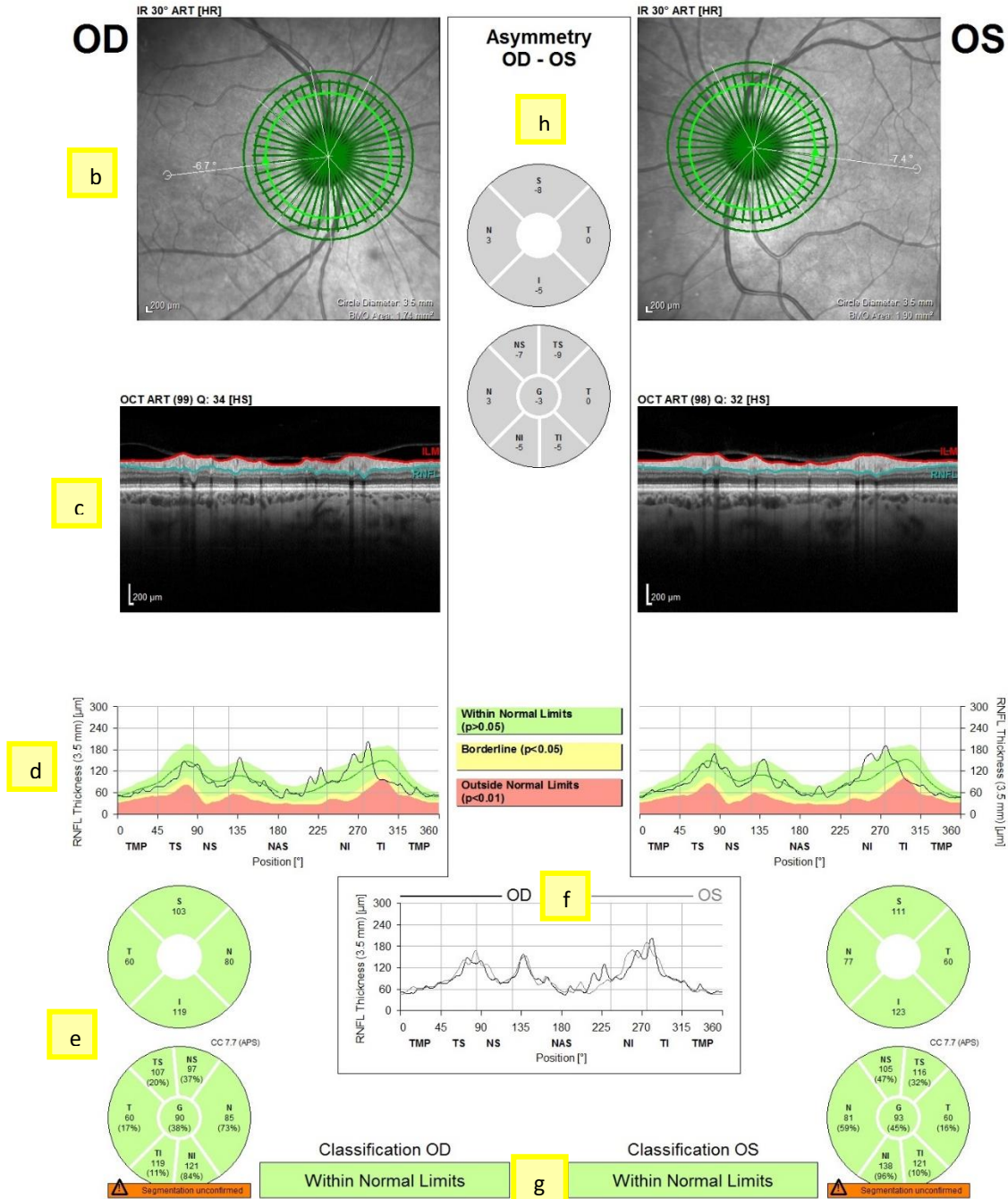
RNFL Single Exam Report OU

Figure 11. Standard RNFL Single Exam Report OU sample results.

Patient:
Patient ID: 2 a 33

1942
Exam.: 3/Jul/2019

Sex: F



Reference database: European Descent (2014)

Software Version: 6.9.5

www.HeidelbergEngineering.com

RNFL Single Exam Report OU

Figure 12. GMPE algorithm RNFL Single Exam Report OU sample results.

3.2.3 VF assessment

Visual field assessments are critical in the clinical diagnosis and monitoring of glaucoma to assess visual function. The Humphrey Visual Field Analyser (HFA; Carl Zeiss Meditec, Dublin, CA) is the predominant method of visual field assessment in glaucoma across the globe, although some clinics have adapted the more recently developed Octopus perimeter (Haag-Streit, Keoniz, Switzerland) or have maintained older testing methods such as Goldmann perimetry.¹⁴² The HFA is an automated static perimeter that assesses threshold visual field sensitivity measurements at various points in the visual field in decibels (dB). Most clinical trials use the HFA full threshold algorithm and this has been the reference standard against which newer algorithms that are compared.¹⁴² The most commonly assessed HFA field sizes for glaucoma are central 10, 24, and 30 degree assessments. In these assessments, a grid of points cover the testing area with the standard full threshold stimulus being 4mm² (size III). The stimulus (flash of light) is presented singularly at one point in the grid until all grid points are assessed to threshold twice. The stimulus changes its intensity in logarithmic stepwise intervals in accordance with the patient's responses (pressing a buzzer in response to seeing the stimulus) utilising a Bayesian thresholding algorithm.¹⁴² A single field analysis output from a HFA (Figure 13) presents information on various aspects of the assessment.

Patient and test information

Patient information is presented along the top strip of the printout (Figure 13 (a)). Patient data including name, identification number, date of birth, examination date, gender and clinician/technician have been removed from Figure 12 in the interest of patient confidentiality. Test information including stimulus size and colour and test strategy are included under the first bar (Figure 13 (aa)).

Reliability indices

Three reliability indices are assessed: patient fixation losses, false positive and false negative responses (Figure 13 (b)). Patient attention is assessed through false negatives, whereby the HFA will present stimulus at a point in the grid that has already been detected by the patient, however at 9dB brighter than previously detected. The HFA also monitors false

positives if a patient responds when no stimulus is presented. Fixation losses are monitored by recording whether a patient responds to a stimulus projected at their blind spot.¹⁴³

Visual field sensitivity

Raw (unadjusted) visual field sensitivity at each of the test points are recorded in dB at each of the test points, as seen in Figure 13 (c). A grayscale map of these quantified values is also presented in the single field analysis results, where light shading indicates high sensitivity and progressively lower sensitivity with progressively darker shading.

Summary statistics

The summary statistics are presented under the grayscale map on the right (Figure 13 (d)), including Visual Field Index (VFI), Mean Deviation (MD) and the Pattern Standard Deviation (PSD). Each patient's results are compared to a large database of age-matched normals to determine whether the results are within normal limits or outside normal limits at the 0.5%, 1%, 2% or 5% probability levels.¹⁴³

The VFI represents the entire visual field as a percentage weighted towards the middle of the field, where 100% represents a normal visual field for that age group and 0% represents a blind visual field for the patient's age.¹⁴⁴ The MD reports the average visual field deviation from normal and age-matched visual field sensitivity values for the testing points. If the MD is negative, this indicates that the patient's visual field sensitivity is lower than healthy age-matched person with a normal visual field. In contrast, if the patient had a visual field sensitivity that was better than healthy age-matched counterparts, the MD would be positive. The PSD quantifies localised visual field sensitivity loss, where localised defects that deviate significantly from healthy and age-matched results will generate a positive result. If a patient has diffuse visual field sensitivity loss, such as in glaucoma, the patient may have a high negative MD alongside a low PSD. Thus, it is possible for PSD to rise in early glaucoma but drop as glaucoma progresses to more advanced stages and MD is more negative.¹⁴³

Glaucoma Hemifield Test (GHT)

The GHT compares five mirrored areas above and below the horizontal midline that are graded based on RNFL anatomy.¹⁴⁵⁻¹⁴⁷ The difference between each mirrored zone (i.e.

superior and inferior) is compared to the difference in each mirrored zone taken from normative data. One of five output messages will be presented (Figure 13 (e)).

1. Outside normal limits: this message is presented if the difference between the mirrored zones is greater than the difference between mirrored zones in 99% of the normal population. This message will also appear if the values in both zones (superior and inferior) are greater than 99.5% of the normal population.
2. Borderline: this message is presented if the difference between mirrored zones is greater than that found in 97% of the normal population.
3. General reduction of sensitivity: this message is presented when neither of the two criteria are met for “outside normal limits” and the minimum depression is greater than what occurs in less than 0.5% of the normal population.
4. Abnormally high sensitivity: this message is presented when the greatest sensitivity is higher than that in 99.5% of the normal population.
5. Within normal limits: this message is presented when none of the above criteria are met.¹⁴³

Total deviation and pattern deviation

The total deviation (TD) plot (Figure 13 (f)) compares the sensitivity of each test point to the sensitivity of each test point in age-matched normal controls. If the number displayed is positive, this indicates that the sensitivity of the patient at that point is higher than the aged-matched controls and negative numbers indicate lower sensitivity compared to age-matched controls. The plot directly under the TD plot shows probability results at each test point (TD probability plot; Figure 13 (g)). A single dot indicates normal sensitivity at that point. Four dots (light stippling) indicates a result outside the normal at the 5% probability limit. Intermediate stippling indicates results outside the normal at 2%, while heavy stippling and solid black indicate results outside the normal at 1% and 0.5% probability limits.¹⁴³

The pattern deviation (PD) plot (Figure 13 (h)) adjusts the results to compensate for diffuse/global sensitivity loss (or gain). This allows for better identification of localised visual field defects. The probability plot below it (Figure 13 (i)) follows the same criteria as above

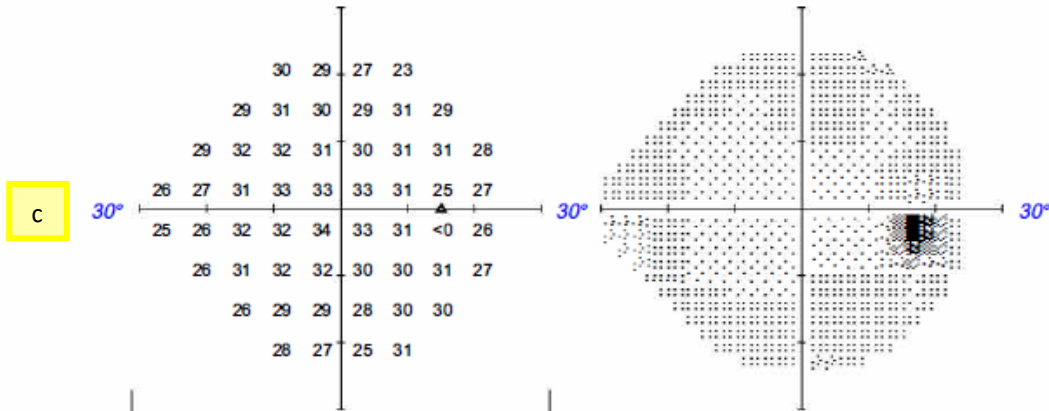
using the pattern deviation plot. This plot can be assessed alongside the TD probability plot. If there is stippling on the TD probability plot but none on the PD probability plot, this means that the sensitivity deficit is purely diffuse. If the stippling in both plots are almost identical, this means that the field loss is purely localised. If there are both types of visual field loss (diffuse and localised), then the probability plots will look similar, but the PD probability plot will show some (but not all) of the TD probability plot stippling.¹⁴³

Patient:
 Date of Birth:
 Gender:
 Patient ID: **a**



OD Single Field Analysis **Central 24-2 Threshold Test**

b Fixation Monitor: Fixation Target: Fixation Losses: False POS Errors: False NEG Errors: Test Duration: Fovea:	Gaze/Blind Spot Central 0/13 0% 2% 05:08 Off	aa Stimulus: Background: Strategy: Pupil Diameter: Visual Acuity: Rx:	III, White 31.5 asb SITA Standard 4.8 mm* Date: Sep 12, 2018 Time: 2:43 PM Age: 31
---	--	--	--



f

1	0	-2	-6
-1	0	-1	-2
-1	0	-2	-3
-3	-4	-1	-1
-3	-5	-1	-2
-4	-1	-1	-1
-5	-3	-3	-4
-2	-3	-6	0

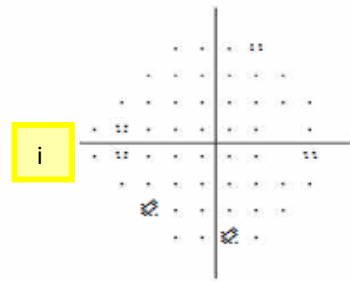
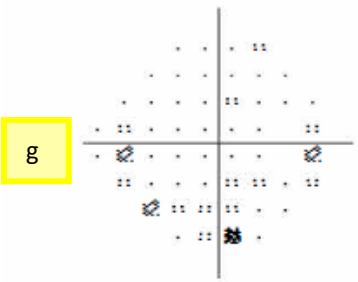
Total Deviation

h

1	0	-2	-6
-1	0	-1	-2
-1	0	-1	-3
-2	-4	-1	-1
-3	-4	-1	0
-4	-1	-1	-1
-5	-3	-3	-4
-2	-3	-6	1

Pattern Deviation

GHT: **Within Normal Limits** **e**
 VFI: **99%**
 MD24-2: **-2.03 dB P < 10%** **d**
 PSD24-2: **1.68 dB**



:: P < 5%
 ☒ P < 2%
 ☒ P < 1%
 ■ P < 0.5%



Figure 13. Sample HFA Single Field Analysis results for a right eye.

3.2.4 RGC assessment

As previously discussed, the underlying pathology in glaucoma is the loss of RGCs including their axons.^{104,105,148} RGC death leads to thinning of the RNFL^{33,125,129} as well as thinning of the neuroretinal rim¹⁴⁸. These structural changes ultimately result in functional changes in the form of reduced visual field sensitivity and potential loss of vision.^{33,112} While the functional loss seen in glaucoma does mirror the pathology and the pattern of structural loss, there is some discordance between these structural and functional changes due to the difference in disease stage that they first present.^{45,106-112,129} These differences have been reported to hinder the ability to detect glaucoma at its early stages.^{149,150} Combined structural (OCT) and functional (HFA) results, through a series of formulas, has been used to estimate RGC count in patients with glaucoma.¹³¹ Calculating RGCs numbers and the rate of their loss over time has been shown to perform significantly better, compared to isolated OCT and HFA assessments, in assessing glaucoma and its progression.¹³¹ Yoshioka and colleagues describe a method for RGC calculation using data from the OCT and HFA.¹⁵¹ However, this method utilises OCT and HFA results from glaucoma clinical test strategies that are not commonly used as baseline glaucoma assessments; these tests include the HFA 10-2 test protocol and ganglion cell layer thickness measurements from the OCT.¹⁵¹ Formulas derived by Medeiros and colleagues, based on the work of Harwerth and colleagues, calculate RGC estimates using standard and widely-used glaucoma assessment test strategies, i.e. the 24-2 HFA test protocol and RNFL thickness assessment from the OCT.^{33,131,152} Their method is described in detail in Chapter 5. Both RGC calculation methods factor in age-related loss of RGCs so as to not confuse glaucomatous RGC loss with normal age-related RGC loss, which is approximately 8000 RGCs per year.^{105,131}

Detection of Apoptosing Retinal Cells (DARC) Technology is a technique that identifies real-time apoptosing retinal cells using fluorescent-labelled annexin-V and excited using an argon laser (488nm), a photodetector system and retinal imaging (snapshot of fluorescence at RGC apoptosis sites shown in Figure 14).^{153,154} This technique has revealed significant correlations between higher DARC counts and increased cup-to-disc ratios ($p=0.0038$) in glaucoma. Overall, DARC counts are significantly elevated in patients with glaucoma

compared to healthy controls ($p < 0.05$), indicating higher rates of RGC death at any given time in patients with glaucoma.¹⁵⁵

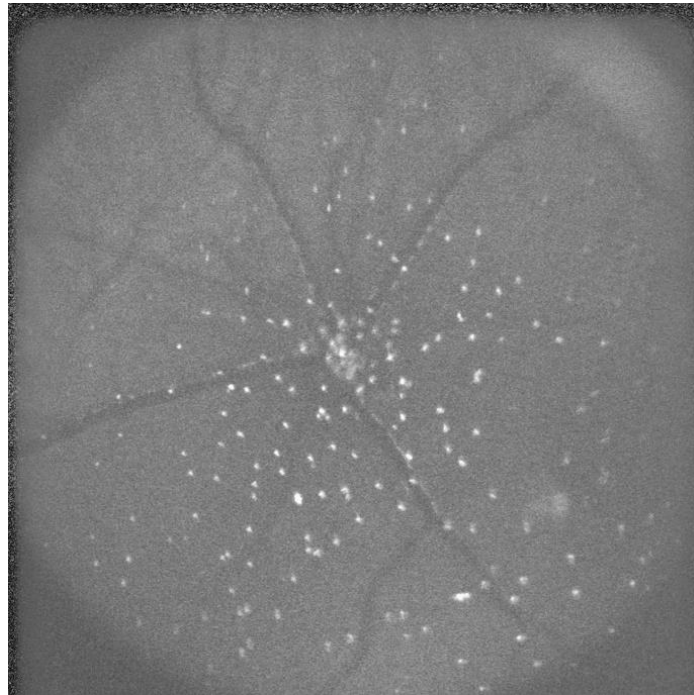


Figure 14. A rat retina showing individual RGC apoptosis at each white spot (fluorescing spots) using DARC Technology. Image taken with permission from Crodeiro et al (2011).¹⁵³

3.3 Vascular markers in Glaucoma

Alongside neurodegenerative changes, glaucoma is also associated with vasculature damage evident in the retina and at the optic nerve head, such as haemorrhages and vein occlusions.^{156,157} Disruption and failure of stable blood flow in the region of the optic nerve can cause ischemic damage of the RGCs, potentially initiating the cascade of glaucomatous damage.^{158,159} This suggests that vascular changes could occur at the very early stages of the glaucoma continuum. Investigations of retinal blood flow during the early stages of glaucoma have revealed increased blood flow in regions of RNFL thinning, with a progressive decline in ocular blood flow with increased glaucomatous progression.¹⁶⁰⁻¹⁶³ Assessment of retinal microcirculation is possible due to the visibility of retinal vasculature using non-invasive means.

3.3.1 Static vascular markers

Modern digitalised retinal photography and computer software have been developed to objectively assess and quantify subtle changes in retinal vasculature. Many static vascular markers have been studied, including:¹⁶⁴

- **Retinal vascular calibre**, which is usually measured as a summary index reflecting the average width of either retinal arterioles or venules, termed central retinal artery equivalent (CRAE) and central retinal vein equivalent (CRVE) respectively. Retinal vascular calibre can also be measured in arteriovenous ratio, which is a dimensionless ratio used to compensate for differences in magnification and refractive error.^{165,166}
- **Retinal vascular tortuosity** reflects vessel curvature and measured as a ratio between the natural length of a vessel from point A to B and the shortest straight-line distance between points A and B.¹⁶⁷
- **Retinal vascular bifurcation angle (RVBA)** is the first angle subtended between two daughter vessels at a vascular junction.¹⁶⁸
- **Fractal dimension** is a calculation of how thoroughly the vessels fill the two dimensional space by looking at the whole branching pattern of the retinal vascular tree.^{169,170}

All of the above listed static vascular markers have been found in reduced states in glaucomatous eyes across various studies.¹⁷¹⁻¹⁸⁰ The most commonly reported reduction is a generalised narrowing of the retinal vasculature as a characteristic of advanced glaucomatous damage. It has been found that the central retinal vessels become narrower as the severity of glaucomatous damage increases.¹⁷² A summary of static vascular changes are reported in Table 1, adapted from Chan et al (2017).¹⁶⁴

Table 1. Summary of static vascular changes in glaucoma

Static glaucomatous vascular changes					
Arteriole calibre	Venular calibre	Fractal dimension	Tortuosity	RVBA	Study
-	-	Reduced	-	-	Ciancanglini et al (2015) ¹⁷¹
Reduced	Reduced	-	-	-	De Leon et al (2015) ¹⁷²
Reduced	Reduced	-	-	-	Gao et al (2015) ¹⁷³
Reduced	-	-	-	-	Yoo et al (2015) ¹⁷⁴
-	-	Reduced	Reduced	Reduced	Wu et al (2013) ¹⁷⁵
Reduced	Reduced	-	-	-	Amerasinghe et al (2008) ¹⁷⁶
Reduced	-	-	-	-	Wang et al (2007) ¹⁷⁷
Not significant	Not significant	-	-	-	Klein et al (2004) ¹⁷⁸
Reduced	Reduced	-	-	-	Mitchell et al (2004) ¹⁷⁹
Not significant	-	-	-	-	Angelica et al (2001) ¹⁸⁰

Previous to the development of computerised and automated machines, retinal vessel calibre had been assessed manually in glaucoma patients.¹⁸¹⁻¹⁸³ Interestingly, these manual means of vessel assessment revealed similar findings to the current computerised methods and found decreased retinal vessel calibre with increasing glaucoma severity. This was more evident in retinal arteries than retinal veins. Furthermore, it has been found that retinal quadrants with greater ONH damage corresponded to narrower retinal arteries.¹⁸¹⁻¹⁸³

The association of reduced vessel calibre in glaucoma is quite interesting and can be explained by two varying theories. The first theory states that RGC loss leads to an auto-regulatory response where vasoconstriction occurs as a means of adjustment to the reduced metabolic demand, which is also consistent with parallel findings of reduced vessel calibre in non-glaucomatous eye that have optic atrophy.¹⁸³⁻¹⁸⁵ The alternate postulation is that RGC loss is related to impaired local autoregulation, vasoactive substance leakage and consequent vasoconstriction.¹⁸⁶ This theory is supported by elevated oxidative stress markers in the aqueous humour, serum and trabecular meshwork of patients with glaucoma.^{187,188}

3.3.2 Dynamic vascular markers

Current technology has advanced to allow for quantitative assessment of ocular blood flow and ocular perfusion. Scanning Laser Doppler Flowmetry (LDF) with automated perfusion imaging analysis quantifies the frequency shift of perfused blood vessels and capillaries by defining and segmenting vessels from which blood flow velocity is then derived from the rate of flow shift. Laser Speckle Flowgraphy (LSF) calculates the velocity of blood flow by assessing the speckle pattern that arises from the scatter of the laser irradiation from an illuminated fundus. Changes in blood flow velocity blur the speckle pattern from which a blur rate is derived.¹⁶⁴ Both methods have revealed reduced blood flow at the ONH and peripapillary area in patients with glaucoma,¹⁸⁹⁻¹⁹¹ as well as patients who are glaucoma suspects, before the development of clinically detectable VF loss.^{192,193} However these methods are limited, as LDF can only evaluate a small area of the retina and LSF is limited in its repeatability due to the absorbance and reflectivity of the optic disc.¹⁶⁴

Ocular perfusion measures ocular blood flow through digital scanning laser angiograms that tracks the passage of blood from the retinal arteries through to the retinal capillaries and hence to the retinal veins. Although this method has revealed a prolonged passage time in glaucoma patients, it is limited by its invasiveness, risk of potential adverse systemic effects on the patient and difficulty in accurate quantification.¹⁹⁴⁻¹⁹⁶ Nonetheless, these findings have helped to attribute the cause of reduced ocular blood flow to a reduction of capillary diameter due to vasospasms or arteriosclerosis.¹⁶⁴

Optical coherence tomography-angiogram (OCT-A) is a non-invasive alternative to traditional angiograms that offers three dimensional analysis of retinal and choroidal microcirculation by mapping erythrocyte movement over time and comparing sequential B-scan OCT angiography images at a given cross section.^{197,198} OCT-A also has the additional advantages of being able to visualise different depths of retinal and choroidal blood flow and generate quantified data on vascular blood flow in terms of retinal and optic disc perfusion. This is advantageous compared to traditional angiography methods using fluorescein or indocyanine green that only provide two dimensional information.¹⁹⁹ Studies using OCT-A readings have found that patients with glaucoma have reduced peripapillary vessel density and reduced optic disc perfusion.²⁰⁰⁻²⁰⁴

Furthermore, greater vascular damage has been reported to be associated with increased glaucomatous structural and functional loss in many studies using OCT-A.²⁰⁵⁻²¹⁰ A study conducted by Yarmohammadi and colleagues (2016) found increasingly sparse peripapillary networks and decreased vessel density at the optic nerve head with progressively worse glaucoma status on the basis of HFA assessment ($p < 0.001$) (Figure 15).²⁰⁵ Furthermore, Cennamo and colleagues (2017) found significantly decreased blood vessel density in patients with pre-perimetric glaucoma compared to healthy eyes ($p = 0.001$).²⁰⁷ More recently, Hou and colleagues (2020) investigated the vessel density at the optic disc in patients with POAG and PACG using OCT-A. They found significantly reduced vessel densities in both groups, compared to their control group. However, the POAG and PACG groups differed in that the POAG group had significantly lower vessel density in the inferior temporal peripapillary region compared to the PACG group ($p < 0.001$).²⁰⁶ Thus OCT-A can be a useful tool in better understanding the pathogenesis in different types and severities of glaucoma.

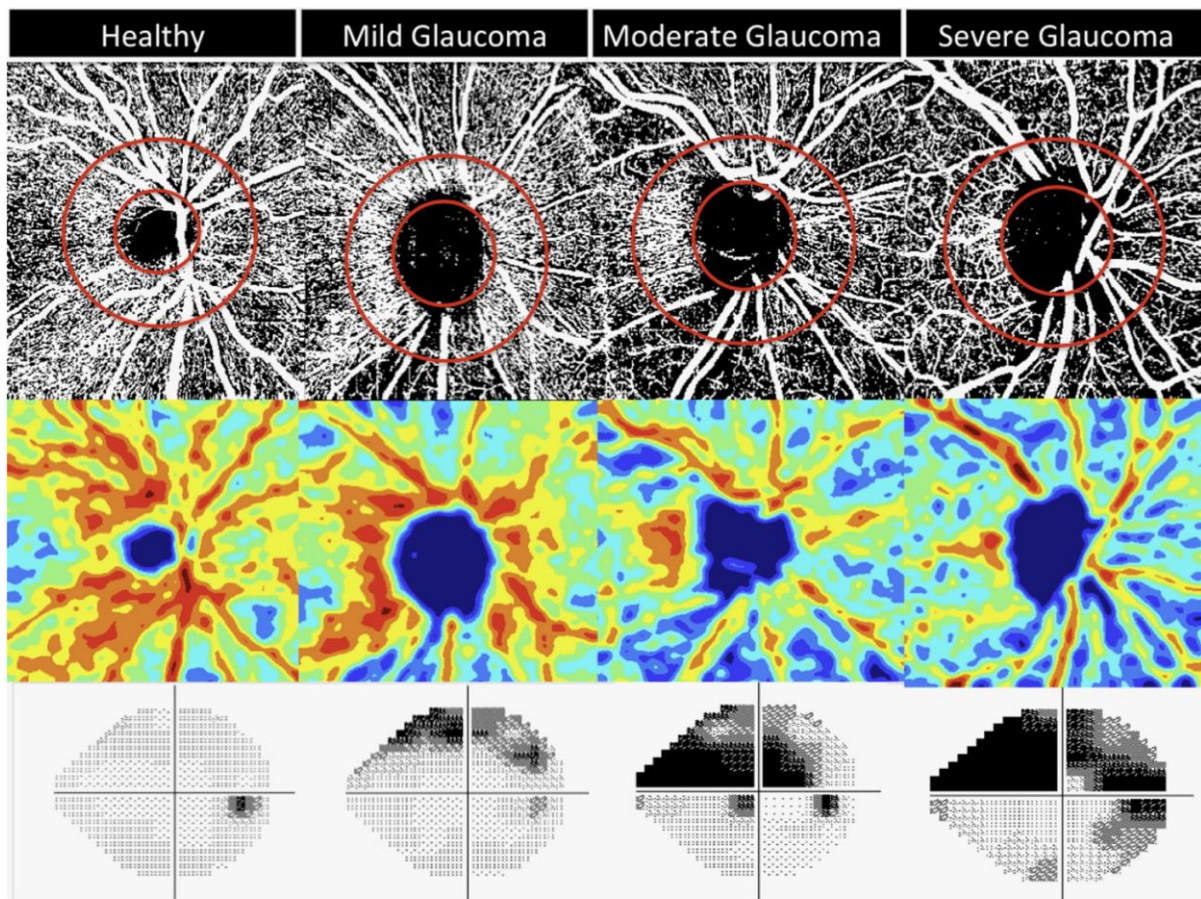


Figure 15. Optic nerve head vessel density map showing declining vessel density with increasing glaucoma severity and visual field loss. Image taken with permission from Yarmohammadi and colleagues (2016).²⁰⁵

Although there are many benefits in the OCT-A over traditional angiograms, there are several limitations. The current most updated OCT-A device only allows a maximum scanning field of $6 \times 6 \text{mm}^2$ and image artefacts are quite common, which may lead to inaccurate assessments.²¹¹ Currently, OCT-A devices utilise amplitude decorrelation to detect blood vessels, however this blood flow is not quantified. Moreover, vessels with slow or absent blood flow that is slower than the OCT's detection threshold cannot be assessed. Moreover, an OCT-A cannot differentiate a vessel that has a higher flow rate than a slower flow rate if both are above the detection threshold.^{205,212}

Blood flow velocity can also be measured using retinal functional imaging that compares erythrocyte movement in a series of retinal images. Elevated mean retinal blood flow velocity has been detected in the peripapillary vasculature, which may reflect a

phenomenon where there is increased flow in retinal vessels when there is decreased retinal capillary perfusion.^{213,214}

3.3.3 Retinal vein characteristics

The average diameter of the retinal veins is dependent on its location in the retina or optic nerve. At the retinal surface, between half to one optic disc diameters from the optic disc, the superior and inferior hemiretinal veins are typically $214 \pm 22 \mu\text{m}$ in diameter and are thicker on the optic disc surface as they approach their junction at the CRV.²¹⁵ The average diameter of the CRV is $200 \mu\text{m}$, which decreases in diameter at the lamina cribrosa and increases slightly once it has passed through the lamina cribrosa into the optic nerve.²¹⁶ The average retinal vein wall thickness is reported to be approximately $12 \pm 1.3 \mu\text{m}$ and variations in the vessel wall thickness affect its compliance characteristics i.e. “the movement of the venous wall in response to pressure change”, which is seen in spontaneous retinal venous pulsations (SVPs).²¹ The vessels lie relatively loose and un-bound on the retina, however at the lamina cribrosa, the CRV wall develops a tight connection with the laminar collagen, which creates a mechanical link between the two structures.²¹⁷

The histology of the endothelial cells of the CRV have an interesting morphology whereby an irregular polygonal morphology, similar to other endothelial cells in the body, is seen along the vessel lining except at the portion that passes through the lamina cribrosa region.²¹⁸ At the lamina cribrosa, the CRV endothelial cells take on a spindle-formation, similar to arterial endothelial cells.²¹⁸ This change in endothelial cell morphology across the venous wall is not seen anywhere else in the human venous system unless there has been a vascular-arterial grafting. In this instance, the vein that has been grafted into the artery is exposed to high shear and shear stress leading to morphologic changes of the endothelium.²¹⁹⁻²²¹ Therefore, the change in morphology of the endothelial cells across the CRV indicate high shear stress and elevated blood velocities at the lamina cribrosa.

This is also an indication that it is a site where the difference in pressure between the intraocular and cerebrospinal areas create a pressure gradient.^{222,223} In fact, this pressure gradient is one of the largest pressure gradients in the human body.²¹ In a healthy state, where IOP and CSFp are within normal range, this translaminar pressure gradient has been

estimated as 20-33mmHg/mm,^{223,224} compared to other vascular pressure gradients found across the body that are typically up to 0.8mmHg/mm²²⁵. Other than the translaminar pressure gradient across the CRV, the largest vascular pressure gradients are typically found within capillaries at 5-12mmHg/mm.^{225,226} The contributing compartments to the pressure gradient across the CRV are the IOP at the optic disc surface and retina. Posterior to this pressure compartment is the CSFp that surrounds the optic nerve up to the posterior portion of the globe in the optic nerve subarachnoid space.²¹

Veins are said to have high compliance, that is, for any per unit variation in the volume of blood, the walls of the blood vessels will alter shape to accommodate the change in pressure.²¹ Transmural pressure is the difference in pressure between the internal vessel pressure and the pressure external to the vessel wall. This plays a large role in vessel distensibility, which is the change in cross-sectional area per unit of pressure change. If transmural pressure is between -1mmHg to 1mmHg, partial vessel collapse occurs at -1mmHg of transmural pressure.²²⁷ When IOP is between 10-35mmHg and greater than CSFp, the retinal vein transmural pressure at the optic disc has been recorded as 0.3mmHg, in both canine²¹¹ and porcine eyes^{228,229} (± 0.9 mmHg and ± 1.5 mmHg respectively). This then increases at one disc diameter from the disc margin in canine (1.3mmHg) and porcine (1.7mmHg) eyes (± 0.8 mmHg and ± 1.2 mmHg respectively).^{211,228,229}

It has been estimated that in humans, the translaminar pressure gradient is 20-33mmHg/mm when IOP and CSFP are within normal range, with a pressure drop of 10mmHg from IOP to retrolaminar tissue pressure.^{21,223,230} In the human eye, a translaminar pressure gradient of 23mmHg/mm and pressure difference of 11mmHg causes blood flow discontinuity and thus pulsations to occur.²³¹

4. Spontaneous retinal venous pulsations (SVPs)

SVPs are changes in caliber of the retinal vein over the optic nerve head, usually at the hemi-veins of the CRV close to where they join to form the CRV, or at the CRV closest to where it exits at the lamina cribrosa.²³² SVPs are considered as another dynamic vascular marker for glaucoma.^{163,233-235} Since the discovery of SVPs in the 1850's,²³⁶ their presence has been variably reported in patients with glaucoma, with some papers reporting absent SVPs.^{163,233} This has created interest in the assessment of SVPs in glaucoma.^{21,163,233-235,237} Recent objective quantification of SVPs has led to an increase in their detection in glaucoma. This is clearly demonstrated in a study reporting an increase in detection of SVPs in glaucoma patients from 64.1% using subjective measures to 100% using objective measures.¹⁶³ These improved methods of detection of SVPs have led to the question of whether the variability in their amplitudes may be indicative of the presence of glaucoma and its stages and whether low amplitude SVPs were simply undetectable using previous methods. The latter was investigated by Morgan and colleagues (2015) who reported that SVP amplitudes are strongly related to whether or not pulsations are observable to the naked eye.²³⁸ However, it is as yet unclear whether the reduction in SVP amplitudes is due to anatomical factors such as variations in vessel dimension and/or changes to vessel pliability. The role of reduced SVPs in the pathogenesis of glaucoma is not clearly defined, though reduced SVP amplitudes have been associated with RNFL loss.^{163,233,235}

4.1 Aetiology and mechanism of SVPs

There has been some controversy over the aetiology of SVPs since they were first observed, particularly in regards to the staging of venous collapse in relation to the cardiac cycle. Initially, it was thought that the influx of blood to the eye at systole caused an increase in IOP, causing venous collapse.²³⁶ Later, it was proposed that the higher IOP compared to the pressure in the retrolaminar CRV at systole, caused venous collapse.²³⁹ This proposition was under question when it was found that retinal venous pressure is greater than IOP at all times,²⁴⁰⁻²⁴² and lead to speculation as to whether IOP impacted the retinal veins.²⁴¹

This then lead to the proposal that the fluctuations of IOP are greater than the fluctuations of the retrolaminar venous pressure, leading to the generation of SVPs where venous

collapse occurs at ocular systole.²⁴³ More recently, the theory that venous collapse occurs at ocular systole has been refuted with evidence that venous collapse occurs at ocular diastole.^{244,245} Kain and colleagues (2010) assessed IOP fluctuation alongside retinal vein diameter in a small sample of ten participants. They found that maximal retinal vein collapse and maximum retinal vein dilation occurred not in line with, but shortly after minimal and maximal IOP levels, suggesting that venous collapse actually occurs shortly after ocular diastole.²⁴⁵ This theory was supported by Kim and colleagues' 2014 study that was conducted on a larger sample of 47 patients using a different approach.²⁴⁶ Similarly, Morgan and colleagues have found that retinal venous collapse occurs in time with minimum CSFp pressure, close to minimum IOP and therefore in time with diastole.²⁴⁵ A schematic of this mechanism is presented in Figure 16.

A collapsible vessel wall will pulsate at the exit point when fluid travels from a pressurized chamber to an external space,^{247,248} with vessel collapse occurring at or close to the exit point where the most negative transmural pressure is induced. In relation to the retinal veins, the CRV is the collapsible vessel that travels through the pressurised chamber (IOP) to the external space (CSFp) with the lamina cribrosa being the exit point. Thus, SVPs are visible close to the lamina cribrosa. The negative transmural pressure in the CRV is suggested to occur in early diastole.²⁴⁶ At diastole, there is a decrease in both IOP and intracranial pressure (ICP),^{245,249} however there is a time difference between the two. A drop in ICP occurs before the drop in IOP at early diastole,^{245,250,251} creating a negative transmural pressure and hence vessel collapse.²⁴⁶ Vessel collapse at diastole has also been explained on the hypothetical theory of varying amplitudes of IOP and ICP at diastole, where the latter has a greater amplitude, leading to a greater pressure gradient at diastole (Figure 16).²⁴⁴ While there is no confirmation that the ICP amplitude is greater than that of IOP, Morgan and colleagues (2012) found that at systole, ICP increases at a more rapid rate than the increase in IOP, causing a reduced rate of venous outflow. This in turn, caused an accumulation of blood within the vessel and therefore CRV dilation at systole.²⁴⁵

Yu and colleagues (2016) found that retinal vein dilation and contraction can be regulated through vasoactive agents (vasocontraction and vasodilation through endothelin-1 and

adenosine respectively), therefore SVPs may not be a completely passive response to changes in blood flow.²²⁷

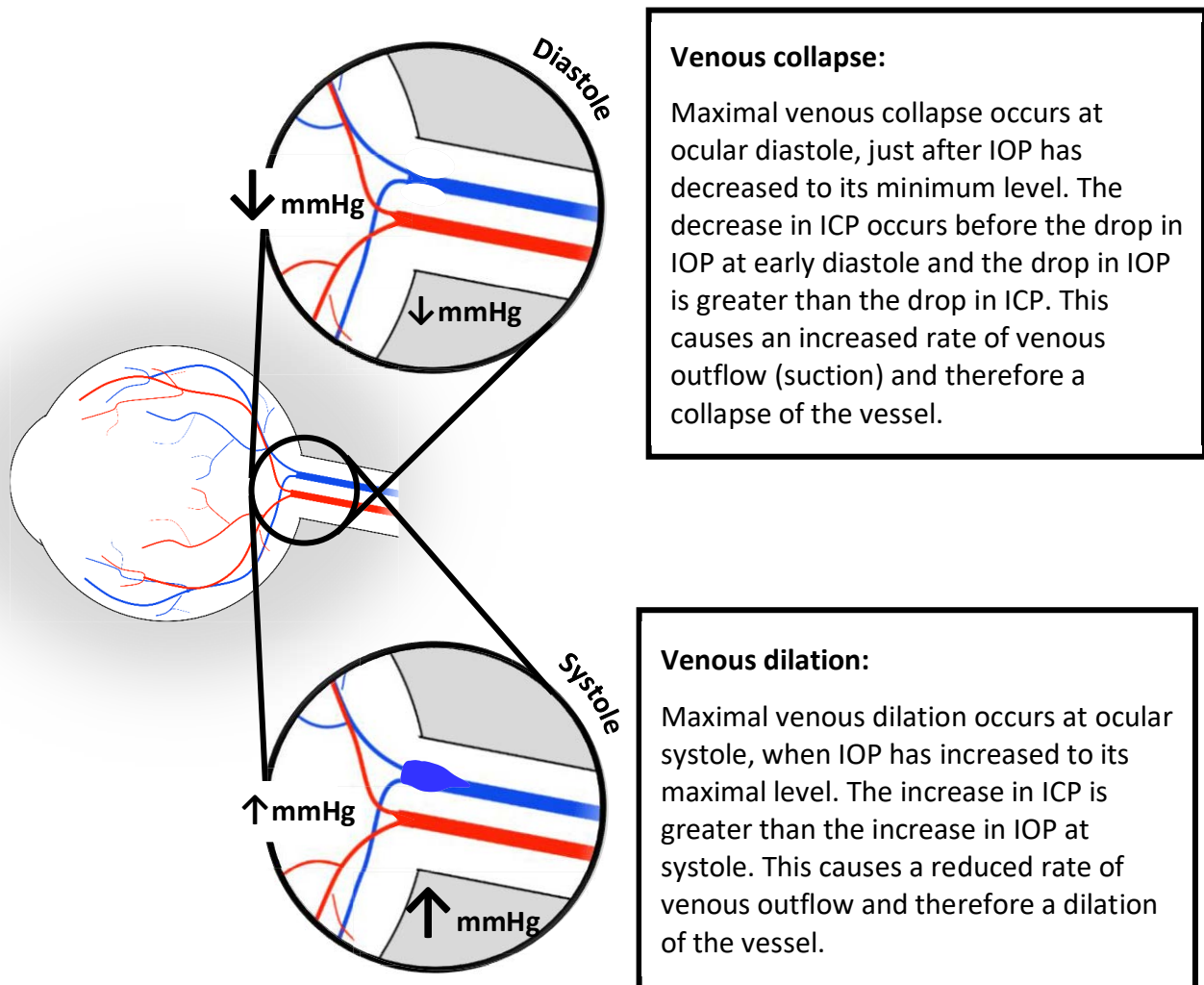


Figure 16. Schematic of SVPs in relation to IOP and ICP. Arrows on the left side correspond to relative increase or decrease of IOP to that of ICP (arrows in the grey area).

4.2 SVPs in healthy eyes

In a healthy state, SVPs are most commonly seen at the CRV close to the lamina cribrosa or at a vessel close to the CRV at the optic disc surface. The anatomical position of the CRV is usually temporal to the CRA both within the lamina cribrosa and at the surface of the optic disc.²¹ However, there can be normal anatomical variation between individuals where the retinal vein can pass beneath an artery which would therefore obstruct its visibility.²¹ While early studies have assessed SVPs using subjective methods, studies detecting SVPs through objective means have reported SVPs in 81.7% to 100% of healthy eyes.^{233,252,253} Moreover, there is an increasing visibility and detection of SVPs with age.^{232,254} This may be due to various factors including increasing mean and pulse arterial blood pressure after the age of 40 years.^{232,255}

4.3 SVP alterations in glaucoma

The most likely explanation for reduced SVP detection in glaucoma is the reduction of SVP amplitude due to an increased resistance of the CRV in glaucoma.²¹ Although CSFp has been reported to be lower,²⁵⁶⁻²⁵⁸ and venous pulsation pressure has been reported to be elevated^{163,233,259,260} in eyes with glaucoma, it has been postulated that the increased resistance and narrowing of the CRV in the lamina region causes the change in venous pulsation pressure in glaucoma.²¹ While the exact cause of this increased resistance is unclear, Yu and colleagues (2014) have proposed that alterations in haemodynamic stress leads to changes to the venous endothelium and the wall of the CRV.²²⁴ In contrast, Roberts and colleagues (2009) proposed lamina remodelling in subjects with glaucoma, causing compressive changes to the CRV.²⁶¹ Narrowing of the vessel is not only reported at the CRV, but also at the superior and inferior retinal vein branches that bifurcate from the CRV. The branch with greatest vein pulsation pressure being likely to pass over the more damaged portion of the optic disc.²³²

Changes in the translaminal pressure gradient can also be a large factor in the visibility of SVPs. As previously described, the translaminal pressure gradient is dependent on the IOP anterior to the lamina cribrosa and the CSFp posterior to the lamina cribrosa.²¹ The pressure gradient increases when the difference between the two compartments changes as a result

of elevation of IOP and/or reduction of CSFp.²⁶² Multiple studies have reported a highly significant reduction of CSFp in patients with glaucoma, compared to healthy eyes (minimum significance in these studies being $p < 0.001$).²⁵⁶⁻²⁵⁸ Therefore, a high translamellar pressure gradient (pressure difference) is associated with glaucoma and may disrupt or minimise the generation of SVPs.²⁶²

4.4 Current SVP detection techniques

4.4.1 Subjective techniques

SVPs were first assessed based on observer detection of whether the pulse is present or absent. The very first detection of SVPs was through direct observation by the use of an ophthalmoscope.²³⁶ Since then, advances in technology have allowed SVPs to also be subjectively assessed using video recordings of the retinal circulation using fundus cameras and OCT devices.²⁶³

4.4.2 Objective techniques

Ophthalmodynamometry and other changes to IOP (vein pulsation pressure)

In the early 1900's ophthalmodynamometry was introduced as a method for taking threshold measurements of the retinal arterial pulsations.²¹ This technique involved applying pressure (force) to the sclera, causing an increase in IOP, while observing through an ophthalmoscope, the retinal vessels over the optic nerve. The ophthalmodynamometric force was recorded as the point at which the applied pressure allowed the first observation of the pulsations. For example, if SVPs are visible without adding pressure, this force is recorded as zero. Vein pulsation pressure can be derived from ophthalmodynamometric force to calculate the induced IOP.^{264,265}

Advancements in ophthalmodynamometry have led to a contact lens systems that allow continuous force recordings as well as increased accuracy.^{21,266,267} Applying pressure (force) to the globe for short periods of time increases aqueous outflow and therefore IOP is physically lowered once the pressure is released.²⁶⁸ In contrast, aqueous suppressants have been used as an alternative to pharmacologically reduce IOP.²⁶⁹ Once IOP is sufficiently reduced, regular observations of the retinal circulation and of IOP are made until SVPs are

visible at which point the IOP is recorded as the endpoint and noted as the vein pulsation pressure.

Videography and image sequencing (retinal vein width assessment)

Videography of the retinal circulation can be used to assess vessel width measurements. The Dynamic Retinal Vessel Analyser (Imedos, Jena, Germany) is currently the only commercial-level device used to assess retinal vascular pulse properties. The device calculates vessel diameter at user-selected points along a vessel. Measurements are made at the transverse axis of vessels, perpendicular to the vessel orientation and therefore SVP amplitudes are measurements of the transverse diameter amplitude.^{237,270} This method only provides two dimensional transverse information without information about vessel depth along the axial dimension. However, mathematical simulations and previous research have demonstrated that the largest venous calibre change is along the axial direction, where there is a flattening of the retinal vein from round to flat or ribbon shaped (Figure 17).²⁷¹⁻²⁷³ Furthermore, this method is limited by its inability to measure vessels that have a transverse diameter measurement less than 90µm and when vessels have insufficient spacing between them.²⁷⁴

Alternatives to the aforementioned method are infrared and near-infrared image sequences. Some Spectralis OCT (Heidelberg Engineering) models allow for up to 30 seconds of videography of the fundus as well as inbuilt software that enables video stabilisation^{252,263,275} or application of principal component analysis²⁷³. These videos can be used to subjectively assess SVPs or to objectively quantify SVPs through manual measurements of the vessel at the transverse axis see in the video. The limitation of this method is the relatively low frame rate.²⁷⁶

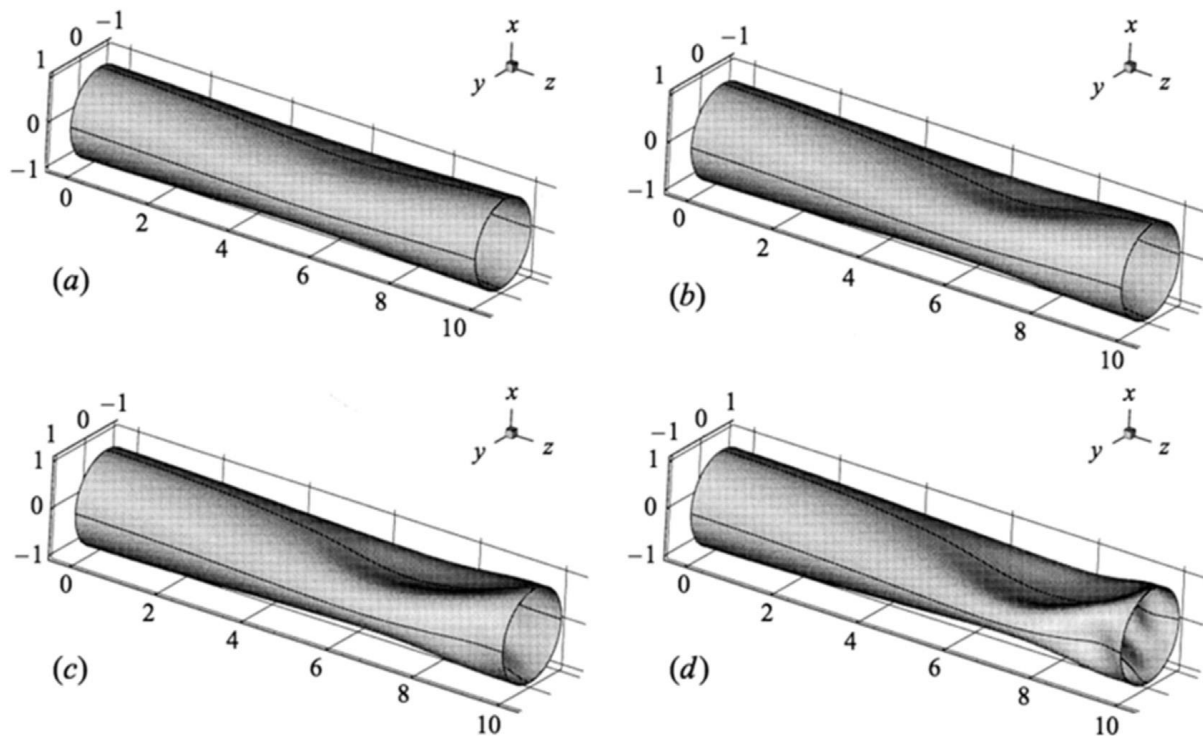


Figure 17. Mathematical model illustrating flattening of the retinal vein from round (a) to flat or ribbon shaped (d) along the z-axis at higher external chamber pressures. Image taken with permission from Heil (1997).²⁷¹

Vessel Mapping of Retinal Image Sequence is a method whereby a series of fundus images are taken at timed intervals to create a video sequence of the retinal circulation. This technique allows pulsatile changes to be measured along an identified vessel segment, compared to other techniques that are used to measure SVPs at a single point. Consequently, many other pulsatile features can be detected using this method, including serpentine movements, which are lateral movements of the vessels, as well as vessel displacement.²⁷⁷

Photoplethysmography and modified photoplethysmography

Photoplethysmography (PPG) detects changes in blood volume in vessels using a light source that illuminates the microvascular bed of tissue of interest. Changes in perfusion volume are detected in the form of varied intensities of reflected light detected by a photodetector.²⁷⁶ Modified photoplethysmography (mPPG) allows for assessment of retinal venous and arterial pulsations along the optic disc and vessels up to one disc diameter from the optic disc through fundus videography.²⁷⁸ The maximal light absorption of haemoglobin

is 550nm, which is also the maximal absorption of the green filter (colour channel) in digital cameras, forming the basis of mPPG.²⁷⁹ Vessel pulsations are detected as changes in absorption of light by the varying amounts of haemoglobin (carried by red blood cells) in the vessel of interest. The assumption that mPPG makes is that the absorption of light is predominantly from the haemoglobin and does not consider the effects of scattering.²⁷⁵ Changes in orientation of the red blood cells may cause significant changes in light absorption and these scattering characteristics have been widely reported in various studies.²⁸⁰⁻²⁸³ A combined approach of mPPG with OCT may be able to address these issues.²⁸⁴

5. Gaps in current literature and thesis outline

Reduced SVP amplitudes have been reported in glaucoma, however, where in the glaucoma disease continuum these changes present themselves is unclear. As described in section 3.3 of this literature review, it is thought that vascular changes may occur at the very early stages of the glaucoma continuum. If this holds true, SVPs have huge potential to be used as an early marker for glaucoma and may even be predictive of glaucoma progression. This potential is also supported by Balaratnasingam and colleagues' 2007 study that found that the ophthalmodynamometric force required to induce SVPs was a strong predictor of glaucomatous disease progression in a sample of glaucoma patients assessed over seven years,²⁸⁵ Absent SVPs have also been found to be predictive of glaucoma progression.²³⁵ As discussed in section 4.3 elevated venous pulsation pressure is higher in glaucoma compared to normal eyes, and VPP being even higher in patients with greater glaucomatous disease progression such as RNFL thinning and visual field defects¹⁶³ compared to venous pulsation pressure in eyes with less glaucomatous progression.^{233,260} There is a need to determine where in the glaucoma continuum these changes to SVPs present themselves in order to explore the possibility of SVPs being used as a potential biomarker for glaucoma screening in clinical practice.

Current devices that can be used to assess SVPs pose many challenges and limitations. These are described in detail in section 4.4 of this literature review. In summary, existing devices are significantly costly, with prices of some devices such as OCT being upwards of

\$100,000(AUD), immobile or not readily portable, with high sensitivity to positional and environmental changes and thus requiring adjustments to calibration, limited resolution and a high degree of technicality for use. These features deem current SVP detection unfeasible for screening outside metropolitan and in remote areas and for use in mobile clinics that service underprivileged and remote communities where there is likely to be many cases of undetected glaucoma.

Recent computer analysis of image sequences (or video frames) have been introduced to SVP analysis methods.^{269,286,287} A novel tablet-based ophthalmoscope will be explored in this thesis as a means of quantifying SVPs using video frames and computer analysis. In this method, fundus videoscropy is performed centred over the optic disc using a tablet attached to a 20D indirect ophthalmoscopy lens and raw images undergo computer analysis to assess SVPs along the transverse axis of the vessel of interest. The feasibility of this method has been described in detail in our paper titled "Objective quantification of spontaneous retinal venous pulsations using a novel tablet-based ophthalmoscope" which is presented in Chapter 3 and also addresses the advantages that this technique offers compared to some of the commercial devices listed previously.²⁸⁶

The ability to detect changes in SVP presence or changes in SVP amplitude can provide a means of assessing the outcomes of glaucoma treatment, whether pharmaceutical or surgical. A glaucoma patient reported to have no visible SVP was re-assessed 12 weeks after surgical glaucoma treatment (in the form of trabeculectomy) and was found to have visible SVPs.²¹ Furthermore, a reduction in IOP has been found to reduce venous pulsation pressure in glaucoma patients.²⁸⁸ These are encouraging reports that fuel the need for further investigation of SVPs as a means of conducting surveillance of the efficacy of glaucoma treatment.

This thesis aims to assess the effectiveness of a novel tablet-based ophthalmoscope to detect and quantify SVPs with the aid of computer analysis. SVPs are assessed in both patients with glaucoma and those who are glaucoma suspects. Following this, quantified SVPs will be examined alongside standard glaucoma clinical test outputs such as RNFL thickness and visual field results to assess correlations between the variables in order to

stage SVPs on the glaucoma continuum. These RNFL thickness and visual field results will also be used to calculate RGC count to further stage SVPs in glaucoma, using methods and formulas derived by Medeiros and colleagues, based on the work of Harwerth and colleagues.^{33,131,152}

This thesis will be presented in the following chapter sequence:

1. Introduction & Review of the Literature. (this chapter)
2. Materials & Methods.
3. Objective Quantification of Spontaneous Retinal Venous Pulsations Using a Novel Tablet-based Ophthalmoscope.
This chapter explores the use of the novel tablet-based ophthalmoscope on a small sample of patients with glaucoma to provide proof of concept of the technique and its ability to be used to detect and quantify SVPs in glaucoma.
4. Objective Assessment of Spontaneous Retinal Venous Pulsations in Glaucoma.
This chapter explores the distribution of SVPs in glaucoma and glaucoma suspects and establishes SVPs as a quantifiable dynamic vascular marker for glaucoma.
5. Spontaneous Retinal Venous Pulsations as a Vascular Marker for Glaucoma.
This chapter explores the relationship between SVP amplitudes and traditional clinical markers of glaucoma including RNFL thickness, visual field loss, IOP, and RGC count.
6. The use of Spontaneous Retinal Venous Pulsation Assessment in Distinguishing Glaucoma Sub-Types
This chapter explores how SVPs compare to common clinical markers including RNFL thickness, visual field loss, IOP as well as RGC count in distinguishing POAG from NTG and glaucoma suspects.
7. Longitudinal Changes in Spontaneous Retinal Venous Pulsations in Glaucoma.
This chapter explores the longitudinal changes in SVPs in glaucoma and glaucoma suspects.
8. Discussion and conclusions.

Chapter 2

Materials & Methods

Chapter Summary

The objective of this research was to establish the use of a novel tablet-based ophthalmoscope to detect and quantify spontaneous retinal venous pulsations in glaucoma. This novel technique was investigated due to the significant benefits that it holds compared to costly and non-portable devices, as described in Chapter 1. Therefore, this thesis required recruitment of suitable participants as well as collection, analysis and interpretation of the data collected. The following chapter is a detailed description of the methodology applied in this thesis.

1. Human ethics

Ethics approval was required for the use of human subjects in this investigation. Approval was granted in June 2017 by the University of Technology Sydney Human Research Ethics Committee (UTS HREC) before the commencement of participant recruitment and data collection (ETH17-1392). Additional ethics approval was obtained from the Human Research Ethics Committee of the University of New South Wales (UNSW; HC08-2014-36). All participants were provided with an information brochure (Appendix 1) about the study and informed consent (Appendix 2) was obtained from each participant prior to the commencement of the study. Data collection, analysis and communication throughout the thesis was performed in accordance with the UTS and UNSW HREC guidelines as well as the guidelines of the Tenants of Helsinki.

2. Participant recruitment

A total of 170 participants were recruited from three ophthalmic clinics in Sydney, Australia from July 2017 to March 2020. These were two Marsden Eye Specialists (MES) clinic locations (n=58), as well as the Centre for Eye Health (CFEH) at the University of New South Wales (n=112). Where possible, follow-up assessments were also conducted at the participants scheduled glaucoma review appointments between 6-12 months from their initial visit. A total of 30 participants had a second assessment. Eligibility criteria for inclusion were: age 18 years or over; patients consenting to the use of their clinical data for research; a diagnosis of glaucoma (open angle) or glaucoma suspect (either new or existing patients at the clinic); no diagnosis of diabetes and/or non-glaucomatous ocular pathology; no neurological comorbidities that would confound visual field assessment results; no history of ocular surgery apart from glaucoma laser treatment (including selective laser trabeculoplasty, peripheral iridotomy), minimally invasive glaucoma surgery, cataract surgery and intraocular lens implantation; no history of ocular trauma; spherical equivalent refractive error between ± 8.00 diopters (spherical equivalent) with no evidence of trial lens rim artefact on visual field assessment and clear ocular media with best corrected visual acuity better than 6/12. Six participants who had a diagnosis other than OAG or glaucoma

suspect (such as pseudoexfoliative (n=3) or pigment dispersion glaucoma (n=3) were excluded from analysis.

2.1 Clinical diagnosis and classification

Recent studies have suggested using the term “high-tension glaucoma” (HTG) to specify the diagnosis of primary open-angle glaucoma (POAG) with elevated IOP in contrast to normal tension glaucoma (NTG).^{289,290} In this thesis, the term “POAG” is used, in place of “HTG”, when referring to diagnosis in order to maintain consistency with the clinical notes that were obtained from participants.

Clinical diagnosis for each group was based on current glaucoma guidelines,^{291,292} including:

Confirmed open angle glaucoma

1. Definite characteristic glaucomatous structural anomalies at the optic nerve head (including, but not limited to increased cup to disc (CD) ratio, CD asymmetry, neuroretinal rim thinning and/or notching).
2. And/or: Definite RNFL anomalies corresponding to optic nerve head changes.
3. And/or a cluster of contiguous points of visual field deficit at the $p < 0.05$ level, Glaucoma Hemifield Test outside normal limits, and/or pattern standard deviation with $p \leq 5\%$.
4. Open anterior chamber angles.
5. NTG: Items 1-4 in the presence of IOP within normal limits (defined as 10-21mmHg on applanation tonometry at the time of diagnosis^{30,37}).
6. POAG: Items 1-4 in the presence of elevated IOP (defined as >21mmHg on applanation tonometry at the time of diagnosis^{30,37}).

All participants with confirmed glaucoma were following the appropriate glaucoma management regimen under the direction of the glaucoma specialists at each respective clinic, predominantly in the form of pharmaceutical treatment.

Glaucoma Suspect

1. Normal HFA results.
2. And/or suspicious appearance of optic disc or RNFL changes suggestive of glaucoma.
3. And/or elevated IOP (defined as >21mmHg on applanation tonometry^{30,37}).
4. And/or family history of glaucoma.
5. Not receiving treatment for glaucoma.

Clinical determinations were made by at least one clinician (one glaucoma specialist at MES and at least two examining clinicians at CFEH).

3. Power Calculation

In Chapter 3 (pilot study), a significant difference of 9% is observed in SVPs between POAG and glaucoma suspects. Furthermore, current models can only correctly predict $\leq 30\%$ of eyes that develop glaucoma.²⁹³ Considering previous studies that suggest visual fields deteriorate in 45% of treated glaucoma patients,⁴⁴ a sample size of 100 (50 in each group) will have a 90% power ($\alpha=0.05$) to detect a significant difference in vascular (SVP) and functional parameters (HFA and RNFL thinning) between glaucoma and glaucoma suspects. The sample size collected consists of $n=106$ glaucoma, and $n=64$ glaucoma suspects, which is greater than the minimum number required, allowing for some group asymmetry.

4. Data breakdown per chapter

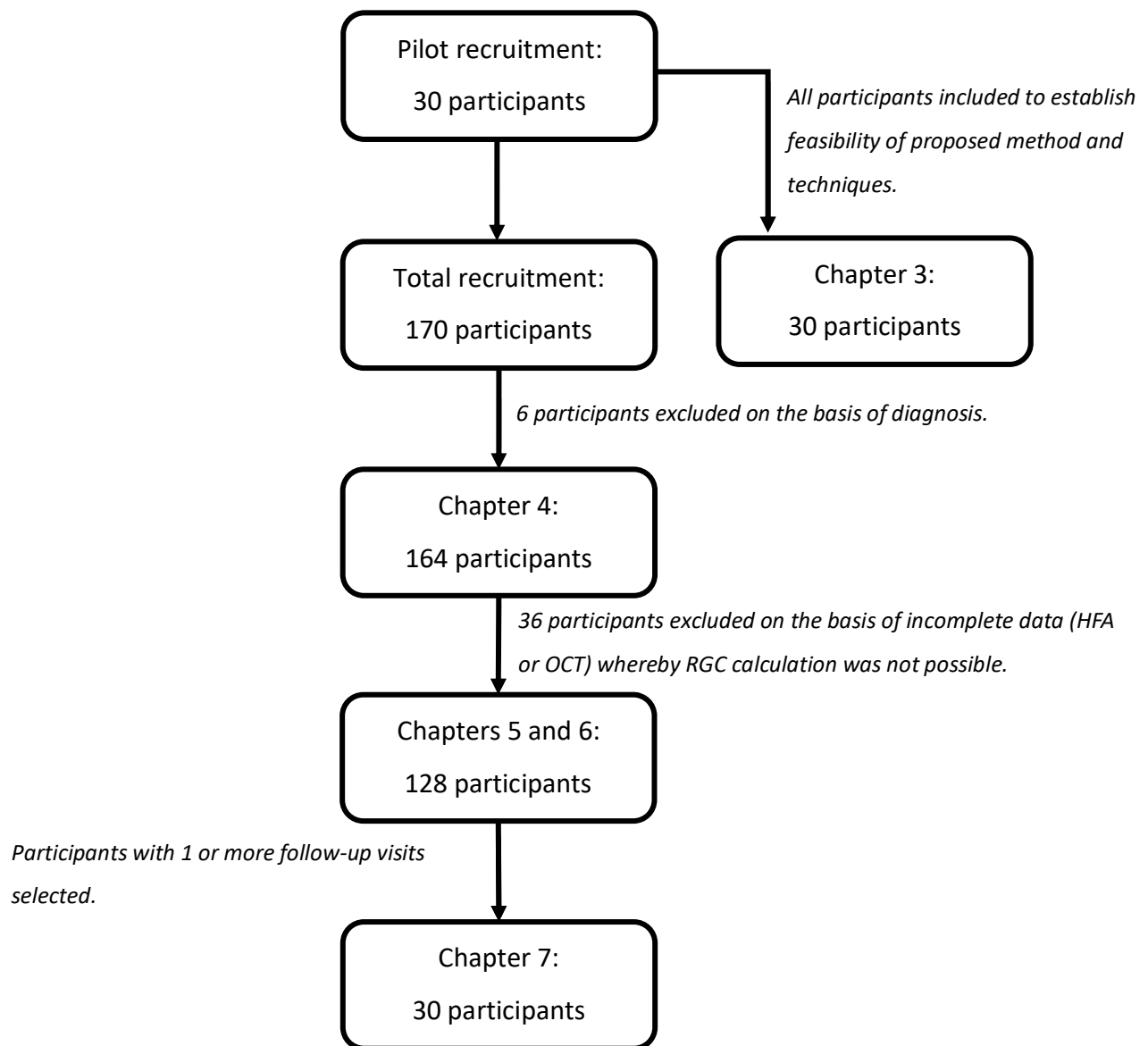


Figure 18. Flow diagram of data collected and used in each chapter of this thesis.

5. Data collection

5.1 Standard ophthalmic workup

Participants had a full ophthalmic workup at MES and CFEH by either a qualified orthoptist or optometrist (respectively) as well as an ophthalmologist (glaucoma specialist) at MES and CFEH. This workup included patient history including a medical history questionnaire (Appendix 3) and best corrected visual acuity assessment at each visit. Where possible, static visual field assessment using the Humphrey Visual Field Analyser (HFA; HFA II-i series or HFA III, using the 24-2 SITA-Standard, SITA-fast or SITA-fastest strategy using a white Goldmann size III stimulus over the 24-2 test grid) and Optical Coherence Tomography (OCT) using either the Spectralis OCT (Heidelberg Eye Explore version 1.10.20 using the retinal nerve fiber layer (RNFL) algorithm; n=96) or the Cirrus HD-OCT (version 5.2.1.12 Optic Disc Cube 200x200; n=68) were conducted at the same visit or at a maximum of 12 months from their assessment. Reliability metrics of interest for HFA assessment were false positive rates (FPR; where possible this value was maintained at <20%). False negative rate (FNR) was not used as an index of reliability as they are elevated in disease.²⁹⁴ Where possible IOP assessment using applanation was also conducted at the same visit.

5.2 Retinal videoscscopy (SVP recording)

At the same visit, all subjects had a dilated (1% Tropicamide (Mydracyl)) 10 second videoscscopy of venous circulation at the optic nerve head using the tablet-based 20D-ophthalmoscope using the ProMovie video camera application on an iOS operating device (iPad Mini4, Apple Inc.). The tablet has a protective case with a tubular attachment between the camera and an indirect 20D lens (as seen in appendix 4a and 4b). The body of the device extends perpendicular from the tubular attachment, enclosing the electrical components, which can be used as a handle to grasp for handheld use, or can be mounted on a slit lamp. In brief, the tablet-based ophthalmoscope was mounted on a slit lamp to maximize stability in this study and all videos were taken at 2.2x zoom with tailored adjustments of focus and exposure to maximize the visibility of vessels. Detailed methodology on SVP assessment is reported in Chapter 3.

5.3 Data management

Data was recorded, collated and sorted on Microsoft Excel 2016 to create spreadsheets for data management.

5.4 SVP quantification

Chapter 3 of this thesis details the SVP quantification process. In summary, each SVP recording was exported from the tablet to a computer and quantified using Image J (previously National Institutes of Health (NIH) Image).²⁹⁵ A summary of the image enhancement process using Image J is presented in Figure 19, taken from Chapter 3.

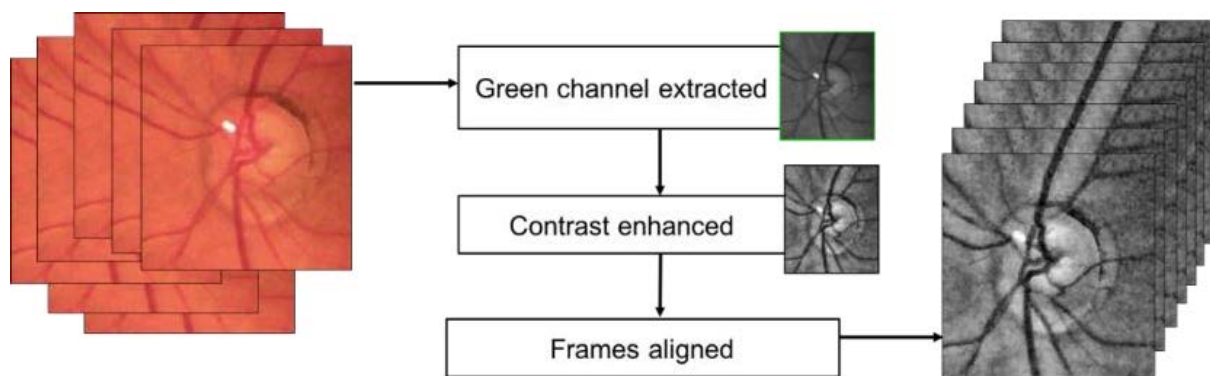


Figure 19. Schematic of image enhancement process using Image J. Image taken from Chapter 3.

Following image enhancement, vessels were manually selected for measurement at the CRV or the closest point to the CRV when it was not visible. Measurements were made perpendicular to the vessel orientation using a method described by Fischer and colleagues (2010).²⁹⁶

A quantified SVP trace was created using the measurements of each vessel. This information was used to calculate the percentage pulse to reveal the SVP amplitude of each participant at each visit. Detailed calculations are presented in Chapter 3.

5.5 Retinal ganglion cell estimation

OCT, HFA data and age were used to calculate RGC estimates. The equations used to estimate RGCs are from the methodology proposed by Medeiros and colleagues^{131,152,297}

based on the work of Harwerth and colleagues³³. An in-depth presentation of formulas used and reasoning is reported in Chapter 5.

5.6 Staging glaucoma

Hoddap-Parrish-Anderson criteria for HVA progression was used to assess glaucoma stages, as summarised below: ²⁹⁸

Early glaucoma:

- MD less than -6dB
- <25% of points depressed below the 5% level, and <10 points depressed below the 1% level on the pattern deviation plot (PDP)
- All points in the central 5° have ≥15dB sensitivity

Moderate glaucoma:

- MD less than -12dB
- <50% of points depressed below the 5% level and <20 points depressed below the 1% level on the PDP
- No points in the central 5° have 0dB sensitivity
- Only 1 hemifield with a point with <15dB sensitivity within central 5°

Severe glaucoma:

- MD greater than -12dB
- >50% of points depressed below the 5% level and >20 points depressed below the 1% level on the PDP
- ≥1 point in the central 5° have 0dB sensitivity
- Both hemifields have points within the central 5° with a <15dB sensitivity

6. Statistical analysis

Data was collected from the right eye of each participant and used for analysis throughout this thesis. The intention of doing so was to maintain consistency and avoid confounding effects that may have arisen due to potential differences in blood flow between left and right eyes.

Descriptive statistics are used throughout this thesis including means and standard deviations (mean \pm standard deviation). Normality of the data was evaluated using the D'Agostino & Pearson test. When comparing the means between two groups, student's t-test was used to determine statistical significance. When comparing means in three groups (Chapter 4), one-way analysis of variance (ANOVA) was used to determine statistically significant differences. A significance cut off of $p < 0.05$ was used for all statistical analysis.

In Chapter 5, linear regression was used to assess the relationship between various parameters and a generalised linear mixed model was used to assess the power of each of the correlations studied. Pearson correlation was used to quantify correlation coefficients.

In Chapter 6, the different diagnoses were distinguished by measuring the area under the receiver operating characteristic curve (AUROC). Pair-wise differences were evaluated by assessing the confidence interval and standard error of the difference between the two AUROCs of interest. This method has been described in detail by DeLong and colleagues.²⁹⁹

In Chapter 7, longitudinal changes in SVPs were assessed by plotting symmetrized percentage of SVP change against the SVP amplitude at visit 1. This is method described by Berry and Ayers (2006).³⁰⁰ Analysis of covariance (ANCOVA) was then used to assess the difference in slopes of the linear regression. This is described in detail in Chapter 7.

Statistical analysis was performed using SPSS (IBM SPSS Statistics 27), on Microsoft Excel 2016 and Graphpad prism (La Jolla, CA, USA).

Chapter 3

Objective Quantification of Spontaneous Retinal Venous Pulsations Using a Novel Tablet-based Ophthalmoscope

Published as:

Shariflou, S., Agar, A., Rose, K., Bowd, C. and Golzan, S.M., 2020. Objective quantification of spontaneous retinal venous pulsations using a novel tablet-based ophthalmoscope. Translational Vision Science & Technology, 9(4), pp.19-19.

Chapter Summary

This chapter explores the use of the novel tablet-based ophthalmoscope on a small sample of patients with glaucoma to provide proof of concept of the technique and its ability to be used to detect and quantify SVPs in glaucoma.

1. Introduction

Spontaneous retinal venous pulsations (SVPs) are changes in caliber of the retinal veins at the optic nerve head, usually at the hemi-veins of the central retinal vein as they join to form the central vein, or where it exits at the lamina cribrosa.²³² The mechanism by which SVPs occur is complex. Intraocular pressure (IOP), retinal venous pressure (RVP) and cerebrospinal fluid pressure (CSFp) are all thought to play a role in their generation. These factors create a pressure gradient between the intraocular and retrobulbar spaces which is said to be the main driver in the generation of SVPs.^{256,301} Reduced or absent SVPs have been reported as a risk factor for glaucoma and its progression,^{163,233,235} with absent SVPs reported in up to approximately 50% of glaucoma subjects.²³³ These findings may be due to elevated RVP, reduced ocular blood flow^{161,162} and/or lower mean CSFp compared to non-glaucomatous patients, which can decrease the amplitude of SVPs.²⁵⁷ Other identified factors known to reduce SVPs are the combination of elevated CSFp and reduced IOP, which can decrease the intravascular pressure gradient.^{228,233,237,245,302}

The first record of SVPs were from Coccius in 1853, using the newly invented direct ophthalmoscope.²³⁶ By the 1920's, SVPs were measured using ophthalmodynamometry, which involved applying digital pressure to the eye resulting in an increase in IOP enabling the visualization of SVPs. The minimum force required to induce SVPs, referred to as ophthalmodynamometric force, was used to quantify SVP.²⁶⁴ Both these methods are subjective and dependent on observation and therefore are disposed to bias and inconsistency. Other factors that may contribute to unreliability in these methods include inter-observer variation, the presence of microsaccades and/or fixation nystagmus and variations in the ophthalmoscope lens power used. Hence, recent studies have focused on developing objective measures of SVP that are able to quantify the presence and degree of SVPs, rather than the subjective binary classification of present or absent. These methods have included quantitative techniques of vessel diameter measurement,²³⁷ lateral displacement of the blood vessels²⁷³ and haemoglobin concentration.²³⁸

The Dynamic Vessel Analyzer (DVA) is an optical-based device used to measure SVP pulsatility along vessel markers based on processing algorithms, producing a continuous SVP

trace. A recent study compared subjective and objective methods of SVP detection using indirect ophthalmoscopy (75D lens) and DVA methods, respectively.¹⁶³ The authors reported subjective SVP detection in only 64.1% of glaucoma subjects when indirect ophthalmoscopy assessment was conducted. In comparison, SVPs were objectively detected in all subjects using the DVA, including those with advanced glaucoma whom have previously been reported as having absent SVPs.¹⁶³ This demonstrates the increased accuracy in SVP detection through objective means.

The use of dynamic imaging (i.e. real-time retinal videography) has previously been used to determine SVP amplitude successfully.^{20,237,287} This study introduces a novel approach to real-time videography and SVP analysis using a tablet (iOS operating system) with an add-on 20D binocular indirect ophthalmoscope lens. Previous methods of SVP analysis have been performed using costly, non-portable devices. This tablet-based ophthalmoscope is both portable and not costly and records the retinal blood vessel pulsatility while maintaining a relatively high frame rate of 30 frames per second. While devices such as the Heidelberg-Spectralis Optical Coherence Tomographer (OCT) have better image quality, they are limited by lower frame rate, mobility and ease of use. The modern DVA technology developed specifically for videography and assessment of retinal vasculature is also non-portable and limited by contrast requirements, where blood vessels do not have sufficient contrast against the retina in some cases, hindering vessel edge detection.²⁷⁰ Our novel approach to videography and SVP analysis address these issues.

2. Methodology

2.1 Data collection

30 participants (average age 71.8 ± 9.7 years; 14 males) were recruited for this study, including 21 with confirmed glaucoma and 9 with suspected glaucoma. Subjects were selected from an ophthalmology clinic and not included if they had diabetes and/or if the patients had current or previous vascular or retinal pathology. All had a standard ophthalmic examination, including medical history, visual acuity corrected with glasses if worn, IOP measurement using Goldmann tonometry and Humphrey Visual Field assessment (HFA; HFA

II-i series, Operating system 5.1) using 24-2 SITA-Standard strategy and stimulus size III (white).

Optic nerve imaging was carried out on OCT, using either the Spectralis OCT (Heidelberg Eye Explore version 1.10.20 using the retinal nerve fiber layer (RNFL) algorithm) for 25 subjects, including eight glaucoma suspects or the Cirrus HD-OCT (version 5.2.1.12 Optic Disc Cube 200x200) for five subjects, one of whom was a glaucoma suspect. All subjects at the same visit had an additional dilated (1% Tropicamide (Mydriacyl)) 10 second videoscropy of venous circulation at the optic nerve head using the tablet-based 20D-ophthalmoscope,

Glaucoma was diagnosed in the presence of definite glaucomatous optic neuropathy and/or visual field defects with mean deviation (MD) ranging from -9.52 to -1.57dB and progressive change in either assessment. Progressive change was established using a minimum of one past assessment and comprehensive assessment was undertaken by an experienced glaucoma specialist (AA), combining conventional indirect ophthalmoscopy, OCT RNFL analysis (Heidelberg Spectralis) and Hoddap-Anderson criteria for HFA progression.²⁹⁸

Glaucoma suspects were defined as having elevated IOP, defined as >21mmHg on applanation tonometry at the time of diagnosis^{30,37}, or suspicious appearing optic disc with no progressive changes in either, and a normal visual field with MD range -1.88-0.59dB, assessed on examination by AA.

2.2 Retinal Videoscropy

Retinal videoscropy was performed using the ProMovie video camera application on an iOS operating device (iPad Mini4, Apple Inc.). Imaging settings such as exposure and focus were adjusted manually as required for each subject to ensure maximum contrast of the optic nerve head and retinal vessels. Videos were taken centered on the optic disc and digital zoom was maintained at 2.2x across all participants to ensure consistency. Participants were instructed to refrain from blinking while a 10 second photographic video was recorded. Although the tablet-based ophthalmoscope is designed for hand-held use, for the purpose of video stability, a slit lamp mount was used. Images of the device set-up are included in Appendix 4a and Appendix 4b.

An additional five healthy individuals were recruited to determine the reproducibility and intra-individual variability of the device. Each individual had retinal videography performed three times, each at 10-minute intervals.

2.3 Data analysis

The digital video recordings were saved and exported as individual frames to an image-analysis program, ImageJ (previously National Institutes of Health (NIH) Image).²⁹⁵ To enhance visibility of the vessels, the color channels of each frame were split, extracting the green channel to reveal the highest contrast of retinal vasculature.³⁰³ A contrast equalization plugin (CLAHE; ImageJ) was then applied to each frame enhance image contrast for greater accuracy in the detection of vessel borders, as seen in Figure 20. All other parameters such as block size, histogram bins and max slope were kept constant across all videos.

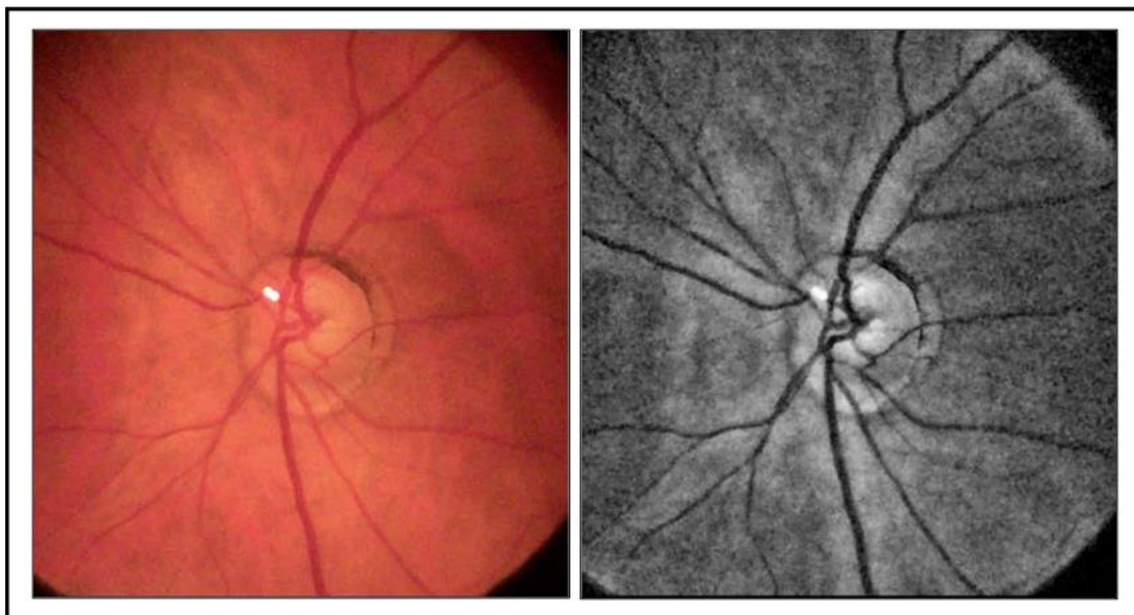


Figure 20. Magnified frames from an SVP video (left eye) from a 68 year-old female captured using a 20D tablet-based ophthalmoscope. Left image is a magnified original frame. The right image is the green channel of the same frame with CLAHE application.

The frames were then aligned to eliminate ocular movements such as those arising from fixation nystagmus or decompensation. For this, the optic disc in the first frame of the video was manually selected and used as a reference for the entire video. Normalised correlation coefficient was then used as the matching method - this function detects the landmark or the most similar image pattern in every slice (in this case the optic nerve). Each slice is adjusted to align the landmark pattern to keep it in the same position throughout the stack. More specifically, the algorithm compares each frame against the reference region of interest (the optic disc) by sliding, i.e. moving the patch one pixel at a time (left to right, up to down) (Figure 21). The algorithm was implemented in the ImageJ software using the “template matching” plugin.

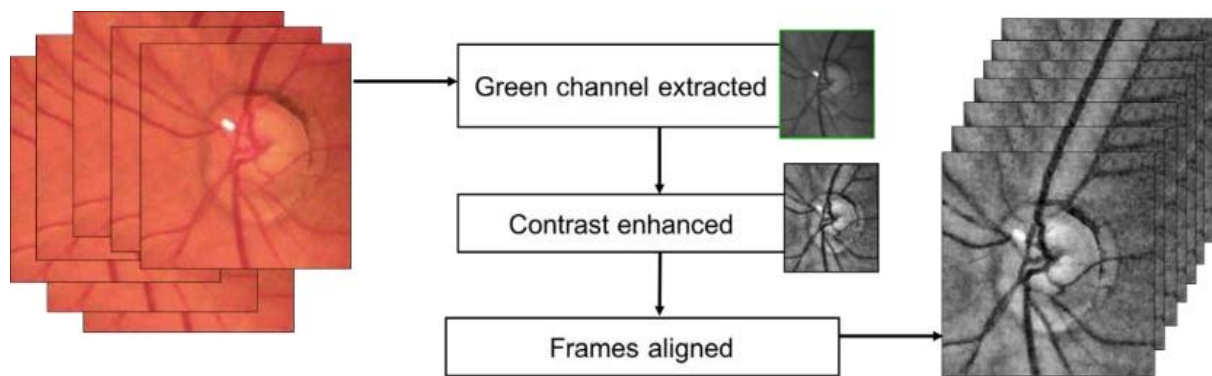


Figure 21. Schematic of image enhancement process using Image J.

The vessels were selected for measurement by an Orthoptist (SS) at the central retinal vein (CRV) where possible. When the CRV was not visible (anatomical variations), the closest point to the CRV at the optic disc was selected for measurement. A manual selection was made along the transverse axis of the vessel, perpendicular to the vessel orientation. All vessel calibres were measured at the vessel of interest, using a method described by Fischer and implemented in Image J.²⁹⁶ In brief, the inner vessel diameter is estimated based on the red blood cell column using a full width at half-maximum algorithm. The diameter of the selected vessel is measured five times in each frame of the video. These five measurements were made using the ImageJ Vessel Diameter plugin algorithm that takes one measurement along the user-defined line (vessel diameter selection) and two measurements on both sides of the line, shifted either one or two pixels parallel to the line.²⁹⁶ A moving average window

of three is then applied to obtain vessel diameter at the selected location on each frame of the video. These measurements were then exported to an excel spreadsheet for analysis. To remove baseline wandering, a moving average algorithm of three points was also applied.

The frame-by-frame change in diameter was plotted against time, producing a quantified SVP trace (Figure 22). SVP amplitude was then determined using a two-step calculation, utilizing the percentage change in vessel caliber to eliminate the effects of vessel size variation between individuals, ensuring that any changes observed in vessel pulsatility are driven by pathophysiological changes rather than inter-individual vessel diameter variation. Firstly, the change in average venous diameter (Δ venous diameter) of each participant was calculated as $\frac{\text{peak-trough}}{\text{meanveincaliber}}$. This information was then used to calculate the average percentile pulse, calculated as $\frac{\text{averageSVPamplitude} \times 100}{\text{meanveincaliber}}$ to reveal the SVP amplitude of each individual.

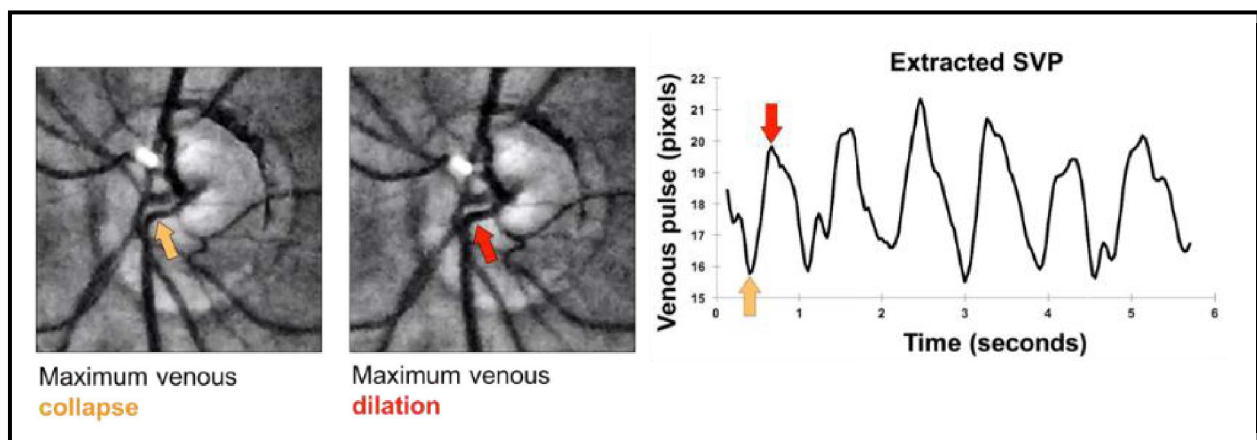


Figure 22. Left images: Two magnified, cropped and enhanced frames from the same eye at 7 frames apart (approximately 0.25 seconds). The yellow arrow points to the vessel location at maximum venous collapse and the red arrow points to the vessel location at maximum venous dilation. **Right image:** Corresponding SVP trace with yellow and red arrows indicating resultant troughs and peaks.

Graphpad prism (La Jolla, CA, USA) was used for data analysis and visualization. Linear regression was applied to visualise the strength of correlations alongside use of Pearson

correlation tests to quantify the correlation strength and statistical significance (significant at the $p < 0.05$ level; 2-tailed). Descriptive statistics were also conducted to reveal the basic distribution of the data.

2.4 Ethics

This study was performed in accordance with the guidelines of the Tenets of Helsinki and approved by the University of Technology Sydney's Human Research Ethics Committee. Written consent was obtained from each subject following an explanation of the nature of the study.

3. Results

The average age of participants was 72 ± 10 years, with glaucoma patients having a significantly higher average age (75 ± 8 years) compared to glaucoma suspects (64 ± 9 years). A summary of patient demographics and mean values for IOP, global average RNFL and HFA is presented in Table 2.

Table 2. Patient Demographics and mean values.

	Glaucoma	Glaucoma suspects	<i>p</i> -value
Gender	9 male	5 male	
Age	75.2 ± 8.3	64.0 ± 8.6	<0.001
IOP (mmHg)	13.9 ± 3.2	16.2 ± 4.2	0.1
RNFL (μm)	80.9 ± 18.1	76.2 ± 16.4	0.5
HFA MD (dB)	-3.5 ± 3.0	-1.9 ± 1.8	0.1

3.1 SVPs were identified in 100% of patients when assessed objectively

Raw videos of retinal circulation were first observed before computer analysis. SVPs were visible to the naked eye in 67% of glaucoma suspects and 62% of patients with confirmed glaucoma. However computer analysis revealed the presence of SVPs in 100% of participants in both groups, with a mean SVP amplitude of $40\% \pm 10\%$ across glaucoma and

glaucoma suspects. Mean SVP amplitudes were significantly lower ($p=0.03$) in suspects ($34\% \pm 6.7$) compared to those with a confirmed diagnosis of glaucoma ($43\% \pm 10.7$).

3.2 SVPs are correlated with RNFL thickness

Data was pooled data from both glaucoma and glaucoma suspects and linear regression was used to study the association between SVP amplitudes, RNFL thickness and HFA MD. We found a positive and significant correlation between SVP amplitudes and RNFL thickness ($p=0.006$, $r=0.49$) (Figure 23). A similar positive association between HFA MD and SVP amplitude across all participants were observed, however, this was not statistically significant ($p=0.58$, $r=0.10$).

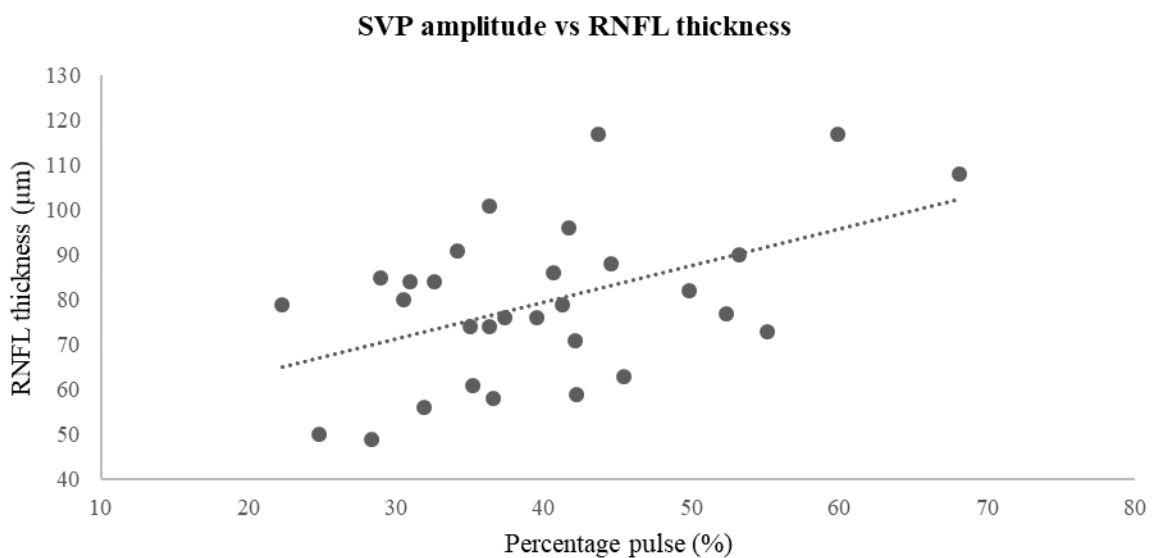


Figure 23. Correlation between SVP amplitude and RNFL thickness ($p=0.006$, $r=0.49$).

3.3 SVP measures are reproducible using the tablet-based ophthalmoscope

The average age of healthy participants recruited for the feasibility study was 27 ± 5 years. The average overall SVP percentile pulse was $12\% \pm 3\%$ across all measurements. The standard deviation of SVP variability for each individual varied from 0.2% - 3.7% with an overall average standard deviation of 2.6% for each participant that was not significantly significant (One-way ANOVA; $p=0.68$).

4. Discussion

In this study, we explored the use of a novel tablet-based ophthalmoscope to objectively detect and quantify SVPs. We also investigated the relationship between SVP amplitudes and other established structural and functional assessment parameters for glaucoma (RNFL thickness and HFA MD). Our results showed that using a tablet-based digital ophthalmoscope, we were able to visualize and quantify SVPs in all participants.

Furthermore, consistent with our previous findings,¹⁶³ we observed a positive correlation between SVP amplitudes and RNFL thickness. Further studies of SVP assessment are required to determine the sensitivity and specificity of SVPs in glaucoma diagnosis and also to explore the addition of SVP assessment as a parameter for glaucoma risk evaluation.

Previous studies of blood vessel width measurement using devices such as the DVA have demonstrated difficulty in taking measurements at the optic nerve head due to image contrast limitations, particularly the reflectivity reported at the optic nerve or lamina cribrosa.²³⁷ Furthermore, the DVA is limited by the need for steady fixation.²⁷⁰ The ProMovie application used in this study overcomes these limitations by allowing live adjustment of image exposure to overcome image contrast and reflectivity issues, allowing reliable measurements of both the optic nerve head and retina. Our custom-written algorithms also address the issue of unsteady fixation. Other advantages of the tablet-based ophthalmoscope used in this study compared to other devices used in previous studies are summarized in Table 3. Although this novel device does not have a gold standard to compare against, our feasibility results show that the numbers obtained for SVPs are testable against current gold standard glaucoma assessments.

Table 3. Comparison of SVP detection devices.

	Ophthalmoscope			Heidelberg-Spectralis OCT	Dynamic Vessel Analyser (DVA)
	Tablet-based	Direct (traditional)	Indirect		
Portability	✓	✓	✓	×	×
Lens strength (D)	20	5	Varied	20	
Approximate cost of device (AUD)	1700	≥ 600	≥ 2500	~120,000	Add-on to Heidelberg Spectralis OCT
Ease of use	Technical training required	Medical training required		Technical training required	
Dilation required	✓	✓	✓	×	✓
Frame rate (fps)	30	n/a	n/a	15	25
Resolution	77µm/pixel	n/a	n/a	10µm/pixel	
Field of view (degrees)	46	5	Varied	25-35 ³⁰⁴	

Consistent with previous studies that have compared subjective and objective means of SVP detection,¹⁶³ this study demonstrates greater detection of SVPs through objective means. SVP amplitudes are often difficult to identify with the naked eye, with reduced amplitudes being below the limits of resolution by the naked eye. This may explain the results of studies that have used subjective means of SVP detection and have detected fewer SVPs in their glaucoma subjects compared to healthy subjects.^{233,305}

Contradictory to previous findings and other reports, we found greater SVP amplitudes in glaucoma patients than in glaucoma suspects. While this is a surprising finding, a previous study conducted by Ren *et al* found abnormally low CSFp in glaucoma patients with normal baseline IOP. This exaggeration of the translaminal pressure gradient causes an exaggeration of SVPs. While baseline IOP, i.e. IOP pre-treatment, was not reported in this study, Ren *et al*'s study provides a possible explanation of the current results.²⁵⁶ A study investigating SVP in glaucoma patients with normal baseline IOP and those with elevated baseline IOP before and after medical treatment is required to further unravel the findings of this study. Secondly, the number of glaucoma suspects was considerably lower than those with a glaucoma diagnosis (n=9 vs 21), and hence the results we have observed may not necessarily be completely representative. Thirdly, it has been reported that SVPs are more frequently observed in older age groups.²⁵⁴ This may also be a contributing factor, given that the average age of patients with a glaucoma diagnosis was higher than glaucoma suspects. Finally, given the positive correlation between SVP amplitudes and RNFL thickness, reduced SVPs are expected with thinner RNFLs. Hence, the difference may simply be due to lower mean RNFL thickness in glaucoma suspects.

It is well known that glaucoma is associated with RNFL thinning, however,^{163,233,235} contrary to previous reports, we found thinner RNFL in glaucoma suspects than in glaucoma patients. Previous investigations of retinal blood flow and RNFL thickness have revealed increased ocular blood flow in regions of RNFL thinning in the early stages of glaucoma,¹⁶⁰ with a progressive decline in ocular blood flow observed with increasing glaucoma severity.¹⁶⁰⁻¹⁶² A study investigating the effect of glaucoma on SVP amplitude found reduced SVP amplitudes in retinal sectors with greater RNFL loss. The authors also report significantly smaller SVP amplitudes and RNFL thickness in glaucoma patients compared to normal controls

($p < 0.0001$). The study also investigated individual quadrant analysis of the RNFL (i.e. superior, inferior, nasal and temporal regions of the RNFL surrounding the optic nerve) and determined positive correlations between SVP amplitude and RNFL thickness.¹⁶³

In our study cohort, only three participants with confirmed glaucoma had moderate glaucoma, the majority had early stage glaucoma²⁹⁸ and may have less damage to the RNFL than is normally observed in larger cohorts of patients with a diagnosis of glaucoma. Larger sample sizes with even distribution between the groups are needed to reflect the true RNFL distribution expected. The discrepancy could also be due to different OCTs used – Leite *et al* demonstrate thinner measurements on the Cirrus OCT compared to the Spectralis OCT ($p < 0.001$).¹³⁸ Faghihi *et al* also found similar results but demonstrated a significant relationship between inter-measurement differences.³⁰⁶ A separate analysis was conducted using only the measures obtained from the Spectralis OCT which was found to exacerbate the difference in RNFL thickness between the groups (mean RNFL thickness was $2.2\mu\text{m}$ greater and $3.8\mu\text{m}$ thinner in the glaucoma and glaucoma suspects groups respectively). A similar analysis was not performed on just the Cirrus OCT results as our participant numbers are too small for statistical comparison with just one participant in the glaucoma suspect group. This participant however, had a thicker average RNFL than the average RNFL thickness in the participants with glaucoma ($91.00\mu\text{m}$ and $73.60\mu\text{m} \pm 10.69\mu\text{m}$ respectively).

Assessment of visual fields are routine in clinical glaucoma practice. It is the major indicator of functional impact of glaucoma in one's quality of life,^{307,308} and results are key in influencing management options.³⁰⁹ Previous studies have demonstrated that worse visual field MD is associated with lower frequency of SVPs in glaucoma.³¹⁰ While the correlation we observed between SVP and HFA MD in our small sample of participants was not significant, future studies using larger sample sizes may reveal stronger correlations that align with previous studies.³¹⁰

Our results demonstrate that the use of a portable and easy-to-use device in detecting and quantifying SVPs is possible and very promising. Further research is necessary to determine the comparability of SVP analysis using this novel technique and established SVP analysis tools and methods, such as the DVA. If these projected studies demonstrate good

comparability between devices, it can be proposed that using a tablet-based ophthalmoscope is a more feasible approach to SVP analysis. Furthermore, it will be useful to establish normal age-related changes in SVP amplitude. Studies have looked at the effect of aging on presence of SVP, however there have been no studies establishing the normal distribution of SVP amplitude with age.²⁵⁴

In conclusion, this study has provided proof of principal that using a 20D binocular indirect ophthalmoscope lens in conjunction with a smart digital hardware may be a feasible means of detecting SVPs and can be used for SVP analysis. There is significant potential for future use of the device given its relatively inexpensive, easy-to-use and portable nature. Future studies with larger sample sizes may resolve the apparently contradictory findings regarding glaucoma suspects.

Chapter 4

Objective Assessment of Spontaneous Retinal Venous Pulsations in Glaucoma

Chapter Summary

Thus far, it has been shown that using tablet-based ophthalmoscopy can objectively detect and quantify spontaneous retinal venous pulsations (SVP). In this chapter, using the technique presented in chapter 3, the distribution of SVPs in normal tension and open angle glaucoma, as well as glaucoma suspects is studied. It was hypothesised that SVPs can be detected in all patients with confirmed glaucoma as well as those who are glaucoma suspects. This establishes SVPs as a quantifiable dynamic vascular marker for glaucoma. In this chapter, it is determined that SVP amplitudes appear to be related to glaucoma subtypes, with NTG displaying the greatest amplitudes than other glaucoma diagnoses.

1. Introduction

Spontaneous retinal venous pulsations (SVPs) are seen as rhythmic fluctuations of the central retinal vein calibre or fluctuations at its bifurcation over the optic nerve head.²¹ The phenomenon has previously been reported to be reduced or absent in patients with glaucoma, particularly when assessed subjectively.^{163,233,238} This may indicate a disruption or alteration in blood flow at the optic nerve, that is reported to cause ischemic damage of the RGCs, potentially initiating the cascade of glaucomatous damage.^{158,159} A factor that plays an important role in this cascade of glaucomatous damage is optic nerve hypoperfusion.^{158,159,311,312} Perfusion pressure is the difference in pressure between the arterial and venous blood supply and is reported to be reduced in glaucoma.³¹³ Therefore, SVPs in un-treated glaucoma are expected to be reduced compared to healthy eyes and some cases of treated glaucoma, which is in line with reports of reduced SVP visibility in glaucoma.^{163,233,238} Intraocular pressure (IOP) is an important risk factor in glaucoma^{29,44-47} and it is also the primary modifiable risk factor for glaucoma progression.³⁰ Lowering IOP has been reported to increase perfusion pressure, therefore improving blood circulation at the optic nerve head in glaucoma.²⁶⁰ Moreover, elevated IOP as well as significant reductions in cerebrospinal fluid pressure in glaucoma²⁵⁶⁻²⁵⁸ can have a significant influence upon the translaminar pressure difference (10mmHg) between the intraocular and retrobulbar spaces.^{21,223,230,231} This pressure difference is thought to be a major driver of SVPs, which coupled with glaucoma-specific pathological changes can reduce the visibility of SVPs.²⁶²

Normal tension glaucoma (NTG) is a sub-classification of glaucoma where patients have IOP within the normal range, however the pathogenesis and progression of NTG is also heavily affected by disruptions to normal ocular blood flow.³¹⁴ Glaucomatous optic neuropathy can still be progressive and irreversible in these patients, regardless of their normal IOP status. Moreover, studies have found pronounced impairment in vascular autoregulation in patients with NTG compared to patients with high tension glaucoma, particularly in progressive NTG compared to stable NTG.^{315,316} A study conducted by Pinto and colleagues (2013) investigated the presence of SVPs in NTG and primary open-angle glaucoma (POAG).

They found a greater decrease in SVP visibility in NTG compared to POAG, with increased disease progression.³¹⁷

While previous studies have reported an absence of subjectively assessed SVPs in some glaucoma patients,^{163,233} this study aims to objectively assess SVPs in normal tension and open angle glaucoma as well as glaucoma suspects. It is hypothesised that by taking an objective approach, SVPs can be detected in all groups in varying degrees due to pathological implications of the disease on SVPs.

2. Methods

2.1 Data collection

The right eyes from 164 participants, including 64 with POAG, 37 with NTG and 63 with suspected glaucoma were included in this study. Subjects were recruited from two ophthalmic clinics with an exclusion criteria of a history of diabetes and/or vascular or retinal pathology. A dilated 10 second video of the venous circulation at the optic nerve head was recorded using a tablet-based ophthalmoscope and pupil dilation using a single drop of 1% Tropicamide (Mydracyl). Visual acuity and IOP, using applanation tonometry, was also performed and documented.

2.2 SVP Quantification

A detailed description of using a tablet-based ophthalmoscope to capture and analyse retinal videos to quantify SVPs has been published and presented in Chapter 3 of this thesis (Shariflou et al, 2020).³¹⁸ In brief, videoscropy of the retinal circulation at the optic nerve was performed on all eyes using an iOS-operating device with an attached add-on 20D indirect ophthalmoscopy lens. Data on SVPs were quantified by exporting individual video frames, adjusting image contrast and stabilizing frames to eliminate eye movements. The central retinal vein diameter, or the closest visible vein was measured at the same place in each frame and plotted against time.

Descriptive statistics including means and standard deviations were conducted and analysed for all eyes. One-way analysis of variance (ANOVA) was used to determine statistically significant differences between means in the three groups. Student's t-test was used to compare means between two groups. A significance cut-off of 5% was used for all statistical analyses. ImageJ (previously National Institutes of Health (NIH) Image) was used for objective quantification of SVPs as detailed in Chapter 3.²⁹⁵. Data analysis and visualisation was performed using GraphPad Prism (CA, USA).

2.3 Ethics

This study was performed in accordance with the guidelines of the Tenets of Helsinki and approved by the University of Technology Sydney and University of New South Wales Human Research Ethics Committees. Written consent was obtained from each subject following an explanation of the nature of the study.

3. Results

Retinal videos were collected from one hundred and sixty-four participant's right eyes (103 male, 66.0±11 years). Patient demographics for each of the three groups (i.e., NTG, POAG and glaucoma suspects) are presented in Table 4. SVPs were detected and quantified in all eyes, with a range of 0.7% - 81.7%, and 95% CI of 22.4% to 29.5%. Analysis for distribution in each group revealed a normal distribution in NTG, POAG, and glaucoma suspects ($K^2=2.6, 3.2, 0.6$; $p=0.2, 0.2, 0.7$ respectively) (Figure 24). There was a significant difference in age between glaucoma suspects and POAG as well as glaucoma suspects and NTG (both $p=0.004$). No significant difference in SVP amplitude between the three groups was observed ($p=0.2$). The highest SVP amplitude was found in the NTG group (32.5%±18.6) (Table 4).

Table 4. Summary of total average findings across clinic sites.

	Number of participants	Age (years)	IOP (mmHg)	SVP amplitude
All eyes	164 (103 males)	66±11	14.5± 3.5	28.6%±14.9
POAG only	64 (41 males)	68±12	15 ±3	28.7%±14.5
NTG only	37 (25 males)	68±8	13 ±2.5	32.5%±18.6
Suspects only	63 (35 males)	62±10	15.5± 3.5	26.3%±13.2

3.1 SVP and age

A significant and positive correlation between SVP amplitude and age was found when all eyes were grouped and analysed together ($r=0.31$, $p<0.0001$). However, when analysing correlations in each of the three groups separately, a significant association was only revealed between SVP amplitudes and age in the NTG group ($r=0.53$, $p<0.001$) (Figure 25).

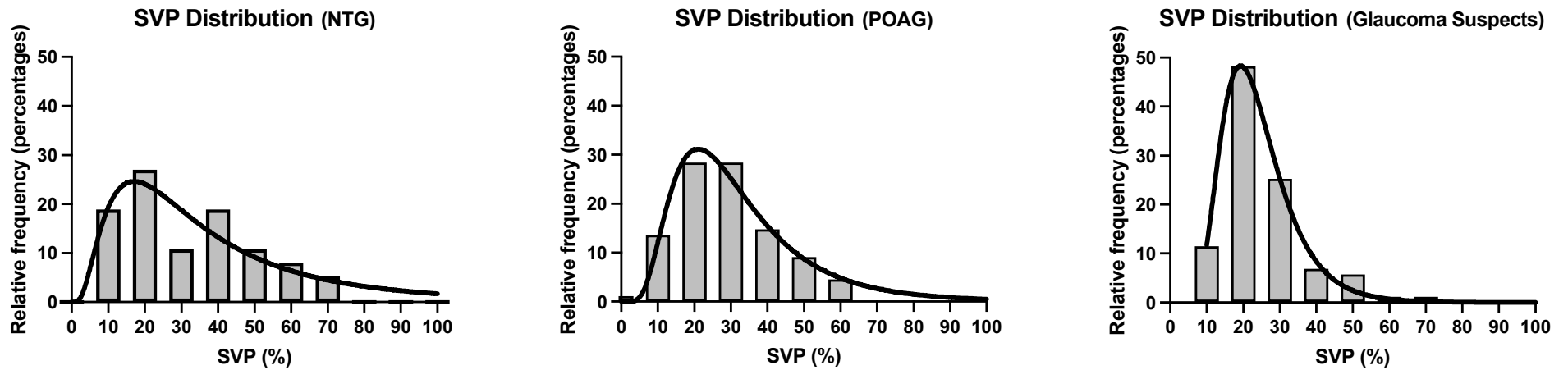


Figure 24. Distribution of SVPs in NTG (n=37), POAG (n=64) and glaucoma suspects (n=63).

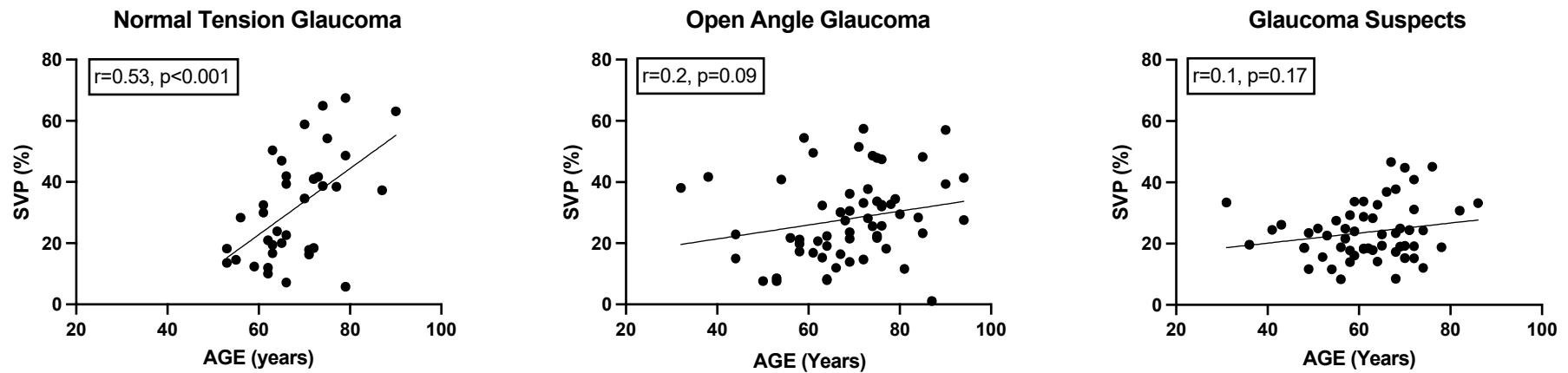


Figure 25. The association between SVP amplitudes and age in each of the three.

3.2 SVP and gender

The mean SVP amplitude in all eyes was slightly higher in females compared to males (29 ± 13 vs 25 ± 13 , $p=0.1$). Separate group analysis revealed that SVPs are only significantly higher in females than males in the NTG group (39 ± 17 vs 26 ± 14 respectively, $p < 0.05$) (Figure 26).

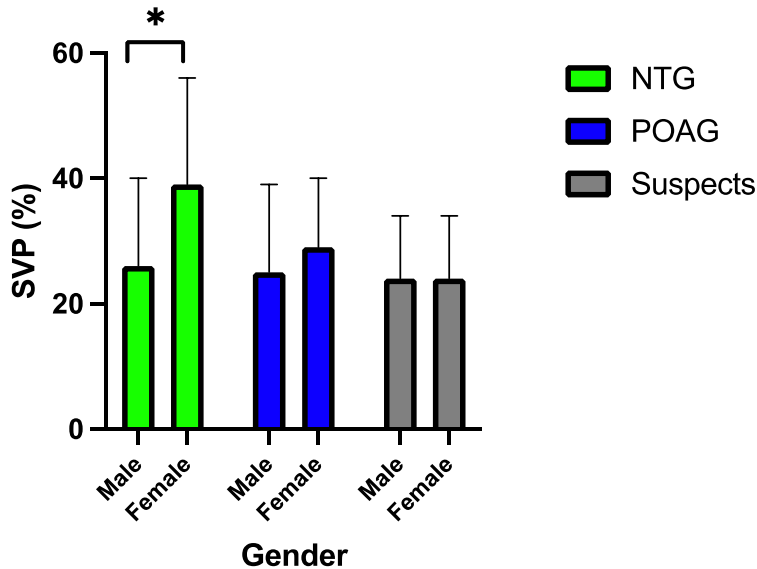


Figure 26. SVP amplitude in females and males across the three groups (* $p < 0.05$).

4. Discussion and conclusions

In this study, SVPs were explored in patients with confirmed glaucoma (POAG and NTG) and those who are glaucoma suspects. These classifications were based on comprehensive assessments of participants by experienced glaucoma specialists (a minimum of one ophthalmologist).

SVP amplitudes were highest in the NTG group, followed by the POAG, and glaucoma suspect groups. A positive and significant association between age and SVP amplitude was observed when all eyes were grouped. However, intra-group analysis showed only a significant association between age and SVP amplitudes in NTG. There was also a significantly higher SVP amplitudes in females compared to males with NTG. Although the difference in SVP amplitude between the glaucoma groups were non-significant, SVPs were quantifiable in all participants in this study. This

is in contrast to the literature which states that SVPs are absent or less visible in glaucoma^{21,160}, however, most previous studies have used subjective approaches to assess the presence or absence of SVPs.

Our results show that patients with NTG had greater SVP amplitudes compared to POAG or glaucoma suspects. Given that NTG patients have normal IOP prior to receiving glaucoma treatment,³¹⁴ it is possible that their SVPs are greater than in POAG when considering the effect of IOP on perfusion pressure and therefore blood flow that can be assessed through SVPs.²⁶⁰ Lowering IOP has been reported to increase perfusion pressure, improving blood circulation at the optic nerve head in glaucoma.²⁶⁰ Thus, it is possible that glaucoma treatment by means of lowering IOP exaggerates the difference in SVP amplitude between patients with NTG and POAG. In contrast, none of the glaucoma suspects were receiving any glaucoma treatment, thus revealing their “natural” SVP amplitude.

Previous evidence has demonstrated that increasing age improves the visibility and detection of SVPs.^{232,254} Our results are consistent with this as we found a significant and positive association between SVP amplitudes and age with higher SVP amplitudes observed in older age. This might also explain the lower SVP amplitude in our glaucoma suspect cohort, as the mean age in this group was significantly lower compared to the combined glaucoma (i.e., NTG and POAG) group. Furthermore, the glaucoma suspect group was furthest from statistical significance when assessing age-related changes in SVP, which may be due to the overall lower age group. While to the best of our knowledge there is no previous study that has specifically assessed SVP presence or absence in females and males, current evidence on gender and glaucoma have demonstrated that women are at an increased risk of POAG³¹⁹ as well as NTG.³²⁰ Female sex hormones have demonstrated implications on vascular resistance and subsequent optic nerve head circulation.⁵² Therefore, it’s not surprising to observe a difference in SVPs amplitudes between men and women in both NTG and POAG.

This study has limitations - firstly, most participants had early-moderate glaucoma and therefore, a greater sample of advanced glaucoma cases may have revealed a greater difference in SVP

amplitude between patients with glaucoma and those who are glaucoma suspects. Secondly, our study did not include healthy controls. Accordingly, differences in SVP amplitude between glaucoma and healthy controls have not been established in this study. Nevertheless, our study is the first to objectively demonstrate SVP distribution in glaucoma and glaucoma suspects. Finally, a larger and more evenly distributed sample size would have been beneficial to further confirm the relationships observed in this study.

In conclusion, contrary to previous reports of the absence of SVPs in glaucoma, this study has revealed that SVPs can be detected in all subjects with glaucoma using our novel technology. The amplitude of SVPs appear to be related to the glaucoma subtype, with NTG having greater amplitudes than both POAG and glaucoma suspects. Higher SVP amplitudes were observed with older age and females with NTG have significantly higher SVP amplitudes than males with NTG.

Chapter 5

Spontaneous Retinal Venous Pulsations as a Vascular Marker for Glaucoma

Chapter Summary

So far, it has been shown that SVPs are present in varying degrees in all glaucoma and glaucoma suspects. The association between SVPs and age and gender have also been confirmed. However, before establishing the assessment of SVPs as a clinical marker for glaucoma, the association between SVP amplitudes and other established markers of glaucoma must be determined. This chapter attempts to identify the relationship between SVP amplitudes and RNFL thickness, visual field loss, IOP, and retinal ganglion cell count. The results reveal a significant positive association between SVP amplitude and structural and functional parameters.

1. Introduction

Glaucoma describes a group of optic neuropathies that can be classified using a 3-stage disease continuum gradually leading to permanent vision loss when undiagnosed and unmanaged.^{33,102} The cascade of glaucomatous vision loss is initiated by progressive loss of retinal ganglion cells (RGCs) through apoptosis, and/or necrosis,¹⁰³ forming the basis of glaucomatous structural damage. Traditionally, it is said that in stage one, RGC loss is not detectable using current technology.^{45,102,104-110} In stage two, retinal nerve fibre layer (RNFL) loss and neuroretinal rim thinning is evident on fundus imaging, with up to 45% of RNFL loss having occurred.¹²⁹ These RNFL changes are said to be the earliest observable defects in glaucoma.^{111,112} However, these changes are unable to be detected through functional testing such as visual field (VF) assessment and remain asymptomatic.^{45,106-110} Therefore, irreversible damage and disease progression will have already ensued by the time glaucoma becomes symptomatic and can be definitively diagnosed. It is estimated that half of all glaucoma cases currently remain undiagnosed, even in well-resourced countries such as Australia.¹¹³ By stage three, visual dysfunction and blindness may develop due to increasing damage to the RGCs and their axons and therefore the optic nerve.¹⁰²

Despite traditional and longstanding beliefs of this three-stage glaucoma continuum, there is evidence to suggest that this is not the course of glaucoma pathology in all patients.¹¹⁵ The occurrence of RGC dysfunction, preceding RGC death has been suggested as an explanation in patients whereby functional changes present before the presence of detectable structural changes.¹¹⁵ RGC dysfunction, opposed to RGC death, may lead to a reduction in VF sensitivity while maintaining a relatively smaller amount of structural reduction. In such cases, functional deficits can exceed the reduction predicted from structural measures alone.¹¹⁶ There is conflicting evidence on the frequency of functional changes preceding structural changes. Data from a large clinical trial has revealed this in as low as 35% percent of patients,⁴⁵ while others have reported this in up to 60-86% of patients.^{117,118} However, these results have been questioned as the identification of relative frequency of these changes (structural vs functional) depend on the accuracy of the criteria to define that structural or functional change has taken place (specificity and sensitivity).¹¹⁵ In a study with test specificity at 90%, functional deterioration alone was

observed in approximately 20% of participants.¹¹⁹ In the same study, when test specificity was increased to 97%, this frequency dropped to 15%.¹¹⁹

Alongside neurodegenerative changes, glaucoma is also associated with vasculature damage evident in the retina and at the optic nerve head, such as RNFL haemorrhages and vein occlusions.^{156,157} Disruption and failure of stable blood flow in the region of the optic nerve can cause ischemic damage of the RGCs, potentially initiating the cascade of glaucomatous damage.^{158,159} This suggests that vascular changes could occur at the very early stages of the glaucoma continuum. Investigations of retinal blood flow during the early stages of glaucoma have revealed increased blood flow in regions of RNFL thinning, with a progressive decline in ocular blood flow with increased glaucomatous progression.¹⁶⁰⁻¹⁶³

Since the discovery of spontaneous retinal venous pulsations (SVPs) in the 1850's,²³⁶ the presence of SVPs has been variably reported in patients with glaucoma, with some papers reporting absent SVPs.^{163,233} This has created interest in the assessment of SVPs in glaucoma.^{21,163,233-235,237} Recent objective quantification of SVPs has led to an increase in SVP detection in glaucoma. This is clearly demonstrated in a study reporting an increase in detection of SVPs in glaucoma patients from 64.1% using subjective measures to 100% using objective measures.¹⁶³ These improved methods of detection of SVPs have led to the question of whether the variability in SVP amplitudes may be indicative of the presence of glaucoma and its stages and whether low amplitude SVPs were simply undetectable using previous methods. The latter was investigated by Morgan and colleagues who reported that SVP amplitudes are strongly related to whether or not pulsations are observable to the naked eye.²³⁸ However, it is as yet unclear whether the reduction in SVP amplitudes is due to anatomical factors such as variations in vessel dimension and/or changes to vessel pliability. The role of reduced SVPs in the pathogenesis of glaucoma is not clearly defined, though reduced SVP amplitudes have been associated with RNFL thinning.^{163,233,235}

The number of RGCs can be estimated using empirical formulas derived from data obtained from measurement of functional and structural changes observed by VF and optical coherence tomography (OCT) analysis respectively.^{33,131} These empirical formulas, developed by Medeiros

and colleagues, based on the work of Harwerth and colleagues, link both the structural and functional changes in glaucoma.^{33,131,152,297}

In comparison to other current methods for studying structural and functional changes in glaucoma, SVP assessment, as a dynamic vascular marker, is relatively easy to perform, inexpensive and scalable. However, due to its inherent subjectivity, there is no evidence on how comparable SVP assessment is to other established biomarkers for glaucoma diagnosis. The aim of this study was to uncover the potential relationship between SVP amplitudes and existing markers for glaucoma assessment including RGC count estimates, RNFL thickness, and VF loss. As these measures represent the different stages of the glaucoma continuum, the findings of this study can also determine the likely phase at which SVP changes occur on the continuum.

2. Methodology

2.1 Data collection

One hundred and twenty-eight eyes from 128 participants, including 31 with confirmed normal tension glaucoma (NTG; 21 males) 48 with confirmed primary open-angle glaucoma (POAG; 33 males) and 49 with suspected glaucoma (28 males) were included in this study.

Subjects were selected to participate from three ophthalmic clinics in Sydney if they had no history of diabetes and/or vascular and/or retinal pathology. Each participant had a full glaucoma assessment, including visual acuity, intraocular pressure (IOP) measured using applanation tonometry, Humphrey Visual Field (HFA; HFA II-i series or HFA III, Carl Zeiss, Meditec, Dublin, CA, Operating system 5.1) testing with SITA-Standard strategy (stimulus size III white), and RNFL assessment using OCT using either a Spectralis OCT (Heidelberg Eye Explore version 1.10.20 using the retinal nerve fiber layer (RNFL) algorithm) or a Cirrus HD-OCT (version 5.2.1.12 Optic Disc Cube 200x200) A 10 second video of the venous circulation at the optic nerve head was then recorded using a tablet-based ophthalmoscope following pharmacologic pupil dilation using a single drop of 1% Tropicamide (Mydracil).

Experienced glaucoma specialists at each site undertook comprehensive assessments of all participants, utilising conventional indirect ophthalmoscopy, RNFL analysis and Hoddap-Anderson criteria for HFA progression to assess glaucoma status, as outlined in Chapter 2.²⁹⁸ All participants with confirmed glaucoma had definite glaucomatous optic neuropathy and/or HFA Mean Deviation (MD) range within -10.2 – 1.7dB and progressive change in either assessment. This group was split in to POAG and NTG, where participants with POAG had HFA MD between -10.2 – 1.7dB and participants with NTG had HFA MD was between -9.5 – 0.9dB. Glaucoma suspects in this study were defined as having elevated IOP or suspicious appearing optic disc with no progressive changes in either and normal HFA result and a HFA MD between -5.15dB and 0.98dB.

2.2 Ethics

This study was approved by the University of Technology Sydney and University of New South Wales Human Research Ethics Committees (ETH17-1392 and HC08-2014-36 respectively) and was conducted in accordance with the guidelines of the Tenants of Helsinki. Verbal and written explanations including aims and nature of the study were provided to each participant prior to obtaining written informed consent.

2.3 Retinal videography

A detailed description of retinal videography using a tablet-based ophthalmoscope to quantify SVP amplitudes has been detailed in Chapters 3 and 4.³¹⁸ Retinal video recordings were taken of the retinal circulation at the optic disc using a 20D tablet-based (iOS operating device; iPad Mini4, Apple Inc.) ophthalmoscope and ProMovie iOS application. This was performed at the same visit as their OCT and HFA, following which participants were dilated and asked to refrain from blinking for 10 seconds while the recordings were taken.

2.4 Estimating retinal ganglion cell count

Methodology proposed by Medeiros and colleagues^{131,152,297} based on Harwerths' equations³³ was used to estimate RGC counts using HFA outputs and RNFL thickness. An in-depth description and discussion of these equations are reported by Medeiros et al (2012).¹³¹ In summary, the formulas use data obtained from each of the HFA test locations (sensitivity in dB) from a 24-2 SITA-Standard HFA assessment to estimate RGC somatas in the corresponding area of the retina (Equation 1). RGC axon estimates are calculated from OCT-obtained RNFL thickness (Equation 2).¹³¹

$$m = [0.054 \times (ec \times 1.32)] + 0.9$$

$$b = [-1.5 \times (ec \times 1.32)] - 14.8$$

$$gc = \frac{(s - 1) - b}{m} + 4.7$$

$$VFrgc = \Sigma 10^{(gc \times 0.1)}$$

Equation 1. RGC somatas estimated from functional testing (VF).¹²⁹

ec = eccentricity of VF test location

m = slope of linear function relating ganglion cell quantity (*gc*) to visual field sensitivity (*s*)

b = intercept of linear function relating *gc* to *s*

VFrgc = total number of RGC somas

$$d = (-0.007 \times \text{age}) + 1.4$$

$$c = (-0.26 \times \text{MD}) + 0.12$$

$$a = \text{average RNFL thickness} \times 10.87 \times d$$

$$RGC_{OCT} = 10^{(\log a \times 10) - c}$$

Equation 2. RGC axons estimated from structural testing (OCT).¹²⁹

d = axonal density (axons/ μm^2)

c = correction factor for the severity of disease

RGC_{OCT} = total number of RGC axons

These functional and structural equations (Equation 1 and Equation 2, respectively) are then combined to create a weighted scale according to disease severity (Equation 3).¹³¹

$$\textit{Combined RGC count} = \left(\frac{1 + \text{MD}}{30} \times \textit{RGC}_{OCT}\right) + \left(\frac{-\text{MD}}{30} \times \textit{RGC}_{VFA}\right)$$

Equation 3. Combined RGC count estimated from structural and functional testing equations (RGC_{OCT} and RGC_{VF} respectively).¹²⁹

MD = HFA mean deviation (dB)

2.5 Statistical analysis

The relationship between SVP and IOP, RNFL, HFA, and RGC estimates were assessed using linear regression. A generalized linear mixed model was also used to assess the power of each correlation with respect to age and IOP as variables known to affect SVP amplitudes. Pearson correlation was used to quantify the correlation coefficients. Statistical significance defined at the $p < 0.05$ level. Descriptive statistics were conducted to reveal basic data distribution and presented in the Mean \pm Standard Deviation format.

3. Results

The mean age of all participants was 65 \pm 11 years, with participants who were glaucoma suspects being significantly younger than POAG participants (61 \pm 11 vs 67 \pm 13; $p < 0.05$). Mean IOP was significantly higher in glaucoma suspects compared to NTG participants (15 \pm 3.5 vs 13 \pm 2.4; $p < 0.05$). Glaucoma suspects had significantly thicker RNFL measurements than those with POAG (84 \pm 12 vs 76 \pm 13 $p < 0.005$). Mean HFA MD was significantly reduced in the participants who had glaucoma (NTG and POAG) in comparison to glaucoma suspects ($p < 0.05$). Mean RGC count was significantly lower in NTG and POAG participants in comparison to glaucoma suspects ($p < 0.005$ and $p < 0.0005$ respectively) (Table 5).

Table 5. Patient demographics and means.

	NTG	POAG	Suspects	p-value
n	31	48	49	--
Gender (males)	21	33	28	--
Age (years)	67±8	67±13*	61±11*	0.02
IOP (mmHg)	13±2.4*	15±3.6	15±3.5*	0.03
RNFL (µm)	78±13	76±13**	84±12**	0.007
HFA MD (dB)	-2.5±2.5*	-2.1±2.6 ⁺	-1±1.7* ⁺	0.007
RGC count (x1000)	699±151**	687±186 [#]	836±193** [#]	0.0001
SVP amplitude (% pulse)	32.6±17 ^{#*}	25.8±10*	22.4±7.1 [#]	0.001

Post hoc analysis; ** $p < 0.05$, *** $p < 0.005$, # $p < 0.0005$

All participants had quantifiable SVPs. There was a significant difference in SVP amplitude across the three groups ($p=0.001$), with SVP amplitude in glaucoma suspects and POAG being significantly lower than NTG ($p < 0.005$ and $p < 0.05$ respectively). Mean values for each parameter in each group are reported alongside patient demographics in Table 5.

3.1 SVP amplitudes and their association with structural-functional parameters in NTG

A positive but non-significant relationship between SVP amplitudes and individual structural and functional parameters (i.e., RNFL, HFA, and RGC estimates) was observed in NTG participants. As SVPs were shown to be associated with age, a linear mixed model was used to account for the effects of age. However, this did not result in a significant change in our results. The highest correlation was found between SVP amplitude and RNFL thickness ($p=0.1$, $r=0.28$) (Table 6).

Table 6. Associations between SVP amplitudes and individual parameters in NTG.

	Coefficient	<i>p</i> -value	<i>r</i> (correlation coefficient)	Standard Error
SVP vs. IOP				
<i>Direct Correlation</i> ¹	0.6	0.6	0.08	1.2
<i>Corrected for Age</i> ²	0.01	0.9	0.59	1
SVP vs. RNFL				
<i>Direct Correlation</i>	0.37	0.1	0.28	0.23
<i>Corrected for Age</i>	0.2	0.2	0.62	0.19
SVP vs. HFA				
<i>Direct correlation</i>	0.83	0.5	0.12	1.26
<i>Corrected for Age</i>	0.64	0.5	0.6	0.62
SVP vs. RGC				
<i>Direct correlation</i>	0.67	0.7	0.05	0.02
<i>Corrected for Age</i>	1.9	0.2	0.61	0.017

¹ Direct Correlation: Linear regression between SVP and the specified parameter

² Corrected for Age: Multiple linear regression with age and the specified parameter as explanatory variables and SVP as outcome variable

3.2 SVP amplitudes and their association with structural-functional parameters in POAG and glaucoma suspects

Linear regression was used to assess the association between SVP amplitudes and individual structural and functional parameters (i.e., RNFL, HFA, and RGC estimates). In addition, as age and IOP are two important features in the pathophysiology of POAG and glaucoma suspects, a linear mixed model was also used to account for the potential impact of these two parameters.

Table 7. Associations between SVP amplitudes and individual parameters in POAG.

	Coefficient	p-value	r (correlation coefficient)	Standard Error
SVP vs. IOP				
<i>Direct Correlation</i>	0.36	0.4	0.12	0.44
<i>Corrected for Age</i>	0.44	0.3	0.27	0.11
SVP vs. RNFL				
<i>Direct Correlation</i>	0.27	0.02	0.33	0.11
<i>Corrected for Age</i>	0.24	0.03	0.38	0.11
<i>Corrected for Age and IOP</i>	0.24	0.03	0.4	0.11
SVP vs. HFA				
<i>Direct correlation</i>	1.33	0.02	0.31	0.58
<i>Corrected for Age</i>	1.5	0.01	0.42	0.57
<i>Corrected for Age and IOP</i>	1.45	0.01	0.43	0.58
SVP vs. RGC				
<i>Direct correlation</i>	1.82	0.03	0.31	0.08
<i>Corrected for Age</i>	2.85	0.001	0.5	0.08
<i>Corrected for Age and IOP</i>	2.77	0.002	0.5	0.08

A positive and significant relationship between SVP amplitudes and individual structural and functional parameters was observed in POAG participants. The highest correlation was observed between SVP amplitudes and RGC count estimates after correcting for age ($p < 0.001$, $r = 0.5$) (Table 7).

In contrast, a negative and significant relationship was found between SVP amplitudes and individual parameters in glaucoma suspects. Similar to POAG, the highest correlation in glaucoma suspects was observed between SVP amplitudes and RGC count estimates after correcting for age and IOP ($p = 0.009$, $r = 0.41$) (Table 8).

Table 8. Association between SVP amplitudes and individual parameters in glaucoma suspects.

	Coefficient	<i>p</i> -value	<i>r</i> (correlation coefficient)	Standard Error
SVP vs. IOP				
<i>Direct Correlation</i>	0.3	0.2	0.17	0.28
<i>Corrected for Age</i>	0.34	0.2	0.18	0.34
SVP vs. RNFL				
<i>Direct Correlation</i>	-0.17	0.02	0.31	0.07
<i>Corrected for Age</i>	-0.19	0.02	0.32	0.08
<i>Corrected for Age and IOP</i>	-0.18	0.05	0.33	0.09
SVP vs. HFA				
<i>Direct correlation</i>	-1.8	0.001	0.44	0.52
<i>Corrected for Age</i>	-1.8	0.001	0.45	0.53
<i>Corrected for Age and IOP</i>	-1.7	0.002	0.46	0.54
SVP vs. RGC				
<i>Direct correlation</i>	-1.3	0.01	0.36	0.05
<i>Corrected for Age</i>	-1.9	0.004	0.4	0.006
<i>Corrected for Age and IOP</i>	-1.8	0.009	0.41	0.006

4. Discussion

In this study, the association between quantified SVP amplitudes and previously established structural and functional measures in NTG, POAG, and glaucoma suspects was investigated. While a positive but non-significant relationship between SVP amplitudes and RNFL thickness, HFA loss, and RGC count estimates in NTG was observed, the results of this study showed a positive and significant association between SVP amplitudes and the aforementioned parameters in POAG. Interestingly, a negative and significant association was observed between SVP amplitudes and the structural and functional measures in glaucoma suspects.

The mechanism by which SVPs occur is complex and has not yet been clearly defined. IOP, retinal venous pressure and cerebrospinal fluid pressure (CSFp) contribute to creating a pressure difference between the intraocular and retrobulbar spaces, also known as the trans-laminar pressure difference, which has been shown to be a major driver of SVP generation.^{256,301} Previous studies that have investigated CSFp in POAG and NTG have shown that CSFp is significantly lower in POAG compared with age-matched controls.^{258,321,322} CSFp is also reduced in NTG compared with not only healthy controls but also POAG patients (NTG: 8.7 ± 1.16 mmHg vs POAG: 9.1 ± 0.77 mmHg vs Controls: 11.8 ± 0.71 mmHg, $p < 0.01$).²⁵⁸ While there are no studies on CSFp levels in glaucoma suspects, interestingly, there have been reports of increased CSFp in ocular hypertension patients compared to healthy controls (12.6 ± 0.85 mm Hg vs. 10.6 ± 0.81 mm Hg; $p < 0.05$).^{258,323} As lower CSFp is associated with higher translaminar pressure difference (leading to higher SVP), our findings of highest SVP amplitudes in NTG, followed by POAG, and glaucoma suspects is consistent with these reports. The positive and negative association between SVP amplitudes and structural and functional measures in glaucoma and glaucoma suspects, respectively, can also be explained by these findings. Lower than normal CSFp levels in POAG leads to higher SVP amplitudes (due to higher translaminar pressure difference) and thus a positive correlation between SVP and RNFL thickness, HFA loss, and RGC count estimates. Conversely, in glaucoma suspects, higher than normal CSFp levels leads to lower SVP amplitudes despite a normal range of RNFL thickness, HFA loss, and RGC count estimates. As a result, a negative correlation between SVP amplitudes and these parameters are observed.

SVPs are increasingly being investigated as an additional glaucoma marker with a growing body of literature providing evidence of links between SVPs and specific glaucoma markers. These include associations between SVPs and IOP,³²⁴ as well as RNFL thickness.¹⁶³ Similarly, a positive correlation between SVPs and RNFL thickness was observed in the POAG cohort. Unfortunately, there is no evidence on the association between SVP amplitudes and structural and functional measures in glaucoma suspects or NTG and thus there are no references to establish whether the observations of this study are in line with other findings.

4.1 RGC estimation and its limitations

The formulas used in this study estimate RGC counts using data obtained from OCT, HFA and patient age to generate a combined output linking structure and function in glaucoma. However, the disagreement between structural and functional tests in detecting glaucomatous disease progression is widely reported.^{109,134,325}

Visual field assessments are generally less sensitive in detecting early changes in glaucoma, while OCT assessments are often more sensitive to early glaucomatous changes and less sensitive in the detection of advanced glaucomatous changes.¹³¹ The differences between detection of structural and functional changes through OCT and VF assessments respectively are reported to be due to differences in measurement algorithms and scales between the devices.^{33,107,131}

The logarithmic (i.e. non-linear) approach in VF analysis compresses the findings of sensitivity loss in early glaucoma and expands the findings in late glaucoma, meaning that VF analysis is more sensitive to small changes in sensitivity in the later stages of glaucoma compared to the small changes in sensitivity in early glaucoma.¹³¹ While there are benefits in a combined approach to detecting glaucomatous disease progression through structural and functional assessments, VF assessments may fail to provide sensitive measures in early glaucoma due to the nature of its measurement scale, thus underestimating RGC loss estimations in early glaucoma.

The formulas used in this paper to calculate RGC estimates address this shortcoming through the use of a weighted system for HFA MD values, which has been summarised above (Equation 3) and explained in detail elsewhere.¹³¹ Furthermore, region-specific calculation of RGCs, i.e. superior-

temporal/nasal and inferior temporal/nasal, may have revealed alternative results due to the characteristic nature of structural and functional loss in glaucoma, particularly as Golzan and colleagues' have found varying but highly significant correlations between SVPs and RNFL thickness in four different retinal segments.¹⁶³

In comparison to isolated structural and functional parameters, combining parameters to estimate RGC counts using the methods described in this paper have demonstrated improved detection of glaucoma and its progression in previous studies.^{131,152,326-331} However, more recently, two studies have indicated that RGC counts estimated through this method have discrepancies with histological data. Both studies have noted that RGC counts differ from the clinical value of combining structural and functional parameters.^{332,333}

Although our results revealed a similar distribution of RNFL thickness across the glaucoma and glaucoma suspect cohorts, there was a significant difference in RGC estimates between the groups (Table 5). This difference in RGC estimates between groups may be due to the differences in HFA MD distribution ($p < 0.005$) and age ($p < 0.05$) between the cohorts (Table 5) which were used in the formulas. A previous study estimating RGC counts in healthy participants and participants with glaucoma found a significantly lower RGC counts in the glaucoma group.¹³¹ Although our current study did not include participants with healthy eyes, our results in the glaucoma cohort had a significantly lower average RGC count than the glaucoma suspect cohort ($p < 0.0005$; Table 5).

Our findings demonstrate that when corrected for age and IOP, SVP amplitudes had the highest correlation with HFA MD in glaucoma suspects. However, in POAG, when corrected for age, SVPs had the highest correlation with RGC count estimates. While it is not clear why this difference exists between the two groups, it can be anticipated that there is a greater amount of RGC damage in POAG compared to glaucoma suspects and the POAG group were undertaking pharmaceutical glaucoma management which may have collectively impacted these findings. While RGC estimates have been shown to be useful in showing glaucomatous progression,¹³¹ the formulas used to calculate the RGC estimates require results from two expensive and non-portable devices. In contrast, SVP recordings were done using a portable and inexpensive device in our

study. Therefore, the SVP quantification method utilised in this thesis may be promising as a non-traditional and economical method to differentiate POAG from glaucoma suspects. With further data, this method may be able to track glaucoma progression. As RGC loss occurs at the very early stages of the glaucoma continuum, our findings demonstrate that objective assessment of SVPs can act as a surrogate marker for identifying the early stages of the disease. However, further studies investigating the diagnostic power of SVPs in glaucoma is needed.

4.2 Study limitations

Several limitations exist within this study. Firstly, our sample size was limited and should be increased in future research in order to strengthen our findings. The increased sample size should also include more even distribution of participants across all studied groups. The NTG group in this study was smaller in comparison to the POAG and glaucoma suspect groups. Although significant findings were found in the studied parameters in the POAG and glaucoma suspect groups, our results only yielded non-significant findings in the NTG group which may be attributed to the lower sample size.

Secondly, our sample did not include any healthy subjects. The inclusion of healthy participants would have allowed us to examine the association between SVPs and structural and functional markers in the healthy state, as well as solidify the stage at which SVP changes occur in the glaucoma continuum. The inclusion of baseline blood pressure from these healthy subjects would also be beneficial in future studies where blood pressure is measured in all study subjects.

Thirdly, two different OCT devices utilising spectral-domain OCT technology were employed in this study; the Cirrus (Carl Zeiss Meditec, Dublin, CA) and Spectralis (Heidelberg Engineering, Dossenheim, Germany) OCTs. Medeiros et al's equations utilised in this paper (Equations 1-3) originally estimate RGC count using RNFL thickness measurements from the Spectralis OCT.¹⁵² This protocol was not able to be implemented in our study due to the lack of availability of Spectralis OCT devices at all data collection sites in this study, hence the need for both Spectralis and Cirrus OCT devices. However, previous studies have reported no significant differences in RNFL thickness parameters obtained between the two OCT devices.^{138,306} Thus, it is unlikely that

the use of two OCT devices has affected the results of this study. A future study comparing RGC counts obtained using data from both devices would confirm this.

5. Conclusions

In this study a positive and significant correlation between SVP amplitude and both structural and functional parameters in patients with confirmed POAG was found, with the strongest correlation being between SVPs and RGC count estimates ($p=0.001$, $r=0.5$). In contrast, a negative correlation was observed between SVP amplitudes and structural and functional parameters in glaucoma suspects, with the strongest correlation also being between SVPs and RGC count estimates ($p=0.002$, $r=0.46$).

This indicates that SVPs may reflect early glaucomatous changes within the first two stages of the glaucoma continuum at the structural level of pathology, as the correlation between SVP amplitude and RNFL thickness was also significant. The potential benefits that this may offer in the early detection of glaucoma and consequent management are substantial. When combined with RGC estimation methods, SVP amplitude analysis may provide more benefits to traditional glaucoma assessments where often structural and functional glaucomatous loss are only clinically detected once substantial RGC loss has already occurred.

The portable, easy-to-use and cost efficient tablet-based ophthalmoscope used in this study for SVP analysis also demonstrates that a feasible approach to glaucoma screening can be taken compared to the traditionally expensive bench-top devices, especially in remote or underserved areas. While this study demonstrates promising results in the use of SVPs and RGC counts as a surrogate method for early glaucoma detection, further studies with larger and more evenly distributed groups are indicated.

Chapter 6

The use of Spontaneous Retinal Venous Pulsation Assessment in Distinguishing Glaucoma Sub-Types

Chapter Summary

The relationship between SVP amplitude and standard clinical assessments including RNFL thickness, VF changes and IOP, as well as RGC count has been established in Chapter 5. This chapter aims to establish how SVPs compare to these common clinical markers in distinguishing glaucoma from glaucoma suspects, as well as in distinguishing between different types of glaucoma, namely NTG and POAG. The results of this chapter show that SVPs are comparable and are as powerful in separating glaucoma sub-types as standard clinical markers for glaucoma.

1. Introduction

Glaucoma is term given to a group of progressive and irreversible neurodegenerative ocular diseases, which in the absence of other ocular diseases and congenital abnormalities, demonstrates characteristic morphological changes in the optic nerve head and retinal nerve fibre layer. Approximately 50% of those with glaucoma are undiagnosed and unaware that they have the condition.^{113,334,335} Biennial ocular checks are recommended by the Royal Australian and New Zealand College of Ophthalmologists; however, there is no formal screening program for glaucoma. Early detection is vital to reduce the number who progress to significant glaucomatous visual loss, therefore improvement in early detection of glaucoma is essential.

Decades ago, glaucoma diagnosis was based purely on elevated intraocular pressure,²⁹ however it has since become clear that intraocular pressure (IOP) on its own is not sensitive or specific to the diagnosis of glaucoma, particularly in cases of normal tension glaucoma (NTG). Visual field assessment through standard automated perimetry (SAP) has been used to diagnose glaucoma as this method offers some level of specificity, however it is not ideal as a screening tool as visual field defects are not detected until 30-50% of RGC axons have been lost.^{105,336-338}

Current diagnosis of glaucoma is based on comprehensive ocular examination including SAP, assessment of the retinal nerve fiber layer (RNFL) and optic nerve to identify associated markers. However, as discussed, visual field defects are not detected by SAP until as much as 50% of retinal ganglion cell axons are lost.^{105,336-338} Substantial RNFL damage also often occurs before its detection.^{45,102,104-110} Therefore, current glaucoma assessments do not always accurately classify glaucoma pathogenesis and there is a need for more sensitive diagnostic assessments of glaucoma.

Biomarkers that may improve diagnostic accuracy are particularly important in glaucoma, as the early stages of the disease continuum can be undetectable using traditional assessments. Changes in retinal vasculature have been suggested as biomarkers for glaucoma, including static markers such as changes in retinal vascular calibre,^{165,166,172} retinal vascular tortuosity⁴⁴ and fractal dimension^{169,170}. Dynamic vascular markers such as spontaneous retinal venous pulsations (SVPs)

have also been identified as a possible biomarker for glaucoma.^{21,163,233-235,237,238} The role of reduced SVPs in the pathogenesis of glaucoma is not clearly defined, however reduced SVP amplitudes have been associated with RNFL thinning.^{163,233,235} Findings described in this thesis have also demonstrated that SVPs may be indicative of early changes in glaucoma. Early diagnosis through assessment of SVPs may be beneficial in reducing the number those who if untreated progress to glaucomatous optic neuropathy.

This study investigates the use and comparability of quantified SVPs, detected using a novel tablet-based ophthalmoscope, against traditional glaucoma markers in distinguishing glaucoma from glaucoma suspects. Gold standard clinical markers of glaucoma such as RNFL thickness and visual field (VF) defects, as well as retinal ganglion cell (RGC) count estimates, will also be investigated as comparisons.

2. Methods

128 eyes from 128 participants, including 31 with confirmed normal tension glaucoma (NTG, 21 males) 48 with confirmed primary open-angle glaucoma (POAG, 33 males) and 49 with suspected glaucoma (28 males) were included in this study. All participants with confirmed glaucoma had definite glaucomatous optic neuropathy and/or HFA changes consistent with glaucoma, with a HFA Mean Deviation (MD) ranging between -9.5–0.9 for NTG and -10.2 – 1.7dB for POAG and progressive changes reported in either neuropathy and/or HFA assessment. All glaucoma suspects had elevated IOP or suspicious appearing optic disc, with no progressive changes in either measure and a normal HFA result and HFA MD between -5.15dB and 0.98dB. Participants were excluded in the presence of diabetes and/or current or previous vascular or retinal pathology.

Each patient underwent standard diagnostic glaucoma assessments, including intraocular pressure (IOP; applanation tonometry), Humphrey Visual Field (HFA; HFA II-i series or HFA III, Carl Zeiss, Meditec, Dublin, CA, Operating system 5.1) testing with SITA-Standard strategy (stimulus size III white), and RNFL assessment using OCT using either a Spectralis OCT (Heidelberg Eye Explore version 1.10.20 using the RNFL algorithm) or a Cirrus HD-OCT (version 5.2.1.12 Optic Disc Cube

200x200) and a dilated (1% Tropicamide (Mydracyl)) 10-second videoscropy of the retinal venous circulation at the optic nerve all at the same visit.

2.1 Ethics

Informed consent was obtained from each participant prior to participation in this study. This study was approved by both the University of Technology Sydney and University of New South Wales Human Research Ethics Committees and all methods were performed in accordance with the guidelines of the Tenants of Helsinki.

2.2 Retinal venous circulation videoscropy and SVP analysis

A tablet-based (iOS operating device) 20D ophthalmoscope was used to take 10 second photographic video recordings. Details are specified in Chapter 3 of this thesis and have been published.²⁸⁶ In brief, videos of the retinal vasculature at the optic disc were taken at 2.2x zoom across all participants, while contrast and focus were adjusted as required for each subject to ensure maximum visibility of the vessels and optic nerve head. Image J was used for video analysis and measurement of retinal veins to create an SVP trace. SVP amplitude was calculated as percentile change in average venous diameter (i.e. $\frac{\text{peak} - \text{trough}}{\text{mean vein caliber}}$) and average percentile pulse was calculated as $\frac{\text{average SVP amplitude} \times 100}{\text{mean vein caliber}}$.

2.3 Retinal ganglion cell estimates

Structural and functional information derived from the HFA and OCT assessments were used to calculate RGC estimates using formulas derived by Medeiros and colleagues^{131,152,297} based on Harweth et al's equations.³³ These methods are detailed in Chapter 5 of this thesis.

2.4 Data analysis

The area under the receiver operating characteristic curve (AUROC) was measured for each of the parameters (i.e. SVP, RNFL, HFA mean deviation (MD), RGC count, and IOP) to allow differentiation of POAG from glaucoma suspects and NTG from POAG participants. Pair-wise differences in AUROC between the parameters was evaluated using a method described by DeLong.²⁹⁹ This

method provides a confidence interval and standard error of the difference between two (or more) AUROCs. The significance level was set at $p < 0.05$. Data analysis was performed using Microsoft Excel and GraphPad prism (CA, USA).

3. Results

The mean age of participants with glaucoma was older compared to glaucoma suspects (67 ± 13 and 61 ± 11 years respectively; $p = 0.02$). A summary of patient demographics and mean values for IOP, RNFL, HFA, RGC and SVP data is presented in Table 9.

Table 9. Patient demographics and mean outputs.

	NTG	POAG	Suspects	<i>p-value</i>
n	31	48	49	--
Gender (males)	21	33	28	--
Age (years)	67 ± 8	$67 \pm 13^*$	$61 \pm 11^*$	0.02
IOP (mmHg)	$13 \pm 2.4^*$	15 ± 3.6	$15 \pm 3.5^*$	0.03
RNFL (μm)	78 ± 13	$76 \pm 13^{**}$	$84 \pm 12^{**}$	0.007
HFA MD (dB)	$-2.5 \pm 2.5^*$	$-2.1 \pm 2.6^+$	$-1 \pm 1.7^{*+}$	0.007
RGC count (x1000)	$699 \pm 151^{**}$	$687 \pm 186^\#$	$836 \pm 193^{**\#}$	0.0001
SVP amplitude (% pulse)	$32.6 \pm 17^{\#\#}$	$25.8 \pm 10^*$	$22.4 \pm 7.1^\#$	0.001

*Post hoc analysis; * $p < 0.05$, ** $p < 0.005$, # $p < 0.0005$*

The accuracy of each parameter was assessed in distinguishing POAG from glaucoma suspects and also POAG from NTG. ROC curve results are presented in Figure 27 and Figure 28. The AUROC for distinguishing POAG from glaucoma suspects was highest for RNFL thickness (0.70) followed by RGC count (0.69) which was very similar to SVP amplitude (0.67) (Table 10). The lowest AUROC was IOP (0.55) followed by HFA MD (0.61). In contrast, when ROC curves distinguishing POAG from

NTG were analysed, the greatest AUROC was for IOP (0.60), followed by SVP amplitude (0.59). The lowest AUROC in differentiating between POAG and NTG was observed for RGC count (0.51) (Table 10).

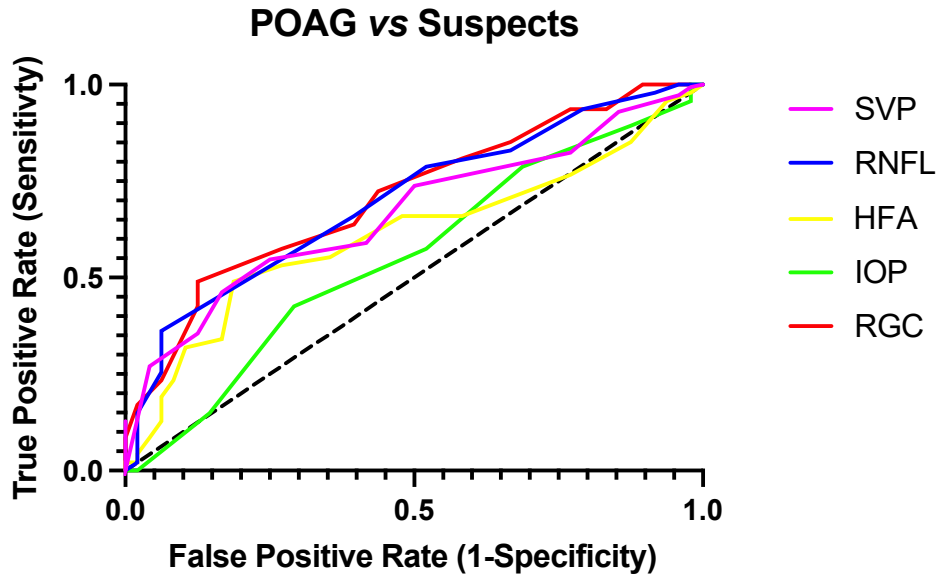


Figure 27. ROC curve of various markers in differentiating between POAG and glaucoma suspects.

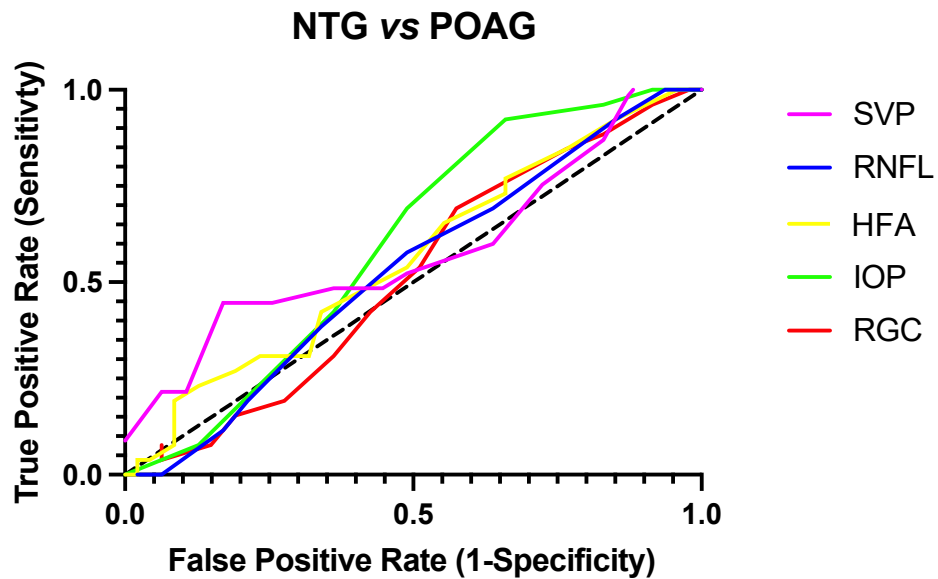


Figure 28. ROC curve of various markers in differentiating between NTG and POAG.

Table 10. AUROC for both ROC curves (POAG vs glaucoma suspects and NTG vs POAG).

	Area Under the Curve (AUROC)	
	<i>POAG vs Suspects</i>	<i>NTG vs POAG</i>
SVP	0.67	0.59
RNFL	0.70	0.53
HFA	0.61	0.54
IOP	0.55	0.60
RGC	0.69	0.51

Pairwise comparison of the AUROC for each of the ROC curves is presented in Table 11. For the ROC curve distinguishing POAG from glaucoma suspects, the AUROC of SVPs was not significantly different to RNFL ($p=0.06$) or RGC ($p=0.1$). This suggests that SVPs are equally effective in distinguishing the two groups, despite the higher AUROC for RNFL and RGC. The AUROC of SVPs were significantly higher than HFA and IOP ($p<0.005$), meaning that SVP is a more effective marker in distinguishing the two groups than these parameters.

For the ROC curve distinguishing POAG from NTG, the AUROC of SVPs was not significantly different to IOP ($p=0.4$), suggesting that SVPs are equally effective in separating the two groups, despite the higher AUROC for IOP. The AUROC of SVPs were significantly higher than RNFL, HFA and RGC ($p<0.005$), indicating that SVPs may be a more effective marker in distinguishing the two groups than these parameters.

Table 11. Pairwise comparison of AUROC.

<i>Paired Parameters</i>	<i>POAG vs Suspects</i>		<i>NTG vs POAG</i>	
	<i>Z Score</i>	<i>p-value</i>	<i>Z Score</i>	<i>p-value</i>
SVP-RNFL	1.9	0.063	3.9	0.000*
SVP-HFA	3.5	0.000*	4.3	0.000*
SVP-IOP	4.9	0.000*	0.8	0.451
SVP-RGC	1.5	0.134	5.4	0.000*
RNFL-HFA	6.4	0.000*	0.8	0.453
RNFL-IOP	6.8	0.000*	3.2	0.001*
RNFL-RGC	0.7	0.469	1.2	0.218
HFA-IOP	3.0	0.003*	3.1	0.002*
HFA-RGC	7.7	0.000*	2.3	0.023
IOP-RGC	7.0	0.000*	4.1	0.000*

* Significant at $p < 0.005$

4. Discussion

This study aimed to explore the performance of SVP analysis in comparison to other structural functional parameters in distinguishing POAG from glaucoma suspects and POAG from NTG. The results have shown that SVP analysis is comparable to other markers in separating the aforementioned groups. More specifically, SVPs can statistically separate POAG from glaucoma suspects as effectively as RNFL thickness. SVPs can also separate POAG from NTGs as effectively as IOP measurements. Interestingly, SVPs outperformed HFA measures in both groups, however whether this demonstrates a higher diagnostic power requires further work with the inclusion of a healthy control for comparison.

4.1 POAG vs glaucoma suspects

SVP analysis results were compared to traditional structural and functional glaucoma markers of RNFL thickness and HFA MD respectively, alongside IOP and analysis through the calculation of RGC count that combines structure and function. The greatest predictive accuracy in distinguishing

POAG from glaucoma suspects, of all the diagnostic markers studied in this study, was RNFL thickness (AUROC 0.70). This is in line with a previous study that reported RNFL thickness to have the highest specificity (AUROC 0.87) compared to HFA results (AUROC 0.73) and fundus photos (AUROC 0.73) in differentiating confirmed glaucoma cases from glaucoma suspects.³³⁹

The AUROC calculated for RNFL thickness in this study falls within the range of AUROC values reported in various other studies (0.69 - 0.99).³⁴⁰⁻³⁴⁸ These studies had sample sizes that included various glaucoma severities. The AUROC value for RNFL thickness has been reported to increase with increasing glaucoma severity, as demonstrated by Wu and colleagues who found that RNFL thickness was successful in diagnosing early glaucoma (AUROC 0.89) and excellent for detecting moderate-advanced glaucoma (AUROC 0.95).³⁴⁸ Therefore, the AUROC value obtained for RNFL thickness in this study, while it fits within previous study AUROC ranges, is on the lower end of this range due to two potential reasons. Firstly, the patient cohort was limited to mostly early glaucoma, and secondly, there was a small sample size. RNFL thickness having the largest AUROC compared to other parameters is to be expected, as RNFL thickness is one of the first observable and quantifiable pathological changes in the glaucoma continuum and often precedes visual field loss.^{111,112}

In comparison to RNFL thickness, HFA MD was found to have a significantly lower AUROC value. Considering the glaucoma sample used in this study were mostly early glaucoma, the results of our study are not surprising, as VF defects are often not detected until later in the glaucoma continuum.^{105,336-338} This also explains why the results of this study yielded a higher AUROC for RGC count than HFA MD. The HFA AUROC value in discriminating between POAG and glaucoma suspect (0.61) in this study is similar to the results of a study conducted by Bowd and colleagues (2008) where the sensitivity of classifying eyes as healthy or glaucomatous at 0.75 specificity using VF MD was 0.64 in their cohort of 225 participants.³⁴⁹

There is currently no literature on the sensitivity of SVPs in differentiating between POAG and glaucoma suspects. Multiple studies, including those in Chapter 5 of this thesis, have demonstrated that there is a link between SVP amplitudes and RNFL thickness, where reduced

SVPs in POAG are correlated to thinner RNFLs.^{163,233,235} This correlation is also reflected in the results of this study, as there were no significant differences in the AUROC of SVPs in distinguishing POAG from glaucoma suspects than RNFL thickness or RGC count. In contrast, SVPs achieved a significantly higher AUROC than HFA MD in distinguishing the two groups. These results suggests that SVPs are comparable and are as powerful as standard clinical markers for glaucoma diagnosis and there is potential to explore SVPs as an early diagnostic marker for glaucoma.

4.2 POAG vs NTG

When separating POAG and NTG, the AUROC of IOP was significantly higher than all other parameters, except SVPs. The main difference between POAG and NTG is the difference in IOP, where NTG presents with normal IOP.³⁵⁰⁻³⁵² Therefore the superiority of IOP compared to other standard clinical markers is expected. Interestingly, SVPs and IOP showed no significant difference in their ability to distinguish between the two groups. As described in Chapter 5, changes in the translaminal pressure difference in glaucoma, particularly NTG, may be a driver of this result. While IOP in NTG is within normal range, there is lower tolerance of normal IOP in eyes that have NTG, causing glaucomatous damage.³⁵² Furthermore, cerebrospinal fluid pressure (CSFp) has been found to be significantly reduced in NTG compared to POAG,²⁵⁸ affecting the translaminal pressure difference more so than in POAG, thus making SVPs more visible in NTG than in POAG. The difference in SVP amplitude between NTG and POAG appear to be sufficient in rendering SVP amplitude equal to IOP in differentiating the two diagnoses (AUROC 0.59 and 0.60 respectively; $p=0.45$).

4.3 Limitations

This study has a number of limitations that should be taken into account in future research. This study has utilised the glaucoma suspects group as a control group, whereas the cited texts have healthy control groups. A larger sample size as well as the inclusion of healthy age-matched controls will be essential in strengthening the results of this study, and will allow more comparable results to previous studies that have healthy control groups. Inclusion of healthy controls will allow analysis of the various markers in differentiating healthy eyes from glaucoma suspects as well as

confirmed glaucoma. Moreover, this additional group would help to establish normative data for SVPs across different age ranges. A greater range of glaucoma severity of each of the different types of glaucoma (POAG and NTG) in a larger cohort would be beneficial to this study to reveal the strength of SVPs in differentiating between different severities of glaucoma and how this compares to the standard clinical markers used in glaucoma (RNFL thickness, HFA MD, IOP) as well as markers such as RGC count.

5. Conclusions

In conclusion, this study demonstrates that SVPs have effective diagnostic ability in differentiating POAG from glaucoma suspects and NTG from POAG in comparison to other established markers. The importance of SVPs in glaucoma pathogenesis is evident in the results of this research, which indicates that SVPs are more closely related to early changes in glaucoma (RNFL thinning and RGC loss) than later (functional) and are a key differentiating marker when distinguishing between NTG and POAG.

While this study indicates that SVP amplitudes can be used alongside traditional clinical markers such as RNFL thickness, HFA MD and IOP in the differentiation of POAG from NTG and glaucoma suspects, further work is required to confirm these results. There is limited data in the literature comparing the relative diagnostic abilities of standard clinical test results for glaucoma in distinguishing glaucoma diagnoses (POAG from NTG) as well as glaucoma suspects from confirmed glaucoma. Early detection is crucial in preventing blindness and preserving visual function, therefore further research in this area is warranted.

Chapter 7

Longitudinal Changes in Spontaneous Retinal Venous Pulsations in Glaucoma

Chapter Summary

The presence of SVPs in all glaucoma, as well as its correlation with structural and functional clinical markers has been demonstrated so far. Moreover, the accuracy in glaucoma diagnosis using SVPs has been shown to be comparable to early structural markers (RNFL thickness and RGC count) in glaucoma. This chapter aims to assess longitudinal changes in SVPs in glaucoma. The results of this chapter reveal that SVP amplitudes change in parallel to structural and functional markers in glaucoma.

1. Introduction

Glaucomatous optic neuropathy involves progressive structural and functional changes related to progressive degeneration of retinal ganglion cells (RGCs) that manifest clinically as deterioration and thinning of the retinal nerve fiber layer (RNFL) and neuroretinal rim.^{30-33,35} Parallel to this progressive neurodegeneration, other structural changes such as progressive parapapillary atrophy and haemorrhages at the optic disc also occur.^{353,354} Changes in retinal vasculature over time in glaucoma have been studied and it has been found that there is a displacement of blood vessels away from the center of the optic nerve head over time.^{355,356} This change has been suggested to be attributed to areas of RNFL thinning in glaucoma and glaucoma suspects that cause tractional forces that pull RGC axons away from the blood vessel(s) in that area. As the RGC axons progressively degenerate and create greater areas of RNFL thinning, this tractional force may increase, further pulling the blood vessels progressively over time.^{356,357}

Other vascular markers in glaucoma have also been studied, as pathological changes to structure and function are also associated with changes in the vasculature and blood flow to the eye, particularly at the optic nerve head.^{156,157,160-163} Ocular blood flow has been reported to increase in the early stages of glaucoma in regions of RNFL thinning, which then declines progressively as glaucomatous pathology progresses.¹⁶⁰⁻¹⁶³ Moreover, retinal vascular calibre is reduced in glaucoma,^{172-174,176} with greater vessel narrowing in areas of greater glaucomatous damage.¹⁸¹⁻¹⁸³ Spontaneous retinal venous pulsations (SVPs) are a dynamic vascular marker for glaucoma,^{163,233-235} which have been reported variably in glaucoma, with some studies noting undetectable SVPs.^{163,233} A number of hypotheses have been proposed for reduced or absent SVPs in glaucoma, including an increased resistance to blood flow and narrowing of the central retinal vein (CRV) and its superior and inferior bifurcations, as well as a decrease in translaminal pressure difference.^{21,232} While SVP changes in glaucoma have been studied, there is no data at present about longitudinal changes in SVP amplitude in glaucoma. This study investigated progressive changes in SVP amplitude in glaucoma and glaucoma suspects in parallel to clinical markers for glaucoma including RNFL thickness and visual field loss, as well as an assessment of retinal ganglion cell count.

2. Methods

A total of thirty participants right eyes including 20 with confirmed primary open angle glaucoma (POAG) and 10 glaucoma suspects, were selected on the basis of availability of follow-up data, from a cohort of 128 participants. Patients recruited from three ophthalmology clinic sites in Sydney were included in the study if they had no history of diabetes and/or vascular and/or retinal pathology. Participants all had at least one follow-up visit within 12 months from their initial visit. A subset of fifteen participants also had a second follow-up visit (totalling three visits). At each visit, participants had a general ophthalmic workup including history, visual acuity and IOP assessment measured using applanation tonometry. RNFL assessment was conducted using optical coherence tomography (OCT) with either the Spectralis OCT (Heidelberg Engineering, Dossenheim, Germany Eye Explore version 1.10.20 using the RNFL algorithm) or the Cirrus HD-OCT (Carl Zeiss Meditec, version 5.2.1.12 Optic Disc Cube 200x200) on 29, 25 and 6 participants at visits 1, 2 and 3 respectively. Humphrey Visual Field (HFA; HFA II-i series or HFA III, Carl Zeiss, Meditec, Dublin, CA, Operating system 5.1) testing with SITA-Standard, SITA-Fast, or SITA-Faster strategy (stimulus size III white) was also performed on 27, 24 and 6 participants at visits 1, 2 and 3 respectively. A dilated 10 second video of the venous circulation at the optic nerve head was recorded following standard ophthalmic assessment in all participants and at all visits, using a tablet-based ophthalmoscope and pupil dilation using a single drop of 1% Tropicamide (Mydracyl).

2.1 Retinal videography and SVP quantification

Chapter 3 of this thesis describes the published detailed methodology of retinal videography using a tablet-based ophthalmoscope.³¹⁸ In brief, videography of the retinal circulation at the optic nerve was performed using an iOS-operating device with an attached add-on 20D indirect ophthalmoscopy lens. SVP video recordings were quantified by exporting individual video frames, manipulating image contrast and stabilizing frames to eliminate eye movements. The central retinal vein diameter or closest visible vein diameter over the optic nerve head was measured in

each frame and plotted against time. The same vessel location that was selected for analysis at the baseline visit was selected for analysis at subsequent visits for each participant.

2.2 Retinal ganglion cell estimates

RGC estimates were calculated in accordance with methods proposed by Medeiros et al^{131,152,297} based on Harwerth and colleagues' equations.³³ An in-depth description and discussion of these equations are reported in by Medeiros et al (2012) and summarised in Chapter 5 of this thesis.¹³¹

2.3 Statistical analysis

All numerical variables are presented in mean \pm standard deviation. Difference in parameters between visit 1 and visit 2 were analysed using a paired t-test. One-way analysis of variance (ANOVA) was used to assess difference in SVPs across the three visits (post-hoc analysis was also performed). Changes in SVP in visits 2 and 3 relative to the baseline visit 1 were assessed by plotting the symmetrised percentage SVP change ($\% \Delta$; Equation 4) against the SVP amplitude at visit 1,³⁰⁰ and then applying analysis of covariance (ANCOVA) to compare the slopes of the linear regression.

$$\text{Symmetrized } \% \Delta = \frac{SVP_f - SVP_1}{SVP_f + SVP_1} \times 100$$

Equation 4. Symmetrized percentage change ($\% \Delta$) in SVP amplitude across visits.

f = Visit number 2 or 3 (representing SVP amplitudes at either visit 2 or visit 3).

SVP_1 = SVP amplitude at the first visit.

2.4 Ethics

This study was performed in accordance with the guidelines of the Tenets of Helsinki and approved by the University of Technology Sydney and University of New South Wales Human Research Ethics Committees. Written and informed consent was obtained from each subject.

3. Results

All participants (n=30, 13 male) had a follow-up visit within 5-12 months of their first assessment. A subset of 15 participants had a second follow-up SVP assessment within 12 months of their second assessment (totalling 3 visits). The number of participants and assessments conducted at each visit is presented in Table 12.

Table 12. Number of glaucoma (and glaucoma suspect) patients assessed at each visit.

	RNFL thickness	Visual field Glaucoma (glaucoma suspects)	RGC count	SVP amplitude
Visit 1	20 (9)	18 (9)	18 (9)	20 (10)
Visit 2	17 (8)	17 (7)	16 (7)	20 (10)
Visit 3	4 (2)	4 (2)	4 (2)	10 (5)

Mean values for age, RNFL thickness, HFA MD, RGC count and SVP amplitude across two visits are presented in Table 13. Paired t-test analysis revealed no significant changes in any of the parameters across the two visits in either group of patients. There was also no significant difference in follow-up times for all patients grouped together ($p=0.15$). Changes in SVPs across three visits are illustrated in Figure 29 – this includes only the patients who had three visits and therefore there is a smaller sample of participants presented. While there is a variation of SVPs between visits, one-way ANOVA (and post-hoc) analysis revealed no significant changes across the visits ($p=0.3$).

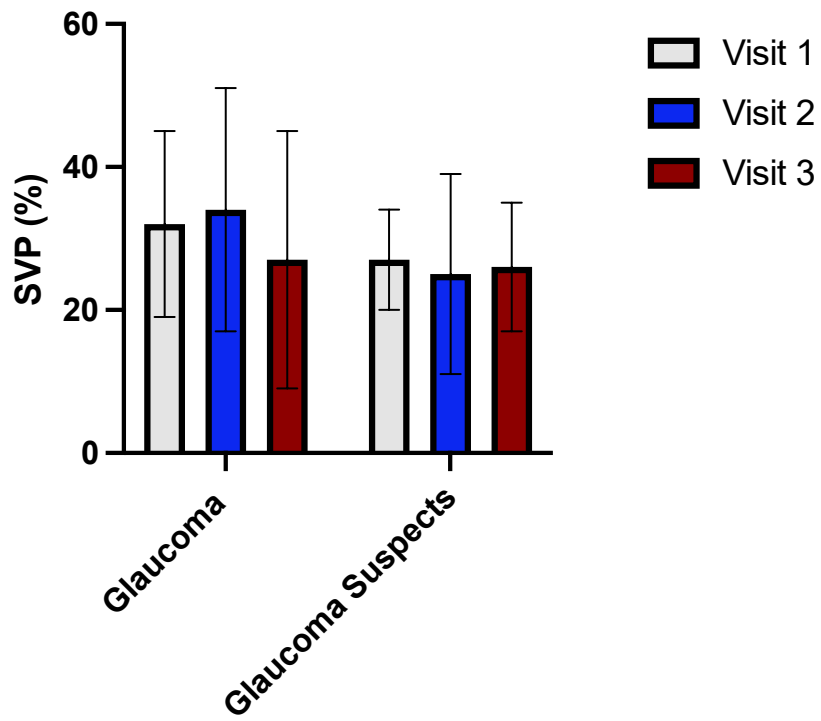


Figure 29. Changes in SVP amplitude across three visits in the subset of patients who had three visits (glaucoma n=10; glaucoma suspects n=5).

Table 13. Mean values for all measured parameter over two visits in patients with glaucoma and glaucoma suspects.

		Visit 1	Visit 2	Ratio (visit 2/visit 1)	<i>p</i> value
Glaucoma	Age (years)	64.7±9.0	65.6±8.8	1.01	0.8
	RNFL (μm)	78.1±15.3	75.3±14.5	0.96	0.6
	HFA MD (dB)	-1.8±2.2	-1.6±1.9	0.88	0.8
	RGC (count) x1000	744±177	718±138	0.96	0.6
	SVP (%)	27.2±14.3	26.7±15.8	0.98	0.9
Glaucoma Suspects	Age (years)	64.6±12.5	65.4±12.5	1.01	0.9
	RNFL (μm)	78.8±14.9	79.6±14.1	1.01	0.9
	HFA MD (dB)	-1.9±2.9	-1.4±2.6	0.73	0.7
	RGC (count) x1000	732±196	742±186	1.01	0.9
	SVP (%)	32.5±11.2	29.5±15.8	0.9	0.8

Changes in SVP relative to the first visit

To evaluate changes in SVP amplitude over the three visits, both in POAG and glaucoma suspects, the slope of symmetrized percentage change³⁰⁰ was assessed in SVPs (%Δ) from visit 2 and visit 3, relative to visit 1 (baseline). Analysis of covariance (ANCOVA) was used to assess difference in slopes between symmetrized %Δ and SVP at baseline in each of the two groups (glaucoma suspects and POAG).

In glaucoma suspects, ANCOVA analysis revealed that if the overall slopes were identical there is a 1.3% chance of randomly choosing data points with slopes this different. Accordingly, it can be

concluded that the differences between the slopes are significant (i.e., slope of Visit 2:Visit 1 vs slope of Visit 3:Visit 1, $p=0.01$) (Figure 30A,B). In POAG, ANCOVA analysis revealed that if the overall slopes were identical, there is a 54% chance of randomly choosing data points with slopes this different. Accordingly, it can be concluded that the differences between the slopes are not significant (i.e., slope of Visit 2:Visit 1 vs slope of Visit 3:Visit 1, $p=0.2$) (Figure 30 C, D). Since the slopes are not significantly different, it is possible to calculate a pooled slope of -0.13.

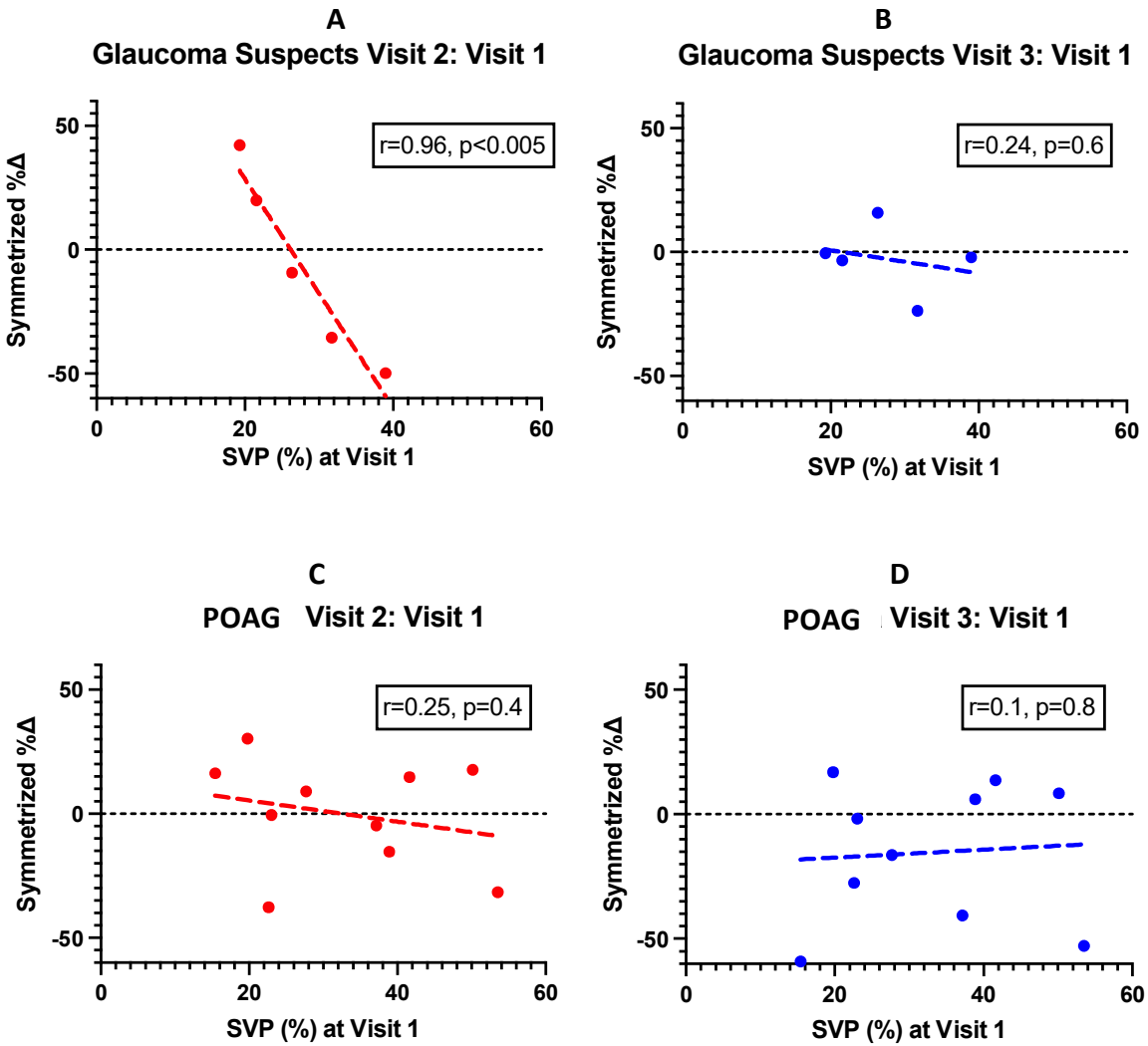


Figure 30. SVP changes relative to the baseline visit in glaucoma suspects (A, B n=5), and POAG (C, D, n=10). A significant difference in slopes between A and B was observed ($p=0.01$).

Linear mixed model regression of pooled data revealed an overall non-significant correlation between time, glaucoma subtype (as predictors) and SVP amplitude (as outcome; $r=0.26$; $p=0.38$). The coefficient for time and glaucoma subtype were $r = -0.01$ ($p=0.24$) and $r=4.23$ ($p=0.5$) respectively.

4. Discussion and conclusion

In this study longitudinal changes in SVP amplitude were observed in POAG and glaucoma suspects. SVPs were captured from the same individuals over a maximum of three visits, representing an approximate 2-year difference between the first and last visit in participants who had three visits. A downward but non-significant trend was observed in SVP amplitudes of both glaucoma and glaucoma suspects. The decline in SVP amplitude over time occurred alongside an expected decline in known structural and functional changes in confirmed glaucoma (RNFL thickness, RGC count and HFA MD). In both groups, there was an improvement in HFA MD that occurred at a faster rate over the two visits than other parameters. Glaucoma suspects demonstrated a decline in all other parameters except RNFL thickness and RGC count.

Studies have reported an increase in ocular blood flow in the early stages of glaucoma, which then declines progressively as the cascade of glaucomatous damage continues.¹⁶⁰⁻¹⁶³ Most participants who had glaucoma in this study had early glaucoma. The phenomenon of increased ocular blood flow in early glaucoma may explain the increase in SVP amplitude at visit two seen in Figure 29 in the glaucoma group. Moreover, there is a slight increase in SVP amplitude in the glaucoma suspect group in Figure 29 at visit three compared to visit two, which may also support this phenomenon. Further studies with a larger sample of glaucoma and glaucoma suspects with a larger spectrum of disease progression are needed to confirm this finding. It is also worth noting that all participants with confirmed glaucoma were receiving glaucoma treatment, therefore SVP amplitudes reported in this group may not be representative of “true” SVP amplitudes in glaucoma. Future studies with larger sample sizes and longer follow-up periods could capture changes in SVP amplitude of patients who progress from glaucoma suspects to confirmed glaucoma diagnosis.

To assess changes in SVP amplitude in visits 2 and 3, relative to visit 1 respectively, the association between symmetrized percentage change³⁰⁰ was evaluated in SVPs (visit 2 vs visit 1 and visit 3 vs visit 1) against baseline SVP values at visit 1, and then compared their slope using an ANCOVA analysis. This approach was chosen as comparing simple percentage change from baseline for each subsequent visit has been demonstrated to be statistically inefficient.³⁵⁸ This is mainly because percentage change does not correct for inter-group imbalance at baseline.³⁵⁸

In glaucoma suspects a significant and negative association was observed in symmetrized % Δ SVP changes at visit 2 relative to visit 1. In other words, patients with higher SVP at baseline had progressed to a significantly lower SVP at visit 2. While this was contrary to RNFL thickness, HFA and RGC count changes that showed a slight improvement from visit 1 to visit 2 (Table 12), it is nonetheless consistent with our findings in Chapter 5 that demonstrated a negative relationship between SVP amplitudes and structural-functional markers in glaucoma suspects. By the third visit SVP amplitude had recovered, and a slightly negative but insignificant association was observed in symmetrized % Δ SVP changes at visit 3 relative to visit 1. While there are no measurements for structural and/or functional parameters at visit 3, this increase of SVP from visit 2 is suggestive of an improvement in the blood flow to the optic nerve head and/or an increase in the translaminal pressure difference (as a result of an increase in IOP or decrease in cerebrospinal fluid pressure). Both of these findings have been demonstrated in previous studies.³⁵⁹

In the POAG group a significant change in SVPs from visit 1 to visit 2 or 3 could not be established. However given the positive association revealed between SVP amplitudes and structural-functional parameters in this cohort, a positive change in SVP amplitudes with a larger sample size and longer follow-up duration is expected.

There are limitations in this study that can be addressed in future research. Firstly, the sample size studied was very limited, which was attributed to difficulty in following up patients exacerbated by recruitment of patients across three different clinics. Having a larger baseline sample would naturally increase the number of patients that have follow-up appointments. Regardless, follow-up appointments should be prioritised in order to establish larger and more equally distributed

sample sizes at subsequent visits. The sample of patients (across all visits) should also be varied in diagnosis with equal distribution of early, moderate and late stage glaucoma. Doing so would strengthen the results of this study and may highlight more significant changes in the parameters.

Secondly, the addition of participants that progress from glaucoma suspect to glaucoma would be invaluable to this study, allowing for observation of changes that occur across diagnoses, not only between the different groups (glaucoma suspects and glaucoma) but also within a group of patients (those who have progressed from glaucoma suspect status to confirmed glaucoma). Moreover, this would allow for the analysis of changes in SVP amplitude and other parameters before and after the commencement of glaucoma treatment. Ideally this would be monitored across visits until the patient has reached stability in their glaucoma status, allowing us to assess whether SVPs can be used as a means to monitor treatment and its efficacy. However this would require longer follow-up periods to allow for these changes to develop. Regardless of glaucoma status, the follow-up period in this study was limited. The relatively short duration of this study can compromise the significance of the changes that were observed.

Thirdly, data on treatment was unavailable to establish the effect of treatment type such as type of pharmaceutical drops, frequency of use and change in course of treatment. In future, data should be extracted regarding each participants treatment. Finally, the addition of a healthy age-matched group would have allowed us to monitor the changes in SVPs and other parameters in reference to normal aging.

In conclusion, SVP amplitudes in POAG change in parallel to structural markers such as RNFL thinning. However in glaucoma suspects, despite a slight improvement in these structural and functional indices, SVPs continued to decline within a 12 month follow up period from baseline. While the significance of the changes could not be statistically established in either of the groups, this can be attributed to a relatively low sample size and short follow up duration. Further studies are required to determine if longitudinal SVP changes are associated with progressive glaucoma and whether they can be used as a marker for monitoring disease progression.

Chapter 8

Conclusions & Future Directions

Chapter Summary

This chapter provides an overview of findings of the previous chapters and how they address the objectives of this thesis. The limitations of this thesis have been outlined as well as future directions for research in the field of SVPs in glaucoma assessment.

1. Conclusions

Several functional, structural, and vascular markers of glaucoma have been developed in the literature and studied clinically in a diverse cohort of patients (early, moderate, severe disease severity, different subtypes, etc). This has resulted in the development of a time stamp of pathophysiological changes associated with glaucoma, with each of the markers directly linked to the various pathophysiological hallmarks. More specifically, OCT scans are now more utilised in the assessment of structural changes observed at the optic nerve head. These changes are known to often precede the functional changes that are evident at the symptomatic stages of the glaucoma, and that are evaluated using standard automated perimetry.

Development of OCT angiography (OCT-A) in 2014, opened a new avenue of research in identifying glaucoma-specific vascular changes. OCT-A is reported as a powerful tool in the assessment of optic disc perfusion through evaluation of peripapillary and macular vessel density. Studies have shown that changes in ocular perfusion are detectable in pre-perimetric patients. As such, assessment of vascular markers has gained immense popularity in the early detection of glaucomatous damage.

Despite all these advances, over half of all people with glaucoma are unaware of their disease, and more than 72% of new cases are detected incidentally during ocular examination for another unrelated reasons.¹⁵⁰ An effective screening program can identify individuals at greater risk of the disease and facilitate appropriate referral pathways to prevent further vision loss and subsequent disability.

However, there is currently no formal program for glaucoma screening in Australia.^{360,361} There are two main reasons for this: firstly, glaucoma screening is not considered to be cost effective and, secondly, an optimal, portable and inexpensive test has not yet been developed. While one may argue that the development of newer devices such as OCT-A addresses part of the second problem, nevertheless, scalability and accessibility of such technology, due to high procurement costs and skilled personnel needed to operate the device, remains as a major hurdle. Considering these limitations and the significant value of vascular markers in glaucoma, particularly in the early

stages of the disease, motivated this study to explore this area of vision science further. More specifically, the purpose was to make use of a tool that is clinically translatable, scalable and also accessible. Furthermore, the decision to focus on a dynamic vascular marker (i.e., spontaneous retinal venous pulsations (SVPs)), was based on its identification as an area that has been underexplored in glaucoma.

To achieve this goal, a novel custom-built tablet-based ophthalmoscope was used. This new device is not only economical, but it's also easy to operate and light weight and thus, has the potential to address the aforementioned limitations, particularly for widespread screening for glaucoma. The specific aims of this thesis were therefore:

1. To determine the feasibility of a novel tablet-based ophthalmoscope in detecting SVPs and objectively quantifying them.
2. To study SVPs, as a dynamic vascular marker of glaucoma, in comparison to established clinical structural and functional markers for glaucoma.

The use of the tablet-based (iOS operating system) indirect ophthalmoscope to detect, and later quantify, SVPs was explored in a sample of individuals with glaucoma in **Chapter 3** of this thesis. Detailed methodology relating to the use of the novel device in detecting SVPs as well as the relevant digital analysis techniques were outlined in this chapter. The results of this chapter demonstrated a proof of principal that the novel device, in conjunction with appropriate computer analysis, can be used successfully to detect and quantify SVPs in all types of glaucoma (suspect, primary open-angle glaucoma (POAG), normal tension glaucoma (NTG)).

In **Chapter 4**, SVPs were quantified in individuals with glaucoma (POAG and NTG) and those who were glaucoma suspects. This chapter demonstrated that SVP detection and quantification is possible using the novel device regardless of glaucoma severity. The magnitude of SVP amplitudes in those participants with NTG, were found to have a significant association with gender (larger in females) and older age. More importantly, it was also revealed that SVP amplitude is related to the severity of glaucoma diagnosis, with NTG having the greatest SVP amplitudes, followed by POAG

and finally the lowest amplitude in was found in glaucoma suspects. These results reveal the potential of SVP quantification to differentiating between various levels of glaucoma diagnoses.

The next aim of this research was to establish the relationship between SVPs and other traditional clinical markers for glaucoma such as RNFL thinning, VF loss, IOP as well as RGC count. Results outlined in **Chapter 5** revealed a positive correlation between SVP amplitude and known structural and functional markers (RNFL thickness and VF loss) in all diagnosed glaucoma participants (POAG and NTG). The strongest correlation in the POAG group was between SVP amplitude and RGC count, while the strongest correlation in the NTG group was between SVP amplitude and RNFL thickness. The correlation between SVP amplitude and RGC count was also the strongest in the glaucoma suspect group. However, this group demonstrated a negative correlation between SVP amplitude and other structural and functional parameters, i.e. there was an increase in RNFL thickness and RGC count with a decreasing SVP amplitude. These results reflect previous literature that have reported an increase in blood flow in areas of RNFL thinning in early glaucoma with a progressive decline in ocular blood flow with increased glaucoma progression.¹⁶⁰⁻¹⁶³ This is similar to the negative correlation found in the glaucoma suspects group in this study. Therefore, this chapter has demonstrated the alignment of SVPs with traditional clinical and scientific markers for glaucoma. Moreover, the significant association between SVP amplitudes and structural parameters demonstrated that SVPs may reflect early glaucomatous change within the first two stages of the glaucoma continuum, when structural changes are present.

SVP analysis, through the use of the novel tablet-based ophthalmoscope technology, was found to be a valid dynamic vascular marker of glaucoma. The next step was to explore the accuracy of SVPs in distinguishing glaucoma sub-types compared to existing clinical markers (RNFL thickness, VF loss, IOP) as well as RGC count. In **Chapter 6**, the accuracy of each marker/parameter was assessed to determine its capacity to distinguish POAG from glaucoma suspects, as well as POAG from NTG. The results of this chapter revealed that SVP amplitudes are almost equally as effective as IOP measurements in distinguishing POAG from NTG. They are also almost equally as effective as RNFL thickness measurements and RGC counts when distinguishing POAG from glaucoma

suspects. In summary, this chapter demonstrated that SVPs are comparable to established markers in differentiating between POAG and glaucoma suspects.

Finally, in **Chapter 7**, longitudinal changes in SVPs overtime were assessed by following a small sample of confirmed glaucoma (POAG) and glaucoma suspects over a minimum of 12 months. There was an overall reduction in SVP amplitude in both confirmed glaucoma participants and those who were glaucoma suspects, demonstrating the potential of SVPs as a marker for monitoring glaucomatous progression. This decline in SVP amplitude was somewhat mirrored by the expected decline in structural and functional changes in all participants with glaucoma. These results indicate that SVPs may be used as a marker to monitor the efficacy of glaucoma treatment as well as a marker for progression towards glaucomatous decline in glaucoma suspects. However, a larger and heterogenous sample size is required to confirm these findings

In summary, the main findings of this thesis are:

1. Tablet-based ophthalmoscopy can be used to detect and objectively quantify SVP amplitudes, which provides a portable and more cost-efficient method that can be used as alongside traditional clinical tools.
2. SVPs can be detected in both confirmed glaucoma and glaucoma suspects, with glaucoma suspects having reduced SVP amplitudes compared to SVPs in POAG.
3. SVPs in NTG are greater than SVPs in both POAG and glaucoma suspects.
4. SVPs are positively correlated to structural and functional changes in confirmed glaucoma.
5. SVPs are negatively correlated to structural and functional changes in glaucoma suspects.
6. SVP amplitudes are almost as equally effective in distinguishing between glaucoma suspects and confirmed glaucoma as established clinical structural markers.
7. There is indication of a potential overall reduction in SVP amplitude in glaucoma and glaucoma suspects over 12months.

2. Future directions

Using a novel tablet-based ophthalmoscope, the potential of SVPs as a dynamic vascular marker of glaucoma was revealed. Propelled by compelling findings from this study, it appears that SVP analysis can also be used for glaucoma screening. However, there are some shortcomings that should be addressed in future research to consolidate the current findings and provide justification for a screening program for glaucoma.

1. An area of importance is for future research to explore these findings in a larger population of patients with glaucoma and suspected glaucoma. A large sample of data was collected for this thesis, however a portion of this data was not useable due to some participants having missing clinical information (e.g. IOP, OCT and HVF results being more than 12 months since their SVP recording or absent). This overall reduced the dataset homogeneity. Furthermore, an enrichment strategy for sampling can be used to selectively recruit participants that would maximise the amount of data for analysis for glaucoma subtypes.
2. A major area of future research to build on the findings of this thesis is the establishment of SVPs in age-matched healthy controls. Establishing normal SVP amplitudes in healthy eyes can further the use of SVPs as a potential early marker for glaucoma. A database of healthy SVP amplitudes at different ages also has potential to be useful in non-ophthalmic settings, such as for patients in hospital intensive care and cardiac care units. Furthermore, having a large sample of healthy controls would be useful to establish intra- and inter-session repeatability. This aspect of SVPs also warrants further exploration.
3. Future investigations of longitudinal changes in SVP amplitude over time would be of great benefit to better understanding the role of SVPs in the natural history of glaucoma, in glaucoma diagnosis and its treatment. Of significant interest and value, would be to track annual or biannual changes in SVPs overtime in participants from early to late adulthood (e.g. 20 to 60 years and beyond) who have healthy eyes and those who are glaucoma suspects as well as those with a confirmed diagnosis of glaucoma. This would be beneficial

in revealing changes in SVP amplitude in healthy ageing eyes, which would possibly confirm reports of increased SVP visibility with older age,^{232,254} that may potentially be due to increased SVP amplitudes possibly related to underlying age-related cardio-vascular changes. Tracking these changes in healthy eyes can be compared to the changes that occur in participants who progress from glaucoma suspect status to confirmed glaucoma. Results from such a study, while time consuming, will reveal significant information that has great potential to aid prediction and diagnosis of glaucoma, and potentially other ocular and systemic conditions as well. Moreover, tracking longitudinal changes in SVPs is beneficial in aiding glaucoma management by assessing the changes in SVP amplitude in glaucoma suspects that have developed glaucoma and are trialling a new management plan. The SVPs may reveal the efficacy of treatment in these patients as well as those who have long-standing glaucoma and require changes to their treatment.

4. Analysis of additional factors such as systemic hypertensive status, sphygmomanometer results, type and duration of glaucoma treatment would also be beneficial in revealing the effects of on SVP amplitude. Moreover, the effect of height and weight should be recorded and analysed for each participant as a means to non-invasively estimate CSFp to establish the correlation between SVP amplitude and CSFp. These factors would aid our understanding on how SVPs change in various individual situations and better understand the effect of glaucoma on SVPs when compounded and isolated from additional factors.
5. Another area of future development is to automate the computer analysis component of the SVP quantification process. The current process has been described in detail in Chapter 3 of this thesis. While the computer analysis process is relatively simple, it is time consuming, which was a major challenge for the analysis of the data collected for this thesis. Collaboration with an information technologist or information technology team would be a practical step forward from this thesis. It would allow the development of an application to be used on the tablet (iOS operating device) to perform the SVP analysis quantification method automatically. This would increase the practicality of the device as a clinical tool requiring no external analysis. Such an application would allow the clinician to

select an ocular blood vessel while the software automatically performs the calculations and analyses to reveal the SVP amplitude, its average diameter and determine whether these parameters falls within the normal range of SVP amplitude for the age group under assessment. Moreover, a more time-effective way to quantify the SVPs may be to use an automated application with an AI-based framework for the tablet. Doing so will increase the usability of the device as a clinical tool not only in glaucoma but other specific conditions. Furthermore, such applications would allow the device to be used as a stand-alone screening tool, capable of use as an initial screening test for glaucoma (before warranting further assessment using the expensive and non-portable benchtop devices) in particular for underserved and rural areas, as well as in mobile clinic services. The introduction of a larger dataset with more longitudinal data will increase the likelihood of accurate screening and monitoring of glaucoma using this tool.

6. Another area of future development in this research is the use of artificial intelligence (AI) to enhance glaucoma detection using SVP videos. So far, a proof-of-principal study has been conducted and published using the data collected for this thesis (full paper included in Appendix 5). The study outlines the development of an AI-based framework that combines the use of static fundus photos and SVP videos to discriminate glaucoma from healthy eyes. The results of this study revealed that this model had a 96.2% accuracy in differentiating glaucoma from healthy eyes, compared to 79.2% accuracy when relied on structural features in static fundus images alone (fundus images). This demonstrates enhanced glaucoma detection compared to traditional artificial neural networks that can be incorporated into the application to be used on the tablet (see point 4 above re proposed potential technological developments).
7. This thesis has demonstrated the potential use of the novel tablet-based ophthalmoscope in detecting and quantifying SVPs in glaucoma and glaucoma suspects, as well as reveal the correlation between SVPs and common clinical markers of glaucoma. However, research is required to evaluate how SVPs compare to other vascular markers in glaucoma that have

been recently identified using OCT-A, such as vessel density.²⁰⁵⁻²⁰⁷ Doing so would provide a better understanding of the pathogenesis of glaucoma.

References

References

1. Snell RS, Lemp MA. *Clinical anatomy of the eye*. John Wiley & Sons; 2013.
2. Prada D, Harris A, Guidoboni G, Rowe L, Verticchio-Vercellin AC, Mathew S. Vascular anatomy and physiology of the eye. In: *Ocular Fluid Dynamics*. Springer; 2019:23-45.
3. Remington LA, Goodwin D. *Clinical anatomy of the visual system E-Book*. Elsevier Health Sciences; 2011.
4. Ogden TE. Nerve fiber layer of the macaque retina: retinotopic organization. *Investigative ophthalmology & visual science*. 1983;24(1):85-98.
5. Hoyt WF, Tudor RC. The course of parapapillary temporal retinal axons through the anterior optic nerve: a Nauta degeneration study in the primate. *Archives of Ophthalmology*. 1963;69(4):503-507.
6. Harrington DO. The Visual Fields. *Academic Medicine*. 1965;40(3):318.
7. Raza AS, Cho J, de Moraes CG, et al. Retinal ganglion cell layer thickness and local visual field sensitivity in glaucoma. *Archives of ophthalmology*. 2011;129(12):1529-1536.
8. Hwang YH, Jeong YC, Kim HK, Sohn YH. Macular ganglion cell analysis for early detection of glaucoma. *Ophthalmology*. 2014;121(8):1508-1515.
9. Kelts EA. The basic anatomy of the optic nerve and visual system (or, why Thoreau was wrong). *NeuroRehabilitation*. 2010;27(3):217-222.
10. Yanoff M, Duker J. Patient workup for cataract surgery. . *Ophthalmology, 2nd Edn, New Delhi, Elsevier*. 2004.
11. Wassle H, Boycott BB. Functional architecture of the mammalian retina. *Physiological reviews*. 1991;71(2):447-480.
12. Rodieck RW, Binmoeller K, Dineen J. Parasol and midget ganglion cells of the human retina. *Journal of Comparative Neurology*. 1985;233(1):115-132.
13. Reinhard K, Münch TA. Visual properties of human retinal ganglion cells. *Plos one*. 2021;16(2):e0246952.
14. Kolb H, Linberg KA, Fisher SK. Neurons of the human retina: a Golgi study. *Journal of comparative neurology*. 1992;318(2):147-187.

15. Kolb H, Dekorver L. Midget ganglion cells of the parafovea of the human retina: a study by electron microscopy and serial section reconstructions. *Journal of Comparative Neurology*. 1991;303(4):617-636.
16. Harris A, Jones-Cuypers CP, Ciulla TA, Kagemann L, Kriegelstein GK. *Atlas of ocular blood flow: vascular anatomy, pathophysiology, and metabolism*. Butterworth-Heinemann Medical; 2003.
17. Guidoboni G, Harris A, Sacco R. *Ocular Fluid Dynamics: Anatomy, Physiology, Imaging Techniques, and Mathematical Modeling*. Springer; 2019.
18. Campbell J, Zhang M, Hwang T, et al. Detailed vascular anatomy of the human retina by projection-resolved optical coherence tomography angiography. *Scientific reports*. 2017;7(1):1-11.
19. Ansari MW, Nadeem A. The Blood Supply to the Eyeball. In: *Atlas of Ocular Anatomy*. Springer; 2016:29-38.
20. Golzan SM, Avolio A, Graham SL. Hemodynamic interactions in the eye: a review. *Ophthalmologica*. 2012;228(4):214-221.
21. Morgan WH, Hazelton ML, Yu DY. Retinal venous pulsation: Expanding our understanding and use of this enigmatic phenomenon. *Prog Retin Eye Res*. 2016;55:82-107.
22. Volpe NJ. Adler's Physiology of the Eye: Clinical Application. *Journal of Neuro-ophthalmology*. 2004;24(4):348.
23. Wybar K. Wolff's Anatomy of the Eye and Orbit. *The British Journal of Ophthalmology*. 1977;61(4):302.
24. Browning DJ. Anatomy and pathologic anatomy of retinal vein occlusions. In: *Retinal Vein Occlusions*. Springer; 2012:1-31.
25. Tham YC, Li X, Wong TY, Quigley HA, Aung T, Cheng CY. Global prevalence of glaucoma and projections of glaucoma burden through 2040: a systematic review and meta-analysis. *Ophthalmology*. 2014;121(11):2081-2090.
26. Stevens GA, White RA, Flaxman SR, et al. Global prevalence of vision impairment and blindness: magnitude and temporal trends, 1990-2010. *Ophthalmology*. 2013;120(12):2377-2384.
27. Bourne RR, Stevens GA, White RA, et al. Causes of vision loss worldwide, 1990-2010: a systematic analysis. *Lancet Glob Health*. 2013;1(6):e339-349.
28. Foster PJ, Buhrmann R, Quigley HA, Johnson GJ. The definition and classification of glaucoma in prevalence surveys. *British journal of ophthalmology*. 2002;86(2):238-242.

29. Cook C, Foster P. Epidemiology of glaucoma: what's new? *Canadian Journal of Ophthalmology*. 2012;47(3):223-226.
30. Jonas JB, Aung T, Bourne RR, Bron AM, Ritch R, Panda-Jonas S. Glaucoma. *The Lancet*. 2017;390:2083-2093.
31. Kwon YH, Fingert JH, Kuehn MH, Alward WL. Primary open-angle glaucoma. *New England Journal of Medicine*. 2009;360(11):1113-1124.
32. Weinreb RN, Khaw PT. Primary open-angle glaucoma. *The Lancet*. 2004;363(9422):1711-1720.
33. Harwerth RS, Wheat JL, Fredette MJ, Anderson DR. Linking structure and function in glaucoma. *Prog Retin Eye Res*. 2010;29(4):249-271.
34. Danesh-Meyer HV, Levin LA. Glaucoma as a neurodegenerative disease. *Journal of Neuro-Ophthalmology*. 2015;35:S22-S28.
35. Almasieh M, Wilson AM, Morquette B, Vargas JLC, Di Polo A. The molecular basis of retinal ganglion cell death in glaucoma. *Progress in retinal and eye research*. 2012;31(2):152-181.
36. Vaajanen A, Vapaatalo H. Local ocular renin–angiotensin system—a target for glaucoma therapy? *Basic & clinical pharmacology & toxicology*. 2011;109(4):217-224.
37. Anderson DR, Drance SM, Schulzer M. Factors that predict the benefit of lowering intraocular pressure in normal tension glaucoma. *American journal of ophthalmology*. 2003;136(5):820-829.
38. Kass MA, Gordon MO, Gao F, et al. Delaying treatment of ocular hypertension: the ocular hypertension treatment study. *Archives of ophthalmology*. 2010;128(3):276.
39. Quigley HA, Broman AT. The number of people with glaucoma worldwide in 2010 and 2020. *Br J Ophthalmol*. 2006;90(3):262-267.
40. Heijl A, Bengtsson B, Hyman L, Leske MC, Group EMGT. Natural history of open-angle glaucoma. *Ophthalmology*. 2009;116(12):2271-2276.
41. Rudnicka AR, Mt-Isa S, Owen CG, Cook DG, Ashby D. Variations in primary open-angle glaucoma prevalence by age, gender, and race: a Bayesian meta-analysis. *Investigative ophthalmology & visual science*. 2006;47(10):4254-4261.
42. Kim KE, Kim MJ, Park KH, et al. Prevalence, awareness, and risk factors of primary open-angle glaucoma: Korea National Health and Nutrition Examination Survey 2008–2011. *Ophthalmology*. 2016;123(3):532-541.

43. Garway-Heath DF, Crabb DP, Bunce C, et al. Latanoprost for open-angle glaucoma (UKGTS): a randomised, multicentre, placebo-controlled trial. *The Lancet*. 2015;385(9975):1295-1304.
44. Leske MC, Heijl A, Hussein M, Bengtsson B, Hyman L, Komaroff E. Factors for glaucoma progression and the effect of treatment: the early manifest glaucoma trial. *Archives of ophthalmology*. 2003;121(1):48-56.
45. Kass MA, Heuer DK, Higginbotham EJ, et al. The Ocular Hypertension Treatment Study: a randomized trial determines that topical ocular hypotensive medication delays or prevents the onset of primary open-angle glaucoma. *Arch Ophthalmol*. 2002;120(6):701-713; discussion 829-730.
46. Lichter PR, Musch DC, Gillespie BW, et al. Interim clinical outcomes in the Collaborative Initial Glaucoma Treatment Study comparing initial treatment randomized to medications or surgery. *Ophthalmology*. 2001;108(11):1943-1953.
47. Medeiros FA, Weinreb RN, Zangwill LM, et al. Long-term intraocular pressure fluctuations and risk of conversion from ocular hypertension to glaucoma. *Ophthalmology*. 2008;115(6):934-940.
48. Sharif NA. Ocular hypertension and glaucoma: a review and current perspectives. *Int J Ophthalmol Vis Sci*. 2017;2:22-36.
49. Investigators A. The Advanced Glaucoma Intervention Study (AGIS): 7. The relationship between control of intraocular pressure and visual field deterioration. *Am J Ophthalmol*. 2000;130:429-440.
50. Amerasinghe N, Aung T. Angle-closure: risk factors, diagnosis and treatment. *Progress in brain research*. 2008;173:31-45.
51. Cedrone C, Mancino R, Cerulli A, Cesareo M, Nucci C. Epidemiology of primary glaucoma: prevalence, incidence, and blinding effects. *Progress in brain research*. 2008;173:3-14.
52. Higginbotham EJ. Does sex matter in glaucoma? *Archives of Ophthalmology*. 2004;122(3):374-375.
53. Mason RP, Kosoko O, Wilson MR, et al. National survey of the prevalence and risk factors of glaucoma in St. Lucia, West Indies: Part I. Prevalence findings. *Ophthalmology*. 1989;96(9):1363-1368.
54. Leske MC, Connell A, Schachat AP, Hyman L. The Barbados Eye Study: prevalence of open angle glaucoma. *Archives of ophthalmology*. 1994;112(6):821-829.

55. Friedman DS, Jampel HD, Munoz B, West SK. The prevalence of open-angle glaucoma among blacks and whites 73 years and older: the Salisbury Eye Evaluation Glaucoma Study. *Archives of ophthalmology*. 2006;124(11):1625-1630.
56. Tielsch JM, Sommer A, Katz J, Royall RM, Quigley HA, Javitt J. Racial variations in the prevalence of primary open-angle glaucoma: the Baltimore Eye Survey. *Jama*. 1991;266(3):369-374.
57. Song W, Shan L, Cheng F, et al. Prevalence of glaucoma in a rural northern china adult population: a population-based survey in kailu county, inner mongolia. *Ophthalmology*. 2011;118(10):1982-1988.
58. Casson R, Newland H, Muecke J, et al. Prevalence of glaucoma in rural Myanmar: the Meiktila Eye Study. *British journal of ophthalmology*. 2007;91(6):710-714.
59. Xu L, Wang Y, Wang S, Wang Y, Jonas JB. High myopia and glaucoma susceptibility: the Beijing Eye Study. *Ophthalmology*. 2007;114(2):216-220.
60. Qiu M, Wang SY, Singh K, Lin SC. Association between myopia and glaucoma in the United States population. *Investigative ophthalmology & visual science*. 2013;54(1):830-835.
61. Perera SA, Wong TY, Tay W-T, Foster PJ, Saw S-M, Aung T. Refractive error, axial dimensions, and primary open-angle glaucoma: the Singapore Malay Eye Study. *Archives of ophthalmology*. 2010;128(7):900-905.
62. Nagaoka N, Jonas JB, Morohoshi K, et al. Glaucomatous-type optic discs in high myopia. *PLoS One*. 2015;10(10):e0138825.
63. Ding X, Chang RT, Guo X, et al. Visual field defect classification in the Zhongshan Ophthalmic Center-Brien Holden Vision Institute High Myopia Registry Study. *Br J Ophthalmol*. 2016;100(12):1697-1702.
64. Scott R, Grosvenor T. Structural model for emmetropic and myopic eyes. *Ophthalmic Physiol Opt*. 1993;13(1):41-47.
65. Saw SM, Gazzard G, Shih-Yen EC, Chua WH. Myopia and associated pathological complications. *Ophthalmic Physiol Opt*. 2005;25(5):381-391.
66. Wang X, Rumpel H, Lim WEH, et al. Finite element analysis predicts large optic nerve head strains during horizontal eye movements. *Investigative ophthalmology & visual science*. 2016;57(6):2452-2462.
67. Ozdek SC, Onol M, Gurelik G, Hasanreisoglu B. Scanning laser polarimetry in normal subjects and patients with myopia. *Br J Ophthalmol*. 2000;84(3):264-267.

68. Tay E, Seah SK, Chan SP, et al. Optic disk ovality as an index of tilt and its relationship to myopia and perimetry. *Am J Ophthalmol.* 2005;139(2):247-252.
69. Melo GB, Libera RD, Barbosa AS, Pereira LM, Doi LM, Melo LA, Jr. Comparison of optic disk and retinal nerve fiber layer thickness in nonglaucomatous and glaucomatous patients with high myopia. *Am J Ophthalmol.* 2006;142(5):858-860.
70. Shoji T, Sato H, Ishida M, Takeuchi M, Chihara E. Assessment of glaucomatous changes in subjects with high myopia using spectral domain optical coherence tomography. *Investigative ophthalmology & visual science.* 2011;52(2):1098-1102.
71. Thorleifsson G, Walters GB, Hewitt AW, et al. Common variants near CAV1 and CAV2 are associated with primary open-angle glaucoma. *Nature genetics.* 2010;42(10):906-909.
72. Thorleifsson G, Magnusson KP, Sulem P, et al. Common sequence variants in the LOXL1 gene confer susceptibility to exfoliation glaucoma. *Science.* 2007;317(5843):1397-1400.
73. Burdon KP, Macgregor S, Hewitt AW, et al. Genome-wide association study identifies susceptibility loci for open angle glaucoma at TMCO1 and CDKN2B-AS1. *Nature genetics.* 2011;43(6):574-578.
74. van Koolwijk LM, Ramdas WD, Ikram MK, et al. Common genetic determinants of intraocular pressure and primary open-angle glaucoma. *PLoS Genet.* 2012;8(5):e1002611.
75. Wiggs JL, Yaspan BL, Hauser MA, et al. Common variants at 9p21 and 8q22 are associated with increased susceptibility to optic nerve degeneration in glaucoma. *PLoS Genet.* 2012;8(4):e1002654.
76. Wiggs JL, Pasquale LR. Genetics of glaucoma. *Human molecular genetics.* 2017;26(R1):R21-R27.
77. Vithana EN, Khor C-C, Qiao C, et al. Genome-wide association analyses identify three new susceptibility loci for primary angle closure glaucoma. *Nature genetics.* 2012;44(10):1142-1146.
78. Khor CC, Do T, Jia H, et al. Genome-wide association study identifies five new susceptibility loci for primary angle closure glaucoma. *Nature genetics.* 2016;48(5):556-562.
79. Aung T, Ozaki M, Lee MC, et al. Genetic association study of exfoliation syndrome identifies a protective rare variant at LOXL1 and five new susceptibility loci. *Nature genetics.* 2017;49(7):993-1004.
80. Gordon MO, Beiser JA, Brandt JD, et al. The Ocular Hypertension Treatment Study: baseline factors that predict the onset of primary open-angle glaucoma. *Archives of ophthalmology.* 2002;120(6):714-720.

81. Jonas JB, Holbach L. Central corneal thickness and thickness of the lamina cribrosa in human eyes. *Investigative ophthalmology & visual science*. 2005;46(4):1275-1279.
82. Nongpiur ME, Png O, Chiew JW, et al. Lack of association between corneal hysteresis and corneal resistance factor with glaucoma severity in primary angle closure glaucoma. *Investigative ophthalmology & visual science*. 2015;56(11):6879-6885.
83. Day AC, Machin D, Aung T, et al. Central corneal thickness and glaucoma in East Asian people. *Investigative Ophthalmology & Visual Science*. 2011;52(11):8407-8412.
84. Quaranta L, Riva I, Gerardi C, Oddone F, Floriano I, Konstas AG. Quality of life in glaucoma: a review of the literature. *Advances in therapy*. 2016;33(6):959-981.
85. Ramulu PY, Maul E, Hochberg C, Chan ES, Ferrucci L, Friedman DS. Real-world assessment of physical activity in glaucoma using an accelerometer. *Ophthalmology*. 2012;119(6):1159-1166.
86. Nelson P, Aspinall P, Papasouliotis O, Worton B, O'Brien C. Quality of life in glaucoma and its relationship with visual function. *Journal of glaucoma*. 2003;12(2):139-150.
87. Burr JM, Kilonzo M, Vale L, Ryan M. Developing a preference-based Glaucoma Utility Index using a discrete choice experiment. *Optom Vis Sci*. 2007;84(8):797-808.
88. Aspinall PA, Johnson ZK, Azuara-Blanco A, Montarzino A, Brice R, Vickers A. Evaluation of quality of life and priorities of patients with glaucoma. *Investigative ophthalmology & visual science*. 2008;49(5):1907-1915.
89. Ramulu P. Glaucoma and disability: which tasks are affected, and at what stage of disease? *Current opinion in ophthalmology*. 2009;20(2):92.
90. Ramulu PY, West SK, Munoz B, Jampel HD, Friedman DS. Driving cessation and driving limitation in glaucoma: the Salisbury Eye Evaluation Project. *Ophthalmology*. 2009;116(10):1846-1853.
91. Campbell MK, Bush TL, Hale WE. Medical conditions associated with driving cessation in community-dwelling, ambulatory elders. *Journal of Gerontology*. 1993;48(4):S230-S234.
92. Freeman EE, Munoz B, Rubin G, West SK. Visual field loss increases the risk of falls in older adults: the Salisbury eye evaluation. *Investigative ophthalmology & visual science*. 2007;48(10):4445-4450.
93. Murphy SL, Dubin JA, Gill TM. The development of fear of falling among community-living older women: predisposing factors and subsequent fall events. *The Journals of Gerontology Series A: Biological Sciences and Medical Sciences*. 2003;58(10):M943-M947.

94. Mabuchi F, Yoshimura K, Kashiwagi K, et al. High prevalence of anxiety and depression in patients with primary open-angle glaucoma. *Journal of glaucoma*. 2008;17(7):552-557.
95. Crish SD, Sappington RM, Inman DM, Horner PJ, Calkins DJ. Distal axonopathy with structural persistence in glaucomatous neurodegeneration. *Proceedings of the National Academy of Sciences*. 2010;107(11):5196-5201.
96. Dai H, Mu K, Qi J, et al. Assessment of lateral geniculate nucleus atrophy with 3T MR imaging and correlation with clinical stage of glaucoma. *American journal of neuroradiology*. 2011;32(7):1347-1353.
97. Chen Z, Lin F, Wang J, et al. Diffusion tensor magnetic resonance imaging reveals visual pathway damage that correlates with clinical severity in glaucoma. *Clinical & experimental ophthalmology*. 2013;41(1):43-49.
98. Helmer C, Malet F, Rougier MB, et al. Is there a link between open-angle glaucoma and dementia? The Three-City–Alienor Cohort. *Annals of neurology*. 2013;74(2):171-179.
99. Tamura H, Kawakami H, Kanamoto T, et al. High frequency of open-angle glaucoma in Japanese patients with Alzheimer's disease. *Journal of the neurological sciences*. 2006;246(1-2):79-83.
100. Zhang X, Beckles GL, Chou C-F, et al. Socioeconomic disparity in use of eye care services among US adults with age-related eye diseases: National Health Interview Survey, 2002 and 2008. *JAMA ophthalmology*. 2013;131(9):1198-1206.
101. Topouzis F, Coleman AL, Harris A, et al. Factors associated with undiagnosed open-angle glaucoma: the Thessaloniki Eye Study. *American journal of ophthalmology*. 2008;145(2):327-335. e321.
102. Weinreb RN, Friedman DS, Fechtner RD, et al. Risk assessment in the management of patients with ocular hypertension. *Am J Ophthalmol*. 2004;138(3):458-467.
103. Vargas JLC, Di Polo A. Neuroinflammation in glaucoma: soluble tumor necrosis factor alpha and the connection with excitotoxic damage. *Neural regeneration research*. 2016;11(3):424.
104. Blumenthal EZ, Weinreb RN. Assessment of the retinal nerve fiber layer in clinical trials of glaucoma neuroprotection. *Survey of Ophthalmology*. 2001;45:S305-S312.
105. Kerrigan-Baumrind LA, Quigley HA, Pease ME, Kerrigan DF, Mitchell RS. Number of ganglion cells in glaucoma eyes compared with threshold visual field tests in the same persons. *Invest Ophthalmol Vis Sci*. 2000;41(3):741-748.

106. Medeiros FA, Alencar LM, Zangwill LM, Bowd C, Sample PA, Weinreb RN. Prediction of functional loss in glaucoma from progressive optic disc damage. *Arch Ophthalmol*. 2009;127(10):1250-1256.
107. Hood DC, Kardon RH. A framework for comparing structural and functional measures of glaucomatous damage. *Prog Retin Eye Res*. 2007;26(6):688-710.
108. Harwerth RS, Carter-Dawson L, Smith EL, 3rd, Barnes G, Holt WF, Crawford ML. Neural losses correlated with visual losses in clinical perimetry. *Invest Ophthalmol Vis Sci*. 2004;45(9):3152-3160.
109. Leung CK, Cheung CY, Weinreb RN, et al. Evaluation of retinal nerve fiber layer progression in glaucoma: a study on optical coherence tomography guided progression analysis. *Invest Ophthalmol Vis Sci*. 2010;51(1):217-222.
110. Medeiros FA, Alencar LM, Zangwill LM, Sample PA, Weinreb RN. The Relationship between intraocular pressure and progressive retinal nerve fiber layer loss in glaucoma. *Ophthalmology*. 2009;116(6):1125-1133 e1121-1123.
111. Hoyt WF, Schlicke B, Eckelhoff RJ. Fundoscopic appearance of a nerve-fibre-bundle defect. *Br J Ophthalmol*. 1972;56(8):577-583.
112. Sommer A, Katz J, Quigley HA, et al. Clinically detectable nerve fiber atrophy precedes the onset of glaucomatous field loss. *Arch Ophthalmol*. 1991;109(1):77-83.
113. Novartis. Facts About Glaucoma. In: Glaucoma Australia; 2018.
114. Anderson D, Artes P, Bengtsson B, et al. VISUAL FUNCTION PROGRESSION. *Progression in Glaucoma*. 2020.
115. Malik R, Swanson WH, Garway-Heath DF. 'Structure–function relationship' in glaucoma: past thinking and current concepts. *Clinical & experimental ophthalmology*. 2012;40(4):369-380.
116. Harwerth RS, Vilupuru AS, Rangaswamy NV, Smith EL. The relationship between nerve fiber layer and perimetry measurements. *Investigative ophthalmology & visual science*. 2007;48(2):763-773.
117. Miglior S, Zeyen T, Pfeiffer N, et al. Results of the European Glaucoma Prevention Study. *Ophthalmology*. 2005;112(3):366-375.
118. Heijl A, Leske MC, Bengtsson B, et al. Reduction of intraocular pressure and glaucoma progression: results from the Early Manifest Glaucoma Trial. *Archives of ophthalmology*. 2002;120(10):1268-1279.

119. Strouthidis NG, Scott A, Peter NM, Garway-Heath DF. Optic disc and visual field progression in ocular hypertensive subjects: detection rates, specificity, and agreement. *Investigative ophthalmology & visual science*. 2006;47(7):2904-2910.
120. Ritch R. Exfoliation syndrome—the most common identifiable cause of open-angle glaucoma. *Journal of glaucoma*. 1994;3(2):176-177.
121. Moroi SE, Lark KK, Sieving PA, et al. Long anterior zonules and pigment dispersion. *American journal of ophthalmology*. 2003;136(6):1176-1178.
122. Nongpiur ME, He M, Amerasinghe N, et al. Lens vault, thickness, and position in Chinese subjects with angle closure. *Ophthalmology*. 2011;118(3):474-479.
123. Dandona L, Dandona R, Mandal P, et al. Angle-closure glaucoma in an urban population in southern India: the Andhra Pradesh Eye Disease Study. *Ophthalmology*. 2000;107(9):1710-1716.
124. Radius RL, Anderson DR. The histology of retinal nerve fiber layer bundles and bundle defects. *Arch Ophthalmol*. 1979;97(5):948-950.
125. Quigley HA, Addicks EM. Quantitative studies of retinal nerve fiber layer defects. *Arch Ophthalmol*. 1982;100(5):807-814.
126. Quigley HA, Sommer A. How to use nerve fiber layer examination in the management of glaucoma. *Trans Am Ophthalmol Soc*. 1987;85:254-272.
127. Tuulonen A, Airaksinen PJ. Initial glaucomatous optic disk and retinal nerve fiber layer abnormalities and their progression. *Am J Ophthalmol*. 1991;111(4):485-490.
128. Joshi GD, Sivaswamy J, Prashanth R, Krishnadas S. Detection of peri-papillary atrophy and RNFL defect from retinal images. Paper presented at: International Conference Image Analysis and Recognition 2012.
129. Quigley HA. Examination of the retinal nerve fiber layer in the recognition of early glaucoma damage. *Trans Am Ophthalmol Soc*. 1986;84:920-966.
130. Airaksinen PJ, Drance SM, Douglas GR, Mawson DK, Nieminen H. Diffuse and localized nerve fiber loss in glaucoma. *Am J Ophthalmol*. 1984;98(5):566-571.
131. Medeiros FA, Zangwill LM, Anderson DR, et al. Estimating the rate of retinal ganglion cell loss in glaucoma. *Am J Ophthalmol*. 2012;154(5):814-824 e811.
132. Leung CK, Yu M, Weinreb RN, Lai G, Xu G, Lam DS. Retinal nerve fiber layer imaging with spectral-domain optical coherence tomography: patterns of retinal nerve fiber layer progression. *Ophthalmology*. 2012;119(9):1858-1866.

133. Lee EJ, Kim TW, Weinreb RN, Park KH, Kim SH, Kim DM. Trend-based analysis of retinal nerve fiber layer thickness measured by optical coherence tomography in eyes with localized nerve fiber layer defects. *Invest Ophthalmol Vis Sci.* 2011;52(2):1138-1144.
134. Artes PH, Chauhan BC. Longitudinal changes in the visual field and optic disc in glaucoma. *Prog Retin Eye Res.* 2005;24(3):333-354.
135. Quigley HA, Miller NR, George T. Clinical evaluation of nerve fiber layer atrophy as an indicator of glaucomatous optic nerve damage. *Archives of Ophthalmology.* 1980;98(9):1564-1571.
136. Leung CK-s, Cheung CY-l, Weinreb RN, et al. Retinal nerve fiber layer imaging with spectral-domain optical coherence tomography: a variability and diagnostic performance study. *Ophthalmology.* 2009;116(7):1257-1263. e1252.
137. Vizzeri G, Weinreb RN, Gonzalez-Garcia AO, et al. Agreement between spectral-domain and time-domain OCT for measuring RNFL thickness. *British Journal of Ophthalmology.* 2009;93(6):775-781.
138. Leite MT, Rao HL, Zangwill LM, Weinreb RN, Medeiros FA. Comparison of the diagnostic accuracies of the Spectralis, Cirrus, and RTVue optical coherence tomography devices in glaucoma. *Ophthalmology.* 2011;118(7):1334-1339.
139. Akman A. Interpretation of Imaging Data from Cirrus HD-OCT. In: Akman A, Bayer A, Nouri-Mahdavi K, eds. *Optical Coherence Tomography in Glaucoma: A Practical Guide.* Cham: Springer International Publishing; 2018:41-54.
140. Bayer A. Interpretation of Imaging Data from Spectralis OCT. In: *Optical Coherence Tomography in Glaucoma.* Springer; 2018:55-76.
141. He L, Ren R, Yang H, et al. Anatomic vs. acquired image frame discordance in spectral domain optical coherence tomography minimum rim measurements. *PloS one.* 2014;9(3):e92225.
142. Turalba AV, Grosskreutz C. A review of current technology used in evaluating visual function in glaucoma. Paper presented at: Seminars in ophthalmology2010.
143. Bosworth CF, Sample PA, Johnson CA, Weinreb RN. Current practice with standard automated perimetry. Paper presented at: Seminars in ophthalmology2000.
144. Bengtsson B, Heijl A. A visual field index for calculation of glaucoma rate of progression. *American journal of ophthalmology.* 2008;145(2):343-353.
145. Asman P. Computer-assisted interpretation of visual fields in glaucoma. *Acta ophthalmologica Supplement.* 1992(206):1-47.

146. Åsman P, Heijl A. Glaucoma hemifield test: automated visual field evaluation. *Archives of ophthalmology*. 1992;110(6):812-819.
147. Åsman P, Heijl A. Evaluation of methods for automated hemifield analysis in perimetry. *Archives of ophthalmology*. 1992;110(6):820-826.
148. Quigley HA, Green WR. The histology of human glaucoma cupping and optic nerve damage: clinicopathologic correlation in 21 eyes. *Ophthalmology*. 1979;86(10):1803-1827.
149. Yoshioka N, Wong E, Kalloniatis M, et al. Influence of education and diagnostic modes on glaucoma assessment by optometrists. *Ophthalmic and Physiological Optics*. 2015;35(6):682-698.
150. Wong EY, Keeffe JE, Rait JL, et al. Detection of undiagnosed glaucoma by eye health professionals. *Ophthalmology*. 2004;111(8):1508-1514.
151. Yoshioka N, Zangerl B, Phu J, et al. Consistency of structure-function correlation between spatially scaled visual field stimuli and in vivo OCT ganglion cell counts. *Investigative ophthalmology & visual science*. 2018;59(5):1693-1703.
152. Medeiros FA, Lisboa R, Weinreb RN, Girkin CA, Liebmann JM, Zangwill LM. A combined index of structure and function for staging glaucomatous damage. *Arch Ophthalmol*. 2012;130(9):1107-1116.
153. Cordeiro M, Migdal C, Bloom P, Fitzke F, Moss S. Imaging apoptosis in the eye. *Eye*. 2011;25(5):545-553.
154. Cordeiro MF, Guo L, Luong V, et al. Real-time imaging of single nerve cell apoptosis in retinal neurodegeneration. *Proceedings of the National Academy of Sciences*. 2004;101(36):13352-13356.
155. Cordeiro MF, Normando EM, Cardoso MJ, et al. Real-time imaging of single neuronal cell apoptosis in patients with glaucoma. *Brain*. 2017;140(6):1757-1767.
156. Budenz DL, Anderson DR, Feuer WJ, et al. Detection and prognostic significance of optic disc hemorrhages during the Ocular Hypertension Treatment Study. *Ophthalmology*. 2006;113(12):2137-2143.
157. Sperduto RD, Hiller R, Chew E, et al. Risk factors for hemiretinal vein occlusion: comparison with risk factors for central and branch retinal vein occlusion: the eye disease case-control study. *Ophthalmology*. 1998;105(5):765-771.
158. Moore D, Harris A, Wudunn D, Kheradiya N, Siesky B. Dysfunctional regulation of ocular blood flow: A risk factor for glaucoma? *Clin Ophthalmol*. 2008;2(4):849-861.

159. Flammer J, Pache M, Resink T. Vasospasm, its role in the pathogenesis of diseases with particular reference to the eye. *Prog Retin Eye Res.* 2001;20(3):319-349.
160. Plange N, Kaup M, Weber A, Arend KO, Remky A. Retrobulbar haemodynamics and morphometric optic disc analysis in primary open-angle glaucoma. *Br J Ophthalmol.* 2006;90(12):1501-1504.
161. Siesky B, Harris A, Racette L, et al. Differences in ocular blood flow in glaucoma between patients of African and European descent. *J Glaucoma.* 2015;24(2):117-121.
162. Flammer J, Orgul S, Costa VP, et al. The impact of ocular blood flow in glaucoma. *Prog Retin Eye Res.* 2002;21(4):359-393.
163. Golzan SM, Morgan WH, Georgevsky D, Graham SL. Correlation of retinal nerve fibre layer thickness and spontaneous retinal venous pulsations in glaucoma and normal controls. *PLoS One.* 2015;10(6):e0128433.
164. Chan KK, Tang F, Tham CC, Young AL, Cheung CY. Retinal vasculature in glaucoma: a review. *BMJ open ophthalmology.* 2017;1(1).
165. Wong TY, Knudtson MD, Klein R, Klein BE, Meuer SM, Hubbard LD. Computer-assisted measurement of retinal vessel diameters in the Beaver Dam Eye Study: methodology, correlation between eyes, and effect of refractive errors. *Ophthalmology.* 2004;111(6):1183-1190.
166. Hubbard LD, Brothers RJ, King WN, et al. Methods for evaluation of retinal microvascular abnormalities associated with hypertension/sclerosis in the Atherosclerosis Risk in Communities Study. *Ophthalmology.* 1999;106(12):2269-2280.
167. Cheung CY-I, Zheng Y, Hsu W, et al. Retinal vascular tortuosity, blood pressure, and cardiovascular risk factors. *Ophthalmology.* 2011;118(5):812-818.
168. Zamir M, Medeiros J, Cunningham T. Arterial bifurcations in the human retina. *The Journal of general physiology.* 1979;74(4):537-548.
169. Liew G, Wang JJ, Cheung N, et al. The retinal vasculature as a fractal: methodology, reliability, and relationship to blood pressure. *Ophthalmology.* 2008;115(11):1951-1956. e1951.
170. Mainster MA. The fractal properties of retinal vessels: embryological and clinical implications. *Eye.* 1990;4(1):235-241.
171. Ciancaglini M, Guerra G, Agnifili L, et al. Fractal dimension as a new tool to analyze optic nerve head vasculature in primary open angle glaucoma. *In Vivo.* 2015;29(2):273-279.

172. De Leon JMS, Cheung CY, Wong T-Y, et al. Retinal vascular caliber between eyes with asymmetric glaucoma. *Graefes Archive for Clinical and Experimental Ophthalmology*. 2015;253(4):583-589.
173. Gao J, Liang Y, Wang F, et al. Retinal vessels change in primary angle-closure glaucoma: the Handan Eye Study. *Scientific reports*. 2015;5(1):1-6.
174. Yoo E, Yoo C, Lee B-r, Lee T-E, Kim YY. Diagnostic ability of retinal vessel diameter measurements in open-angle glaucoma. *Investigative ophthalmology & visual science*. 2015;56(13):7915-7922.
175. Wu R, Cheung CY-L, Saw SM, Mitchell P, Aung T, Wong TY. Retinal vascular geometry and glaucoma: the Singapore Malay Eye Study. *Ophthalmology*. 2013;120(1):77-83.
176. Amerasinghe N, Aung T, Cheung N, et al. Evidence of retinal vascular narrowing in glaucomatous eyes in an Asian population. *Investigative ophthalmology & visual science*. 2008;49(12):5397-5402.
177. Wang S, Xu L, Wang Y, Wang Y, Jonas JB. Retinal vessel diameter in normal and glaucomatous eyes: the Beijing eye study. *Clinical & experimental ophthalmology*. 2007;35(9):800-807.
178. Klein R, Klein BE, Tomany SC, Wong TY. The relation of retinal microvascular characteristics to age-related eye disease: the Beaver Dam eye study. *American journal of ophthalmology*. 2004;137(3):435-444.
179. Mitchell P, Leung H, Wang JJ, et al. Retinal vessel diameter and open-angle glaucoma: the Blue Mountains Eye Study. *Ophthalmology*. 2005;112(2):245-250.
180. Angelica MM, Sanseau A, Argento C. Arterial narrowing as a predictive factor in glaucoma. *International ophthalmology*. 2001;23(4-6):271-274.
181. Jonas JB, Nguyen XN, Naumann G. Parapapillary retinal vessel diameter in normal and glaucoma eyes. I. Morphometric data. *Investigative ophthalmology & visual science*. 1989;30(7):1599-1603.
182. Rader J, Feuer WJ, Anderson DR. Peripapillary vasoconstriction in the glaucomas and the anterior ischemic optic neuropathies. *American journal of ophthalmology*. 1994;117(1):72-80.
183. Rankin S, Drance SM. Peripapillary focal retinal arteriolar narrowing in open angle glaucoma. *Journal of glaucoma*. 1996;5(1):22-28.
184. Frisén L, Claesson M. Narrowing of the retinal arterioles in descending optic atrophy: a quantitative clinical study. *Ophthalmology*. 1984;91(11):1342-1346.

185. Papastathopoulos KI, Jonas JB. Follow up of focal narrowing of retinal arterioles in glaucoma. *British journal of ophthalmology*. 1999;83(3):285-289.
186. Zheng Y, Cheung N, Aung T, Mitchell P, He M, Wong TY. Relationship of retinal vascular caliber with retinal nerve fiber layer thickness: the Singapore Malay Eye Study. *Investigative ophthalmology & visual science*. 2009;50(9):4091-4096.
187. Saccà SC, Pascotto A, Camicione P, Capris P, Izzotti A. Oxidative DNA damage in the human trabecular meshwork: clinical correlation in patients with primary open-angle glaucoma. *Archives of Ophthalmology*. 2005;123(4):458-463.
188. Sorkhabi R, Ghorbanihaghjo A, Javadzadeh A, Rashtchizadeh N, Moharrery M. Oxidative DNA damage and total antioxidant status in glaucoma patients. *Molecular vision*. 2011;17:41.
189. Yokoyama Y, Aizawa N, Chiba N, et al. Significant correlations between optic nerve head microcirculation and visual field defects and nerve fiber layer loss in glaucoma patients with myopic glaucomatous disk. *Clinical ophthalmology (Auckland, NZ)*. 2011;5:1721.
190. Tobe LA, Harris A, Hussain RM, et al. The role of retrobulbar and retinal circulation on optic nerve head and retinal nerve fibre layer structure in patients with open-angle glaucoma over an 18-month period. *British Journal of Ophthalmology*. 2015;99(5):609-612.
191. Piltz-Seymour JR. Laser Doppler flowmetry of the optic nerve head in glaucoma. *Survey of ophthalmology*. 1999;43:S191-S198.
192. Michelson G, Langhans MJ, Harazny J, Dichtl A. Visual field defect and perfusion of the juxtapapillary retina and the neuroretinal rim area in primary open-angle glaucoma. *Graefe's archive for clinical and experimental ophthalmology*. 1998;236(2):80-85.
193. Piltz-seymour JR, Grunwald JE, Hariprasad SM, Dupont J. Optic nerve blood flow is diminished in eyes of primary open-angle glaucoma suspects. *American journal of ophthalmology*. 2001;132(1):63-69.
194. Arend O, Remky A, Plange N, Martin B, Harris A. Capillary density and retinal diameter measurements and their impact on altered retinal circulation in glaucoma: a digital fluorescein angiographic study. *British journal of ophthalmology*. 2002;86(4):429-433.
195. Huber K, Plange N, Remky A, Arend O. Comparison of colour Doppler imaging and retinal scanning laser fluorescein angiography in healthy volunteers and normal pressure glaucoma patients. *Acta Ophthalmologica Scandinavica*. 2004;82(4):426-431.
196. Plange N, Kaup M, Remky A, Arend KO. Prolonged retinal arteriovenous passage time is correlated to ocular perfusion pressure in normal tension glaucoma. *Graefe's Archive for Clinical and Experimental Ophthalmology*. 2008;246(8):1147-1152.

197. Spaide RF, Klancnik JM, Cooney MJ. Retinal vascular layers imaged by fluorescein angiography and optical coherence tomography angiography. *JAMA ophthalmology*. 2015;133(1):45-50.
198. Jia Y, Wei E, Wang X, et al. Optical coherence tomography angiography of optic disc perfusion in glaucoma. *Ophthalmology*. 2014;121(7):1322-1332.
199. Moghimi S, Hou H, Rao HL, Weinreb RN. Optical Coherence Tomography Angiography and Glaucoma: A Brief Review. *The Asia-Pacific Journal of Ophthalmology*. 2019;8(2):115-125.
200. Liu L, Jia Y, Takusagawa HL, et al. Optical coherence tomography angiography of the peripapillary retina in glaucoma. *JAMA ophthalmology*. 2015;133(9):1045-1052.
201. Lévêque P-M, Zéboulon P, Brasnu E, Baudouin C, Labbé A. Optic disc vascularization in glaucoma: value of spectral-domain optical coherence tomography angiography. *Journal of ophthalmology*. 2016;2016.
202. Chen C-L, Bojikian KD, Gupta D, et al. Optic nerve head perfusion in normal eyes and eyes with glaucoma using optical coherence tomography-based microangiography. *Quantitative imaging in medicine and surgery*. 2016;6(2):125.
203. Akagi T, Iida Y, Nakanishi H, et al. Microvascular density in glaucomatous eyes with hemifield visual field defects: an optical coherence tomography angiography study. *American journal of ophthalmology*. 2016;168:237-249.
204. Bojikian KD, Chen C-L, Wen JC, et al. Optic disc perfusion in primary open angle and normal tension glaucoma eyes using optical coherence tomography-based microangiography. *PloS one*. 2016;11(5):e0154691.
205. Yarmohammadi A, Zangwill LM, Diniz-Filho A, et al. Relationship between optical coherence tomography angiography vessel density and severity of visual field loss in glaucoma. *Ophthalmology*. 2016;123(12):2498-2508.
206. Hou T-Y, Kuang T-M, Ko Y-C, Chang Y-F, Liu CJ-L, Chen M-J. optic Disc and Macular Vessel Density Measured by optical coherence tomography Angiography in open-Angle and Angle-closure Glaucoma. *Scientific reports*. 2020;10(1):1-9.
207. Cennamo G, Montorio D, Velotti N, Sparnelli F, Reibaldi M, Cennamo G. Optical coherence tomography angiography in pre-perimetric open-angle glaucoma. *Graefe's Archive for Clinical and Experimental Ophthalmology*. 2017;255(9):1787-1793.
208. Geyman LS, Garg RA, Suwan Y, et al. Peripapillary perfused capillary density in primary open-angle glaucoma across disease stage: an optical coherence tomography angiography study. *British Journal of Ophthalmology*. 2017;101(9):1261-1268.

209. Shin JW, Lee J, Kwon J, Choi J, Kook MS. Regional vascular density–visual field sensitivity relationship in glaucoma according to disease severity. *British Journal of Ophthalmology*. 2017;101(12):1666-1672.
210. Yarmohammadi A, Zangwill LM, Manalastas PIC, et al. Peripapillary and macular vessel density in patients with primary open-angle glaucoma and unilateral visual field loss. *Ophthalmology*. 2018;125(4):578-587.
211. Spaide RF, Fujimoto JG, Waheed NK. Image artifacts in optical coherence angiography. *Retina (Philadelphia, Pa)*. 2015;35(11):2163.
212. Tokayer J, Jia Y, Dhalla A-H, Huang D. Blood flow velocity quantification using split-spectrum amplitude-decorrelation angiography with optical coherence tomography. *Biomedical optics express*. 2013;4(10):1909-1924.
213. Jangi A, Spielberg L, Landa G, et al. Peripapillary blood flow velocity in glaucoma evaluated by the retinal functional imager (RFI). *Investigative ophthalmology & visual science*. 2010;51(13):2692-2692.
214. Burgansky–Eliash Z, Bartov E, Barak A, Grinvald A, Gatton D. Blood-flow velocity in glaucoma patients measured with the retinal function imager. *Current eye research*. 2016;41(7):965-970.
215. Wong TY, Islam FA, Klein R, et al. Retinal vascular caliber, cardiovascular risk factors, and inflammation: the multi-ethnic study of atherosclerosis (MESA). *Investigative ophthalmology & visual science*. 2006;47(6):2341-2350.
216. Taylor A, Sehu W, Williamson T, Lee W. Morphometric assessment of the central retinal artery and vein in the optic nerve head. *Canadian journal of ophthalmology Journal canadien d'ophtalmologie*. 1993;28(7):320-324.
217. Hayreh SS, Vrabec F. The structure of the head of the optic nerve in rhesus monkey. *American Journal of Ophthalmology*. 1966;61(1):136-150.
218. Kang MH, Balaratnasingam C, Paula KY, et al. Morphometric characteristics of central retinal artery and vein endothelium in the normal human optic nerve head. *Investigative ophthalmology & visual science*. 2011;52(3):1359-1367.
219. Shimada N, Ohno-Matsui K, Harino S, et al. Reduction of retinal blood flow in high myopia. *Graefes Arch Clin Exp Ophthalmol*. 2004;42(4):284-288.
220. Ando J, Yamamoto K. Vascular mechanobiology. *Circulation Journal*. 2009;73(11):1983-1992.

221. DePaola N, Gimbrone Jr MA, Davies PF, Dewey Jr CF. Vascular endothelium responds to fluid shear stress gradients. *Arteriosclerosis and thrombosis: a journal of vascular biology*. 1992;12(11):1254-1257.
222. Morgan WH, Yu D-Y, Alder VA, et al. The correlation between cerebrospinal fluid pressure and retrolaminar tissue pressure. *Investigative ophthalmology & visual science*. 1998;39(8):1419-1428.
223. Balaratnasingam C, Morgan WH, Johnstone V, Pandav SS, Cringle SJ, Yu D-Y. Histomorphometric measurements in human and dog optic nerve and an estimation of optic nerve pressure gradients in human. *Experimental eye research*. 2009;89(5):618-628.
224. Yu D-Y, Paula KY, Cringle SJ, Kang MH, Su E-N. Functional and morphological characteristics of the retinal and choroidal vasculature. *Progress in Retinal and Eye Research*. 2014;40:53-93.
225. Zweifach BW. Quantitative studies of microcirculatory structure and function: I. Analysis of pressure distribution in the terminal vascular bed in cat mesentery. *Circulation Research*. 1974;34(6):841-857.
226. Lipowsky HH, Kovalcheck S, Zweifach BW. The distribution of blood rheological parameters in the microvasculature of cat mesentery. *Circulation research*. 1978;43(5):738-749.
227. Yu D-Y, Su E-N, Cringle SJ, Morgan WH, McAllister IL, Paula KY. Local modulation of retinal vein tone. *Investigative Ophthalmology & Visual Science*. 2016;57(2):412-419.
228. Morgan WH, Yu DY, Cooper RL, Alder VA, Cringle SJ, Constable IJ. Retinal artery and vein pressures in the dog and their relationship to aortic, intraocular, and cerebrospinal fluid pressures. *Microvasc Res*. 1997;53(3):211-221.
229. Westlake WH, Morgan WH, Yu DY. A pilot study of in vivo venous pressures in the pig retinal circulation. *Clinical & experimental ophthalmology*. 2001;29(3):167-170.
230. Yu D-Y, Cringle SJ, Balaratnasingam C, Morgan WH, Paula KY, Su E-N. Retinal ganglion cells: energetics, compartmentation, axonal transport, cytoskeletons and vulnerability. *Progress in retinal and eye research*. 2013;36:217-246.
231. Tang C, Zhu L, Akingba G, Lu X-Y. Viscous flow past a collapsible channel as a model for self-excited oscillation of blood vessels. *Journal of Biomechanics*. 2015;48(10):1922-1929.
232. Morgan WH, Balaratnasingam C, Hazelton ML, House PH, Cringle SJ, Yu DY. The force required to induce hemivessel pulsation is associated with the site of maximum field loss in glaucoma. *Invest Ophthalmol Vis Sci*. 2005;46(4):1307-1312.

233. Morgan WH, Hazelton ML, Azar SL, et al. Retinal venous pulsation in glaucoma and glaucoma suspects. *Ophthalmology*. 2004;111(8):1489-1494.
234. Golzan M, Georgevsky D, Bowd C, Weinreb RN, Graham SL. Visual field sensitivity is decreased with reduced spontaneous venous pulsation in glaucoma eyes. ARVO Annual Meeting; 2017; Baltimore.
235. Graham SL, Butlin M, Lee M, Avolio AP. Central blood pressure, arterial waveform analysis, and vascular risk factors in glaucoma. *J Glaucoma*. 2013;22(2):98-103.
236. Coccius EA. Ueber die Anwendung des Augen-Spiegels: nebst Angabe eines neuen Instrumentes. . *Müller*. 1853.
237. Golzan SM, Graham SL, Leaney J, Avolio A. Dynamic association between intraocular pressure and spontaneous pulsations of retinal veins. *Curr Eye Res*. 2011;36(1):53-59.
238. Morgan WH, Abdul-Rahman A, Yu DY, Hazelton ML, Betz-Stablein B, Lind CR. Objective detection of retinal vessel pulsation. *PLoS One*. 2015;10(2):e0116475.
239. Elliot R. The retinal pulse. *The British journal of ophthalmology*. 1921;5(11):481.
240. Glucksberg MR, Dunn R. Direct measurement of retinal microvascular pressures in the live, anesthetized cat. *Microvascular research*. 1993;45(2):158-165.
241. Duke-Elder WS. The venous pressure of the eye and its relation to the intra-ocular pressure. *The Journal of physiology*. 1926;61(3):409.
242. Attariwala R, Giebs CP, Glucksberg MR. The influence of elevated intraocular pressure on vascular pressures in the cat retina. *Investigative ophthalmology & visual science*. 1994;35(3):1019-1025.
243. Levine DN. Spontaneous pulsation of the retinal veins. *Microvascular research*. 1998;56(3):154-165.
244. Kain S, Morgan WH, Yu D-Y. New observations concerning the nature of central retinal vein pulsation. *British journal of ophthalmology*. 2010;94(7):854-857.
245. Morgan WH, Lind CR, Kain S, Fatehee N, Bala A, Yu DY. Retinal vein pulsation is in phase with intracranial pressure and not intraocular pressure. *Invest Ophthalmol Vis Sci*. 2012;53(8):4676-4681.
246. Kim M, Lee EJ, Seo JH, Kim T-W. Relationship of spontaneous retinal vein pulsation with ocular circulatory cycle. *PLoS one*. 2014;9(5):e97943.

247. Meyer-Schwickerath R, Kleinwächter T, Papenfuß H-D, Firsching R. Central retinal venous outflow pressure. *Graefe's archive for clinical and experimental ophthalmology*. 1995;233(12):783-788.
248. Low H, Chew Y, Winoto S, Chin R. Pressure/flow behaviour in collapsible tube subjected to forced downstream pressure fluctuations. *Medical and Biological Engineering and Computing*. 1995;33(4):545-550.
249. Dardenne G, Dereymaeker A, Lacheron J. Cerebrospinal fluid pressure and pulsatility. *European neurology*. 1969;2(4):193-216.
250. Jones HC, Terasaki T. Fluids and Barriers of the CNS: a new journal encompassing Cerebrospinal Fluid Research. In: Springer; 2011.
251. Evans DW, Hosking SL, Embleton SJ, Morgan AJ, Bartlett JD. Spectral content of the intraocular pressure pulse wave: glaucoma patients versus normal subjects. *Graefe's archive for clinical and experimental ophthalmology*. 2002;240(6):475-480.
252. McHugh JA, D'Antona L, Toma AK, Bremner FD. Spontaneous venous pulsations detected with infrared videography. *Journal of Neuro-Ophthalmology*. 2020;40(2):174-177.
253. Lee E, Kim T-W, Kim J-A, Kim JA, Kim H. Spontaneous retinal venous pulsation in unilateral primary open-angle glaucoma with low intraocular pressure. *Journal of Glaucoma*. 2017;26(10):896-901.
254. Lorentzen SE. Incidence of spontaneous venous pulsation in the retina. *Acta Ophthalmol (Copenh)*. 1970;48(4):765-770.
255. Mitchell GF, Wang N, Palmisano JN, et al. Hemodynamic correlates of blood pressure across the adult age spectrum: noninvasive evaluation in the Framingham Heart Study. *Circulation*. 2010;122(14):1379-1386.
256. Ren R, Jonas JB, Tian G, et al. Cerebrospinal fluid pressure in glaucoma: a prospective study. *Ophthalmology*. 2010;117(2):259-266.
257. Berdahl JP, Allingham RR, Johnson DH. Cerebrospinal fluid pressure is decreased in primary open-angle glaucoma. *Ophthalmology*. 2008;115(5):763-768.
258. Berdahl JP, Fautsch MP, Stinnett SS, Allingham RR. Intracranial pressure in primary open angle glaucoma, normal tension glaucoma, and ocular hypertension: a case-control study. *Investigative ophthalmology & visual science*. 2008;49(12):5412-5418.
259. Fang L, Baertschi M, Mozaffarieh M. The effect of flammer-syndrome on retinal venous pressure. *BMC ophthalmology*. 2014;14(1):121.

260. Pillunat KR, Ventzke S, Spoerl E, Furashova O, Stodtmeister R, Pillunat LE. Central retinal venous pulsation pressure in different stages of primary open-angle glaucoma. *British Journal of Ophthalmology*. 2014;98(10):1374-1378.
261. Roberts MD, Grau V, Grimm J, et al. Remodeling of the connective tissue microarchitecture of the lamina cribrosa in early experimental glaucoma. *Investigative ophthalmology & visual science*. 2009;50(2):681-690.
262. Jonas JB. Role of cerebrospinal fluid pressure in the pathogenesis of glaucoma. *Acta ophthalmologica*. 2011;89(6):505-514.
263. Seo JH, Kim T-W, Weinreb RN, Kim YA, Kim M. Relationship of intraocular pressure and frequency of spontaneous retinal venous pulsation in primary open-angle glaucoma. *Ophthalmology*. 2012;119(11):2254-2260.
264. Morgan WH, Cringle SJ, Kang MH, et al. Optimizing the calibration and interpretation of dynamic ocular force measurements. *Graefes Arch Clin Exp Ophthalmol*. 2010;248(3):401-407.
265. Lowe R. Calibration of Bailliar's ophthalmodynamometer. *Archives of Ophthalmology*. 1962;67(4):424-427.
266. Jonas J. Reproducibility of ophthalmodynamometric measurements of central retinal artery and vein collapse pressure. *British journal of ophthalmology*. 2003;87(5):577-579.
267. Sisler HA, HA S. Optical-corneal pressure ophthalmodynamometer. 1972.
268. Parsa C. Spontaneous venous pulsations should be monitored during glaucoma therapy. *British journal of ophthalmology*. 2002;86(10):1187-1187.
269. Golzan SM, Kim MO, Seddighi AS, Avolio A, Graham SL. Non-invasive estimation of cerebrospinal fluid pressure waveforms by means of retinal venous pulsatility and central aortic blood pressure. *Annals of biomedical engineering*. 2012;40(9):1940-1948.
270. Garhofer G, Bek T, Boehm AG, et al. Use of the retinal vessel analyzer in ocular blood flow research. *Acta Ophthalmol*. 2010;88(7):717-722.
271. Heil M. Stokes flow in collapsible tubes: computation and experiment. *Journal of Fluid Mechanics*. 1997;353(1):285-312.
272. Moreno AH, KATZ AI, GOLD LD, Reddy R. Mechanics of distension of dog veins and other very thin-walled tubular structures. *Circulation research*. 1970;27(6):1069-1080.
273. Moret F, Reiff CM, Lagreze WA, Bach M. Quantitative Analysis of Fundus-Image Sequences Reveals Phase of Spontaneous Venous Pulsations. *Transl Vis Sci Technol*. 2015;4(5):3.

274. Seifert B, Vilser W. Retinal Vessel Analyzer (RVA)-design and function. *Biomed Tech.* 2002;47:1.
275. Wartak A, Beer F, Desissaire S, Baumann B, Pircher M, Hitzenberger CK. Investigating spontaneous retinal venous pulsation using Doppler optical coherence tomography. *Scientific reports.* 2019;9(1):1-11.
276. Moret F, Poloschek CM, Lagreze WA, Bach M. Visualization of fundus vessel pulsation using principal component analysis. *Investigative ophthalmology & visual science.* 2011;52(8):5457-5464.
277. Kumar DK, Aliahmad B, Hao H, Che Azemin MZ, Kawasaki R. A Method for Visualization of Fine Retinal Vascular Pulsation Using Nonmydriatic Fundus Camera Synchronized with Electrocardiogram. *ISRN Ophthalmology.* 2013;2013:865834.
278. Abdul-Rahman A, Morgan W, Yu D-Y. Measurement of normal retinal vascular pulse wave attenuation using modified photoplethysmography. *PloS one.* 2020;15(5):e0232523.
279. Morgan WH, Hazelton ML, Betz-Stablein BD, et al. Photoplethysmographic measurement of various retinal vascular pulsation parameters and measurement of the venous phase delay. *Investigative ophthalmology & visual science.* 2014;55(9):5998-6006.
280. Bernucci MT, Merkle CW, Srinivasan VJ. Investigation of artifacts in retinal and choroidal OCT angiography with a contrast agent. *Biomedical optics express.* 2018;9(3):1020-1040.
281. Seidel G, Aschinger G, Singer C, et al. Estimating retinal blood flow velocities by optical coherence tomography. *JAMA ophthalmology.* 2016;134(10):1104-1110.
282. Cimalla P, Walther J, Mittasch M, Koch E. Shear flow-induced optical inhomogeneity of blood assessed in vivo and in vitro by spectral domain optical coherence tomography in the 1.3 μm wavelength range. *Journal of biomedical optics.* 2011;16(11):116020.
283. Srinivasan VJ, Atochin DN, Radhakrishnan H, et al. Optical coherence tomography for the quantitative study of cerebrovascular physiology. *Journal of Cerebral Blood Flow & Metabolism.* 2011;31(6):1339-1345.
284. Lam J, Chan G, Morgan WH, et al. Structural characteristics of the optic nerve head influencing human retinal venous pulsations. *Experimental Eye Research.* 2016;145:341-346.
285. Balaratnasingam C, Morgan WH, Hazelton ML, et al. Value of retinal vein pulsation characteristics in predicting increased optic disc excavation. *British journal of ophthalmology.* 2007;91(4):441-444.

286. Shariflou S, Agar A, Rose K, Bowd C, Golzan SM. Objective quantification of spontaneous retinal venous pulsations using a novel tablet-based ophthalmoscope. *Translational Vision Science & Technology*. 2020;9(4):19-19.
287. Golzan SM, Butlin M, Kouchaki Z, Gupta V, Avolio A, Graham SL. Characterizing dynamic properties of retinal vessels in the rat eye using high speed imaging. *Microvasc Res*. 2014;92:56-61.
288. Morgan WH, House PH, Hazelton ML, et al. Intraocular pressure reduction is associated with reduced venous pulsation pressure. *PloS one*. 2016;11(1):e0147915.
289. Turgut B, Turgut F. Differences between the Characteristics of Normal Tension Glaucoma and High Tension Glaucoma. *Adv Ophthalmol Vis Syst*. 2017;7(7):00250.
290. Pruzan NL, Myers JS. Phenotypic differences in normal vs high tension glaucoma. *Journal of Neuro-Ophthalmology*. 2015;35:S4-S7.
291. Casson RJ, Chidlow G, Wood JP, Crowston JG, Goldberg I. Definition of glaucoma: clinical and experimental concepts. *Clinical & experimental ophthalmology*. 2012;40(4):341-349.
292. Prum BE, Rosenberg LF, Gedde SJ, et al. Primary open-angle glaucoma preferred practice pattern® guidelines. *Ophthalmology*. 2016;123(1):P41-P111.
293. Weinreb RN, Zangwill LM, Jain S, et al. Predicting the onset of glaucoma: the confocal scanning laser ophthalmoscopy ancillary study to the Ocular Hypertension Treatment Study. *Ophthalmology*. 2010;117(9):1674-1683.
294. Phu J, Khuu SK, Agar A, Kalloniatis M. Clinical evaluation of swedish interactive thresholding algorithm—faster compared with swedish interactive thresholding algorithm—standard in normal subjects, glaucoma suspects, and patients with glaucoma. *American journal of ophthalmology*. 2019;208:251-264.
295. Girish V, Vijayalakshmi A. Affordable image analysis using NIH Image/ImageJ. *Indian journal of cancer*. 2004;41(1):47.
296. Fischer MJ, Uchida S, Messlinger K. Measurement of meningeal blood vessel diameter in vivo with a plug-in for ImageJ. *Microvasc Res*. 2010;80(2):258-266.
297. Medeiros FA, Zangwill LM, Bowd C, Mansouri K, Weinreb RN. The structure and function relationship in glaucoma: implications for detection of progression and measurement of rates of change. *Invest Ophthalmol Vis Sci*. 2012;53(11):6939-6946.
298. Susanna R, Jr., Vessani RM. Staging glaucoma patient: why and how? *Open Ophthalmol J*. 2009;3:59-64.

299. DeLong ER, DeLong DM, Clarke-Pearson DL. Comparing the areas under two or more correlated receiver operating characteristic curves: a nonparametric approach. *Biometrics*. 1988;837-845.
300. Berry DA, Ayers GD. Symmetrized percent change for treatment comparisons. *The American Statistician*. 2006;60(1):27-31.
301. Morgan WH. Central venous pulsations: new findings, clinical importance and relation to cerebrospinal fluid pressure. *J Glaucoma*. 2013;22 Suppl 5:S15-16.
302. Wong SH, White RP. The clinical validity of the spontaneous retinal venous pulsation. *J Neuroophthalmol*. 2013;33(1):17-20.
303. Abràmoff MD, Magelhaes P, Ram S. Image processing with ImageJ. 2004.
304. Witmer MT, Parlitsis G, Patel S, Kiss S. Comparison of ultra-widefield fluorescein angiography with the Heidelberg Spectralis® noncontact ultra-widefield module versus the Optos® Optomap®. *Clinical ophthalmology (Auckland, NZ)*. 2013;7:389.
305. Harder B, Jonas JB. Frequency of spontaneous pulsations of the central retinal vein. *Br J Ophthalmol*. 2007;91(3):401-402.
306. Faghihi H, Hajizadeh F, Hashemi H, Khabazkhoob M. Agreement of two different spectral domain optical coherence tomography instruments for retinal nerve fiber layer measurements. *J Ophthalmic Vis Res*. 2014;9(1):31-37.
307. Nelson P, Aspinall P, Papasouliotis O, Worton B, O'Brien C. Quality of life in glaucoma and its relationship with visual function. *J Glaucoma*. 2003;12(2):139-150.
308. Hyman LG, Komaroff E, Heijl A, Bengtsson B, Leske MC, Early Manifest Glaucoma Trial G. Treatment and vision-related quality of life in the early manifest glaucoma trial. *Ophthalmology*. 2005;112(9):1505-1513.
309. Canadian Glaucoma Study G. Canadian Glaucoma Study: 1. Study design, baseline characteristics, and preliminary analyses. *Can J Ophthalmol*. 2006;41(5):566-575.
310. Seo JH, Kim TW, Weinreb RN, Kim YA, Kim M. Relationship of intraocular pressure and frequency of spontaneous retinal venous pulsation in primary open-angle glaucoma. *Ophthalmology*. 2012;119(11):2254-2260.
311. Hayreh SS. Evaluation of optic nerve head circulation: review of the methods used. *Journal of glaucoma*. 1997;6(5):319-330.
312. Anderson DR. Introductory comments on blood flow autoregulation in the optic nerve head and vascular risk factors in glaucoma. *Survey of ophthalmology*. 1999;43:S5-S9.

313. Quaranta L, Katsanos A, Russo A, Riva I. 24-hour intraocular pressure and ocular perfusion pressure in glaucoma. *Survey of ophthalmology*. 2013;58(1):26-41.
314. Fan N, Wang P, Tang L, Liu X. Ocular blood flow and normal tension glaucoma. *BioMed Research International*. 2015;2015.
315. Kaiser HJ, Schoetzau A, STÜMPFIG D, Flammer J. Blood-flow velocities of the extraocular vessels in patients with high-tension and normal-tension primary open-angle glaucoma. *American journal of ophthalmology*. 1997;123(3):320-327.
316. Grunwald JE, Piltz J, Hariprasad SM, DuPont J. Optic nerve and choroidal circulation in glaucoma. *Investigative ophthalmology & visual science*. 1998;39(12):2329-2336.
317. Abegao Pinto L, Vandewalle E, De Clerck E, Marques-Neves C, Stalmans I. Lack of spontaneous venous pulsation: possible risk indicator in normal tension glaucoma? *Acta Ophthalmol*. 2013;91(6):514-520.
318. Shariflou S, Agar A, Rose K, Bowd C, Golzan M. Objective quantification of spontaneous retinal venous pulsations using a novel tablet-based ophthalmoscope *Trans Vis Sci Tech*. 2020;0(0).
319. Hulsman CA, Westendorp IC, Ramrattan RS, et al. Is open-angle glaucoma associated with early menopause? The Rotterdam Study. *American journal of epidemiology*. 2001;154(2):138-144.
320. Drance S, Anderson DR, Schulzer M, Group CN-TGS. Risk factors for progression of visual field abnormalities in normal-tension glaucoma. *American journal of ophthalmology*. 2001;131(6):699-708.
321. Baneke AJ, Aubry J, Viswanathan AC, Plant GT. The role of intracranial pressure in glaucoma and therapeutic implications. *Eye*. 2020;34(1):178-191.
322. Fleischman D, Allingham RR. The role of cerebrospinal fluid pressure in glaucoma and other ophthalmic diseases: A review. *Saudi Journal of Ophthalmology*. 2013;27(2):97-106.
323. Ren R, Zhang X, Wang N, Li B, Tian G, Jonas JB. Cerebrospinal fluid pressure in ocular hypertension. *Acta ophthalmologica*. 2011;89(2):e142-e148.
324. Donnelly SJ, Subramanian PS. Relationship of intraocular pulse pressure and spontaneous venous pulsations. *American journal of ophthalmology*. 2009;147(1):51-55. e52.
325. Wollstein G, Schuman JS, Price LL, et al. Optical coherence tomography longitudinal evaluation of retinal nerve fiber layer thickness in glaucoma. *Arch Ophthalmol*. 2005;123(4):464-470.

326. Medeiros FA, Lisboa R, Weinreb RN, Liebmann JM, Girkin C, Zangwill LM. Retinal ganglion cell count estimates associated with early development of visual field defects in glaucoma. *Ophthalmology*. 2013;120(4):736-744.
327. Meira-Freitas D, Lisboa R, Tatham A, et al. Predicting progression in glaucoma suspects with longitudinal estimates of retinal ganglion cell counts. *Investigative Ophthalmology & Visual Science*. 2013;54(6):4174-4183.
328. Tatham AJ, Weinreb RN, Zangwill LM, Liebmann JM, Girkin CA, Medeiros FA. The relationship between cup-to-disc ratio and estimated number of retinal ganglion cells. *Investigative ophthalmology & visual science*. 2013;54(5):3205-3214.
329. Gracitelli CP, Tatham AJ, Zangwill LM, Weinreb RN, Liu T, Medeiros FA. Estimated rates of retinal ganglion cell loss in glaucomatous eyes with and without optic disc hemorrhages. *PLoS One*. 2014;9(8):e105611.
330. Zhang C, Tatham AJ, Weinreb RN, et al. Relationship between ganglion cell layer thickness and estimated retinal ganglion cell counts in the glaucomatous macula. *Ophthalmology*. 2014;121(12):2371-2379.
331. Hirooka K, Izumibata S, Ukegawa K, Nitta E, Tsujikawa A. Estimating the rate of retinal ganglion cell loss to detect glaucoma progression: an observational cohort study. *Medicine*. 2016;95(30).
332. Raza AS, Hood DC. Evaluation of a method for estimating retinal ganglion cell counts using visual fields and optical coherence tomography. *Investigative ophthalmology & visual science*. 2015;56(4):2254-2268.
333. Swanson WH, Horner DG. Assessing assumptions of a combined structure-function index. *Ophthalmic and Physiological Optics*. 2015;35(2):186-193.
334. Topouzis F, Coleman AL, Harris A, et al. Factors associated with undiagnosed open-angle glaucoma: the Thessaloniki Eye Study. *Am J Ophthalmol*. 2008;145(2):327-335.
335. Mitchell P, Smith W, Attebo K, Healey PR. Prevalence of open-angle glaucoma in Australia. The Blue Mountains Eye Study. *Ophthalmology*. 1996;103(10):1661-1669.
336. Quigley HA, Addicks EM, Green WR. Optic nerve damage in human glaucoma. III. Quantitative correlation of nerve fiber loss and visual field defect in glaucoma, ischemic neuropathy, papilledema, and toxic neuropathy. *Arch Ophthalmol*. 1982;100(1):135-146.
337. Quigley HA, Dunkelberger GR, Green WR. Retinal ganglion cell atrophy correlated with automated perimetry in human eyes with glaucoma. *Am J Ophthalmol*. 1989;107(5):453-464.

338. Bowd C, Zangwill LM, Berry CC, et al. Detecting early glaucoma by assessment of retinal nerve fiber layer thickness and visual function. *Invest Ophthalmol Vis Sci.* 2001;42(9):1993-2003.
339. Blumberg DM, De Moraes CG, Liebmann JM, et al. Technology and the glaucoma suspect. *Investigative ophthalmology & visual science.* 2016;57(9):OCT80-OCT85.
340. Burgansky-Eliash Z, Wollstein G, Chu T, et al. Optical coherence tomography machine learning classifiers for glaucoma detection: a preliminary study. *Investigative ophthalmology & visual science.* 2005;46(11):4147-4152.
341. Huang M-L, Chen H-Y. Development and comparison of automated classifiers for glaucoma diagnosis using Stratus optical coherence tomography. *Investigative ophthalmology & visual science.* 2005;46(11):4121-4129.
342. Naithani P, Sihota R, Sony P, et al. Evaluation of optical coherence tomography and heidelberg retinal tomography parameters in detecting early and moderate glaucoma. *Investigative ophthalmology & visual science.* 2007;48(7):3138-3145.
343. Barella KA, Costa VP, Gonçalves Vidotti V, Silva FR, Dias M, Gomi ES. Glaucoma diagnostic accuracy of machine learning classifiers using retinal nerve fiber layer and optic nerve data from SD-OCT. *Journal of ophthalmology.* 2013;2013.
344. Bizios D, Heijl A, Hougaard JL, Bengtsson B. Machine learning classifiers for glaucoma diagnosis based on classification of retinal nerve fibre layer thickness parameters measured by Stratus OCT. *Acta ophthalmologica.* 2010;88(1):44-52.
345. Larrosa JM, Polo V, Ferreras A, García-Martín E, Calvo P, Pablo LE. Neural network analysis of different segmentation strategies of nerve fiber layer assessment for glaucoma diagnosis. *Journal of glaucoma.* 2015;24(9):672-678.
346. Muhammad H, Fuchs TJ, De Cuir N, et al. Hybrid deep learning on single wide-field optical coherence tomography scans accurately classifies glaucoma suspects. *Journal of glaucoma.* 2017;26(12):1086.
347. Xu J, Ishikawa H, Wollstein G, et al. Three-dimensional spectral-domain optical coherence tomography data analysis for glaucoma detection. *PLoS one.* 2013;8(2):e55476.
348. Wu H, De Boer JF, Chen TC. Diagnostic capability of spectral-domain optical coherence tomography for glaucoma. *American journal of ophthalmology.* 2012;153(5):815-826. e812.
349. Bowd C, Hao J, Tavares IM, et al. Bayesian machine learning classifiers for combining structural and functional measurements to classify healthy and glaucomatous eyes. *Investigative ophthalmology & visual science.* 2008;49(3):945-953.

350. Lee BL, Bathija R, Weinreb RN. The definition of normal-tension glaucoma. *Journal of glaucoma*. 1998;7(6):366-371.
351. Trivli A, Koliarakis I, Terzidou C, et al. Normal-tension glaucoma: Pathogenesis and genetics. *Experimental and therapeutic medicine*. 2019;17(1):563-574.
352. Killer H, Pircher A. Normal tension glaucoma: review of current understanding and mechanisms of the pathogenesis. *Eye*. 2018;32(5):924-930.
353. Bengtsson B, Leske MC, Yang Z, Heijl A, group E. Disc hemorrhages and treatment in the early manifest glaucoma trial. *Ophthalmology*. 2008;115(11):2044-2048.
354. Budde WM, Jonas JB. Enlargement of parapapillary atrophy in follow-up of chronic open-angle glaucoma. *American journal of ophthalmology*. 2004;137(4):646-654.
355. Varma R, Spaeth GL, Hanau C, Steinmann WC, Feldman RM. Positional changes in the vasculature of the optic disk in glaucoma. *American journal of ophthalmology*. 1987;104(5):457-464.
356. Radcliffe NM, Smith SD, Syed ZA, et al. Retinal blood vessel positional shifts and glaucoma progression. *Ophthalmology*. 2014;121(4):842-848.
357. Xin D, Talamini CL, Raza AS, et al. Hypodense regions (holes) in the retinal nerve fiber layer in frequency-domain OCT scans of glaucoma patients and suspects. *Investigative ophthalmology & visual science*. 2011;52(10):7180-7186.
358. Vickers AJ. The use of percentage change from baseline as an outcome in a controlled trial is statistically inefficient: a simulation study. *BMC medical research methodology*. 2001;1(1):1-4.
359. Siaudvytyte L, Januleviciene I, Daveckaite A, et al. Literature review and meta-analysis of translaminal pressure difference in open-angle glaucoma. *Eye*. 2015;29(10):1242-1250.
360. Health N, Council MR. NHMRC Guidelines: For the Screening, Prognosis, Diagnosis, Management and Prevention of Glaucoma 2010. 2010.
361. Tuulonen A. Cost-effectiveness of screening for open angle glaucoma in developed countries. *Indian journal of ophthalmology*. 2011;59(Suppl1):S24.

Appendices

Appendix 1:
Participant information sheet

PARTICIPANT INFORMATION SHEET

Name of Project: **Assessing Spontaneous Venous Pulsations in Glaucoma**

UTS HREC APPROVAL NUMBER: ETH17-1392

WHO IS DOING THE RESEARCH?

My name is Sahar Shariflou and I am a PhD research student at UTS. My supervisor is Dr Mojtaba Golzan (Ph. 9514 4083, Email: mojtaba.golzan@uts.edu.au). This research is being conducted in collaboration with Dr Ashish Agar (Marsden Eye Specialists).

WHAT IS THIS RESEARCH ABOUT?

This research is to find out about how the vessels at the back of the eye (retina) may be affected during Glaucoma, compared to non-glaucoma eyes. Glaucoma is an inherited progressive eye condition that causes irreversible gradual loss of vision. Currently there is no treatment and those with Glaucoma receive therapy to slow its progression.

The purpose of this study is to correlate any changes in the eye vasculature in Glaucoma. If this mechanism is better understood, it will present new opportunities for the wider community, especially those with a family history of Glaucoma, in preventative medicines, drug therapy and disease management of glaucoma. If this study finds strong correlations between vascular changes in Glaucoma, a new screening tool may be implemented in eye health services to aid the early detection of Glaucoma, which is crucial in the management in the disease to slow its progression.

Additionally, we aim to determine if there are any correlations between glaucoma and cognitive decline including attention, concentration, memory, language and orientation. This will be tested through a questionnaire-type cognition assessment.

FUNDING

Funding for this research has been provided by the University of Technology Sydney.

IF I SAY YES, WHAT WILL IT INVOLVE?

If you are an existing glaucoma patient at Marsden Eye Specialists and you decide to participate in this study, you will be assessed during your normal 6-monthly check-ups. The additional assessments for this study will be free of charge and may extend your appointment time for up to 1 hour. If you are not a glaucoma patient, you will be asked to visit the UTS Orthoptic Clinic (Level 13, 15 Broadway, Ultimo) for about an hour.

The following table is an indication of the schedule of visits and tests to be conducted. An explanation of the tests are listed below the table.

Tests	Visits 1-6
	Month 0, 6, 12, 18, 24, 30
Completion of questionnaire	✓
Medical history & medications	✓
Blood pressure & eye pressure	✓
Corneal thickness measurement & anaesthetic	✓
Visual field test	✓
OCT (images the back of the eye)	✓
Eye examination & pupil dilation	✓
Video recording of the vessels at the back of your eye	✓

Blood pressure & eye pressure: Your blood pressure will be checked using an arm cuff, similar to how your GP would check your blood pressure. Your eye pressure will be determined by placing an

instrument called a tonometer on your eyes. You will have received anaesthetic drops before this, so you will not feel anything on your eye.

Corneal thickness measurement: This is a measurement of the front clear part of your eye. You will require anaesthetic to be dropped in each eye for this to temporarily numb the surface of your eye. These drops may cause slight irritation at first, but the irritation is fast passing and is normal. These drops do not affect your vision.

Visual Field Test: Your visual function (vision) will be tested by checking your ability to see spots of white light in your central and peripheral (side) vision.

OCT (Ocular Coherence Tomography): This is a non-invasive and non-contact imaging technique to image the different layers of your retina (back of your eye).

Eye examination & pupil dilation: Eye drops will be dropped on the surface of your eyes to dilate the pupils (the black circle in the centre of your eye) so that an examination of the front and back of your eyes can take place. This assessment will take place on a device called a Slit Lamp, where you will place your chin on a chin rest and forehead against a support bar and a narrow beam of light will be pointed to your eye. It is a non-invasive non-contact test that will allow us to look through the Slit Lamp to examine your eyes. The effect of the drops will last 1-2 hours. Driving after pupil dilation is discouraged, if you do not have transport arranged, please discuss with us.

Video recording of the vessels at the back of your eye: This is also conducted on the Slit Lamp and is also non-invasive and non-contact. A bright light will be pointed at your eyes to illuminate the inside of your eye so that a video recording can be taken to visualise the small vessels at the back of your eye.

ARE THERE ANY RISKS/INCONVENIENCE?

The eye drops when first put on the eye can cause slight irritation which will pass after a few seconds. There is a possibility of light sensitivity following the tests because of the dilated pupil and you will not be able to drive immediately after testing.

The device used to take video recordings of the vessels at the back of your eye has a bright light which may be inconvenient to you. You may see an "after image" once the videorecording has been taken, however this is a normal reaction to light and will return to normal after a few minutes.

We ask that you don't participate in this study if you know you are allergic to tropicamide or proxymetacine (the eye drops).

We also ask that you don't participate in this study if:

- a) you are feeling ill on the day of the study
- b) you have eye problems on the day of the study
- c) you have asthma or "wheezy bronchitis"

WHY HAVE I BEEN ASKED?

You have been approached because you are either:

- a) A suitable glaucoma patient under Dr Agar's care
- OR**
- b) A healthy individual of suitable age (<40-80 years of age) with no eye problems or systemic diseases

DO I HAVE TO SAY YES?

Participation in this research is completely voluntary.

WHAT WILL HAPPEN IF I SAY NO?

You are free to withdraw from participating in this research at any time without consequences. I will thank you for your time so far and won't contact you about this research again.

IF I SAY YES, CAN I CHANGE MY MIND LATER?

You can change your mind at any time. However, changing your mind after data collection may affect analysis and research outcomes. Please advise as soon as possible of any intention to withdraw. I will thank you for your time so far.

WHAT IF I HAVE CONCERNS OR A COMPLAINT?

If you have concerns about the research that you think I or my supervisor can help you with, please feel free to contact us:

Dr. Mojtaba Golzan: Ph. 9514 4083, Email: mojtaba.golzan@uts.edu.au.

Miss Sahar Shariflou: Ph. 9514 4105, Email: sahar.shariflou@uts.edu.au

NOTE:

This study has been approved by the University of Technology Sydney Human Research Ethics Committee (UTS HREC). If you have any concerns or complaints about any aspect of the conduct of this research, please contact the Ethics Secretariat on ph.: +61 2 9514 2478 or email: Research.Ethics@uts.edu.au), and quote the UTS HREC reference number. Any matter raised will be treated confidentially, investigated and you will be informed of the outcome.

Appendix 2:
Participant consent form

INFORMED CONSENT FORM

Name of Project: **Assessing Spontaneous Venous Pulsations in Glaucoma**

UTS HREC APPROVAL NUMBER: ETH17-1392

I, _____ (*participant's name*), agree to participate in the research project 'Assessment of Spontaneous Venous Pulsations in Glaucoma' (UTS HREC approval number: eth17-1392) being conducted by Dr Mojtaba Golzan and Miss Sahar Shariflou, in collaboration with Dr Ashish Agar (Marsden Eye Specialists).

Dr. Mojtaba Golzan: Ph. 9514 4083, Email: mojtaba.golzan@uts.edu.au.

Miss Sahar Shariflou: Ph. 9514 4105, Email: sahar.shariflou@uts.edu.au

Funding for this research has been provided by the University of Technology Sydney.

I understand that the purpose of the study is to correlate any changes in the eye vasculature with Glaucoma. If this mechanism is better understood it will present new opportunities for the wider community in preventative medicine, drug therapy and disease management for Glaucoma.

I understand that I have been asked to participate in this research because I am a suitable Glaucoma patient **OR** am a healthy individual within the age groups of interest and that my participation in this research will involve 6-monthly eye check-ups at Marsden Eye Specialists (for existing glaucoma patients) **OR** UTS Orthoptics Clinic (for healthy individuals) which may last up to an hour (for glaucoma patients this is an hour additional to your normal appointment time). I also understand the various tests that will be conducted at the appointments.

I agree to be:

Video recorded

I agree that the research data gathered from this project may be published in a form that:

Does not identify me in any way

May be used for future research purposes

I am aware that I can contact Dr. Mojtaba Golzan or Miss Sahar Shariflou if I have any concerns about the research. I also understand that I am free to withdraw my participation from this research project at any time I wish, without consequences, and without giving a reason. If you are a UTS student or staff member, withdrawal from the research will not prejudice your future career, academic progress or employment.

I agree that Dr Mojtaba Golzan and/or Dr Ashish Agar and/or Miss Sahar Shariflou have answered all my questions fully and clearly.

Name and Signature (participant)

____/____/____
Date

Name and Signature (researcher or delegate)

____/____/____
Date

NOTE:

This study has been approved by the University of Technology Sydney Human Research Ethics Committee (UTS HREC). If you have any concerns or complaints about any aspect of the conduct of this research, please contact the Ethics Secretariat on ph.: +61 2 9514 2478 or email: Research.Ethics@uts.edu.au, and quote the UTS HREC reference number. Any matter raised will be treated confidentially, investigated and you will be informed of the outcome.

Appendix 3:
Participant questionnaire

Study:

Assessment of Spontaneous Venous Pulsations in Glaucoma

ID _____

Date:..... Name:.....

Date of Birth:..... Gender: Male (0) Female (1)

Address:.....

Post Code:..... Telephone number:.....

Email:

Height: _____(m) Weight: _____(kg)

Ethnic Group: African Aboriginal/Pacific Islander Caucasian

Hispanic Middle Eastern North East Asian South East Asian Other

Waist circumference _____ (cm) Birth weight: _____ (kg)

Hip circumference _____ (cm)

Wish to receive summary of results of whole study? Yes No

PERSONAL MEDICAL HISTORY

Have you ever been told that you have, or have had the following (please tick and indicate age)?

1. High blood pressure

- No (0)
- ISH (2) _____
- EH (3) _____
- Yes (1) _____

2. High cholesterol

- No (0)
- Yes (1) _____

3. Diabetes

- No (0)
- Type I (2) _____
- Type II (3) _____
- Yes (1) _____

4. Stroke

- No (0)
- TIA (2)
- CVA (3)
- Yes (1)

5. Peripheral vascular disease

- No (0)
- Yes (1) _____

6. Chronic heart disease

- No (0)
- Angina (2)
- MI (3)
- Yes (1)

FAMILY MEDICAL HISTORY

Please tick and indicate family member and age.

1. High blood pressure

- No (0)
- ISH (2) _____
- EH (3) _____
- Yes (1) _____

2. Family History of CV Disease (<60 years)

- No (0)
- Yes (1) _____

If yes:

Stroke

- No (0)
- Yes (1) _____

Angina

- No (0)
- Yes (1) _____

Heart attack

- No (0)
- Yes (1) _____

Peripheral vascular disease

- No (0)
- Yes (1) _____

WOMEN ONLY

Please tick and indicate age.

1. Currently Pregnant No (0)
Yes (1)

2. Been Pregnant No (0)
Yes (1) _____

Number of Times _____

3. High blood pressure in pregnancy
No (0)
Yes (1) _____

4. Mother High blood pressure in pregnancy
No (0)
Yes (1) _____

5. Oral contraceptive pill
Never (0)
Previous (1) _____
Current (2) _____

6. Currently breast feeding
No (0)
Yes (1)

LIFESTYLE

1. Smoking

Do you smoke cigarettes? No (0)
Yes (1)
Past Smoker (2)

If yes, how many per day? _____

Pack Years? _____

How many years since you quit? _____

2. Alcohol

Units per week _____

3. Exercise

No (0)
Yes (1)

If yes:

Frequency of exercise per week

Duration of exercise (minutes)

Type of exercise

CURRENT DRUG THERAPY

No (0)
CVD (1)
Other (2)

Taken blood pressure lowering medication today

No (0)
Yes (1)

OTHER PAST MEDICAL HISTORY

.....
.....
.....
.....
.....

OTHER EXCLUSION CRITERIA

Current acute illness

No (0)
Yes (1)

Current eye problems

No (0)
Yes (1)

Suffer from asthma or "wheezy bronchitis"

No (0)
Yes (1)

Current active malignancy (cancer)

No (0)
Yes (1)

Kidney disease

No (0)
Yes (1)

Known allergy to

tropicamide EXCLUDE
glyceryl trinitrate EXCLUDE
proxymetacine EXCLUDE
gluten
lactose

Explanation of questionnaire:

The investigator will go through the questionnaire with the participant and explain each section.

Numbers (0), (1), (2) etc. refer to the codes to be entered into the final database containing all data for analysis.

It is not expected that all participant will know the answers to all questions, but they will be asked to answer to the best of their ability.

Acronyms:

EH: essential hypertension

CHD: chronic heart disease

CV: cardiovascular

CVA: cerebrovascular accident

CVD: cardiovascular disease

ISH: isolated systolic hypertension

MI: myocardial infarction

TIA: transient ischaemic attack

F1	
F2	
F3	
F4	
F5	
F6	
F7	
F8	
F9	
F10	

Appendix 4a:

Image of SVP assessment using a tablet-based ophthalmoscope mounted on a slit lamp

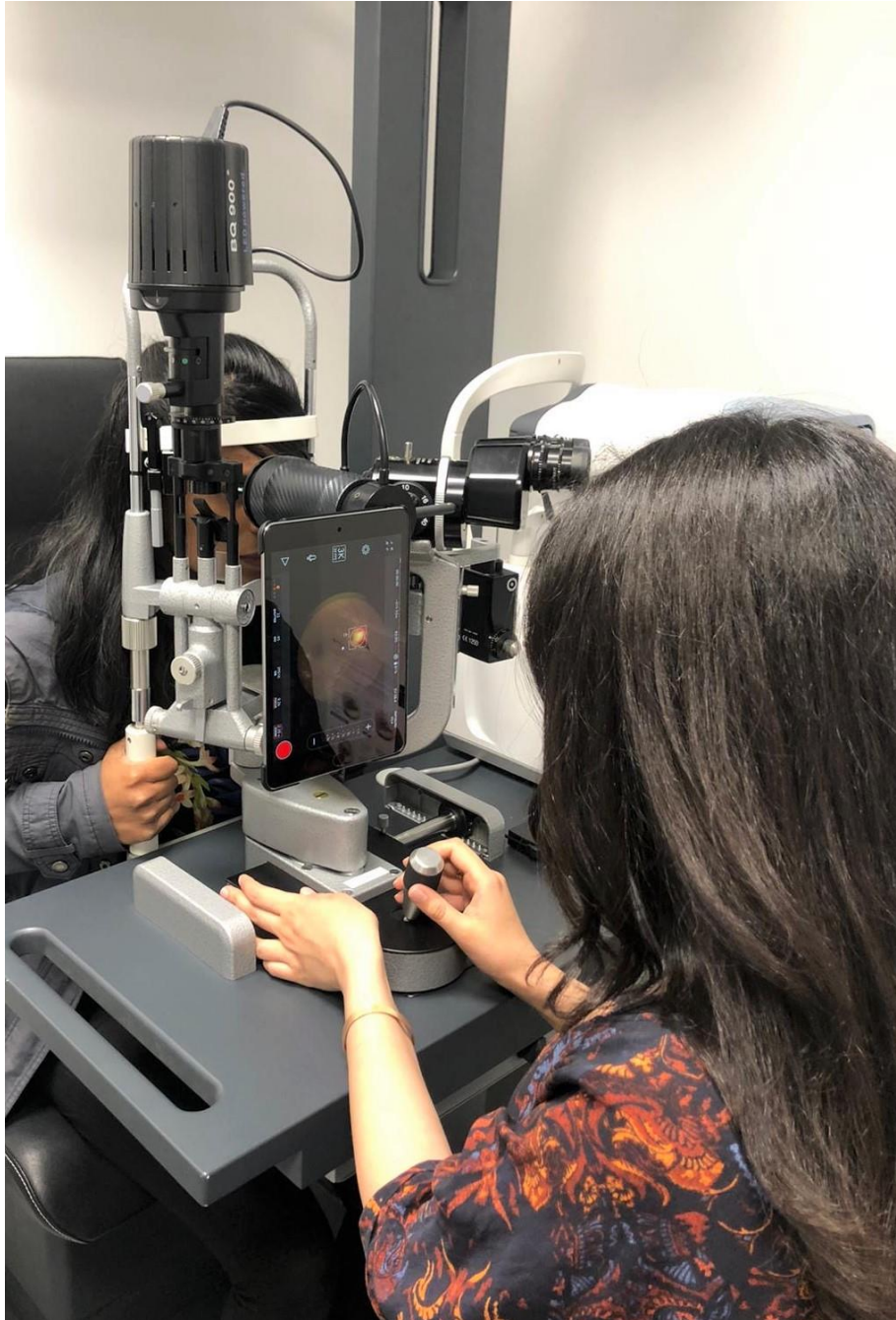


Image 1. SVP assessment using a tablet-based ophthalmoscope mounted on a slit lamp.

Appendix 4b:
Image of SVP-setup on slit lamp



Image 2. Patient and tablet-based ophthalmoscope position during SVP assessment.

Appendix 5:
**A combined convolutional and recurrent neural network for enhanced
glaucoma detection**



OPEN A combined convolutional and recurrent neural network for enhanced glaucoma detection

Soheila Gheisari^{1✉}, Sahar Shariflou¹, Jack Phu^{2,5}, Paul J. Kennedy³, Ashish Agar⁴, Michael Kalloniatis^{2,5} & S. Mojtaba Golzan¹

Glaucoma, a leading cause of blindness, is a multifaceted disease with several patho-physiological features manifesting in single fundus images (e.g., optic nerve cupping) as well as fundus videos (e.g., vascular pulsatility index). Current convolutional neural networks (CNNs) developed to detect glaucoma are all based on spatial features embedded in an image. We developed a combined CNN and recurrent neural network (RNN) that not only extracts the spatial features in a fundus image but also the temporal features embedded in a fundus video (i.e., sequential images). A total of 1810 fundus images and 295 fundus videos were used to train a CNN and a combined CNN and Long Short-Term Memory RNN. The combined CNN/RNN model reached an average F-measure of 96.2% in separating glaucoma from healthy eyes. In contrast, the base CNN model reached an average F-measure of only 79.2%. This proof-of-concept study demonstrates that extracting spatial and temporal features from fundus videos using a combined CNN and RNN, can markedly enhance the accuracy of glaucoma detection.

Glaucoma is a chronic disease associated with age. It is described as an ocular disorder that encompasses a group of progressive optic neuropathies with established pathophysiological changes at the optic nerve head (ONH)¹. The glaucoma continuum describes the optic neuropathy associated with progressive glaucomatous damage as RGC loss during the initial and asymptomatic stages of the disease followed by detectable retinal nerve fibre layer (RNFL) thinning and ultimately visual field (VF) defects². Previous studies have shown that, in untreated patients, due to missed diagnosis, the risk of progressing from ocular hypertension to unilateral vision loss (i.e., legal blindness) is 1.5% to 10.5%³. Accordingly, early diagnosis is vital to prevent disease progression and vision loss.

Fundus photographs provide a 30-degree image of the ONH and an opportunity to quantify a number of glaucoma specific morphological features⁴, including neuroretinal rim loss, and an increased cup-to-disc ratio⁵. Despite the computer-aided approach for objective assessment of these features, there is well known inter- and intra- observer variation in analysing images obtained from the ONH⁶. Another major limitation of single fundus imaging is that it does not reveal markers associated with blood flow dysregulation, a well-established phenomenon in glaucoma⁷. To overcome this limitation, a number of recent studies have focused on analysing fundus videos (i.e. image sequences) in search of markers associated with blood flow. Through analysing fundus videos, temporal features such as alteration in the amplitude of spontaneous venous pulsations (SVP)⁸ and blood column variations⁹ can be obtained, both of which have been linked to glaucoma^{10–12}. Taken together, it is imperative to incorporate both spatial and temporal features for any approach aimed at glaucoma assessment.

Computer aided diagnosis (CAD) systems play an important role in making an accurate, reliable and fast diagnosis of glaucoma¹³. Recent advances in computational power capabilities have allowed implementation of convolutional neural networks (CNN) facilitating autonomous classification of glaucoma based on complex features derived from thousands of available fundus images. The specificity and sensitivity of these models range between 85 to 95%, with the transfer-trained models (as opposed to native trained) achieving the highest performance in separating glaucoma from healthy fundus images^{14–16}. While these experimental results show that pre-trained CNNs have the ability to achieve superior results in classifying glaucomatous fundus images, the complexity of glaucoma pathology poses unique challenges for CNNs trained on fundus images only. More

¹Vision Science Group, Graduate School of Health, University of Technology Sydney, Sydney, Australia. ²Centre for Eye Health, School of Optometry and Vision Science, University of New South Wales, Sydney, Australia. ³Center for Artificial Intelligence, Faculty of Engineering and Information Technology, University of Technology Sydney, Sydney, Australia. ⁴Department of Ophthalmology, Prince of Wales Hospital, Sydney, Australia. ⁵School of Optometry and Vision Science, University of New South Wales, Sydney, Australia. ✉email: soheila.gheisari@uts.edu.au

	Glaucoma	Normal
Number of participants	379	316
Gender (female)	158	151
Gender (male)	221	165
Average age (years, SD)	65.1 ± 13	47 ± 15

Table 1. Participant demographics and data distribution.

specifically, population differences in optic disc size and colouration¹⁷ as well myopic discs¹⁸ are a potential source of errors for these networks as they have strong correlations with critical ONH structural parameters such as cup-disc ratio and neuroretinal rim thickness relevant to glaucoma diagnosis. Accordingly, such networks can only reach certain levels of accuracy and precision without compromising on false positive rates.

As glaucoma encompasses a range of spatial and temporal features, for any autonomous approach, it is essential to treat it as a video classification problem, rather than a static image problem. By taking such approach, spatial features such as changes to ONH morphology as well as temporal features such as amplitude of spontaneous venous pulsations are taken into account. In this study, we propose a novel approach through which a combined CNN and recurrent neural network (RNN) is used to extract spatial and temporal features embedded in fundus videos to detect glaucoma.

Methods

Data collection. Fundus images and videos were collected from 489 and 206 participants attending the Centre for Eye Health (University of New South Wales, Sydney, Australia), Marsden Eye Clinic, and Vision Research Clinic (UTS). For fundus videos, participants had a bilateral dilated funduscopy and a minimum 5-s recording (30 frames per second at a 46/60 degrees' field of view of the retina, and 2.2 image magnification) centred on the optic disc (Table 1). All subjects were required to be > 18 years of age, visual acuity better than 6/12, and have sufficiently clear ocular media for accurate capturing of fundus photos and videography.

We included patients with glaucoma who had primary open-angle (either high- or low-tension glaucoma), pseudoexfoliative or pigmentary glaucoma. Glaucoma patients were diagnosed clinically on the basis of characteristic structural losses observed on dilated stereoscopic examination of the optic nerve head (including but not limited to the following features: increased cup-to-disc ratio, cup-to-disc ratio asymmetry, localised or generalised neuroretinal rim thinning or notching, deepening of the optic cup, and glaucomatous disc haemorrhages) with or without concordant visual field defects on conventional white-on-white standard automated perimetry (Humphrey Field Analyzer, 24-2 SITA-Standard; Carl Zeiss Meditec, Dublin, CA). Glaucomatous visual field defects were not attributable to other diseases of the visual pathway and were defined as any of the following: three or more contiguous points of sensitivity reduction with a significance level of $p < 0.05$, of which at least one point is significant at the $p < 0.01$ level, on the pattern deviation map; a pattern standard deviation result with a significance level of $p < 0.05$; or three consecutive Glaucoma Hemifield Tests that were outside normal limits. Elevated intraocular pressure was not required for a diagnosis of glaucoma. In all cases, a glaucoma specialist was responsible for diagnosis of glaucoma.

Normal subjects were required to have a normal visual field (pattern standard deviation not less than $p < 0.05$; Glaucoma Hemifield Test within normal limits; and no cluster of points of depression as described above), normal ocular health on comprehensive dilated fundus examination and intraocular pressure below 22 mmHg. A glaucoma specialist was also involved in identifying these patients as ophthalmically normal (i.e. no glaucoma). For all subjects, optical coherence tomography was used as an adjunct to the diagnostic process, but no specific numerical cut-offs were used to determine whether or not a patient had glaucoma.

This study was performed in accordance with the guidelines of the tenets of the Declaration of Helsinki and approved by the University of New South Wales and University of Technology Sydney's Human Research Ethics Committee. Informed consent was obtained from each subject following an explanation of the nature of the study.

Preprocessing of data. Prior to developing the deep learning architecture, one of the authors (SG) normalized all the images and frames and then marked the center of the optic disc in all of the frames in each video. An automated algorithm (custom written in MATLAB, The Mathworks, Massachusetts, USA) was then applied to crop all images to a square region centered on the optic disc and limited to two disc diameters surrounding the manually marked disc center. This approach was chosen as glaucoma-specific static and dynamic features are mainly manifested on retinal tissue surrounding the ONH. Furthermore, a previous study by Orlando and colleagues has shown that cropping images around the optic disc is more efficient than using the whole images for training CNNs¹⁹. Finally, we employed a data augmentation procedure to solve the imbalance issue in our dataset and to increase the amount of normal images in the training set. The training images were augmented through random rotation, zooming and horizontal flipping. As the default size of the input images to the network is 224×224 , we resized the images to match this specification (Fig. 1).

Convolutional neural network (CNN): extracting spatial features from retinal images. We evaluated two different deep learning architectures in this study: VGG16²⁰ and ResNet50²¹. These architectures were selected as they have been widely used for medical image classification tasks²². Both networks have a similar architecture and comprise of convolutional layers, pooling layers and a final fully connected layer that produces a

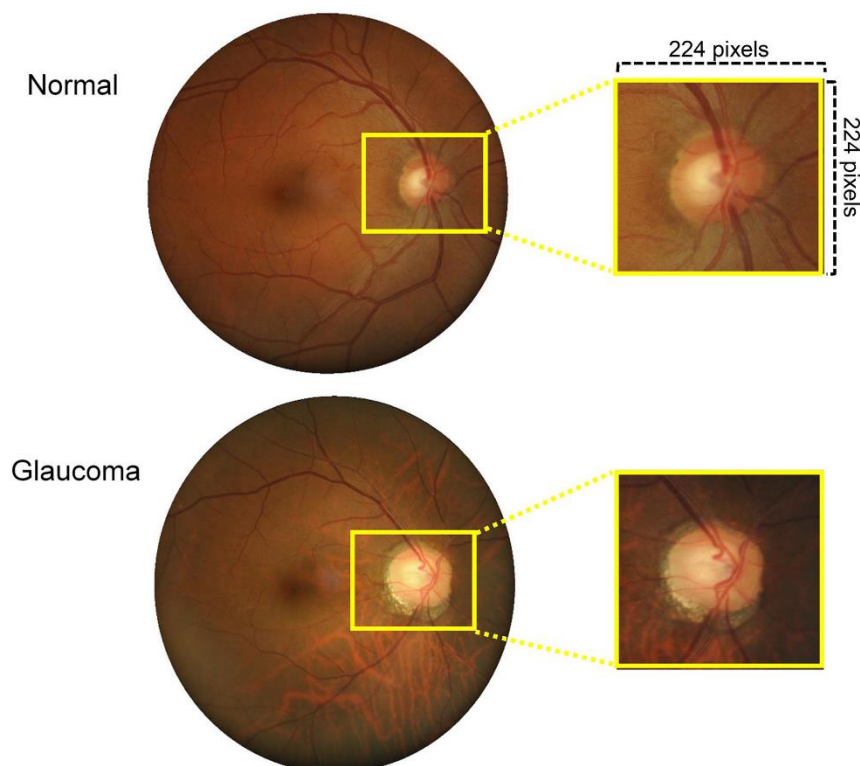


Figure 1. Examples of the original and cropped fundus images. All images were labeled as normal or glaucoma.

label for the input image (Fig. 2). The depth of VGG16 is 16 layers (13 convolutional layers and 3 fully connected layer). ResNet50 contains 50 layers (16 residual layers and 2 fully connected layers, each residual layer contains 3 convolutional layers). The input of the networks was set to 224×224 pixel images that are passed through a stack of convolutional layers. The convolutional layers filter images with a kernel size of 3×3 . Each convolutional block, a group of convolutional layers, is followed by a max-pooling layer. Applying the max-pooling layer not only allows the higher layer outputs to be resilient to subtle changes in the input, but also reduces the overall computational cost. A stack of convolutional layers is followed by fully connected (FC) layers to map the convolutional features to the feature vectors. The CNNs act like a feature extractor that extract static features of the input image.

Recurrent neural network: extracting temporal features from retinal videos. Recurrent neural networks (RNN) are specifically designed to identify patterns in sequences of data or, in our scenario, images. In a traditional neural network, all inputs are treated as being independent of each other. The limitation of such approach is in tasks that require the network to remember events from previous data, such as predicating a word in a sentence or predicating a frame in a video. As RNNs perform the same task for every element of a sequence, they are called *recurrent*. In these networks, the output depends on previous computations. Moreover, these networks have a “memory” which captures information about what has been calculated so far. The most popular RNN network is Long Short Term Memory (LSTM), originally proposed by Hochreiter and Schmidhuber²³, to learn long term dependencies. The superior performance of LSTM in language translation and speech processing has made it the first RNN of choice for tasks that feature extraction from a sequence of data is required (i.e. videos).

The LSTM architecture comprises memory blocks with each block containing a number of memory cells. Each memory cell consists of three gates: forget, input and output gate. The forget gate is an σ function that decides which information to retain and which to forget. The input gate decides what new information is to be stored in each cell. The output gate selects useful information from the current cell state and displays it as an output (Fig. 3).

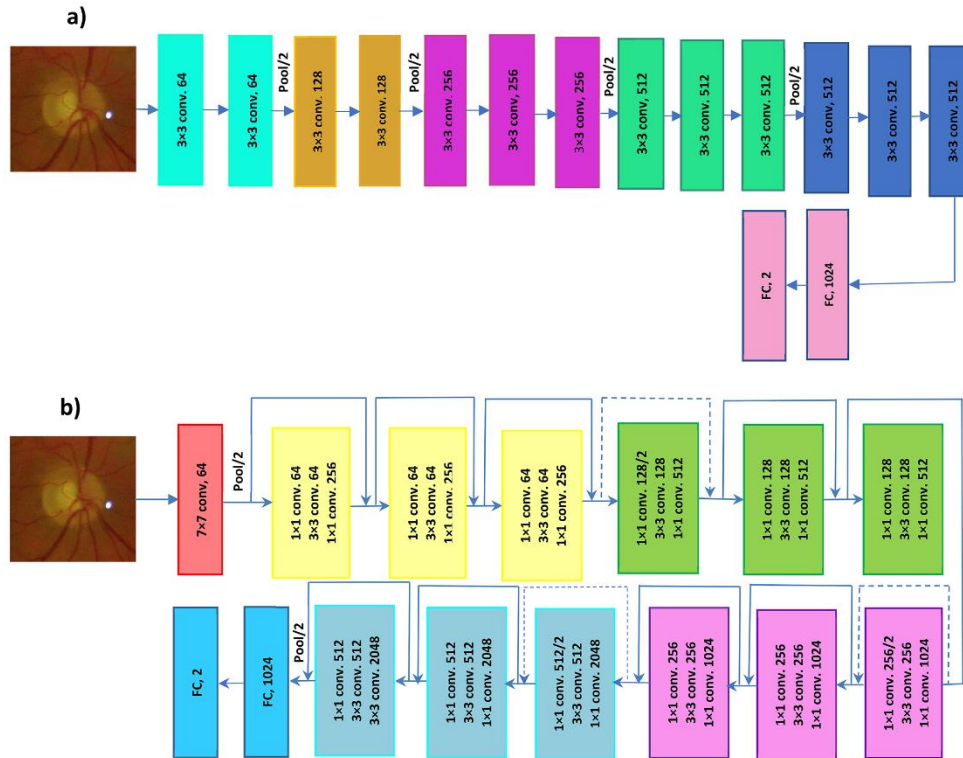


Figure 2. Overall framework of convolutional neural networks. (a) VGG16, (b) ResNet50.

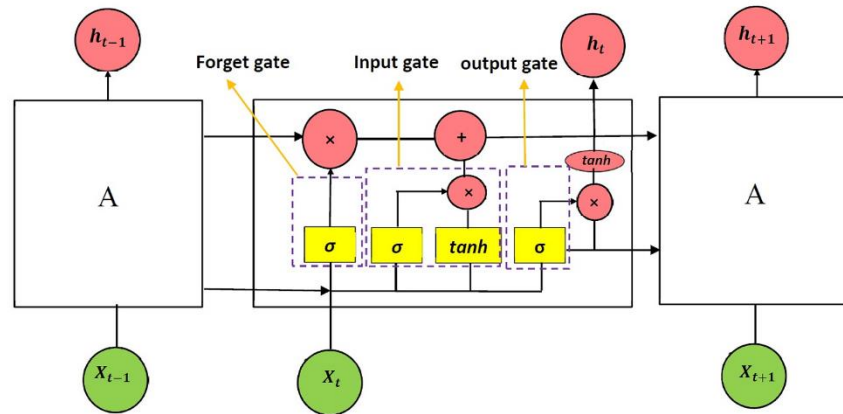


Figure 3. Structure of the Long Short Term Memory (LSTM), encompassing the three gates; forget, input and output. X denotes the input of the memory, h is the prediction at time t , and σ is a function that selects which information to retain or forget.

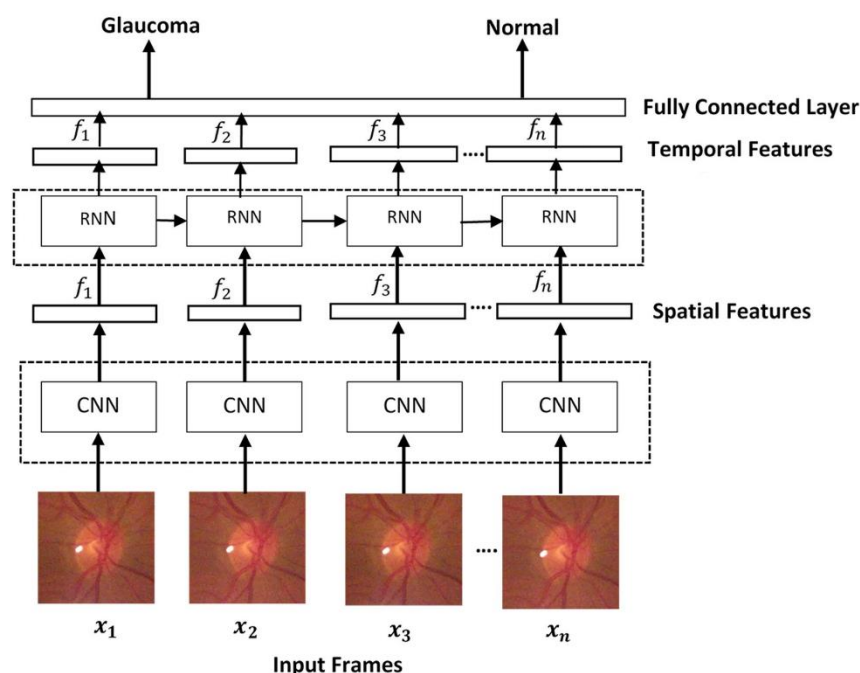


Figure 4. Overall framework of the fused Convolutional Neural Network-Recurrent Neural Network (CNN-RNN). The extracted spatial features from the CNN passes through the RNN to create the temporal features.

Combining CNN and RNN. We developed a combined CNN (VGG16 and ResNet 50) and RNN (LSTM) architecture to extract spatial and temporal features, respectively. The overall framework of our approach is shown in Fig. 4. Each video is converted into sequential images and passed onto the CNN to extract spatial features. The outputs are then passed into a recurrent sequence learning model (i.e. LSTM) to identify temporal features within the image sequence. The combined features are finally passed on to a fully connected layer to predict the classification for the full input sequence.

Network training. We evaluated the networks described earlier using transfer learning. In transfer learning, as opposed to native training, model weights are initialized based on the ImageNet dataset, a large benchmark dataset in object category classification and detection on hundreds of object categories and millions of images. Transfer learning is to initialize the model weights based on a huge general image dataset, except for the fully connected layers which are trained on our constructed fundus dataset. To train and evaluate the models, we divided the dataset randomly into three subsets: training (85% of total images), testing (10% of total images), and validation (5% of total images) and quantified the F-measure, precision and recall. This procedure was repeated ten times and the average of F-measures, precisions and recalls are reported. To ensure a homogenous training and testing, all images and videos from an individual participant were included in the same subset. In other words, all the images and videos used for testing the network were not “seen” by the network as part of the training and validation step.

Local interpretable model-agnostic explanations: uncovering the black box. We employed the Local Interpretable Model-Agnostic Explanations (LIME) algorithm to visualize sections of the image that the model is using to produce its final prediction. Briefly, LIME works based on creating a new dataset that contains permuted samples and the associated predictions. The new dataset is then used to train a new model which is weighted by the proximity of various features in the input image to the feature of interest. As a result, the weights are continuously updated based on whether they are contributing to the prediction or are against it. The fully trained new model is then used to interpret and explain the predictions²⁴.

Network evaluation. For each of the models; VGG16, Resnet50, VGG16 + LSTM and Resnet50 + LSTM, the performance was evaluated on the training and test datasets using sensitivity, specificity, and F-measure. The

Models	Sensitivity	Specificity	F-measure (%)
CNN			
VGG16	0.59 ± 0.1	0.65 ± 0.23	70.3 ± 5
Resnet50	0.71 ± 0.19	0.76 ± 0.13	79.2 ± 11.6
CNN + RNN			
VGG16 + LSTM	0.95 ± 0.02	0.96 ± 0.02	96.19 ± 1.7
Resnet50 + LSTM	0.89 ± 0.04	0.97 ± 0.02	94.03 ± 2.1

Table 2. Performance of the various models on the total dataset.

Models	Sensitivity	Specificity	F-measure (%)
CNN			
VGG16	0.59	0.55	56.4
Resnet50	0.72	0.70	70.3
CNN + RNN			
VGG16 + LSTM	0.94	0.86	89.9
Resnet50 + LSTM	0.88	0.79	83.9

Table 3. Performance of the various models on the age-matched dataset.

area under the receiver operating characteristics curve (AUC) was also used to evaluate the performance of each model.

Results

The combination of VGG16 and LSTM achieved the highest performance. To determine the best performance for each model, we ran several experiments varying the number of epochs, batch size and learning rate. A batch size of eight, 20 epochs, and a learning rate of 0.001 were determined as the optimum values to achieve the best performance. Table 2 summarizes the sensitivity, specificity and F-measure achieved for each of the models, using the aforementioned parameters. Our results show that the combination of VGG16 and LSTM achieved the highest accuracy, outperforming the models trained and tested on spatial features only.

As our overall database had a significant age difference between the glaucoma and normal group, a subsequent analysis was performed on a subgroup of age-matched glaucoma and normals to determine whether age may have a likely effect on the end results. A total of 23 glaucomatous fundus videos (obtained from 22 glaucoma participants, 67 ± 12 years) and 26 normal fundus videos (obtained from 17 healthy participants, 64 ± 18 years) were selected and tested using each of the models (no significant difference in age; $p > 0.05$). Table 3 summarizes the sensitivity, specificity and F-measure achieved for each model. Consistent with earlier results, aggregation of VGG16 and ResNet50 with LSTM achieved the higher F-measure, sensitivity and specificity, with the combined VGG16 and LSTM achieving the highest performance amongst all the models.

Combined CNN and RNN models achieved significantly higher performance than CNNs alone. An inter-group analysis was performed to evaluate the performance of each model in comparison to others. A one-way ANOVA applied to the average sensitivity, specificity and F-measure revealed a significant difference amongst all models ($p < 0.0001$, $p < 0.001$, $p < 0.0001$, respectively). Post-hoc analysis showed that a combined CNN and RNN, outperformed sole CNN models across all measures of sensitivity, specificity, and F-measure. The combination of VGG16 and LSTM achieved the highest performance in comparison to VGG16 for separating glaucoma from healthy image and videos, with a sensitivity of 0.95 (vs. 0.59; $p < 0.0001$), specificity of 0.96 (vs. 0.65; $p < 0.0001$), and F-measure of 96 (vs. 70; $p < 0.0001$). (detailed post-hoc results available in supplementary file, tables S1-S3).

Combined VGG16 and LSTM achieved the highest AUC in separating glaucoma from healthy eyes. To evaluate each model's performance in separating glaucoma from healthy eyes, we compared the area under the Receiver Operating Characteristic Curves (AUC). The VGG16 and ResNet50 models achieved an AUC of 0.6 and 0.83, respectively. However, these values increased to 0.99 and 0.97 for VGG16 + LSTM and ResNet50 + LSTM, respectively. Consistent with previous results, the combined VGG16 and LSTM achieved the highest AUC (Fig. 5).

The loss and accuracy plots over the epochs for the train dataset are shown in Figs. 6 and 7. From the curves, we can see that our methods have a good behavior of convergence.

Temporal features drive the accuracy of the end prediction. To evaluate whether the increased accuracy observed in the combined models are driven by temporal features (and is not due to the increased

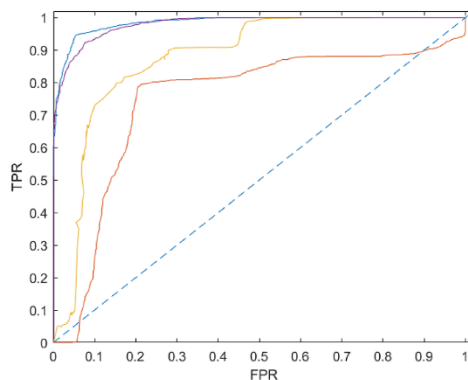


Figure 5. The receiver operating characteristic curves (AUC) for all the different models.

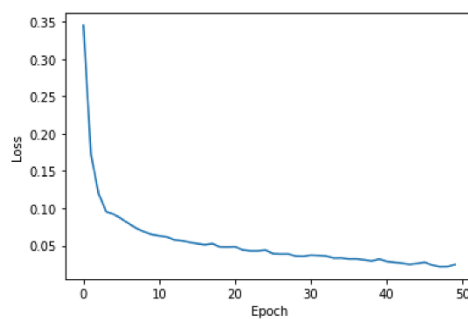


Figure 6. The loss over the epochs for the train dataset.

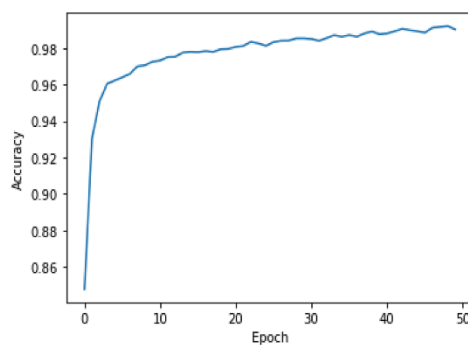


Figure 7. The accuracy over the epochs for the train dataset.

Models	Sensitivity	Specificity	F-measure (%)
VGG16 + LSTM	0.51	0.58	63
Resnet50 + LSTM	0.76	0.64	82

Table 4. Performance of combined CNN with RNN trained on images and tested on sequential images.

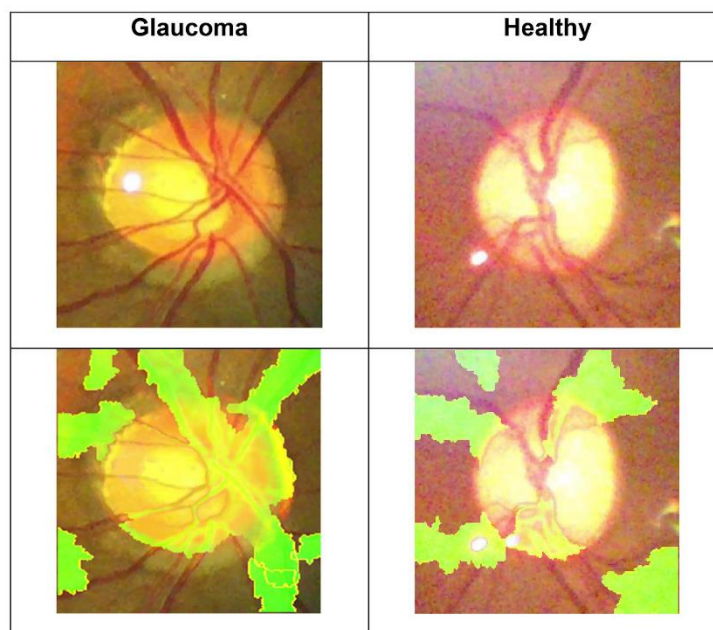


Figure 8. Average intensity map (60 sequential frames) from the LIME algorithm applied to the combined models showing significant regions of the image used to predict glaucoma and healthy. Regions with brighter intensity (green) indicate a larger impact compared to regions with lower intensity (yellow).

sample size as result of multiple frames), we trained the combined models using fundus images, tested with sequential frames, all whilst eliminating the sequential frames from the training set. A significant decrease in the performance of both combined models was noted, further confirming that temporal features played a significant role in achieving the higher performance shown earlier (Table 4).

Vascularized regions were predominantly influential in predicting end-classification. The LIME algorithm was employed to uncover regions of the image that the combined CNN/RNN model is using to extract spatial and temporal features and to produce its final class prediction (i.e., glaucoma or normal). The vascularized regions of superior and inferior retina were identified as regions of “influence” the VGG16 + LSTM has utilized in determining the final classification (Fig. 8). As we applied CNN + RNN on sequential frames of a video, the LIME algorithm is applied on one frame of a video to visualize the difference between a healthy and a glaucoma eye.

Discussion

In this study, we show, for the first time, that training a combined CNN and RNN on retinal image sequences, can extract both spatial and temporal features, resulting in significantly improved detection of glaucoma. More specifically, the combination of a VGG16 or ResNet50 network with an LSTM architecture, reached significantly higher sensitivity and specificity rates compared with a base VGG16 or ResNet50 network. The VGG16 + LSTM combination reached the highest performance, amongst all other networks, achieving a sensitivity of 0.95, specificity of 0.96, F-measure of 96.19% and an AUC of 0.99 in separating glaucoma from healthy eyes. The concept

described here provides the first solid evidence that by treating glaucoma as a video classification task, a highly accurate and autonomous AI-based approach for glaucoma detection can be developed.

While the retinal structures are static in nature, our reasoning for improved performance of the combined model is based on the dynamic changes of retinal vasculature observed at the ONH. More specifically, there is now evidence that the amplitude of spontaneous venous pulsations (SVP) are linked to glaucomatous pathology with lower SVPs associated with thinner RNFL thickness and visual field defects²⁵. While the origin of SVPs is a matter of debate, there is a consensus that the trans-laminar pressure difference is the main driver behind these pulsations. The trans-laminar pressure is governed by the difference in IOP and the pressure of the cerebrospinal fluid surrounding the optic nerve sheath; both of which have been linked to glaucomatous pathology^{26,27}. Furthermore, using a modified photoplethysmography tool (i.e., using the green channel of a colour fundus video to visualise blood column variation in the axial direction and across all regions of the retina.), Morgan et al. have shown a reduction in blood column intensity of glaucoma patients compared to normal⁹. It is these vascular changes that manifest themselves through temporal features of a fundus video and in combination with spatial features of the ONH, result in an overall improved performance of the combined model, as demonstrated in this study.

Deep CNNs have proven to be an efficient AI-based tool in identifying clinically significant features from retinal fundus images^{28–31}. Deep CNNs trained on glaucomatous fundus images have achieved a varied performance ranging from 0.75 to 0.9 in sensitivity and 0.65 to 0.97 specificity^{16,32,33} and these differences may be related to sample size. A recent study by Liu et al.³⁴, using a deep CNN architecture applied to 3,788 fundus photographs, showed a 87.9% in sensitivity and 96.5% in specificity in glaucomatous disc identification. A follow-up study by Christopher et al.¹⁵, using a similar approach on 14,822 fundus photographs, showed a network sensitivity and specificity of 0.84 and 0.83 in distinguishing glaucoma eyes from healthy eyes. There have been other attempts at applying deep learning to a combination of retinal imaging modalities, mainly fundus images and optical coherence tomography (OCT) scans, to improve network performance. Such networks have achieved an area under the ROC curve of 0.94 in separating glaucoma from normal healthy eyes³⁵. While promising, the approach requires access to both modalities and double the data, limiting scaling for large screening programs, mainly in remote and rural areas where access to OCT can be scarce. Furthermore, such approach is, again, based on spatial features only, neglecting the potential impact of temporal features. In contrast, our approach only requires a single device that can capture retinal image and videos.

Collectively, while deep learning methods have been capable of classifying glaucoma based on fundus images, they are yet to be utilised in a clinical setting mainly due to a high proportion of false positive rates and low precision. To overcome this limitation, we developed a model combining a deep spatial feature extractor (i.e. VGG16 and ResNet 50) with a model that can learn to recognize and synthesize temporal features (i.e. LSTM). By taking this approach, our aim was to combine glaucoma-specific temporal features (extracted from image sequences) with spatial biomarkers (extracted from fundus images) to significantly improve classification results compared with a model trained on fundus images only.

To compare results between base and combined models, we constructed and trained a number of architectures; VGG16, ResNet50, VGG16 + LSTM, and ResNet50 + LSTM. For all networks, a transfer training approach was used. This method was chosen mainly for two reasons. First, Christopher et al.¹⁵, has shown that a model encompassing transfer learning achieves a statistically significantly higher performance than natively trained models. Second, our sample size is relatively small and thus native training may not have achieved the intended results we were anticipating. All networks were trained and tested on images and sequential frames extracted from the videos. Our results showed that overall a combined CNN and RNN outperforms sole CNNs.

Amongst all the models trained, the combined VGG16 and LSTM achieved the highest performance. Intra-group analysis revealed a marginal statistically significant difference between the VGG16 and ResNet50 network ($p = 0.04$), with the latter achieving a higher F-measure. This is consistent with a previous report demonstrating higher performance of ResNet50 compared with VGG16¹⁵. We also observed a non-significant difference between the VGG16 + LSTM and ResNet50 + LSTM ($p = 0.19$). While ResNet50 outperformed VGG16, it was the combination of VGG16 and LSTM that achieved the highest performance. This could be attributed to the network structure within each model. Our trained ResNet50 had a total of 50 layers compared with 16 layers in the VGG16. Deeper networks extract more complicated features and achieve higher accuracy. The fact that the combination of VGG16 with LSTM achieved higher performance, demonstrates that the temporal features are possibly a dominant factor in predicting output classification compared to spatial features. As the output dimension of the ResNet50 is higher than VGG16, its connection with the LSTM needs more parameters. Both networks, VGG16 + LSTM and ResNet50 + LSTM are trained with the same dataset. However, ResNet50 + LSTM requires more training data since it has more free parameters. Therefore, under similar conditions, the network with more free parameters (i.e. VGG16 + LSTM) achieves higher accuracy.

To help understand and visualize the temporal features of the image sequence the combined model is utilizing to distinguish glaucoma from healthy videos, we used the LIME algorithm. Results showed that the vascularized regions of superior and inferior retina have the greatest impact on the model prediction. This is consistent with our previous studies that showed a dynamic vascular change in glaucoma eyes^{10,36}. We further evaluated the significance of temporal features on the model prediction by training the combined models using fundus images and testing with sequential images. This resulted in an average 22% decrease in the F-measure of the combined models, further proof that temporal features play a significant role in increasing model performance.

Limitations. Our study has a number of limitations. First, our sample size is relatively small and is from a racially homogenous population. This has resulted in lower network accuracy of the stand-alone VGG16 and ResNet50 compared to other research reports. However, the primary goal of our study was not to develop a

highly precise model for glaucoma detection, but rather demonstrate that adding recurrent connections to stand-alone CNNs could significantly increase a network's performance in separating glaucoma from healthy images. Nonetheless, we acknowledge that a larger and heterogeneous sample size is required to further support our findings. Second, videos obtained from glaucoma and normal participants, encompassing our final dataset, were not age-matched. However, we performed an analysis on a subgroup of age-matched glaucoma and controls, with results confirming our initial findings; combined CNN/RNN performed superior compared with CNN-only models. Third, the ground truth was based on the clinical evaluation of two different expert clinicians, with one labelling the images and the other labelling the videos. Accordingly, we cannot determine agreement. However, given that a benchmark inclusion and exclusion criteria was used for each of the two groups, we do not anticipate a significant impact on our findings. Finally, the camera used to capture retinal fundus videos was different to that of used for capturing retinal fundus images. As a result, the effect of such approach on our results cannot be determined.

In conclusion, this study presented a novel AI-based approach for glaucoma detection based on unification of spatial (static structural) and temporal (dynamic vascular) features. By considering glaucoma as a video classification task, our proposed method demonstrated promising performance in separating glaucoma from healthy compared with models solely reliant on spatial features as their input. Static features such as disc size, cup and rim size, and cup-to-disc ratio are variable across different populations³⁷, and therefore, have hindered development of models with high sensitivity and specificity³⁸. The method proposed here achieved a sensitivity of 0.95 and specificity of 0.96 in identifying glaucoma and thus, may provide an impetus for large-scale screening programs. However, further evaluation on a larger, heterogeneous population is required.

Received: 22 June 2020; Accepted: 5 January 2021
Published online: 21 January 2021

References

- Casson, R. J., Chidlow, G., Wood, J. P., Crowston, J. G. & Goldberg, I. Definition of glaucoma: Clinical and experimental concepts. *Clin. Exp. Ophthalmol.* **40**, 341–349. <https://doi.org/10.1111/j.1442-9071.2012.02773.x> (2012).
- Weinreb, R. N. *et al.* Primary open-angle glaucoma. *Nat. Rev. Dis. Primers* **2**(1), 160–167. <https://doi.org/10.1038/nrdp.2016.67> (2016).
- Weinreb, R. *et al.* Risk assessment in the management of patients with ocular hypertension. *Am. J. Ophthalmol.* **138**, 458–467. <https://doi.org/10.1016/j.ajo.2004.04.054> (2004).
- Wiley, H. & Ili, F. Nonproliferative diabetic retinopathy and diabetic macular edema. *Retina Fifth Edn.* **2**, 940–968 (2012).
- Spaeth, G. L. *et al.* The disc damage likelihood scale: Reproducibility of a new method of estimating the amount of optic nerve damage caused by glaucoma. *Trans. Am. Ophthalmol. Soc.* **100**, 181–186 (2002).
- Garway-Heath, D. F. *et al.* Inter- and intraobserver variation in the analysis of optic disc images: Comparison of the Heidelberg retina tomograph and computer assisted planimetry. *Br. J. Ophthalmol.* **83**(6), 664–669. <https://doi.org/10.1136/bjo.83.6.664> (1999).
- Flammer, J. *et al.* The impact of ocular blood flow in glaucoma. *Prog. Retina Eye Res.* **21**(4), 359–393. [https://doi.org/10.1016/s1350-9462\(02\)00008-3](https://doi.org/10.1016/s1350-9462(02)00008-3) (2002).
- Golzan, S. M., Graham, S., Leaney, J. & Avolio, A. Dynamic association between intraocular pressure and spontaneous pulsations of retinal veins. *Curr. Eye Res.* **36**, 53–59. <https://doi.org/10.3109/02713683.2010.530731> (2011).
- Morgan, W. H. *et al.* Photoplethysmographic measurement of various retinal vascular pulsation parameters and measurement of the venous phase delay. *Investig. Ophthalmol. Vis. Sci.* **55**(9), 5998–6006. <https://doi.org/10.1167/iov.14-15104> (2014).
- Golzan, S. M., Morgan, W. H., Georgevsky, D. & Graham, S. L. Correlation of retinal nerve fibre layer thickness and spontaneous retinal venous pulsations in glaucoma and normal controls. *PLoS ONE* **10**(6), 1–12. <https://doi.org/10.1371/journal.pone.0128433> (2015).
- Golzan, S. M., Georgevsky, D., Bowd, C., Weinreb, R. & Graham, S. Visual field sensitivity is decreased with reduced spontaneous venous pulsation in glaucoma eyes. *Investig. Ophthalmol. Vis. Sci.* **58**(8), 734 (2017).
- Morgan, W. H., Hazelton, M. L. & Yu, D.-Y. Retinal venous pulsation: Expanding our understanding and use of this enigmatic phenomenon. *Prog. Retina Eye Res.* **55**, 82–107. <https://doi.org/10.1016/j.preteyeres.2016.06.003> (2016).
- Cheriguene, S., Azizi, N., Djellali, H., Bunakha, O., Aldwairi, M. & Ziani, A. New computer-aided diagnosis system for glaucoma disease based on twin support vector machine. In *International Conference on Embedded Distributed Systems (EDIS)*, pp. 1–6, (2017).
- Al-Bander, B., Al-Nuaimy, W., Al-Tae, M. A. and Zheng, Y. Automated glaucoma diagnosis using deep learning approach. In *14th International Multi-Conference on Systems, Signals & Devices (SSD)*, pp. 207–210 (2017).
- Christopher, M. *et al.* Performance of deep learning architectures and transfer learning for detecting glaucomatous optic neuropathy in fundus photographs. *Sci. Rep.* <https://doi.org/10.1038/s41598-018-35044-9> (2018).
- Diaz-Pinto, A., Morales, S., Naranjo, V., Thomas, K. & Mossi, J. M. CNNs for automatic glaucoma assessment using fundus images: An extensive validation. *BioMed. Eng.* **18**(29), 1–19. <https://doi.org/10.1186/s12938-019-0649-y> (2019).
- Huynh, S. C., Wang, X. Y., Rochtchina, E., Crowston, J. G. & Mitchell, P. Distribution of optic disc parameters measured by OCT: Findings from a population-based study of 6-year-old Australian children. *Investig. Ophthalmol. Vis. Sci.* **47**(8), 3276–3285. <https://doi.org/10.1167/iov.06-0072> (2006).
- Tan, N. Y. Q., Sng, C. C. A. & Ang, M. Myopic optic disc changes and its role in glaucoma. *Curr. Opin. Ophthalmol.* **30**(2), 89–96 (2019).
- Orlando, I., Prokofyeva, E., Fresno, M., and Blaschko, M. Convolutional neural network transfer for automated glaucoma identification. In *International Symposium on Medical Information Processing and Analysis*, pp. 241–250 (2017).
- Simonyan, K. and Zisserman, A. Very deep convolutional networks for large image recognition. In *International Conference Learning Representation*, pp. 1–14 (2015).
- Szegedy, C., Ioffe, S. and Vanhoucke, V. Inception-v4, Inception-ResNet and the impact of residual connections on learning. In *Computer Vision and Pattern Recognition (CVPR)* 2016.
- Geert, L. *et al.* A survey on deep learning in medical image analysis. *Med. Image Anal.* **42**, 60–88. <https://doi.org/10.1016/j.media.2017.07.005> (2017).
- Hochreiter, S. & Schmidhuber, J. Long short-term memory. *Neural Comput.* **9**(8), 1735–1780 (1997).
- Ribeiro, M. T., Singh, S. & Guestrin, C. Why should I trust you? Explaining the predictions of any classifier. In *Proceedings of the 22nd ACM SIGKDD International Conference on Knowledge Discovery and Data Mining*, pp. 1135–1144 (2016). <https://doi.org/10.1145/1454008.1454050>.

25. Golzan, S. M., Morgan, W. H., Georgevsky, D. & Graham, S. L. [†]Correlation of retinal nerve fibre layer thickness and spontaneous retinal venous pulsations in glaucoma and normal controls. *PLoS ONE* <https://doi.org/10.1371/journal.pone.0128433> (2015).
26. Jonas, J. B., Ritch, R. & Panda-Jonas, S. Cerebrospinal fluid pressure in the pathogenesis of glaucoma. *Prog. Brain Res.* **221**, 33–47 (2015).
27. Price, D. A., Harris, A., Slesky, B. & Mathew, S. The influence of translaminal pressure gradient and intracranial pressure in glaucoma: A review. *J. Glaucoma* **29**(2), 141–146 (2020).
28. Wen, J. C. *et al.* Forecasting future humphrey visual fields using deep learning. *PLoS ONE* <https://doi.org/10.1371/journal.pone.0214875> (2018).
29. De Paauw, I. *et al.* Clinically applicable deep learning for diagnosis and referral in retinal disease. *Nat. Med.* **24**(9), 1342–1350 (2018).
30. Schmidt-Erfurth, U., Sadeghipour, A., Gerendas, B. S., Waldstein, S. M. & Bogunovic, H. Artificial intelligence in retina. *Prog. Retinal Eye Res.* **67**, 1–29. <https://doi.org/10.1016/j.preteyeres.2018.07.004> (2018).
31. Hogarty, D., Mackey, D. & Hewitt, A. Current state and future prospects of artificial intelligence in ophthalmology: A review: Artificial intelligence in ophthalmology. *Clin. Exp. Ophthalmol.* **47**, 128–139. <https://doi.org/10.1111/ceo.13381> (2018).
32. Devasia, T., Jacob, K. and Thomas, T. Automatic early stage glaucoma detection using cascade correlation neural network. In *Second International Conference on Smart Computing and Informatics (SCI)*, pp. 659–669, (2019).
33. Zheng, C., Johnson, T. V., Garg, A. & Boland, M. V. Artificial intelligence in glaucoma. *Curr. Opin. Ophthalmol.* **30**(2), 97–103 (2019).
34. Liu, S. *et al.* A deep learning-based algorithm identifies glaucomatous discs using monoscopic fundus photographs. *Ophthalmol. Glaucoma* **1**(1), 15–22 (2018).
35. Medeiros, F. A., Jammal, A. A. & Thompson, A. C. From machine to machine: An oct-trained deep learning algorithm for objective quantification of glaucomatous damage in fundus photographs. *Ophthalmology* **126**(4), 513–521. <https://doi.org/10.1016/j.ophtha.2018.12.033> (2019).
36. Golzan, S. M., Graham, S. L., Leany, J. & Avolio, A. Dynamic association between intraocular pressure and spontaneous pulsations of retinal veins. *Curr. Eye Res.* **36**(1), 53–59. <https://doi.org/10.3109/02713683.2010.530731> (2011).
37. Zangwill, L. M. *et al.* Racial differences in optic disc topography: Baseline results from the confocal scanning laser ophthalmoscopy ancillary study to the ocular hypertension treatment study. *JAMA Ophthalmol.* **122**(1), 22–28. <https://doi.org/10.1001/archophth.122.1.22> (2004).
38. Ervin, A. M., *et al.* Screening for glaucoma *comparative effectiveness*. Agency for Healthcare Research and Quality, *Report No. 12-EHC037-EE*, 2012.

Acknowledgements

SMG is a recipient of an NHMRC-ARC Dementia Research Fellowship. Guide Dogs NSW/ACT provides salary support for MK and JP. We thank the staff at the Centre for Eye Health, University of New South Wales, Australia, for their technical and clinical assistance.

Author contributions

Methodology, SG; Resources, SS, JP, PJK, AA, MK; Software, SG; Supervision, SMG; Writing original draft, SG; Writing: review and editing, SS, JP, PK, AA, MK and SMG.

Competing interests

The authors declare no competing interests.


Additional information

Supplementary Information The online version contains supplementary material available at <https://doi.org/10.1038/s41598-021-81554-4>.

Correspondence and requests for materials should be addressed to S.G.

Reprints and permissions information is available at www.nature.com/reprints.

Publisher's note Springer Nature remains neutral with regard to jurisdictional claims in published maps and institutional affiliations.

 **Open Access** This article is licensed under a Creative Commons Attribution 4.0 International License, which permits use, sharing, adaptation, distribution and reproduction in any medium or format, as long as you give appropriate credit to the original author(s) and the source, provide a link to the Creative Commons licence, and indicate if changes were made. The images or other third party material in this article are included in the article's Creative Commons licence, unless indicated otherwise in a credit line to the material. If material is not included in the article's Creative Commons licence and your intended use is not permitted by statutory regulation or exceeds the permitted use, you will need to obtain permission directly from the copyright holder. To view a copy of this licence, visit <http://creativecommons.org/licenses/by/4.0/>.

© The Author(s) 2021

Appendix 6:
**Objective Quantification of Spontaneous Retinal Venous Pulsations Using a
Novel Tablet-Based Ophthalmoscope**

Objective Quantification of Spontaneous Retinal Venous Pulsations Using a Novel Tablet-Based Ophthalmoscope

Sahar Shariflou¹, Ashish Agar¹⁻⁴, Kathryn Rose¹, Christopher Bowd⁵, and S. Mojtaba Golzan¹

¹ Vision Science Group, Discipline of Orthoptics, Graduate School of Health, University of Technology Sydney, NSW, Australia

² Ophthalmology Department, Prince of Wales Hospital, Sydney, NSW, Australia

³ Department of Ophthalmology, University of New South Wales, Sydney, NSW, Australia

⁴ Marsden Eye Specialists, Sydney, NSW, Australia

⁵ Hamilton Glaucoma Centre, Shiley Eye Institute, University of California, San Diego, San Diego, CA, USA

Correspondence: Sahar Shariflou, Graduate School of Health, UTS, 100 Broadway, Chippendale NSW 2008, Australia. e-mail: sahar.shariflou@student.uts.edu.au

Received: July 16, 2019

Accepted: December 24, 2019

Published: March 18, 2020

Keywords: spontaneous retinal venous pulsation; transclinal pressure gradient; spontaneous venous pulsation; lamina cribrosa; glaucoma

Citation: Shariflou S, Agar A, Rose K, Bowd C, Golzan SM. Objective quantification of spontaneous retinal venous pulsations using a novel tablet-based ophthalmoscope. *Trans Vis Sci Tech.* 2020;9(4):19. <https://doi.org/10.1167/tvst.9.4.19>

Purpose: Dynamic assessment of retinal vascular characteristics can aid in identifying glaucoma-specific biomarkers. More specifically, a loss of spontaneous retinal venous pulsations (SVPs) has been reported in glaucoma, but a lack of readily available tools has limited the ability to explore the full potential of SVP analysis in glaucoma assessment. Advancements in smart technology have paved the way for the development of portable, noninvasive, and inexpensive imaging modalities. By combining off-the-shelf optical elements and smart devices, the current study aims to determine whether SVPs can be detected and quantified using a novel tablet-based ophthalmoscope in glaucoma and glaucoma suspects.

Methods: Thirty patients, including 21 with confirmed glaucoma (9 men; average age 75 ± 8 years) and 9 glaucoma suspects (5 men; average age 64 ± 9 years), were studied. All patients had intraocular pressure measurements, Humphrey visual field assessment, optical coherence tomography, and a 10-second videography of the retinal circulation. The retinal vasculature recordings (46° field of view at 30 frames per second) were analyzed to extract SVP amplitudes.

Results: SVPs were detected and quantified in 100% of patients with glaucoma and those with suspected glaucoma using the novel device. The average SVP amplitudes in glaucoma and glaucoma suspects were $42.6\% \pm 10.7\%$ and $34\% \pm 6.7\%$, respectively.

Conclusions: Our results suggest that a novel tablet-based ophthalmoscope can aid in documenting and objectively quantifying SVPs in all patients.

Translational Relevance: Outcomes of this study provide an innovative, portable, noninvasive, and inexpensive solution for objective assessment of SVPs, which may have clinical relevance in glaucoma screening.

Introduction

Spontaneous retinal venous pulsations (SVPs) are changes in caliber of the retinal veins at the optic nerve head, usually at the hemi-veins of the central retinal vein as they join to form the central vein or where it exits at the lamina cribrosa.¹ The mechanism by which SVPs occur is complex. Intraocular pressure (IOP), retinal venous pressure (RVP), and cerebrospinal fluid pressure (CSFp) are all thought to play a role in their generation. These factors create a pressure gradi-

ent between the intraocular and retrobulbar spaces, which is said to be a main driver in the generation of SVPs.^{2,3} Reduced or absent SVPs have been reported as a risk factor for glaucoma and its progression,⁴⁻⁶ with absent SVPs reported in up to approximately 50% of patients with glaucoma.⁵ These findings may be due to elevated RVP, reduced ocular blood flow^{7,8} and/or lower mean CSFp compared with nonglaucomatous patients, which can decrease the amplitude of SVPs.⁹ Other identified factors known to reduce SVPs are the combination of elevated CSFp and reduced IOP, which can decrease the intravascular pressure gradient.^{5,10-13}

Copyright 2020 The Authors
tvst.arvojournals.org | ISSN: 2164-2591

This work is licensed under a Creative Commons Attribution-NonCommercial-NoDerivatives 4.0 International License.



The first record of SVPs were from Coccius in 1853, using the newly invented direct ophthalmoscope.¹⁴ By the 1920s, SVPs were measured using ophthalmodynamometry, which involved applying digital pressure to the eye, resulting in an increase in IOP and enabling the visualization of SVPs. The minimum force required to induce SVPs, referred to as ophthalmodynamometric force, was used to quantify SVP.¹⁵ Both these methods are subjective and dependent on observation and therefore are disposed to bias and inconsistency. Other factors that may contribute to unreliability in these methods include interobserver variation, the presence of microsaccades and/or fixation nystagmus, and variations in the ophthalmoscope lens power used. Hence, recent studies have focused on developing objective measures of SVP that are able to quantify the presence and degree of SVPs rather than the subjective binary classification of present or absent. These methods have included quantitative techniques of vessel diameter measurement,¹³ lateral displacement of the blood vessels,¹⁶ and hemoglobin concentration.¹⁷

The Dynamic Vessel Analyzer (DVA) is an optical-based device used to measure SVP pulsatility along vessel markers based on processing algorithms, producing a continuous SVP trace. A recent study compared subjective and objective methods of SVP detection using indirect ophthalmoscopy (75D lens) and DVA methods, respectively.⁴ The authors reported subjective SVP detection in only 64.1% of patients with glaucoma when indirect ophthalmoscopy assessment was conducted. In comparison, SVPs were objectively detected in all patients using the DVA, including those with advanced glaucoma who have previously been reported as having absent SVPs.⁴ This demonstrates the increased accuracy in SVP detection through objective means.

The use of dynamic imaging (i.e., real-time retinal videography) has previously been used to determine SVP amplitude successfully.^{13,18,19} This study introduces a novel approach to real-time videography and SVP analysis using a tablet (iOS operating system) with an add-on 20D binocular indirect ophthalmoscope lens. Previous methods of SVP analysis have been performed using costly, nonportable devices. This tablet-based ophthalmoscope is both portable and not costly and records the retinal blood circulation while maintaining a relatively high frame rate of 30 frames per second. While devices such as the Heidelberg-Spectralis optical coherence tomographer (OCT) have better image quality, they are limited by lower frame rate, mobility, and ease of use. The modern DVA technology developed specifically for videography and assessment of retinal vasculature is also nonportable and limited by contrast requirements.²⁰ Our novel approach to videography and SVP analysis addresses these issues.

Method

Data Collection

Thirty participants (average age 71.8 ± 9.7 years; 14 men) were recruited for this study, including 21 with confirmed glaucoma and 9 with suspected glaucoma. Patients were selected from an ophthalmology clinic and not included if they had diabetes and/or if the patients had current or previous vascular or retinal pathology. All had a standard ophthalmic examination, including medical history, visual acuity corrected with glasses if worn, IOP measurement using Goldmann tonometry, and Humphrey Visual Field (HVF) assessment (HFA II-i series, operating system 5.1, Dublin, CA) using the SITA-Standard strategy and stimulus size III (white).

Optic nerve imaging was carried out on OCT, using either the Spectralis OCT (Heidelberg Eye Explore version 1.10.20, Dossenheim, Germany, using the retinal nerve fiber layer [RNFL] algorithm) for 25 patients, including 8 glaucoma suspects, or the Cirrus HD-OCT (version 5.2.1.12 Optic Disc Cube 200×200 , Carl Zeiss Meditec, Dublin, CA) for 5 patients, one of whom was a glaucoma suspect. All patients at the same visit had an additional dilated (1% tropicamide [Mydracil] Alcon, Macquarie Park, Sydney, NSW) 10-second videography of venous circulation at the optic nerve head using the tablet-based 20D ophthalmoscope.

Glaucoma was diagnosed in the presence of definite glaucomatous optic neuropathy and/or visual field defects with mean deviation (MD) ranging from -9.52 to -1.57 dB and progressive change in either assessment. A comprehensive assessment was undertaken by an experienced glaucoma specialist (AA), combining conventional indirect ophthalmoscopy, OCT RNFL analysis (Heidelberg Spectralis), and Hoddap-Anderson criteria for HVF progression.²¹

Glaucoma suspects were defined as having elevated IOP or a suspicious-appearing optic disc with no progressive changes in either and a normal visual field with MD range of -1.88 to 0.59 dB, assessed on examination by AA.

Retinal Videography

Retinal videography was performed using the ProMovie video camera application on an iOS operating device (iPad Mini4; Apple, Inc., Cupertino, CA, USA). Imaging settings such as exposure and focus were adjusted manually as required for each patient to ensure maximum contrast of the optic nerve head and retinal vessels. Videos were taken centered on the optic disc and digital zoom was maintained at $2.2\times$ across all

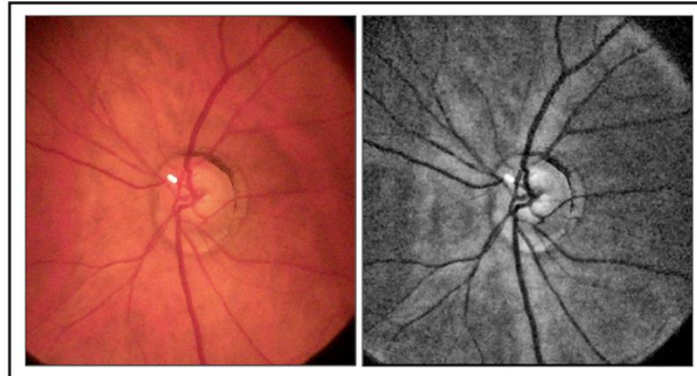


Figure 1. Magnified frames from an SVP video (left eye) from a 68-year-old woman captured using a 20D tablet-based ophthalmoscope. *Left* image is a magnified original frame. The *right* image is the *green* channel of the same frame with Contrast Limited Adaptive Histogram Equalization (CLAHE) application.

participants to ensure consistency. Participants were instructed to refrain from blinking while a 10-second photographic video was recorded. Although the tablet-based ophthalmoscope is designed for handheld use, for the purpose of video stability, a slit-lamp mount was used. Images of the device setup are included in Appendix 1.

An additional five healthy individuals were recruited to determine the reproducibility and intraindividual variability of the device. Each individual had retinal videography performed three times, each at 10-minute intervals.

Data Analysis

The digital video recordings were saved and exported as individual frames to an image-analysis program, ImageJ (previously National Institutes of Health [NIH] Image).²² To enhance visibility of the vessels, the color channels of each frame were split, extracting the green channel to reveal the highest contrast of retinal vasculature.²³ A contrast equalization plugin (CLAHE; ImageJ) was then applied to each frame enhance image contrast for greater accuracy in the detection of vessel borders, as seen in Figure 1.

The frames were then aligned to eliminate ocular movements such as those arising from fixation nystagmus or decompensation. For this, the optic disc in the first frame of the video was manually selected and used as a reference for the entire video. Normalized correlation coefficient was then used as the matching method—this function detects the landmark or the most similar image pattern in every slice (in this

case, the optic nerve). Each slice is adjusted to align the landmark pattern to keep it in the same position throughout the stack. More specifically, the algorithm compares each frame against the reference region of interest (the optic disc) by sliding (i.e., moving) the patch one pixel at a time (left to right, up to down) (Fig. 2). The algorithm was implemented in the ImageJ software using the “template matching” plugin.

The vessels were selected for measurement by an orthoptist (SS) at the central retinal vein (CRV) where possible. When the CRV was not visible (anatomical variations), the closest point to the CRV at the optic disk was selected for measurement. A manual selection was made along the transverse axis of the vessel, perpendicular to the vessel orientation. All vessel calibers were measured at the vessel of interest, using a method described by Fischer et al.²⁴ and implemented in Image J. In brief, the inner vessel diameter is estimated based on the red blood cell column using a full width at half-maximum algorithm. The diameter of the selected vessel is measured five times in each frame of the video. A moving average window of three is then applied to obtain vessel diameter at the selected location on each frame of the video. These measurements were then exported to an Excel (Microsoft, Redmond, WA, USA) spreadsheet for analysis. To remove baseline wandering, a moving average algorithm was also applied.

The frame-by-frame change in diameter was plotted against time, producing a quantified SVP trace (Fig. 3). SVP amplitude was then determined using a two-step calculation, utilizing the percentage change in vessel caliber to eliminate the effects of vessel size variation between individuals, ensuring that any changes

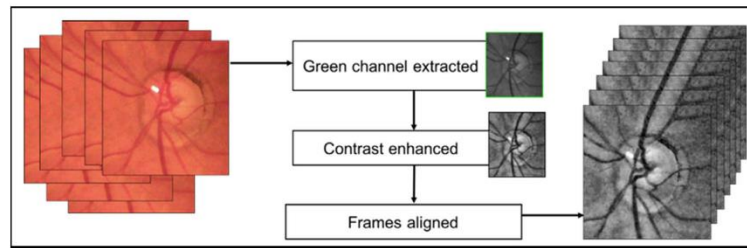


Figure 2. Schematic of image enhancement process using ImageJ.

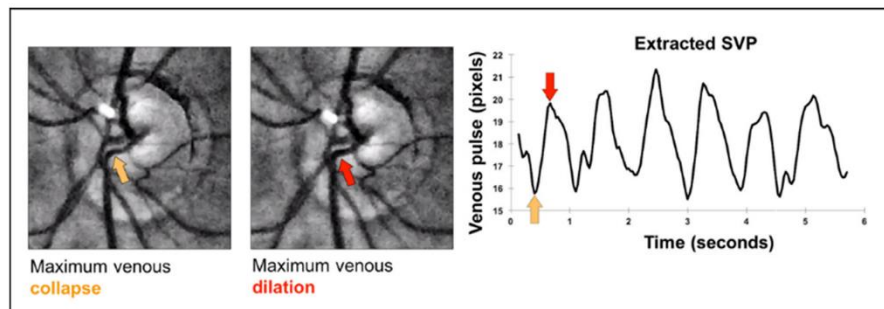


Figure 3. Left images: Two magnified, cropped, and enhanced frames from the same eye at seven frames apart (approximately 0.25 seconds). The yellow arrow points to the vessel location at maximum venous collapse and the red arrow points to the vessel location at maximum venous dilation. Right image: Corresponding SVP trace with yellow and red arrows indicating resultant troughs and peaks.

observed in vessel pulsatility are driven by pathophysiologic changes rather than interindividual vessel diameter variation. First, the change in average venous diameter (Δ venous diameter) of each participant was calculated as $\frac{\text{peak}-\text{trough}}{\text{mean vessel caliber}}$. This information was then used to calculate the average percentile pulse, calculated as $\frac{\Delta \text{ venous diameter} \times 100}{\text{mean vessel caliber}}$, to reveal the SVP amplitude of each individual.

GraphPad Prism (GraphPad Software, La Jolla, CA, USA) was used for data analysis and visualization. Linear regression was applied to visualize the strength of correlations alongside use of Pearson correlation tests to quantify the correlation strength and statistical significance (significant at the $P < 0.05$ level; two-tailed). Descriptive statistics were also conducted to reveal the basic distribution of the data.

Ethics

This study was performed in accordance with the guidelines of the tenets of the Declaration of Helsinki and approved by the University of Technology Sydney's Human Research Ethics Committee.

Written consent was obtained from each patient following an explanation of the nature of the study.

Results

The average age of participants was 72 ± 10 years, with patients with glaucoma having a significantly higher average age (75 ± 8 years) compared with glaucoma suspects (64 ± 9 years). A summary of patient demographics and mean values for IOP, global average RNFL, and HVF is presented in Table 1.

SVPs were Identified in 100% of Patients when Assessed Objectively

Raw videos of retinal circulation were first observed before computer analysis. SVPs were visible to the naked eye in 67% of glaucoma suspects and 62% of patients with confirmed glaucoma. However, computer analysis revealed the presence of SVPs in 100% of participants in both groups, with a mean SVP

Table 1. Patient Demographics and Mean Values

Characteristic	Glaucoma	Glaucoma Suspects	<i>P</i> value
Sex, male, No.	9	5	
Age	75.2 ± 8.3	64.0 ± 8.6	<0.001
IOP (mm Hg)	13.9 ± 3.2	16.2 ± 4.2	0.1
RNFL (μm)	80.9 ± 18.1	76.2 ± 16.4	0.5
HVF MD (dB)	-3.5 ± 3.0	-1.9 ± 1.8	0.1

Values are presented as mean ± SD unless otherwise indicated.

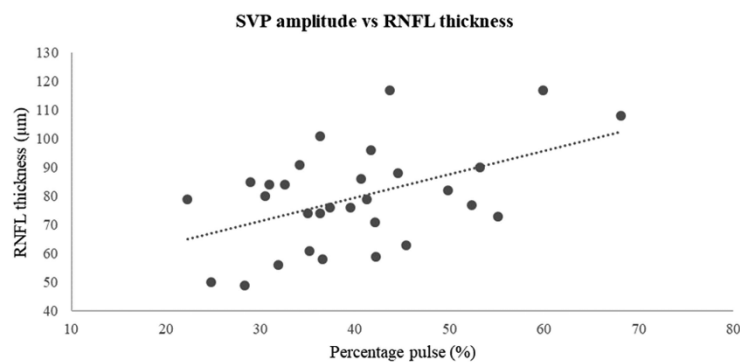


Figure 4. Correlation between SVP amplitude and RNFL thickness ($P = 0.006$, $r = 0.49$).

amplitude of $40\% \pm 10\%$ across patients with glaucoma and glaucoma suspects. Mean SVP amplitudes were significantly lower ($P = 0.03$) in suspects ($34\% \pm 6.7\%$) compared with those with a confirmed diagnosis of glaucoma ($43\% \pm 10.7\%$).

SVPs are Correlated with RNFL Thickness

Data were pooled from both patients with glaucoma and glaucoma suspects, and linear regression was used to study the association between SVP amplitudes, RNFL thickness, and HVF MD. We found a positive and significant correlation between SVP amplitudes and RNFL thickness ($P = 0.006$, $r = 0.49$) (Fig. 4). A similar positive association between HVF MD and SVP amplitude across all participants were observed, but this was not statistically significant ($P = 0.58$, $r = 0.10$).

SVP Measures are Reproducible Using the Tablet-Based Ophthalmoscope

The average age of healthy participants recruited for the feasibility study was 27 ± 5 years. The average overall SVP percentile pulse was $12\% \pm 3\%$ across

all measurements. The standard deviation of SVP variability for each individual varied from 0.2% to 3.7% with an overall average standard deviation of 2.6% for each participant that was not significantly significant (one-way analysis of variance; $P = 0.68$).

Discussion

In this study, we explored the use of a novel tablet-based ophthalmoscope to objectively detect and quantify SVPs. We also investigated the relationship between SVP amplitudes and other established structural and functional assessment parameters for glaucoma (RNFL thickness and HVF MD). Our results showed that using a tablet-based digital ophthalmoscope, we were able to visualize and quantify SVPs in all participants. Furthermore, consistent with our previous findings,⁴ we observed a positive correlation between SVP amplitudes and RNFL thickness. Further studies of SVP assessment are required to determine the sensitivity and specificity of SVPs in glaucoma diagnosis and also to explore the addition of SVP assessment as a parameter for glaucoma risk evaluation.

Table 2. Comparison of SVP Detection Devices

Characteristic	Ophthalmoscope			Heidelberg-Spectralis OCT	Dynamic Vessel Analyzer (DVA)
	Tablet Based	Direct (Traditional)	Indirect		
Portability	✓	✓	✓	×	×
Lens strength (D)	20	5	Varied		20
Approximate cost of device (AUD)	1700	≥600	≥2500	~120,000	Add-on to Heidelberg-Spectralis OCT
Ease of Use	Technical Training Required	Medical Training Required		Technical Training Required	
Dilation required	✓	✓	✓	×	✓
Frame rate (fps)	30	n/a	n/a	15	25
Resolution	77 μm/pixel	n/a	n/a		10 μm/pixel
Field of view (degrees)	46	5	Varied		25–35 ²⁵

n/a, not applicable.

Previous studies of blood vessel width measurement using devices such as the DVA have demonstrated difficulty in taking measurements at the optic nerve head due to image contrast limitations, particularly the reflectivity reported at the optic nerve or lamina cribrosa.¹³ Furthermore, the DVA is limited by the need for steady fixation.²⁰ The ProMovie application used in this study overcomes these limitations by allowing live adjustment of image exposure to overcome image contrast and reflectivity issues, allowing reliable measurements of both the optic nerve head and retina. Our custom-written algorithms also address the issue of unsteady fixation. Other advantages of the tablet-based ophthalmoscope used in this study compared with other devices used in previous studies are summarized in Table 2. Although this novel device does not have a gold standard to compare against, our feasibility results show that the numbers obtained for SVPs are highly reproducible.

Consistent with previous studies that have compared subjective and objective means of SVP detection,⁴ this study demonstrates greater detection of SVPs through objective means. SVP amplitudes are often difficult to identify with the naked eye, with reduced amplitudes being below the limits of resolution by the naked eye. This may explain the results of studies that have used subjective means of SVP detection and have detected fewer SVPs in their patients with glaucoma compared with healthy individuals.^{5,26}

Contradictory to previous findings and other reports, we found greater SVP amplitudes in patients with glaucoma than in glaucoma suspects. While this is a surprising finding, a previous study conducted by Ren et al.² found abnormally low CSFp in patients with glaucoma with normal baseline IOP. This exaggeration of the translaminal pressure gradient causes an exaggeration of SVPs. While baseline IOP (i.e., IOP pretreatment) was not reported in this study, Ren et al.² provide a possible explanation of the current results. A study investigating SVP in patients with glaucoma with normal baseline IOP and those with elevated baseline IOP before and after medical treatment is required to further unravel the findings of this study. Second, the number of glaucoma suspects was considerably lower than those with a glaucoma diagnosis ($n = 9$ vs. 21), and hence the results we have observed may not necessarily be completely representative. Third, it has been reported that SVPs are more frequently observed in older age groups.²⁷ This may also be a contributing factor, given that the average age of patients with a glaucoma diagnosis was higher than glaucoma suspects. Finally, given the positive correlation between SVP amplitudes and RNFL thickness, reduced SVPs are expected with thinner RNFLs. Hence, the difference may simply be due to lower mean RNFL thickness in glaucoma suspects.

It is well known that glaucoma is associated with RNFL thinning, but contrary to previous reports,⁴⁻⁶

we found thinner RNFL in glaucoma suspects than in patients with glaucoma. Previous investigations of retinal blood flow and RNFL thickness have revealed increased ocular blood flow in regions of RNFL thinning in the early stages of glaucoma,²⁸ with a progressive decline in ocular blood flow observed with increasing glaucoma severity.^{7,8,28} A study investigating the effect of glaucoma on SVP amplitude found reduced SVP amplitudes in retinal sectors with greater RNFL loss. The authors also report significantly smaller SVP amplitudes and RNFL thickness in patients with glaucoma compared with normal controls ($P < 0.0001$). The study also investigated individual quadrant analysis of the RNFL (i.e., superior, inferior, nasal, and temporal regions of the RNFL surrounding the optic nerve) and determined positive correlations between SVP amplitude and RNFL thickness.⁴

In our study cohort, only three participants with confirmed glaucoma had moderate glaucoma, and the majority had early stage glaucoma²¹ and may have less damage to the RNFL than is normally observed in larger cohorts of patients with a diagnosis of glaucoma. Larger sample sizes with even distribution between the groups are needed to reflect the true RNFL distribution expected. The discrepancy could also be due to different OCTs used—Leite et al.²⁹ demonstrated thinner measurements on the Cirrus OCT compared with the Spectralis OCT ($P < 0.001$). Faghihi et al.³⁰ also found similar results but demonstrated a significant relationship between intermeasurement differences. A separate analysis was conducted using only the measures obtained from the Spectralis OCT, which was found to exacerbate the difference in RNFL thickness between the groups (mean RNFL thickness was 2.2 μm greater and 3.8 μm thinner in the glaucoma and glaucoma suspects groups, respectively). A similar analysis was not performed on just the Cirrus OCT results as our participant numbers are too small for statistical comparison, with just one participant in the glaucoma suspect group. This participant, however, had a thicker average RNFL than the average RNFL thickness in the participants with glaucoma (91.00 μm and 73.60 \pm 10.69 μm , respectively).

Assessment of visual fields is routine in clinical glaucoma practice. It is the major indicator of functional impact of glaucoma in one's quality of life,^{31,32} and results are key in influencing management options.³³ Previous studies have demonstrated that worse visual field MD is associated with lower frequency of SVPs in glaucoma.³⁴ While the correlation we observed between SVP and HVF MD in our small sample of participants was not significant, future studies using larger sample sizes may

reveal stronger correlations that align with previous studies.³⁴

Our results demonstrate that the use of a portable and easy-to-use device in detecting and quantifying SVPs is possible and very promising. Further research is necessary to determine the comparability of SVP analysis using this novel technique and established SVP analysis tools and methods, such as the DVA. If these projected studies demonstrate good comparability between devices, it can be proposed that using a tablet-based ophthalmoscope is a more feasible approach to SVP analysis. Furthermore, it will be useful to establish normal age-related changes in SVP amplitude. Studies have looked at the effect of aging on the presence of SVP, but there have been no studies establishing the normal distribution of SVP amplitude with age.²⁷

In conclusion, this study has provided proof of principle that using a 20D binocular indirect ophthalmoscope lens in conjunction with a smart digital hardware may be a feasible means of detecting SVPs and can be used for SVP analysis. There is significant potential for future use of the device given its relatively inexpensive, easy-to-use, and portable nature. Future studies with larger sample sizes may resolve the apparently contradictory findings regarding glaucoma suspects.

Acknowledgments

Supported by an National Health and Medical Research Council (NHMRC) PhD scholarship (SS), an NHMRC-Australian Research Council (ARC) dementia research fellowship (SMG), and National Institutes of Health R21EY027945 (CB).

Disclosure: **S. Shariflou**, None; **A. Agar**, None; **K. Rose**, None; **C. Bowd**, None; **S.M. Golzan**, None

References

1. Morgan WH, Balaratnasingam C, Hazelton ML, House PH, Cringle SJ, Yu DY. The force required to induce hemivessel pulsation is associated with the site of maximum field loss in glaucoma. *Invest Ophthalmol Vis Sci*. 2005;46:1307–1312.
2. Ren R, Jonas JB, Tian G, et al. Cerebrospinal fluid pressure in glaucoma: a prospective study. *Ophthalmology*. 2010;117:259–266.
3. Morgan WH. Central venous pulsations: new findings, clinical importance and relation to

- cerebrospinal fluid pressure. *J Glaucoma*. 2013; 22(suppl 5):S15–S16.
4. Golzan SM, Morgan WH, Georgevsky D, Graham SL. Correlation of retinal nerve fibre layer thickness and spontaneous retinal venous pulsations in glaucoma and normal controls. *PLoS One*. 2015;10:e0128433.
 5. Morgan WH, Hazelton ML, Azar SL, et al. Retinal venous pulsation in glaucoma and glaucoma suspects. *Ophthalmology*. 2004;111:1489–1494.
 6. Graham SL, Butlin M, Lee M, Avolio AP. Central blood pressure, arterial waveform analysis, and vascular risk factors in glaucoma. *J Glaucoma*. 2013;22:98–103.
 7. Siesky B, Harris A, Racette L, et al. Differences in ocular blood flow in glaucoma between patients of African and European descent. *J Glaucoma*. 2015;24:117–121.
 8. Flammer J, Orgul S, Costa VP, et al. The impact of ocular blood flow in glaucoma. *Prog Retin Eye Res*. 2002;21:359–393.
 9. Berdahl JP, Allingham RR, Johnson DH. Cerebrospinal fluid pressure is decreased in primary open-angle glaucoma. *Ophthalmology*. 2008;115:763–768.
 10. Morgan WH, Yu DY, Cooper RL, Alder VA, Cringle SJ, Constable IJ. Retinal artery and vein pressures in the dog and their relationship to aortic, intraocular, and cerebrospinal fluid pressures. *Microvasc Res*. 1997;53:211–221.
 11. Morgan WH, Lind CR, Kain S, Fatehee N, Bala A, Yu DY. Retinal vein pulsation is in phase with intracranial pressure and not intraocular pressure. *Invest Ophthalmol Vis Sci*. 2012;53:4676–4681.
 12. Wong SH, White RP. The clinical validity of the spontaneous retinal venous pulsation. *J Neuroophthalmol*. 2013;33:17–20.
 13. Golzan SM, Graham SL, Leaney J, Avolio A. Dynamic association between intraocular pressure and spontaneous pulsations of retinal veins. *Curr Eye Res*. 2011;36:53–59.
 14. Coccia EA. Ueber die Anwendung des Augenspiegels: nebst Angabe eines neuen Instrumentes. Müller, 1853.
 15. Morgan WH, Cringle SJ, Kang MH, et al. Optimizing the calibration and interpretation of dynamic ocular force measurements. *Graefes Arch Clin Exp Ophthalmol*. 2010;248:401–407.
 16. Moret F, Reiff CM, Lagreze WA, Bach M. Quantitative analysis of fundus-image sequences reveals phase of spontaneous venous pulsations. *Transl Vis Sci Technol*. 2015;4:3.
 17. Morgan WH, Abdul-Rahman A, Yu DY, Hazelton ML, Betz-Stablein B, Lind CR. Objective detection of retinal vessel pulsation. *PLoS One*. 2015;10:e0116475.
 18. Golzan SM, Butlin M, Kouchaki Z, Gupta V, Avolio A, Graham SL. Characterizing dynamic properties of retinal vessels in the rat eye using high speed imaging. *Microvasc Res*. 2014;92:56–61.
 19. Golzan SM, Avolio A, Graham SL. Hemodynamic interactions in the eye: a review. *Ophthalmologica*. 2012;228:214–221.
 20. Garhofer G, Bek T, Boehm AG, et al. Use of the retinal vessel analyzer in ocular blood flow research. *Acta Ophthalmol*. 2010;88:717–722.
 21. Susanna R Jr, Vessani RM. Staging glaucoma patient: why and how? *Open Ophthalmol J*. 2009;3:59–64.
 22. Girish V, Vijayalakshmi A. Affordable image analysis using NIH Image/ImageJ. *Indian J Cancer*. 2004;41:47.
 23. Abramoff MD, Magelhaes P, Ram S. Image processing with ImageJ. *Biophotonics Int*. 2004;11:36–42.
 24. Fischer MJ, Uchida S, Messlinger K. Measurement of meningeal blood vessel diameter in vivo with a plug-in for ImageJ. *Microvasc Res*. 2010;80:258–266.
 25. Witmer MT, Parlitsis G, Patel S, Kiss S. Comparison of ultra-widefield fluorescein angiography with the Heidelberg Spectralis noncontact ultra-widefield module versus the Optos Optomap. *Clin Ophthalmol (Auckland, NZ)*. 2013;7:389.
 26. Harder B, Jonas JB. Frequency of spontaneous pulsations of the central retinal vein. *Br J Ophthalmol*. 2007;91:401–402.
 27. Lorentzen SE. Incidence of spontaneous venous pulsation in the retina. *Acta Ophthalmol (Copenh)*. 1970;48:765–770.
 28. Plange N, Kaup M, Weber A, Arend KO, Remky A. Retrobulbar haemodynamics and morphometric optic disc analysis in primary open-angle glaucoma. *Br J Ophthalmol*. 2006;90:1501–1504.
 29. Leite MT, Rao HL, Zangwill LM, Weinreb RN, Medeiros FA. Comparison of the diagnostic accuracies of the Spectralis, Cirrus, and RTVue optical coherence tomography devices in glaucoma. *Ophthalmology*. 2011;118:1334–1339.
 30. Faghihi H, Hajizadeh F, Hashemi H, Khabazkhoob M. Agreement of two different spectral domain optical coherence tomography instruments for retinal nerve fiber layer measurements. *J Ophthalmic Vis Res*. 2014;9:31–37.

31. Nelson P, Aspinall P, Pappasoulotis O, Worton B, O'Brien C. Quality of life in glaucoma and its relationship with visual function. *J Glaucoma*. 2003;12:139–150.
32. Hyman LG, Komaroff E, Heijl A, Bengtsson B, Leske MC; Early Manifest Glaucoma Trial Group. Treatment and vision-related quality of life in the early manifest glaucoma trial. *Ophthalmology*. 2005;112:1505–1513.
33. Canadian Glaucoma Study Group. Canadian Glaucoma Study: 1. Study design, baseline characteristics, and preliminary analyses. *Can J Ophthalmol* 2006;41:566–575.
34. Seo JH, Kim TW, Weinreb RN, Kim YA, Kim M. Relationship of intraocular pressure and frequency of spontaneous retinal venous pulsation in primary open-angle glaucoma. *Ophthalmology*. 2012;119:2254–2260.

Appendix 1

Images 1 and 2.



Image A2. Patient and tablet-based ophthalmoscope position during SVP assessment.



Image A1. SVP assessment using a tablet-based ophthalmoscope mounted on a slit lamp.